GOLD THIN FILMS PRODUCED FROM LASER STIMULATED PLASMA REACTION PRODUCTS

By

CHARLES GEORGE SIMON

A DISSERTATION PRESENTED TO THE GRADUATE SCHOOL OF
THE UNIVERSITY OF FLORIDA
IN PARTIAL FULFILLMENT OF THE REQUIREMENTS FOR THE
DEGREE OF DOCTOR OF PHILOSOPHY

UNIVERSITY OF FLORIDA

1988

To my wife, Diane,
to my parents, Sam and Bernice,
and
to Bobby Sammons.

ACKNOWLEDGEMENTS

The author wishes to express his gratitude to all who contributed to this work and to his education at the University of Florida. In particular, he wishes to express his appreciation for all of the effort and guidance provided by his research director and committee chairman, Samuel Colgate.

The author would like to thank his peers and the faculty and staff members at the University of Florida (U.F.) and the University of South Florida (U.S.F.) who contributed to this effort: at U.F., Mark Hail and Roy King for quadrupole MS analyses, Mehdi Moini for FTICRMS experiments, Dan Lesson for cluster beam TOFMS experiments, Paul McCaslin and Jack Davis, Jr., for XPS analyses; at U.S.F., Alfred D'Agostino and Carl Biver for XPS analyses, and Mike Ammons and Alicia Slater for SEM/EDS analyses. Specials thanks are also extended to Stephanie Boggess at U.F. for her invaluable assistance throughout the course of this work, and to Bobby G. Sammons of Stone Container Corporation, Port Wentworth, Georgia, for providing that special impetus.

Finally, the author wishes to thank his committee members for their contributions to this work, especially Martin Vala and John Eyler who provided laboratory equipment and time, and The Florida High

Technology and Industry Council for their financial support (FHTIC Grant #85092726).

TABLE OF CONTENTS

LIST OF TABLES

Abstract of Dissertation Presented to the Graduate School of the University of Florida in Partial Fulfillment of the Requirements for the Degree of Doctor of Philosophy

GOLD THIN FILMS PRODUCED FROM LASER STIMULATED PLASMA REACTION PRODUCTS

by

Charles George Simon

December 1988

Chairman: Samuel O. Colgate
Major Department: Chemistry

Superfine particles of gold in the 100-400 nanometer size range were produced in a plasma stimulated by 10.6 micron radiation from a pulsed carbon dioxide laser. The production of the particles was shown to be highly dependent on the types and pressures of the gases used in the plasma, and the incident power density. The best conditions determined for production of the particles were a partial pressure of 350 Pascals of methane gas mixed with hydrogen to a total pressure of 700-1400 Pascals, and an incident power density of 3×10^9 watts/cm^2.

The particles were used to coat tungsten, glass, and polymeric substrates. The coated tungsten and glass substrates were subjected to air and hydrogen anneals convectively at temperatures up to 600 K, and by 10.6 and 0.532 micron laser radiation. Selected sample films were then subjected to analyses by optical microreflectometry, X-ray photoelectron spectroscopy, scanning electron microscopy, energy dispersive spectroscopy, and electrical resistance.

The results of these analyses showed that the gold films had highly variable properties depending on the substrate and annealing

conditions. The average mass concentration of gold in the films was 95% (54 atomic %). High quality continuous gold lines could be written on coated glass substrates using continuous wave 0.532 micron argon ion laser radiation. Three distinct colors could be developed in the films using thermal input. This property makes the product a viable candidate for use as a multi-level optical encoding media.

Film collapse did not occur until 490 K and there were no other contaminants in the films due to the containerless evaporation technique. These properties indicate that the plasma reaction products may be suitable high temperature replacements for gold blacks.

CHAPTER I
INTRODUCTION

Methods for producing submicron gold film patterns are of current interest to the microelectronic industry for use as interconnect metallization as device sizes shrink in VLSI (very large scale integration) circuitry. Interconnects provide communication routes between single devices and each other, between single devices and the outside world and between active regions within a single device. Since propagation time delay along the interconnect is directly proportional to film resistivity and inversely proportional to the film thickness, as well as varying with the square of the length,[1] it is important to produce short and relatively thick (compared to the width) films with good electrical properties in order to minimize operating times. Current micron-size interconnects are patterned using aluminum, but industry progression to submicron-size devices will eliminate aluminum for this use because of electromigration problems. Gold is an ideal substitute for aluminum because of its low resistivity, high conductivity, and resistance to electromigration.

Chemical vapor deposition (CVD) is the only currently available technique for producing gold thin films that met both the selective deposition and high throughput requirements necessary for mass-producing submicron patterns in VLSI circuits. Volatile gold compounds are used in the CVD process to form the thin metal films by decomposing

on activated surfaces, leaving the metal atom on the surface and the remaining molecular constituents in the gas phase. Thus, there is a concurrent interest in high yield, cost effective methods for synthesizing suitable compounds for use in gold CVD processes.

An alternative method to conventional solution based synthetic chemistry that offers several advantages is the in situ gas phase production of suitable gold compounds. This technique could be integrated into a CVD system and produce volatile gold compounds on demand, eliminating the need to store and handle such compounds, and removing the processor's dependency on off-site precursor production. The ideal system would use solid gold and non-toxic reactive gases to form the volatile species upstream from the CVD chamber. After passing through the CVD chamber, any unused gold compounds would be easily recovered for recycle or gold reclamation. The following report describes efforts to explore and understand novel chemical means which might support the development of such a system based on production of gas phase gold compounds in a pulsed laser stimulated plasma using a solid gold target and non-toxic reactant gases.

A brief review of the physical properties and mechanisms of currently available materials and methods utilized in interconnect formation will illustrate the limitations that need to be overcome. The advantages of using gold for interconnect metallization and the effectiveness of CVD for submicron patterning will be described. Evidence of the gas phase production of gold compounds using energetic plasmas will also be presented. Finally, a brief description of the proposed technique will be given, followed in Chapter II by a complete

description of all equipment and procedures and in Chapter III by a discussion of the results.

Among the elements only gold, silver, copper, and aluminum have high enough electrical conductivities at device operating temperatures (> 300 K) to be considered for use in interconnect formation.[2] Both silver and copper are highly reactive and subject to catastrophic oxidation. While aluminum is more stable to oxidation, it is far more susceptible to electromigration than gold. Electromigration results from mobility of the metal ions in the film driven by the friction forces exerted by the flowing electrons. The ultimate result of electromigration is the formation of a void large enough to cause a discontinuity in the interconnect resulting in device failure.[3] When the factors responsible for electromigration are considered, the advantages of gold over aluminum become clear.

In the polycrystalline thin metallic films which make up interconnect lines, electromigration can be evaluated by considering the total atomic flux, F, which can be expressed as the sum of the atomic fluxes through the interior of the grain (equivalent to the flux in the bulk metal) and the flux across the grain boundaries. Huntington and Grone[4] derived an expression for the flux in bulk material, while Ho and d'Heurle[5] did so for the added atomic flux across grain boundaries. Both approaches are based on statistical distribution of mobile atoms and adjacent vacancies in the crystal lattice or grain boundaries. Combining their two expressions yields an equation for F as a function of the current density J, the atomic density N, the atomic diffusion coefficient D, the absolute temperature

T, the effective charge Z*q, the bulk conductivity c_b, and the film conductivity c_f:

$$F = NDZ^*qJ/c_bkT + (NDZ^*qJ/c_fkT)(s/d)$$

where k is the Boltzman constant, s is the average separation distance between grain boundaries, and d is the average grain size. This model is only an approximation since it ignores the geometrical orientation of the grains and impurities adsorbed on the grain boundaries, and it assumes that transport across grain boundaries occurs via channels between the grains.

It is immediately apparent that the lower atomic density of gold, 0.098 moles/cm^3, compared to aluminum, 0.167 moles/cm^3,[6] leads to a lower F value for gold. Also, the lower effective nuclear charge of the gold atom and the gold (+1) and (+3) ions (Z* = 0.65, 1.0, and 3.0, respectively, using Slater's Rules) compared to the aluminum atom and (+3) ion (Z* = 3.15 and 4.2, respectively, using Slater's Rules)[7] results in a further lowering of the F value for gold.

Since movement of atoms within a crystal is highly restricted, and the grain boundary area in these polycrystalline metal thin film interconnects is many times greater than the external surface area, the atomic flux within the thin film interconnect is dominated by diffusion across the grain boundaries.[8] Thus, the heavier, more bulky gold atoms, possessing a lower relative charge than aluminum, but having a similar net bulk resistivity of ca. 2.5 microohms/cm, are far less prone to electromigration at high current densities. Typically,

current densities > 10^5 amp/cm^2 cause serious electromigration problems in aluminum and its alloys, while gold does not experience serious problems until current densities exceed approximately 10^9 amp/cm^2.[9] The next generation of electronic devices are expected to be of submicron dimensions and operate at current densities up to 10^8 amp/cm^2.[10] Thus gold appears to be a suitable material for interconnect metallization in future devices. There are several problems associated with the use of gold in silicon based circuitry. Most notably, the high diffusivity of gold in silicon and silicon dioxide necessitates the use of a barrier metal such as tungsten between the two materials.[11] While industrial methods for mass-producing submicron patterns of tungsten based on CVD techniques currently exist,[11-16] there are no methods currently available for mass-producing submicron patterns of gold. If an inexpensive, readily available source of volatile gold species with low toxicity and good deposition characteristics could be developed, it would greatly facilitate efforts in this area.

A review of the methods available for producing gold thin films reveals significant problems associated with the application of each method to the mass-production of submicron patterning. There are seven general categories of techniques currently employed to form gold films:

1) electroplating
2) sputtering (including reactive sputtering)
3) vacuum evaporation
4) ionized cluster deposition
5) superfine particle deposition

6) chemical vapor deposition (CVD)

7) direct write (including laser, electron, and ion beam techniques).

Electroplating gold from solutions has been used extensively by the electronic industry to form thin film devices and structures with dimensions greater than several microns.[17] However, the films produced are typically porous and have significantly lower conductivities than bulk gold. These plated films also contain alkali ion contaminants that migrate in the electric fields and accumulate at junctions where they change the device operating characteristics. There is also the problem of dendritic growth experienced in electroplated gold films, which can lead to formation of short circuits in adjacent conductors.[18]

A recent improvement in conventional electroplating was developed by C. Patton using a laser-enhanced jet plating technique.[19] This method produced high quality gold spots and lines by directing a 25-Watt continuous-wave argon ion laser beam through a focusing lens and into a free-standing jet of electrolyte that acted as an optical wave guide and a gold ion source. The laser energy and the fine jet stream of electrolyte were directed onto a rastered cathode surface where deposition rates as high as 30 microns/sec. were reported. The inherently low throughput of this rastered system precludes its use as a technique for mass-production of submicron gold patterns.

Sputtering is a physical vapor deposition (PVD) technique that uses ionized gases (usually argon) to bombard a target composed of the metal to be deposited. The energetic ion collisions dislodge surface and near surface neutral metal atoms which then travel randomly to the

substrate where they are deposited. Masks and etching techniques are used to form patterns. Several variations have been developed, such as adding a reactive gas to the ambient, or heating and/or applying a radio-frequency (rf) bias to the substrate. These modifications improve step coverage on the substrate surface, and well-defined step coverage is essential for small scale device and interconnect formation.[11,20-23] Non-uniform step coverage results in "thin" areas that lead to early device failure. The improvements have not completely solved the step coverage problems for small dimensions, and the methodology is still considered non-conformal.[22] This major disadvantage along with the non-selectivity of the deposition process precludes the use of sputtering techniques for mass-production of submicron gold patterns.

Vacuum evaporation is also a physical vapor deposition process. Thermal convection, resistance heating, laser vaporization, or electron gun vaporization is used to evaporate the metal in a vacuum. The atoms then travel by line of sight to the substrate where they condense and form a thin film.[21] Masking and etching techniques are used to form patterns. This methodology is limited by non-conformal step coverage and non-selectivity of the deposited films.[22] These limitations exclude evaporation techniques from use in the mass-production of submicron gold patterns.

Ionized cluster beam deposition is a recently developed technique that utilizes ionized clusters of up to several thousand atoms to form thin films.[21,24] The clusters are formed by homogeneous or heterogeneous nucleation either in the vapor phase in the plume exhaust

from a nozzle fitted onto a hot crucible containing the molten source material, or on the side walls of the crucible itself before exiting through the nozzle. The clusters are subsequently ionized by electron bombardment with a current of several milliamps and energies in the 80-100 eV range. They are then accelerated through a 1-10 KV potential and directed to the substrate surface where they deposit non-selectively with enough energy per atom (1-10 eV) to facilitate surface mobility without inducing defect damage associated with higher impact energies.

A recent study by Knauer and Poeschel showed that under optimum conditions only about 1% of the total metal flux from a crucible filled with molten gold or silver was in the form of clusters in the size range of several hundred to several thousand atoms.[25] Since only a few percent of these clusters were ionized in the electron bombardment step, the net efficiency of metal use was very low. This limitation, together with the need for line of sight deposition (which implies non-conformal step coverage) and the non-selectivity of the process, preclude its use for mass-production of submicron gold film patterns.

Another recently developed technique for producing gold thin films, also based on homogeneous and heterogeneous nucleation of particles in the gas phase, involves the production of "ultra-fine" particles in the 5-65 nanometer size range (10^3-10^7 atoms/particle) that are subsequently deposited non-selectively on a substrate.[26-28] Metal vapors are produced using a laser beam, arc discharge, or electron beam in the presence of inert or reactive gases. At least one group applied the technique to gold.[28] The same limitations of non-

selectivity and non-conformal step coverage eliminate this method from consideration as a viable procedure for submicron patterning of gold films. However, investigators claim that high yields of metal compounds can be formed by the activated clusters in reactive gas streams.[27] This is an interesting point which will be discussed further below.

Chemical vapor deposition techniques do not depend on a flux of condensible species reaching the substrate by direct line of sight and hence are not subject to non-conformal step coverage problems.[22] Substrates are surrounded by metal-bearing volatile species that do not decompose without some form of additional energy input.[20] In principle, this allows close packing of the substrates in the deposition chamber and selective deposition via selective energization of pre-patterned barrier metal surfaces. There are many variations of the basic CVD methodology designed to optimize performance of a particular metal deposition system, but they all utilize a volatile species that is forced to decompose on the substrate areas of interest and leave behind a thin film of relatively pure metal.[16,20-23]

Chemical vapor deposition is the only category of currently available metallization technology that meets the requirements of selective deposition and high throughput necessary for mass-production of submicron gold thin film patterns. To date, no reports of simultaneous patterning of large arrays of submicron features with gold have been published. Non-selective CVD of gold from triarylphosphine-goldchlorides using thermal decomposition was demonstrated by Mann, Wells, and Purdie in 1937.[29] House and Colgate recently reported

similar results using the same compounds and rf stimulated thermal decomposition.[30] There are other examples of non-selective CVD of gold from organometallic compounds such as AuR(CNR'), and (R) PAuOSi(R), where R and R' are methyl, ethyl, or phenyl groups.[31,32] The most recent compounds to be used for CVD of gold are dimethylacetylacetonatogold(III) and its tri- and hexafluoro derivatives. Larson and Baum reported the formation of high quality gold films from these compounds by thermal decomposition at 300°C.[33] Films produced from the fluorinated derivatives were relatively free from contamination and had resistance values about twice that of bulk gold. This work represents the current state of the art for gold CVD methods. While the compounds used performed well, they are difficult to synthesize and have low synthetic yields.[34] These compounds are available commercially at a cost of several hundred dollars per gram.[35] Clearly a cheaper, more readily available source of volatile gold species would be of benefit.

The only examples of submicron selective gold deposition reported utilized various direct write methods, such as the laser-jet electroplating technique described earlier,[19] or ion beam pyrolysis of solid (spun-on) organometallic films.[36] Most groups have used focused laser, ion, or electron beams to induce selective CVD of gold from volatile compounds.[37-44] Again, the fluorinated derivatives of dimethylacetylacetonatogold(III) formed the highest quality submicron sized gold lines and spots. Despite the high quality of the gold films produced by these methods, their inherently slow rate of throughput precludes their economic use in mass-production scenarios.

As previously mentioned, one possible alternate source of organogold compounds for use in CVD systems that offers the advantages of low cost and availability on demand is the in situ production of such compounds from solid gold and inocuous gases. Techniques exist for producing gold oxides and halides from solid targets using sputter gun evaporation in the presence of the reactive gases.[45] Araya et al. claim that goldcarbide superfine particles can be generated in the gas phase from Nd:YAG pulsed laser stimulated plasmas using solid gold targets in the presence of methane or Freon gases.[27] There are also examples of organogold ions formed in ion cyclotron resonance mass spectrometer experiments using high-voltage spark and carbon dioxide pulsed laser stimulated vaporization/ionization of solid targets in the presence of aliphatic or aromatic hydrocarbons, alkylhalides, and alcohols.[46-49]

In another related field of research, investigators have been producing gold bearing plasma polymerized films using PVD sputtering or evaporation techniques.[50-58] These studies have shown that the metal is incorporated in the films in the form of small particles that drastically alter the optical and electrical properties of the polymers.

Gold carbonyls and organogold compounds have been formed in matrix isolation studies by cocondensation of gold atoms with carbon monoxide, acetylene, ethylene, and propylene.[59-62] These studies illustrate the high reactivity of gold atoms with carbonaceous molecules, even at very low temperatures.

Taking this evidence into consideration, it would seem possible to develop a continuous process method for generating gaseous gold species from solid gold and gaseous compounds in an energetic plasma. Such a process could be incorporated in a CVD production line to provide volatile gold compounds on demand. This technique would also eliminate the need to store and handle synthetic compounds, a major economic and safety factor advantage in itself.

Materials produced by the method would be evaluated by considering the following criteria:

1) production rate
2) volatility
3) thermal stability
4) temperature of decomposition
5) film properties (resistance, purity, morphology, stability)
6) properties of by-products (should be non-contaminating to the substrate and non-toxic)
7) ability to recycle or reclaim gold.

In addition to these considerations, the toxicity of the starting materials would be a primary concern.

A plasma reaction system was designed and constructed to investigate the feasibility of producing gas phase gold compounds in large enough quantities to be used in mass-producing CVD submicron gold patterns. The procedures and results of that investigation are presented in the following chapters.

CHAPTER II
EXPERIMENTAL

The scope of this study was limited to the investigation of reactions occurring between non-toxic or low-toxic gaseous species and pulsed CO2 laser stimulated gold vapors and plasmas. Particular emphasis was placed on utilization of permanent carbonaceous gases. The study consisted of three major parts: 1) production of gas phase gold-bearing species in high yields in the plasma, 2) determination of volatility of high-yield species, and 3) characterization of gold thin films produced from the high-yield species. Detailed descriptions of experimental equipment and procedures are presented together in this chapter. Each major part of the study is treated autonomously. Conditions leading to equipment or procedure modifications are mentioned but are not discussed until the following chapter.

Production of Gas-Phase Gold Species: The Plasma Reaction System

The plasma reaction system was composed of four sub-systems:

1) the pulsed carbon dioxide laser and associated optics
2) the gas handling system
3) the plasma reaction chambers
4) the product-recovery/substrate-coating systems.

Each sub-system is described in detail together with pertinent operational procedures followed during the course of the study.

Carbon Dioxide Laser, Optics, and Operation

The foremost criterion for development of a successful method for producing gaseous gold compounds for the intended use was a high production rate. An energy source was needed that could provide both a high flux of gold vapor and the additional energy needed to form a reactive plasma from the volatilized gold and reactive gases. A Lumonics pulsed TEA (transversely excited atmosphere) carbon dioxide laser, model 101-1, that had previously demonstrated high volatilization rates for refractory metals[63] was available for use in this study. This laser was capable of producing an optical pulse energy of 2.5 joules with a pulse halfwidth of 250 nanoseconds and a power density of approximately 3×10^9 watts/cm^2 when optimally focused through a 200 mm focal length lens. Maximum pulse repetition rate was 1 hz, giving the laser a duty time of approximately one millisecond per hour. The emitted wavelength of 10.6 microns corresponds to the P(20) line in the 001-100 band.

The laser's pulse energy could be varied by adjusting the nitrogen gas pressure and flow rate to the spark gap trigger, by adjusting the composition and flow rate of the helium/nitrogen/carbon-dioxide lasing gas mixture, or by adjusting the operating voltage. During the course of this study these parameters were maintained in a state that resulted in maximum energy output.

The laser energy output was measured after major maintenance events, such as disassembly and cleaning of the optics or electrodes, using a Scientech 365 laser power/energy meter. During subsequent operation, the laser output was monitored by exposing a piece of thermal paper (Hewlett Packard #820-51A) to single pulses of the unfocused, 28 mm dimeter beam and comparing the resultant discoloration patterns to standard patterns that were produced under measured conditions (see Figure 1).

The laser beam was directed into the plasma reaction chamber through the optic path using a 5 cm square face coated silver mirror during initial screening experiments. This mirror was subsequently removed from the system and the laser was positioned in a direct line of fire with the optics and the chamber at a distance of ca. 0.5 meters in order to transmit as much energy as possible to the target.

An externally mounted 5 cm diameter germanium meniscus lens with a 200 mm focal length (Oriel model 4365) was used to focus the laser beam during the first half of the study. A similar lens with a focal length of 250 mm (II-VI, Inc., model 5-5741-1) replaced the initial lens for the final half of the study. (This was necessary as a result of physical damage sustained by the 200 mm lens during a cleaning procedure accident.) Both lenses had an anti-reflection coating for maximum transmission at 10.6 microns.

The lenses were held in a clamp mounted to an optical stand with three degrees of freedom. This arrangement allowed the lens to be positioned closer to the target than the optimum focal distance during the course of an experimental run, thus distributing the laser energy

Figure 1. Thermal Paper Exposed to Single Pulses of the Carbon Dioxide Laser
(a) Laser performing well (nominal)
(b) Laser performing poorly (gas mixture not optimized for power level and pulse repetition rate

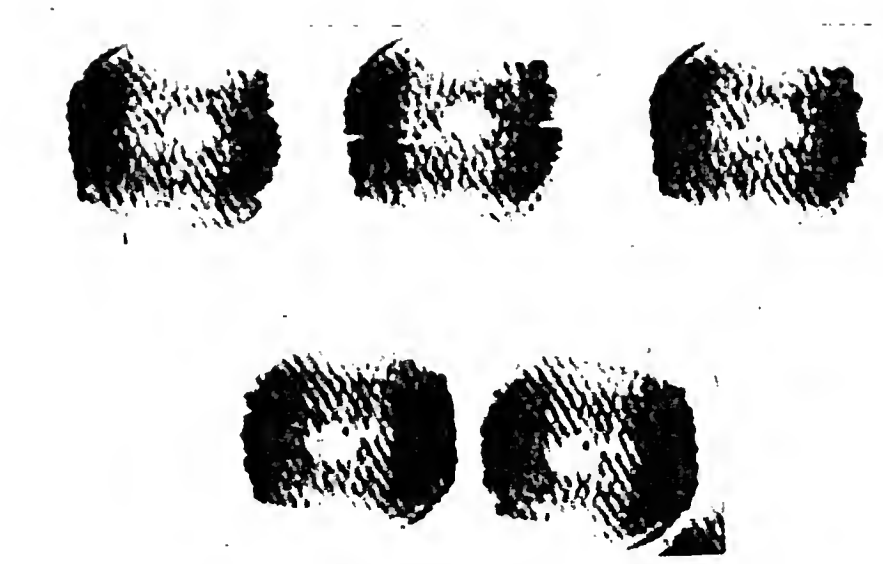

(a)

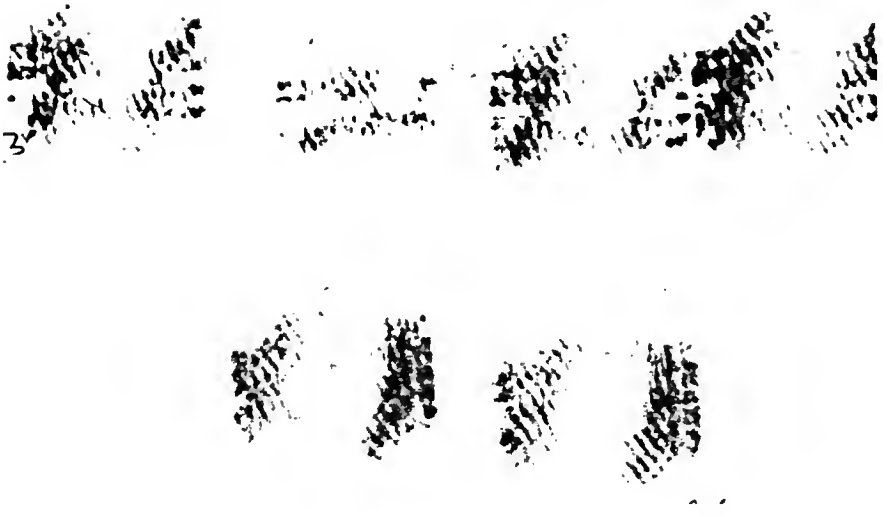

(b)

over a larger surface area. This procedure was used in all experiments where the effects of lower than maximum power densities were investigated.

The optimum focal length for each lens was determined experimentally by exposing thermal paper (in air) to the partially focused beam at distances equivalent to 10, 60, 85, 135, and 195 percent of the expected focal lengths. The average spot diameters from each point were plotted against the distance from the back edge of the lens. The intersection of the two lines drawn through the points gave the optimum focal length (Figure 2). The value determined for the two lenses were 199 mm and 254 mm. These values were confirmed by microscopic examination of target impact craters after exposure to the highly focused beam.

After passing through the focusing lens, the beam entered the reaction chamber through a 3.8 cm diameter zinc selenide window (II-VI, Inc., #-746-7) which also had an anti-reflection coating for maximum transmission at 10.6 microns. The distance between the lens and the window was kept to a minimum in order to prevent damage of the latter by interaction of the partially focused laser beam with surface contaminants. This distance was ca. 0.5 cm for the 200 mm focal length lens and ca. 2 cm for the 250 mm focal length lens.

Gas Handling System and Procedures

All of the gases used in this study, except one, were gaseous at STP and were supplies from pressurized cylinders. Standard one and two stage gas regulators and associated fittings were used to deliver these

Figure 2. Germanium Lens Focal Length Determination

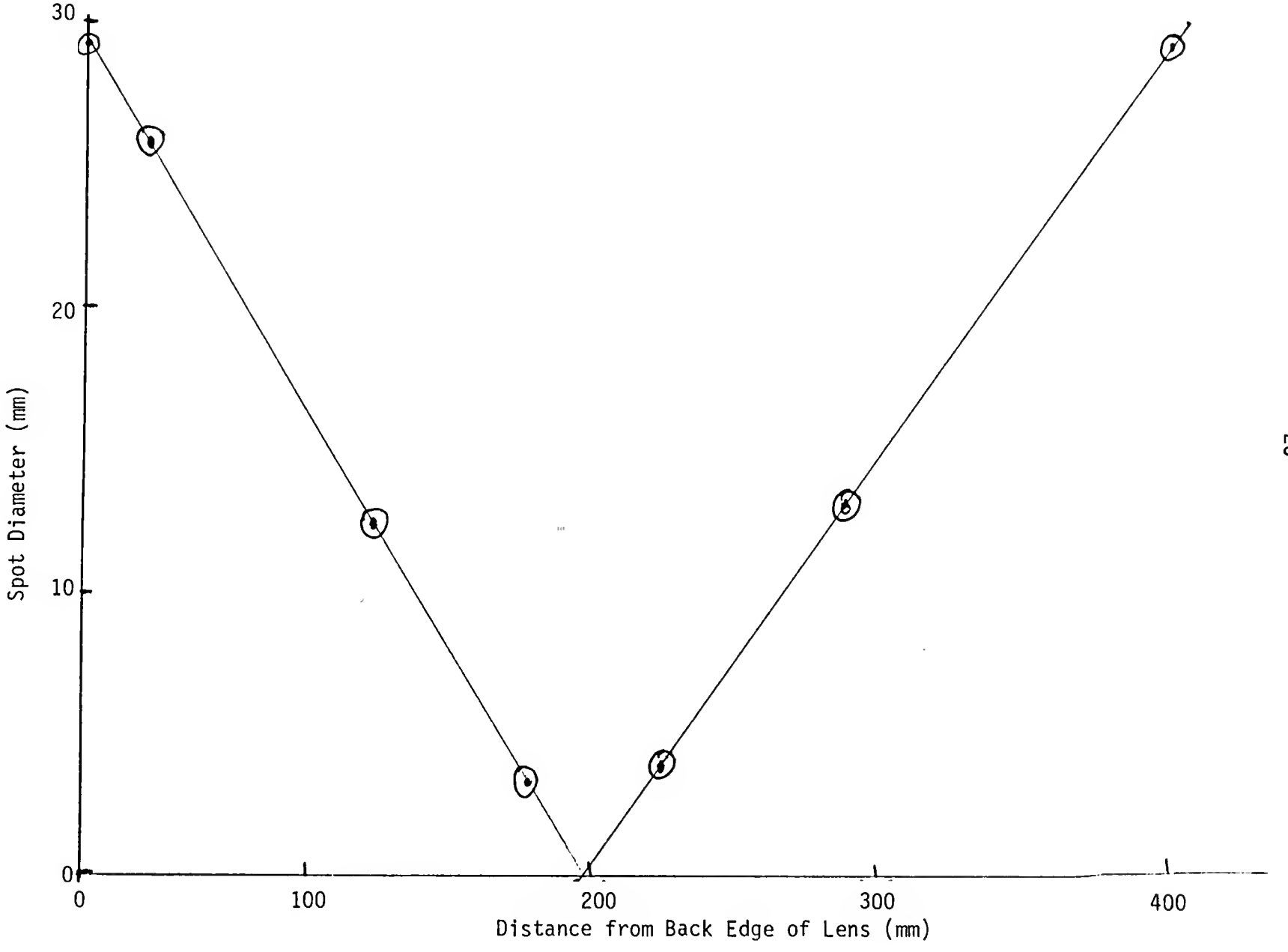
30
20
10
0
Spot Diameter (mm)
0
100
200
300
400
Distance from Back Edge of Lens (mm)

gases to the mixing system through 0.635 cm o.d. polypropylene tubing.

The one compound that was liquid at room temperature, dicyclopentadiene, was placed in a 50 ml glass impinger and helium gas from the gas handling system was bubbled through 30 ml of the liquid at 120 ml/min before entering the plasma chamber. This effectively saturated the gas with the volatile liquid. Teflon tubing and fittings were used to connect the impinger to the plasma chamber during this experiment (Figure 3).

The gas mixing system used in all experiments, except the one noted above, consisted of the following components:

1) three variable area flowmeters with built-in needle valves (Cole-Parmer models J-3217-12 and J-3217-18), mounted together on an aluminum plate,

2) a 120 ml acrylic gas drying column with O-ring sealed aluminum end caps (Altech Associates 100 psi model, sold by Cole-Parmer as model J-1418-100) half filled with indicating drierite and half filled with molecular sieves,

3) a 100 ml glass bubble-tube flowmeter,

4) a brass on/off plug valve with elastomeric O-ring seals (Nupro model B-4P4T) and two brass fine metering valves (Nupro model B-SS4),

5) an oil-filled mechanical vacuum pump (Precision Scientific model 25), and

6) a capacitance manometer (Baratron Type 220BA-01000A2B) with a digital readout (MKS type (PDR-D-1).

Figure 3. Dicyclopentadiene Gas Delivery System

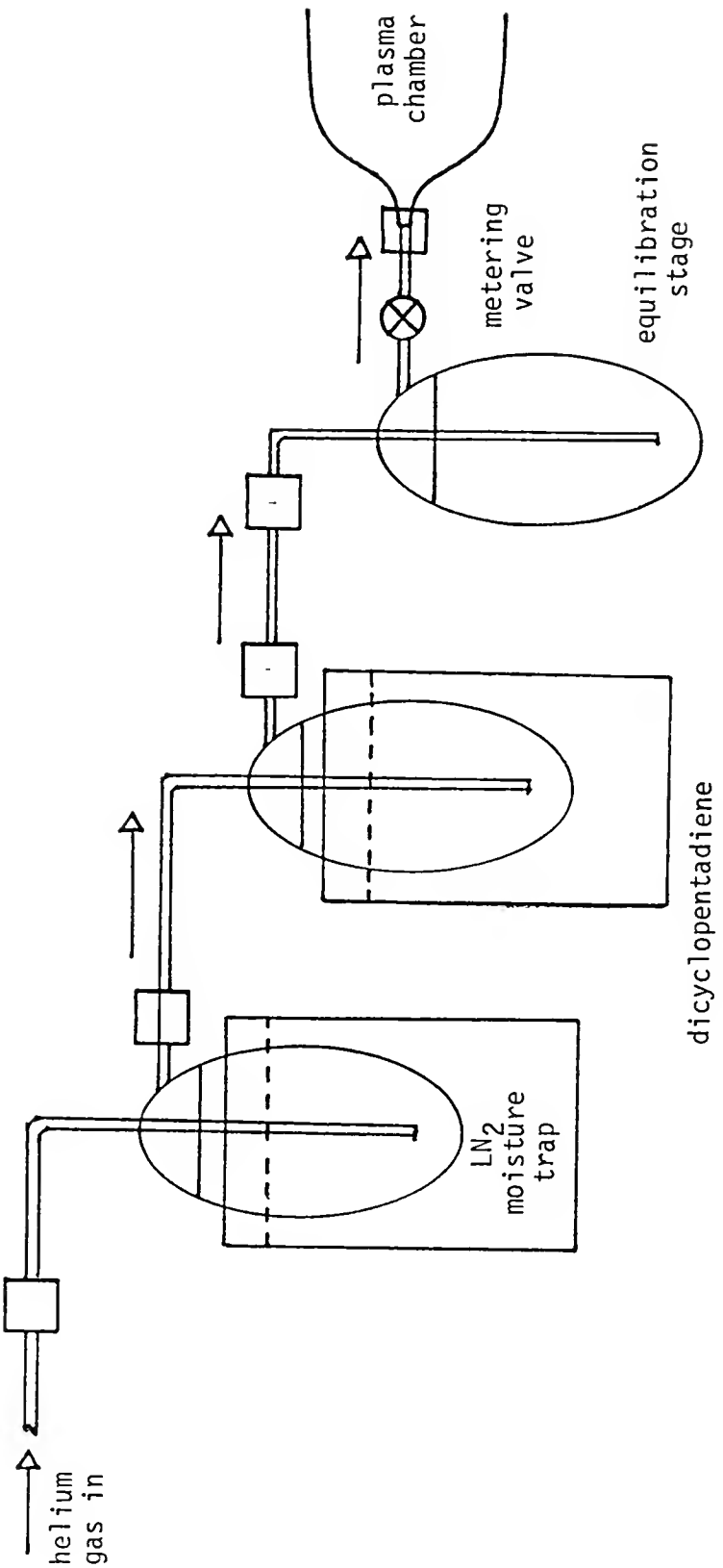
plasma chamber
metering valve
equilibration stage
dicyclopentadiene
LN_2 moisture trap
helium gas in

A diagram of the system components and the gas flow pattern is presented in Figure 4.

Gases were supplied to the flowmeters at 69,000 Pascals (10 psi) pressure and the flow rates adjusted using the variable area flowmeter needle valves. Copper tubes (1/4 in o.d.) from the flowmeter exit ports were teed together a few centimeters downstream using brass compression fittings. The gases then passed through the drying column, which also acted as a mixing chamber. Nominal total flow rates were 200-400 ml/min. After exiting the drying column the gases flowed through a teflon tee. One arm of the tee went to the bubble-tube flowmeter (which was vented to the atmosphere through the building hood exhaust), and the other arm went to the plasma chamber on/off valve. Thus, when the on/off valve was closed, the total gas flow passed through the bubble-tube flowmeter. When the on/off valve was open, part of the gas stream (about half) flowed through the plasma chamber while the remainder was vented through the bubble-tube flowmeter. This arrangement assured that no atmospheric gases were introduced into the plasma reaction chamber through the gas handling system.

Flow rates were set using the flowmeter needle valves and measured using the bubble-tube flowmeter and a stopwatch while the chamber on/off valve was closed. When more than one gas was used for an experiment, the flow rates were determined by addition, starting with the lowest flow and ending with the highest flow. The bubble-tube flowmeter was also used to monitor the excess gas flow to the atmosphere during plasma reaction experiments. The variable area

Figure 4. Gas Mixing and Delivery System

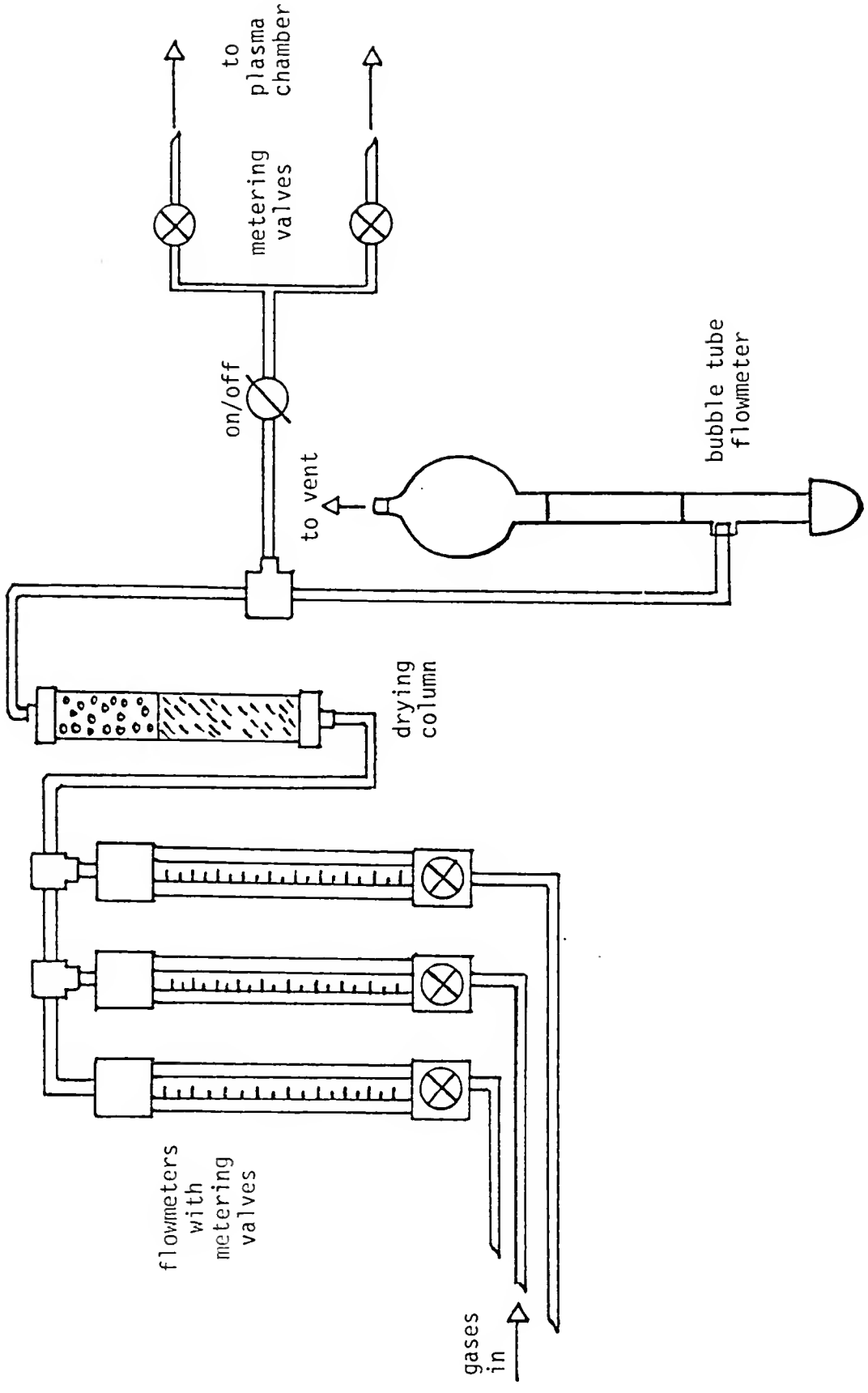
to plasma chamber
metering valves
on/off
to vent
bubble tube flowmeter
drying column
flowmeters with metering valves
gases in

flowmeters were used to monitor the individual gas flows (comprising the reaction mixtures) during experiments.

The gas flow to the plasma chamber was controlled by one or both of the metering valves in most experiments. These valves were located just downstream from the on/off valve and were used to separately control the gas flow through two inlets into the plasma chamber. (One inlet was located at the bottom of the chamber, beneath the target, and the other inlet was located on the optic side arm adjacent to the zinc selenide window. (See the plasma chamber description for further details of the gas inlets.) In experiments where the chamber pressure was 530 Pascals (4 torr) or greater, the gas flow was split equally between the two inlets using the respective needle valves. In experiments where the pressure was 133-533 Pascals (1-4 torr), one needle valve and inlet were plugged and the entire gas flow was directed through the optic side arm inlet. In experiments where the chamber pressure was < 133 Pascals (< 1 torr), the Nupro metering valves were replaced by an in-house fabricated, low-flow, 1000:1 taper valve.

All experiments used the mechanical vacuum pump to provide the driving force for gas flow through the system. The plasma chamber pressure was monitored with the capacitance manometer which had a range of 0-1000 torr in 0.1 torr increments (0-133,323 Pascals in 13 Pascal increments). The manometer was calibrated using a standard mercury-filled McLeod gauge.

The Plasma Reaction Chambers

Two plasma reaction chambers were used during the course of this study. Their function was to provide a controlled environment for the interaction of solid gold and gaseous compounds and elements. An initial screening study was conducted using an all glass reaction chamber. The remainder of the study was conducted using a more versatile aluminum reaction chamber. A description of the all glass chamber is presented first, followed by a description of the aluminum chamber.

General features common to both chambers included a target holder/manipulator for positioning the solid gold target, a zinc selenide window for introducing the laser light, gas inlets for introducing the reactant and inert gases, and a gas outlet for delivering the reaction products and unreacted gases to the product collection system and the vacuum pump. The major difference between the two chambers was the design pressure rating. The glass chamber used in the screening study was designed to operate in the pressure range of 667-186,650 Pascals (5-1,400 torr), while the aluminum chamber used throughout the rest of the study was designed to operate in the pressure range of 0.133 to 93,000 Pascals (0.001 torr to ~ 0.9 atmospheres).

The glass, plasma reaction chamber. This chamber was designed to be utilized for initial screening of prospective gases and gas mixtures for their effectiveness in producing and transporting gas phase gold-bearing species. This involved the determination of optimum pressure

and laser energy density conditions for gases showing positive results. The protocol also included the study of the interaction of the focused, pulsed CO_2 laser beam with several inert and reactive gases and gas mixtures at pressures approaching 200,000 Pascals (ca. 2 atm.). The transparent chamber facilitated the observation of gas breakdown. This phenomenon resulted in absorption of most of the laser pulse energy by the gases, leaving very little energy to vaporize the solid gold. (A further discussion of this topic is presented in the following chapter.)

A diagram of this plasma reaction chamber is presented in Figure 5. The two-piece borosilicate glass body was fabricated in the Scientific Glass-Blowing Shop at the University of Florida and had a total volume (including side arms) of 588 ml. Two 50 mm i.d. glass O-ring seal joints (Kimax No. 50) were used as the base structures. One of the joints was modified by tapering the blank end and butt-sealing it to a 12 mm o.d. by 9 mm i.d. by 4 cm long piece of glass tubing. The overall length of the resultant bell-shaped structure was 20 cm. A 9 mm o.d. by 6 mm i.d. by 14 cm long piece of perforated teflon tubing was press-fitted into the narrow end of the bell structure from the inside. This tube extended about 1 cm into the 12 mm o.d. glass extension tube. The rest of the teflon perf-tube extended through the center of the bell structure and ended about 2 cm from the wide end. A 50 mm dia. by 2 mm thick teflon perforated plate was then attached to the teflon tube by threading a stainless steel screw through the center hold of the perf-plate and into the end of the teflon tube. This unit comprised the main gas inlet to the plasma chamber. The perforated

Figure 5. The Glass Plasma Reaction Chamber

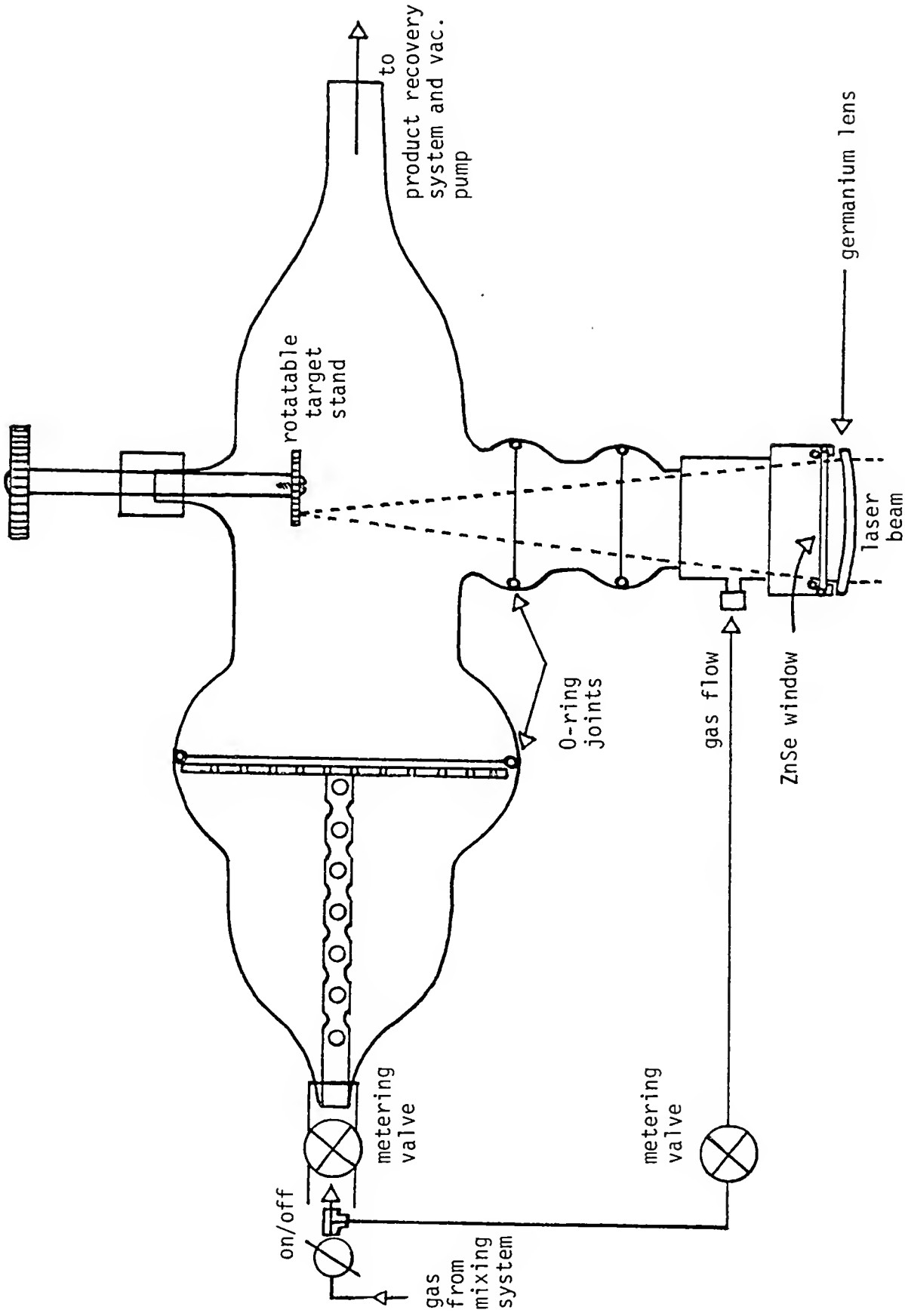
to
product recovery
system and vac.
pump
germanium lens
rotatable
target
stand
laser
beam
O-ring
joints
gas flow
ZnSe window
metering
valve
metering
valve
on/off
gas
from
mixing
system

tube and plate distributed the gas flow evenly to the plasma reaction zone. A length of copper tubing coming from one of the gas handling system metering valves was attached to the narrow end of the glass, gas-inlet structure with a brass, O-ring sealed, quick-connect fitting.

The other 50 mm i.d. glass O-ring joint was also tapered and butt-sealed to a 12 mm o.d. by 4 cm long piece of glass tubing to form a 20 cm long bell-shaped structure. The narrow end was the plasma chamber outlet and was attached to the product recovery system and a mercury manometer using a brass quick-connect fitting. Another 12 mm o.d. by 4 cm long piece of glass tubing was sealed to the large diameter sidewall of the bell structure 5 cm (on center) from the mouth and served as a guide shaft for the sample holder. A 20 mm i.d. glass O-ring joint (Kimax No. 20) was sealed to the opposite sidewall 6 cm (on center) from the mouth and served as the optic side arm attach point. The offset center lines allowed the use of a large diameter target that was rotated past the beam impact point.

The sample holder shaft was an aluminum rod 15 cm long by 9 mm o.d. that was slip-fitted through the chamber side arm, as mentioned above, and sealed by sliding a length of tightly fitted, 3 mm thick silicon rubber tubing over the joint. The part of the aluminum shaft that contacted the silicon rubber tube was coated with vacuum grease (Dow Corning silicon high vacuum grease) to facilitate sealing during shaft rotation. A 7 cm dia. aluminum cogwheel was attached to the exterior end of the aluminum shaft and used to rotate the sample manually. The other end of the shaft extended into the chamber and had a threaded center hole that was used as a target attach point. The

shaft, and target, could be moved toward the beam input opening a maximum of 3 cm in order to shorten the optic path.

The two piece optic side arm was constructed from glass and aluminum. The piece closest to the plasma chamber was made from a 20 mm i.d. glass O-ring joint butt-sealed to a 30 mm i.d. glass O-ring joint (Kimax No. 30). There were actually two such pieces fabricated. One was 5 cm long and the other was 8 cm long. This provided different path lengths between the zinc selenide window and the target surface. By exchanging these pieces, and moving the target back and forth, the optical path length between the backside of the window and the target surface could be varied by 6 cm. This allowed adjustment of the incident energy density of the laser beam while maintaining a minimum distance between the external focusing lens and the window. (This arrangement minimized the probability of damage to the window surface, as previously mentioned.)

The aluminum window holder was machined to match the 30 mm i.d. glass O-ring joint on one end. The other end was machined to hold the zinc selenide window described earlier. The window was sealed using a rotary O-ring gland that incorporated the window edge and the inside circumference of the aluminum holder as sealing surfaces. Two teflon rings with inside diameters 2 mm smaller than the window o.d. were used as spacers on either side of the window. The window and spacers were held in place using an aluminum ring with the same i.d. as the teflon rings and an o.d. equal to that of the aluminum holder. This ring was attached to the end of the holder with four screws. A brass swage fitting (1/4 in. pipe thread to 1/4 in. tube) was located 1 cm (on

center) from the edge of the window seat on the side of the holder. A 1/4 in. copper tube coming from the gas handling system's other metering valve was connected to this fitting and provided a sweep of incoming gases across the window surface to help minimize contamination of the surface.

Butadiene elastomeric O-rings were used where required throughout the system. Pinch clamps held the glass O-ring joints together when the system was not under low pressure. The rotary seal on the window and the seal on the sample holder shaft had moderate leak rates and the chamber could be pumped down only to 13 Pascals (0.1 torr). While this operational parameter met the rough-vacuum design criterion, the affect of the residual pressure of air on the proposed reactions was unknown. Therefore, a study of the affect of increased levels of air in successful gas mixtures was included in the screening study protocol. The affect of very low concentrations of residual air in successful gas mixtures was investigated using the aluminum reaction chamber.

The aluminum plasma reaction chamber. This chamber was fabricated by the author from aluminum (Alcoa alloy 2024) using available facilities in the Department of Chemistry at the University of Florida. A diagram of the chamber, including the sample holder, optic side arm, and observation ports is presented in Figure 6. The screening study was completed, and all other experiments were conducted using this chamber.

Figure 6. The Aluminum Plasma Reaction Chamber

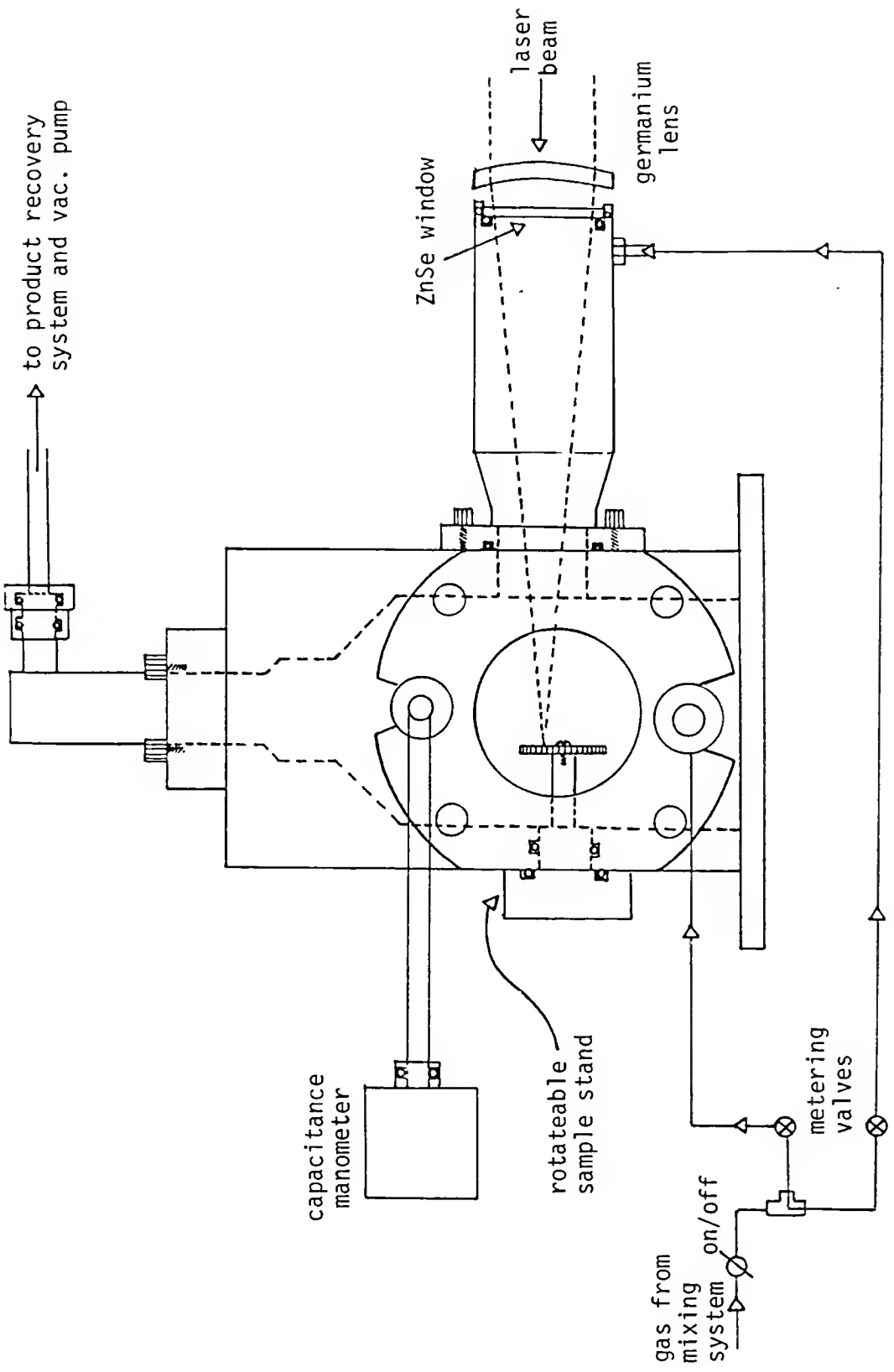
to product recovery
system and vac. pump
laser
beam
germanium
lens
ZnSe window
capacitance
manometer
rotateable
sample stand
metering
valves
on/off
gas from
mixing
system

The aluminum plasma reaction chamber consisted of five parts:

1) the main body, including two gas inlet inserts, a gas outlet flange, and a capacitance manometer insert,

2) two glass observation ports and their flanges,

3) the baseplate,

4) the optic side arm, and

5) the sample holder.

All of the components were fabricated from aluminum except the glass ports and the main body inserts and outlet flange (which were machined from brass). Viton or butadiene elastomeric O-rings were used for all seals. All tubing, fittings, and inserts leading from the gas handling system and capacitance manometer that were subject to vacuum were either brazed or connected with O-ring quick-couples.

The completed system was leak checked using a mass spectrometer helium leak detector (Veeco Leak Indicator MS17) previously calibrated with a standard leak (Veeco Sensitivity Calibrator Type SC-4). The detector response indicated that the leak rate was $< 2 \times 10^{-9}$ cc-atm/sec (air equivalent) at each union and overall under He flood conditions.

The main body was machined from a single block of aluminum 9.5 cm wide by 7.6 deep by 15.2 cm high. The reaction zone was formed by boring a 5.1 cm dia. by 9.5 cm deep hole through the center of the block, starting on the bottom face. The top of this cavity was tapered 30° and narrowed to 1.0 cm in two steps before exiting the center of the top face of the block. Static face seal O-ring glands and four-

hole bolt circles were machined around both holes for attachment of the gas outlet flange and the chamber baseplate.

Several different outlet flanges were used to connect the plasma chamber to the various product recovery systems. All of the flanges were sealed to the chamber using the O-ring face seal and connected to the product recovery system by an O-ring quick-connect type coupler. A 1.2 cm dia. hole was bored on one of the 9.5 cm wide sides 2 cm (on center) from the bottom of the chamber. A 6 cm long insert with a rotary O-ring gland was inserted through this opening. The insert had a 6 mm hole bored from the incoming end and turned 90° at the outlet end. This design allowed the incoming gas to be directed toward or away from the plasma reaction zone by rotating the insert. Another 1.2 cm dia. hole was bored in the same face 9 cm (on center) from the bottom of the chamber. A 6 mm i.d. plug insert with a rotary O-ring gland was used to connect the plasma reaction zone with the capacitance manometer via a 30 cm length of 1/4 in. o.d. tubing.

A 2.0 cm diameter hole was bored into one of the 7.6 cm wide faces 5.5 cm (on center) from the bottom of the chamber. The O-ring gland and four-hole bolt circle were machined around this opening. This was the optic side arm attach point.

A 3.3 cm dia. hole was bored into the other 7.6 cm wide face 4.7 cm (on center) from the bottom of the chamber. The sample holder was inserted through this opening. A rotary O-ring gland was machined into the circumference of the opening 3.0 mm from the outer edge. This O-ring sealed the sample holder even when it was being rotated. A

four-hole bolt circle was machined around the port to secure the sample holder with its O-ring face seal.

Two 5.0 cm dia. ports were cut into the 9.5 cm wide sides directly opposite from each other and 5.0 cm (on center) from the bottom of the chamber. Static face seal O-ring glands and four-hole bolt circles were machined around each port. Two 1.0 cm thick port flanges with matching O-ring glands and bolt holes held and sealed 6.0 cm dia. by 6.0 mm thick lead glass windows over each port.

The baseplate was 12.7 cm square by 2.5 cm thick and had four bolt holes that matched the bolt circle on the bottom face of the chamber. In addition, the baseplate had four holes at the corners that were used to attach the chamber assembly to a table. Block spacers were placed under the baseplate to raise the chamber optic arm to the same height as the laser beam.

The single piece, 3.0 cm i.d., optic side arm used the same type of rotary O-ring gland as described above to center the zinc selenide window. An O-ring face seal gland was cut into the aluminum holder and used to form the primary vacuum seal against the face of the window. A precisely machined teflon spacer, and an aluminum ring flange similar to the one described above, provided the necessary squeeze to form the seal without unduly stressing the window. A 6.0 mm dia. hole was bored into the side arm 5.0 mm (on center) from the window face seal edge and used as the sweep gas inlet. A brass insert with a rotary O-ring gland connected the inlet to one of the gas handling system metering valves. The optic side arm was attached to the plasma chamber using the bolt circle and face seal described earlier.

The sample stand was also made from a single piece of aluminum. The sample attach point was a threaded hole in the end of a 1.4 cm dia. by 2.3 long section of the stand. This section ended in a 3.3 cm dia. by 1.5 cm long section that acted as the sealing surface for the rotary seal in the chamber throat. The outer section of the one-piece stand was 7.5 cm in diameter and 1.3 cm thick and acted as the flange. This section contained a face seal O-ring gland that formed the primary vacuum seal, and a series of arced bolt slots that matched the bolt circle on the chamber. The rotary seal allowed the sample to be rotated manually while under vacuum by loosening the face seal bolts. (Depending on target thickness, this was done once or twice an hour during most experiments.) The bolts were retightened after the sample rotation was completed. This was necessary because particles and frictional wear frequently caused minor leaks in the rotary seal.

The Product-Recovery/Substrate-Coating Systems

There were several product-recovery/substrate-coating systems used throughout the study. Many of the systems used common components assembled in different sequences and maintained at different temperatures. Many of these arrangements were designed to investigate the volatility, or other physical properties, of the plasma reaction products. The system descriptions are presented below along with their respective operational parameters. Results are discussed in Chapter III.

Heated quartz tube. A 2 mm i.d. by 4 mm o.d. by 50 cm long quartz tube was attached directly to the glass plasma chamber outlet using a

silicon rubber sleeve seal. The tube was placed in a Linberg tube furnace with a 30 cm long high temperature zone. The furnace was heated to 600-890 K during experiments in order to decompose any gold bearing species that passed through. The gas flow rates were adjusted to allow a residence time of 3-194 milliseconds in the hot zone. In practice this resulted in visible deposits varying in color (from black to purple to red to gold) and position along the tube. In some experiments the quartz tube was followed by a glass wool plug and/or a cold finger (size 14/22 or 24/40) in a dry-ice/acetone bath (see Figure 7).

Staged cold traps. Several experiments used multiple cold traps at progressively colder temperatures to observe product collection characteristics. The various schemes used are pictured in Figure 8. The first such scheme used a cold finger (CF) in water-ice (273 K) followed by a second CF in dry-ice/acetone (195 K), and a third CF in liquid nitrogen (77 K). Clogging of the CF in liquid nitrogen resulted in its replacement with a second CF in dry-ice/acetone. The next modification incorporated a glass wool plug before the cold traps. This scheme was then modified by placing the glass wool between the first CF, which was kept at room temperature, and a second cold trap made from a 1/4 in. (6.35 mm) o.d. by 25 cm long glass U-tube kept in crushed dry ice. Another scheme used a small test-tube inserted in the gas stream at the plasma chamber outlet ahead of the U-tube in dry ice. The test-tube was either maintained at ambient temperature or was filled with dry ice. The flange which held this tube could also accommodate a quartz window in place of the test-tube. Finally,

Figure 7. Heated Quartz Tube Product Recovery System

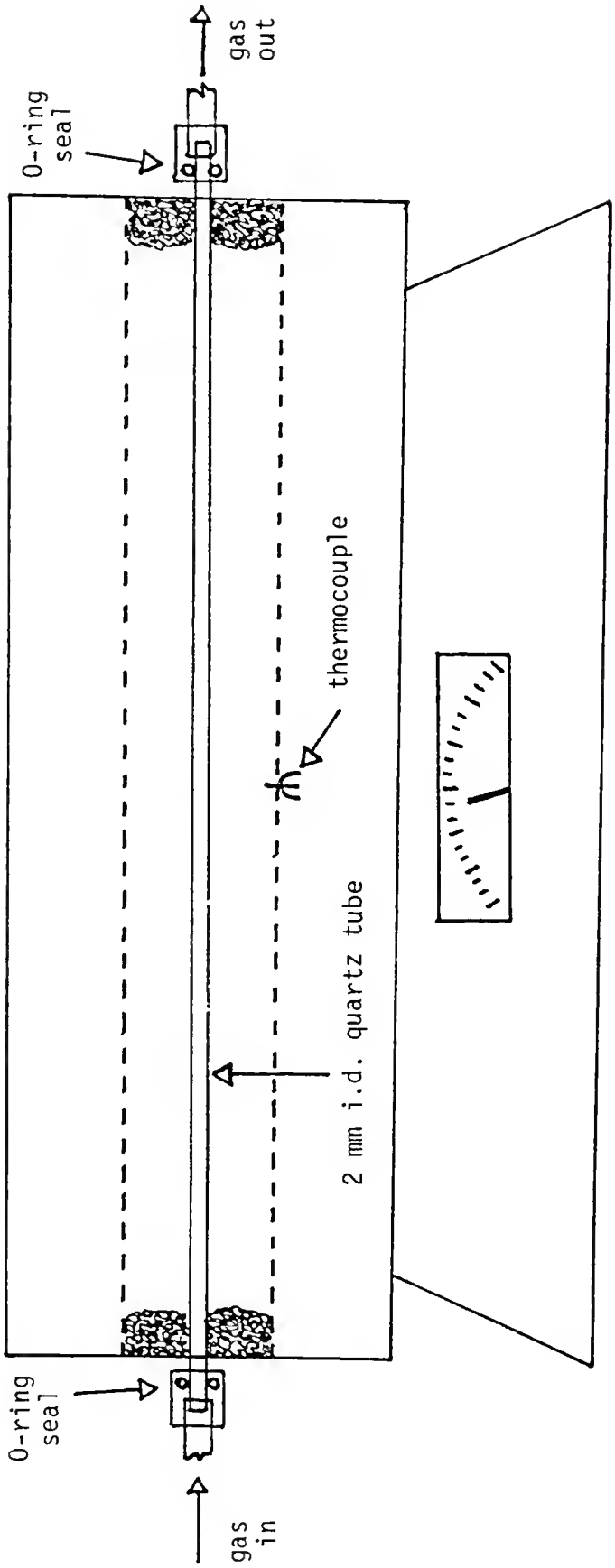
gas out
O-ring seal
thermocouple
2 mm i.d. quartz tube
O-ring seal
gas in

Figure 8. Staged Cold Traps Used for Product Recovery
(a) Three cold fingers
(b) Cold finger with U-tube
(c) Test-tube with U-tube

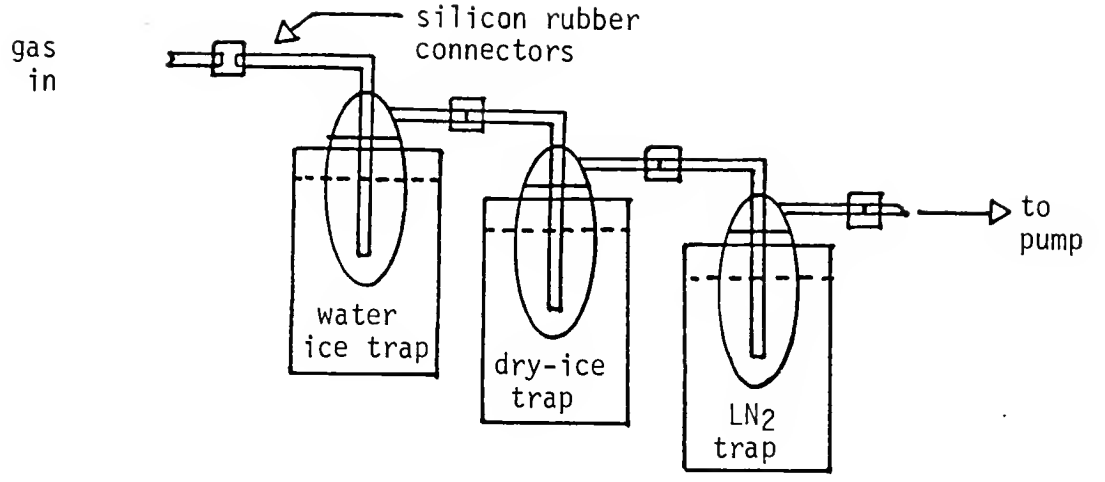
gas
in
silicon rubber
connectors
water
ice trap
dry-ice
trap
LN_2
trap
to
pump

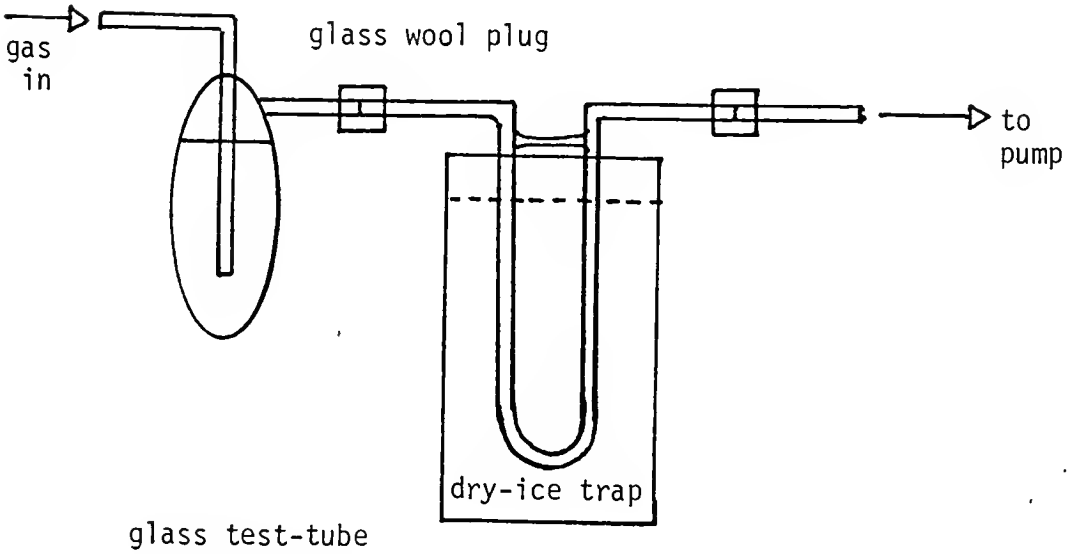
gas
in
glass wool plug
to
pump
dry-ice trap

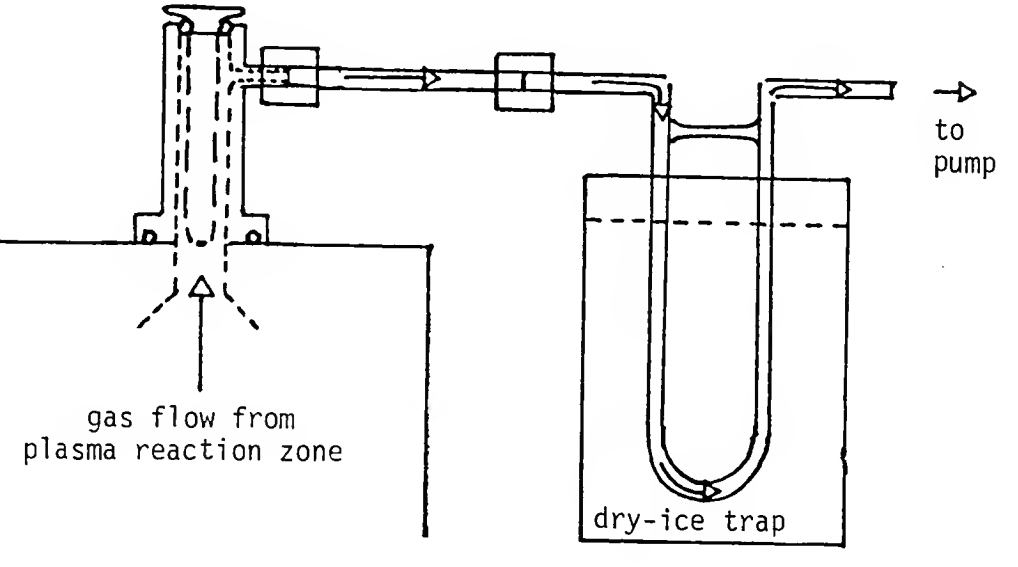
glass test-tube
insert
to
pump
gas flow from
plasma reaction zone
dry-ice trap

the system was limited to the U-tube in crushed dry-ice (or dry-ice/acetone) since this proved sufficient for trapping the plasma reaction products for later use. A fresh trap was used for each experiment. The 1/4 in. o.d. glass U-tubes were eventually replaced with 3/8 in. (9.525 mm) o.d. glass U-tubes. One of these U-tube cold traps was used in all subsequent experiments either alone or after a substrate coating chamber.

Substrate coating chambers. Substrates were coated with the plasma reaction products during experiments by sticking them to the inside of the chamber windows (using Scotch clear adhesive tape), by placing them in the connecting tubing leading to the U-tube cold trap, or by placing them in one of the three coating chambers pictured in Figure 9. The first two chambers were fabricated from glass in the Scientific Glass Blowing Shop at the University of Florida. The third chamber was constructed from aluminum by the author using available facilities in the Department of Chemistry at the University of Florida. All of the chambers were placed in line after the plasma chamber and before the U-tube cold trap. The two glass coating chambers were mounted perpendicular to the plasma chamber via an elbow quick-couple. The aluminum coating chamber was connected directly to the top of the plasma chamber using a straight quick-couple.

The first chamber was made by truncating a 20 mm i.d. glass O-ring seal joint (Kimax No. 20) 3 cm from the sealing end and attaching 1/4 in. o.d. by 5 cm long glass tubes on opposite sides, perpendicular to the seal face. These tubes acted as the inlet and outlet. A 25 mm dia. by 1 mm thick quartz window was placed on the O-ring and held in

Figure 9. Substrate Coating Chambers
(a) Small glass chamber showing a ceramic feed-through in place
(b) Large glass chamber showing the 3-tier sample rack

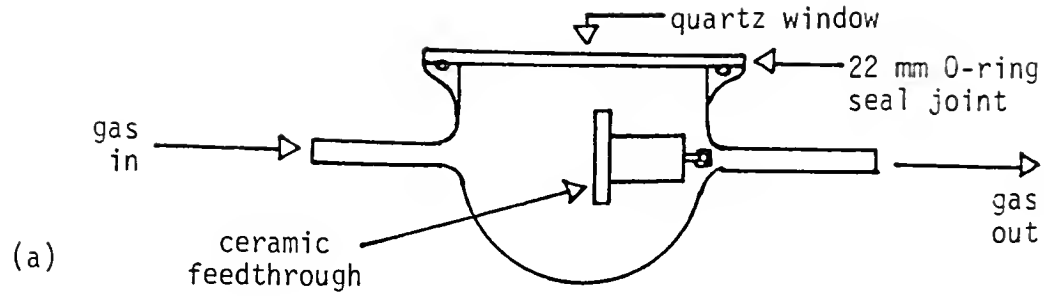

(a)

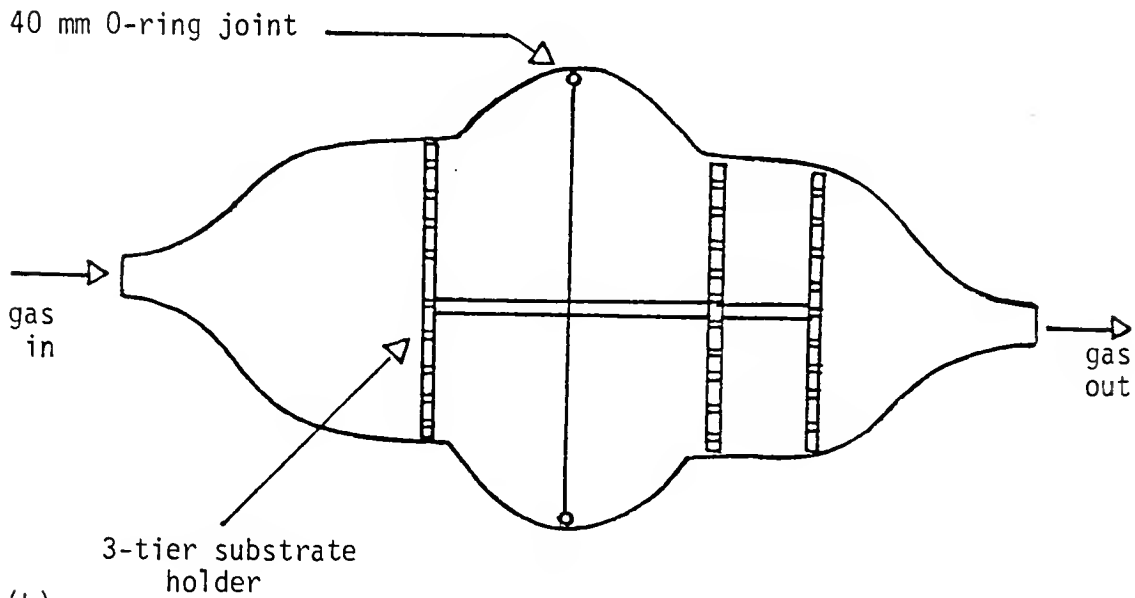

(b)

to heater controller

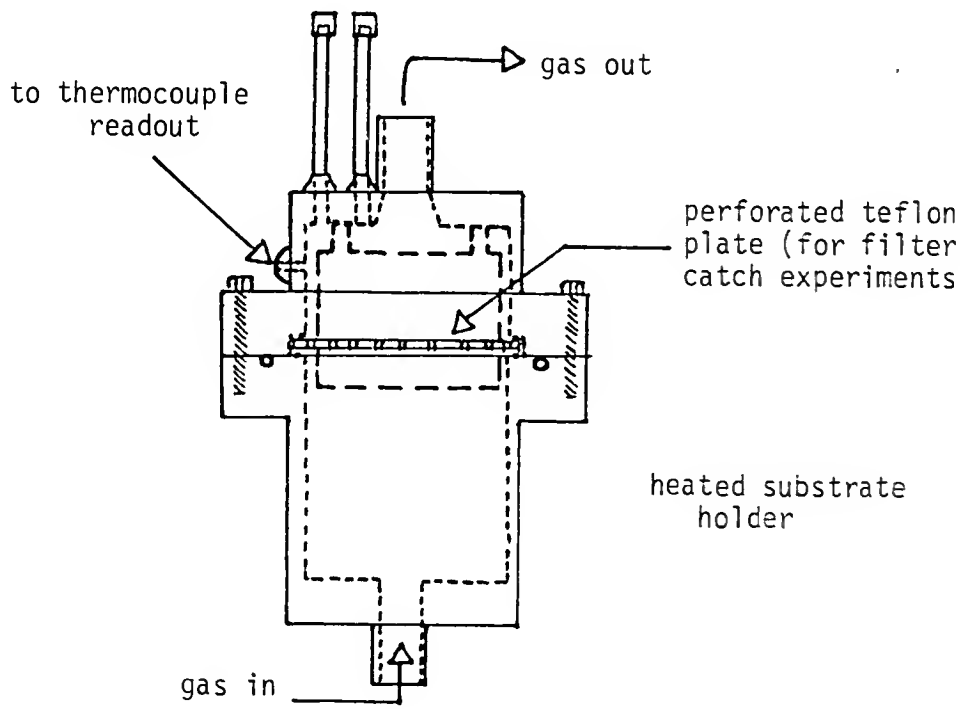

(c)

place by the system vacuum. Total volume of the chamber was 20 ml. Substrates could be placed in this chamber and exposed to a 5 watt Argon ion laser beam (Spectra Physics 165) while plasma reaction products flowed through.

A second, larger coating chamber was constructed from two 40 mm i.d. glass O-ring seal joints (Kimax No. 40). The joints were tapered and sealed to 1/4 in. tubing on the ends. The two halves were held together with a pinch clamp when the system was not under vacuum. The assembled unit was 20 cm long and had a total volume of 145 ml. A three-tiered substrate holder rack was made by the author using three 38 mm dia. by 2 mm thick perforated aluminum plates connected by a central stainless steel shaft. Substrates were placed on the different rack plates in either equatorial or axial positions in order to observe shadowing effects during coating.

A third, more versatile coating system was machined from aluminum stock (Alcoa alloy 2024). This chamber was also a two-piece design and had an O-ring face seal between the halves. The bottom half started with a 1/2 in. (12.7 mm) o.d. by 1.9 cm long inlet segment that sealed directly to the top of the plasma chamber via a 1/2 in. brass quick-couple. This section had an inside diameter of 1.0 cm. The next segment of the bottom piece had an o.d. of 5.0 cm and an i.d. of 4.0 cm and was 4.4 cm long. The final segment was 7.6 cm wide by 1.2 cm thick and contained the O-ring gland, a four-hole bolt circle, and a seat on the inside diameter for a 4.0 mm wide by 3.0 mm thick teflon ring spacer. This segment acted as a flange to connect the two pieces of the chamber.

The top half started with a matching flange segment with a 3.0 mm thick by 48 mm dia. teflon perforated plate press-fitted into the 4.0 mm wide seat on the inside diameter. This was followed by a 5.0 cm o.d. by 4.0 cm i.d. by 1.9 cm long segment and a 1.0 cm i.d. by 1/2 in. (12.7 mm) o.d. by 2.3 cm long outlet segment. The assembled chamber was 13 cm long and had an internal volume of 87 ml.

The teflon perforated plate and spacer were used to hold a 47 mm diameter borosilicate glass fiber filter that had a retention rating of 0.98 at 0.2 microns (Micro Filtration Systems GB 100 R47 mm). The filter faced the gas flow and was backed by the perforated plate. The teflon ring held the filter in place without damaging it. This arrangement was used to trap particles that were produced in the plasma chamber. Particles that were transported 20 cm up from the plasma reaction zone, through the narrow plasma chamber outlet and up to the filter, were very efficiently trapped. Other particles that impinged on the plasma chamber sidewalls or fell to the bottom of the chamber were not collected by the filter. Most large particles ("chunks" and "flakes" tens of microns in size) that made it to the filter rebounded on impact and were found in the bottom of the collection chamber. Large particles that adhered to the filter were easily distinguished using visual microscopy. Thus, the arrangement provided a semi-quantitative method for comparing relative abundances and gold content of particles entrained in the gas stream using gravimetric and atomic absorption analyses, respectively.

Heated substrate mount. Several experiments were performed with substrates attached to a heated mount shown in Figure 9. The 3.5 cm

dia. by 3.0 cm high mount consisted of a potted nichrone heating element covered with a 2 mm thick aluminum plate that had a series of threaded holes. Flat head screws were used to attach substrates to the plate using the threaded holes. The mount was positioned in the top of the aluminum collection chamber with the heated substrates facing the gas flow. Three small ceramic posts minimized the area of contact between the mount and the top of the collection chamber.

The heating element wires extended through the top of the chamber through two glass inserts that were epoxy sealed (J. B. Weld Co., Sulphur Springs, TX) to the aluminum. Rubber septa and sealing putty (Apiezon Q) were used to seal the wires at the exit of the glass inserts. There was a small leak at this point, ca. 0.01 ml air/min determined by differential pressure measurements. However, its location downstream from the plasma reaction zone and the substrate coating zone, and the results of earlier experiments that showed the relative insensitivity of selective plasma reactions to air, minimized concern over the leak.

Temperature control for the heated mount was provided by a 12 V dc power convertor driven by a variable voltage auto-transformer. Temperatures were controlled to $\pm$ 5% of the set point. A thermocouple junction (type K) was implanted in the aluminum hot plate and connected to a digital multi-meter (Kiethly 177 Microvolt DMM). The thermocouple was calibrated using water ice and boiling deionized water.

Production of Gas-Phase Gold Species: Experimental Conditions and Materials

Screening Study Experiments

The purpose of the screening study was to identify gases and/or gas mixtures, operating pressures, and laser power density parameters that resulted in the production of relatively large amounts of gas-phase gold species. The screening study was continued throughout the duration of the overall study. The product recovery systems described above were used to separate the gold species from the gas stream. Visual observation was used as an initial method of evaluation since the relative abundances of gold species collected in individual experiments varied drastically. Cold traps containing the recovered products were sealed and heated in a bunsen burner and then opened to the atmosphere and reheated. Observations of the relative quantities of gold films formed on the glass surfaces were utilized to identify successful operating conditions.

Glass fiber filter catches were determined gravimetrically using a Mettler analytical balance. (Filter blank measurement methods and data are presented in Appendix A). Quantitative measurements of the amounts of gold collected in some of the cold traps, and on most of the glass fiber filters, were performed using Atomic Absorption (AA) analyses (Perkin Elmer Model 303 AA) and standard analytical techniques.[64] Samples were either extracted/ suspended in acetone, or dissolved in aqua regia and diluted. Calibration data and response curves are presented in Appendix C.

The initial gold target used in the screening study was formed by melting and casting ca. 10 grams of Au wire (0.999 purity) into a 2-3 mm thick crescent shape. A machined graphite block was used as a mold for the casting. A Canadian Maple Leaf 1 oz gold coin (0.999 purity) was also used as a target during the screening study and in all substrate coating experiments. This target required recasting after extended use, but its total mass was never less than 23 grams, and its thickness was never less than 3 mm. A 1.0 cm thick by 2.5 cm diameter piece of graphite (mass = 23.7 grams) was used as a target in two experiments and a 6 mm thick by 18 mm wide by 28 mm long OFHC copper target (mass = 28.0 grams) was used in two other experiments.

Gases used in the study were obtained from several different sources. The gases are listed in Table 1 along with their respective vendor sources and purity ratings. No attempts were made to further purify any of the gases beyond the removal of excess moisture in the gas drying column already described, with one exception. The helium gas used in test No. 861126B was passed through two liquid nitrogen cold traps in order to remove traces of water which otherwise would have reacted with the liquid dicyclopentadiene, causing it to gelatinize.

Table 2 lists all of the experiments contained in the screening study along with their respective experimental conditions. Each experiment was given a six numeral identification number based on the year, month, and day that it was performed. A letter was added to the numerical code when more than one experiment was performed in the same day. For example, "860602A" refers to the first experiment performed

Table 1. Gases Used in the Plasma Reaction Study

Gas	Vendor	Purity Rating
helium	Airco	standard grade
argon	Airco	standard grade
air	(laboratory ambient)	N/A
air	Airco	breathing quality
hydrogen	Airco	standard grade
	Linde	standard grade
dicyclopentadiene (liquid)	Aldrich Chemical	reagent grade
chlorodifluoro-methane	Allied Chemical Corp.	refrigerant grade
dichlorodifluoro-methane	Allied Chemical Corp.	refrigerant grade
hexafluoroethane	PCR, Inc.	99%
acetylene	Airco	welder's grade
carbon monoxide	Matheson Specialty Gases	99.9%
methane	Matheson Specialty Gases	99.9% and 99%
natural gas	Gainesville Regional Gas Company (through laboratory lines)	commercial grade

Table 2. Screening Study Plasma Reaction Experiments

Expt. No. (target)	Gas Mix (%)	Pressure (Pascal)	*Flow Rate Through Reaction Zone ml/min (atm.)	cm/sec	CO_2 Laser Conditions Focal Point (mm dia.)	Pulses (x 1000)	**Product Recovery System
860602A (none)	He (100)	161,500	N/A	N/A	optimum	0.20	none
		156,100	N/A	N/A	optimum	0.20	
		141,500	N/A	N/A	optimum	0.20	
		134,800	N/A	N/A	optimum	0.20	
		128,100	N/A	N/A	optimum	0.20	
		121,500	N/A	N/A	optimum	0.20	
		114,800	N/A	N/A	optimum	0.20	
		107,900	N/A	N/A	optimum	0.20	
		101,500	N/A	N/A	optimum	0.20	
		94,790	N/A	N/A	optimum	0.20	
		88,130	N/A	N/A	optimum	0.20	
		72,130	N/A	N/A	optimum	0.20	
		58,800	N/A	N/A	optimum	0.20	
		36,130	N/A	N/A	optimum	0.20	
		26,800	N/A	N/A	optimum	0.20	
		18,800	N/A	N/A	optimum	0.20	
860602B (none)	Air (100)	101,500	(open to atm)		optimum	0.60	none
860530 (Au)	H_2 (100)	110,900	3500	162	optimum-5.6	2.70	none
		106,390	3500	169	optimum	1.80	
860605 (Au)	He/H_2 (80/20)	13,870	40	15	optimum	2.20	790 K QT, 194 msec
860606 (Au)	He/H_2 (75/25)	6,800	51	39	optimum	1.72	790 K QT, 75 msec

Table 2 (continued)

Expt. No. (target)	Gas Mix (%)	Pressure (Pascal)	*Flow Rate Through Reaction Zone ml/min (atm.)	cm/sec	CO_2 Laser Conditions Focal Point (mm dia.)	Pulses (x 1000)	**Product Recovery System
860612 (Au)	He/H_2 (75/25)	800	54	346	optimum	6.36	790 K QT, 8 msec
861022B (Au)	He (100)	800	(54)	(346)	optimum	1.20	GWP, UT
861124 (Au)	He (100)	1,330	125	484	optimum	16.20	UT
870226 (Au)	Ar/H_2 (75/25)	1,390	(90)	(350)	optimum	3.60	300 K TT, UT
	(55/45)	670	(40)	(310)	optimum	7.68	
		750	(55)	(380)	optimum	6.96	
860724 (Au)	He/CO (77/23)	4,930	315	330	optimum	0.30	GWP, two 195 K CFs
		2,670	N/A	N/A	optimum	0.30	
		1,600	N/A	N/A	optimum	0.60	
		1,200	22	95	optimum	12.90	
861106 (Au)	He/CO						UT
	(100/0)	1,600	N/A	N/A	optimum	0.06	
	(99/1.2)	1,600	N/A	N/A	optimum	0.09	
	(98/1.7)	1,600	N/A	N/A	optimum	0.09	
	(96/3.8)	1,600	N/A	N/A	optimum	0.09	
	(95/5.2)	1,470	N/A	N/A	optimum	0.06	
	(90/10)	1,600	N/A	N/A	optimum	0.06	
		4,000	N/A	N/A	optimum	0.06	
	(88/12)	9,070	N/A	N/A	optimum	1.50	

Table 2 (continued)

Expt. No. (target)	Gas Mix (%)	Pressure (Pascal)	*Flow Rate Through Reaction Zone ml/min (atm.)	cm/sec	CO_2 Laser Conditions Focal Point (mm dia.)	Pulses (x 1000)	**Product Recovery System
861110 (Au)	He/CO (79/21)	1,530	210	707	optimum	14.40	195 K CF, GWP, UT
861126B (Au)	He (sat. with dicyclopentadiene)	1,330	(125)	(484)	optimum	12.42	UT
861205 (Au)	He/C_2H_2 (81/19)	1,400	(125)	(460)	optimum	10.08	195 K TT, UT
861210 (Au)	He/C_2H_2 (98/2.5)	1,400	(130)	(490)	optimum	9.78	195 K TT, UT
870121 (Au)	H_2/C_2H_2 (92/8.3)	1,360	(130)	(490)	optimum	11.04	300 K TT, UT
861022A (Au)	CH_4 (100)	1,200	(200)	(860)	optimum	3.96	GWP, UT
860701 (Au)	He/CH_4 (77/23)	1,730	(300)	(890)	optimum	5.40	893 K QT, 3 msec, 195 K CF
860702 (Au)	He/CH_4 (75/25)	1,600	(290)	(935)	optimum	7.02	573 K QT, 3 msec, 195 K CF

Table 2 (continued)

Expt. No. (target)	Gas Mix (%)	Pressure (Pascal)	*Flow Rate Through Reaction Zone ml/min (atm.)	cm/sec	CO_2 Laser Conditions Focal Point (mm dia.)	Pulses (x 1000)	**Product Recovery System
860704 (Au)	He/CH_4 (75/25)	2,000	(330)	(850)	0.59 optimum	2.46 15.12	273 K CF, 195 K CF, 77 K CF
860722 (Au)	He/CH_4 (75/25)	1,470	286	510	optimum	19.62	GWP, two 195 K CFs
861012 (Au)	He/CH_4 (72/28)	2,130	(350)	(850)	optimum	19.62	GWP, UT
861023 (Au)	He/CH_4 (70/30)	1,600	(220)	(710)	optimum	14.40	78 K CF, GWP, UT
861022C (carbon)	He/CH_4 (75/25)	800	N/A	N/A	optimum	3.90	UT
861016 (Au)	$He/CH_4/air$ (71/25/4)	1,200	(200)	(860)	optimum	6.90	GWP, UT
861017 (Au)	$He/CH_4/air$ (75/21/4)	1,200	(200)	(860)	optimum	10.38	UT
861018 (Au)	$He/CH_4/air$ (71/25/4)	1,600	(290)	(935)	optimum	6.78	300 K CF, UT
870109 (Au)	H_2/CH_4 (80/20)	1,310	(125)	(490)	optimum	15.00	195 K TT, UT

Table 2 (continued)

Expt. No. (target)	Gas Mix (%)	Pressure (Pascal)	*Flow Rate Through Reaction Zone ml/min (atm.)	cm/sec	CO_2 Laser Conditions Focal Point (mm dia.)	Pulses (x 1000)	**Product Recovery System
870324 (Au)	H_2/CH_4 (84/16)	1,350	(130)	(500)	2.4 1.1	4.20 2.94	300 K TT, UT
870313 (Au)	H_2/Natural Gas (75/25)	1,420	(130)	(470)	optimum	10.20	300 K TT, UT
880218 (Au)	Ar (100)	1,390	75	278	optimum	29.82	GFF,UT
880222 (Au)	He (100)	1,370	116	436	optimum	29.82	GFF, UT
880223 (Au)	H_2/CH_4 (76/24)	1,350	145	550	optimum	21.60	GFF, UT
880224 (Au)	H_2/CH_4 (74/26)	1,390	200	750	optimum	21.60	GFF, UT
880302 (Au)	H_2/CH_4 (74/26)	1,380	195	730	optimum	21.60	GFF, UT
880303 (Au)	H_2/CH_4 (74/26)	670	81	620	optimum	22.02	GFF, UT
880304 (Au)	H_2/CH_4 (74/26)	2,710	653	1,240	optimum	21.60	GFF, UT

Table 2 (continued)

Expt. No. (target)	Gas Mix (%)	Pressure (Pascal)	*Flow Rate Through Reaction Zone ml/min (atm.)	cm/sec	CO_2 Laser Conditions Focal Point (mm dia.)	Pulses (x 1000)	**Product Recovery System
880307 (Au)	CH_4 (100)	1,470	(240)	(840)	optimum	21.60	GFF, UT
880309 (Au)	H_2/CH_4 (48/52)	670	72	550	optimum	21.60	GFF, UT
880311 (Au)	H_2/CO (75/27)	1,390	(125)	(465)	optimum	19.98	GFF, UT
880317 (Au)	H_2/CO_2 (75/25)	1,390	125	465	optimum	21.60	GFF, UT
880329 (Au)	$He/CHClF_2$ (74/26)	1,470	145	510	optimum	3.66	GFF, UT
880415 (Au)	$He/CHClF_2$ (76/24)	300	110	1,890	optimum	5.16	GFF, UT
880421 (Au)	He/CCl_2F_2 (76/24)	1,360	190	790	optimum	16.56	GFF, UT
880425 (Au)	$He/CCl_2F_2/H_2$ (82/14/3.6)	1,370	175	660	optimum	20.70	GFF, UT
880427 (Au)	He/C_2F_6 (73/27)	1,240	110	413	optimum	19.98	GFF, UT

Table 2 (continued)

Expt. No. (target)	Gas Mix (%)	Pressure (Pascal)	*Flow Rate Through Reaction Zone ml/min (atm.)	cm/sec	CO_2 Laser Conditions Focal Point (mm dia.)	Pulses (x 1000)	**Product Recovery System
880720 (carbon)	H_2/CH_4 (74/26)	1,350	200	760	optimum	9.77	GFF, UT
880723 (copper)	H_2/CH_4 (74/26)	1,350	200	760	optimum	8.34	GFF, UT
880724 (copper)	H_2/CH_4 (74/26)	27	0	0	optimum	0.01	GFF, UT
		1,320	(195)	(760)	optimum	0.03	
		1,230	(185)	(780)	0.28	0.03	
		1,230	(185)	(780)	0.56	0.03	
		200	N/A	N/A	0.56	0.03	
		750	(80)	550	optimum	0.03	
		1,410	(210)	(770)	optimum	10.44	
		2,450	330	690	optimum	0.37	

*Flowrate values in parentheses are estimates based on measurements made under similar conditions.

**QT = quartz tube; GWP = glass wool plug; UT = 195 K U-tube; GFF = glass fiber filter; TT = test-tube; CF = cold finger. See text for detailed descriptions.

on June 2, 1986. The gas mixtures, total pressures, and flow rates through the plasma reaction system are also listed in this table. The pulsed laser focal point diameter at target impact and the total number of pulses for each experiment are included as well.

Volumetric flow rates were measured in ml/min at atmospheric pressure using the bubble-tube flowmeter. Linear flow rates (L) in cm/sec through the plasma reaction zone were calculated using the following equation:

$$L = (F)(101{,}325/P)/\pi r^2$$

where F is the volumetric flow rate in ml/sec measured at atmospheric pressure, P is the plasma reaction chamber pressure in Pascals, and r is the radius of the reaction zone in cm. Some values (listed in parentheses) were estimated from measurements made during similar experiments utilizing the same nominal gas mixture and pressure and the same settings on the variable-area flowmeters.

The diameter (d) for the laser beam at the target impact point was calculated using the absolute value of the difference (x) between the focal length of the lens (f) and the measured separation of the lens and target, and the measured diameter (D) of the unfocused laser beam:

$$(d/2)/x = (D/2)/f$$

The impact point diameter was varied by moving the lens closer to or farther away from the target.

The first experiment listed in Table 2 investigated the onset of gas breakdown in helium under pressures ranging from 18,800 to 161,500 (Pascals (141-1211 torr). The second test listed demonstrated the same effect in air at 101,500 Pascals (761.5 torr). In both of these experiments the laser beam was focused into the center of the plasma chamber. The target and target stand were removed from the system. The third experiment listed demonstrated gas breakdown in hydrogen at 106,390 and 110,900 Pascals (798 and 832 torr) pressure when focusing the laser on a gold target. The focusing lens was moved back 3 cm from the optimum distance in order to observe the effect on the gas breakdown. This same phenomenon was also observed in several other gas mixtures at lower pressures during the course of the study. Observations and results are discussed in the next chapter.

Gases were supplied to the chamber under pressure during segments of the first and third experiments when reactor chamber pressures were greater than the ambient pressure. Flow rates were controlled by a metering valve at the chamber exit, upstream from the mechanical pump. At lower pressures (< 101,500 Pascals) in these and all remaining experiments, the pressures and gas flow rates were controlled using the gas handling system described earlier and the metering valve before the pump.

The last four experiments listed in Table 2 were attempts to generate pure carbonaceous and copper-bearing species in the plasma chamber using the carbon and copper targets, respectively, and a 3:1 $H2CH_4$ gas mix. The remaining experiments listed in Table 2 were all attempts to generate gold species that would remain entrained in the

gas stream and subsequently be trapped in the product recovery system. The reader is directed to the table for a detailed presentation of the experimental conditions. The results of each experiment are discussed in Chapter III.

Substrate Coating and Annealing Experiments

Several different types of substrates were coated with the plasma reaction products during the course of the study. Experiments that produced the coated substrates are listed in Table 3 along with the respective substrates and their physical positions in the plasma-reaction or product-recovery systems during the coating process. In all of the coating experiments the pulsed CO_2 laser was operated at its maximum voltage level (40 KV) and the focusing lens was adjusted to provide an optimum focus at the target impact point. All coating experiments were carried out at a nominal pressure of 1,330 Pascals (10 torr). A nominal gas mixture of 75% hydrogen and 25% methane was used in all of these experiments with four exceptions. Two experiments were performed using 100% helium, one test used 78% helium and 22% carbon monoxide mixture, and one test used a mixture of 75% hydrogen and 25% natural gas.

Eleven different types of substrates were coated with the plasma reaction products:

1) glass plates cut from standard 1 mm thick microscope slides (Corning No. 2947), varying in size from 5 mm by 10 mm to 25 mm by 40 mm,

2) quartz optical windows, 1 mm thick by 27 mm diameter,

Table 3. *Substrate Coating Experiments

Expt. No.	Total # of Laser Pulses (x 1000)	Substrates Coated	Position in System
861117 (78% He/22% CO)	15.00	W coated polycrystalline (pc) Si chip	placed in U-tube inlet
861124 (100% He)	16.20	glass plates	taped to plasma chamber windows; placed in bottom of plasma chamber
861126A (100% He)	7.20	W coated pc Si chip with an etched area; patterned W on single crystal (sc) SI; glass plates	W/Si chips taped to glass plates; glass plates taped to windows and placed in bottom of plasma chamber
870313 (75% H_2/25% natural	10.20	W ribbon coil gas)	placed in U-tube inlet, Ar ion laser beam directed through glass tube onto leeward area
870326	12.60	W ribbon	placed in plasma chamber outlet, Ar ion laser beam directed through quartz window onto W
870416	13.92	ceramic feedthrough	placed in small coating chamber
870427	40.74	9 ceramic feedthroughs	placed in glass coating chamber (GCC) on three-tiered rack
871106	27.66	glass plate	taped into GCC inlet
870721	63.12	W on pc and sc SI chips; patterned Al on sc Si chip	taped to first tier of rack in GCC
870801	11.76	glass plate	taped into GCC inlet
870819	23.10	glass plate	taped into GCC inlet
870901	55.92	3 patterned W, 2 patterned Al on sc SI chips	taped onto glass plate that was taped into GCC inlet

Table 3 (continued)

Expt. No.	Total # of Laser Pulses (x 1000)	Substrates Coated	Position in System
880527	33.55	3 W on pc Si and 3 W on sc Si chips	taped to perf-plate in the aluminum coating chamber (ACC)
880602	31.32	7 W on pc Si and 5 W on sc Si chips	taped to perf-plate in ACC
880617	27.56	3 W on pc Si and 3 W on sc Si chips	clipped to 373 K hot plate in ACC
880623	23.46	2 W on sc Si chips; 2 glass plates	clipped to 373 K hot plate in ACC
880629	20.58	3 W on sc Si chips; 5 glass plates; strip of Scotch tape, adhesive side up, with an area of W thin film stuck to the adhesive	taped to perf-plate in ACC
880708	6.41	2 charged aluminum plates (+275 and -125) volts dc potential)	pressed into center of perf-plate
880711	9.98	Si chip with a central strip of W on one side charged with -125 volt dc potential; two 2.5 cm dia. quartz optical flats; 4 glass chips	placed near sidewall in ACC taped to plasma chamber windows

*All experiments were conducted at a nominal pressure of 1,330 Pascals using a nominal gas mixture of 75% H_2 and 25% CH_4, except where noted.

3) tungsten ribbon, 1.5 mm wide by 0.2 mm thick (H. Cross Company),

4) ceramic electrical feedthroughs, 1 cm diameter surface,

5) blanket coated CVD tungsten (500-600 nm) on a silicon wafer with one polycrystalline (pc) side and one single crystal (sc) side (Harris Corporation) cut into 5 mm by 15 mm chips,

6) same as (5), with areas of tungsten etched away (1 M $K_3Fe(CN)_6$:0.1 M ethylene diamene) to expose the silicon surface,

7) VLSI circuit patterned CVD tungsten on sc silicon with silicon dioxide surfaces surrounding the 5-50 micron size tungsten features (Harris Corporation), cut into 5 mm by 15 mm chips,

8) VLSI circuit patterned CVD aluminum on sc silicon with silicon dioxide surfaces surrounding the 5-50 micron size features (Harris Corporation), cut into 5 mm by 15 mm chips,

9) aluminum plates, 10 mm by 20 mm by 1 mm thick,

10) Scotch brand adhesive tape, and

11) Scotch brand black electrical tape.

All of the substrates, except the two polymeric tapes, were cleaned in spectral grade acetone, rinsed in spectral grade methanol, placed in clean glass petri dishes, and dried in a 383 K oven for at least one hour. After carefully mounting the cooled substrates onto the plasma chamber windows or in the substrate coating chamber using rolled Scotch tape, they were rinsed off with dry nitrogen and placed in line. Coated substrates were stored in air in glass petri dishes or plastic-stoppered glass vials.

In most of the experiments the substrates were positioned in one of the product-recovery/substrate-coating systems described earlier and coated at room temperature (ca. 300 K). In one experiment a 5 cm long piece of tungsten ribbon was coiled and placed in the inlet arm of the glass U-tube cold trap and irradiated with an unfocused cw Argon ion laser beam (4.5 watts, 514.5 nm). In another experiment a 1.5 cm long piece of the tungsten ribbon was placed in the top of the plasma reaction chamber at the exit union with the product recovery system flange (see Figure 9) and exposed to the unfocused Ar ion laser beam through a quartz window. This caused the ribbon to glow a dull red when the chamber was under vacuum. When the system gas flow was turned on the glow disappeared. In both experiments the laser beam was impacting the leeward face of the ribbon. These were attempts to observe thermal decomposition of gold species entrained in the gas stream and subsequent deposition of gold along the thermal gradient induced by the laser beam.

Two experiments utilized the hot plate described earlier to heat glass plates and CVD tungsten coated pc and sc silicon chips to 373 $\pm$ 5 K during the coating process. Problems associated with channeling of the gas stream around the hot plate limited the efficiency of this process, but several substrates were effectively coated in each experiment and then subjected to spectral and microscopic analyses.

A list of the coated substrates that were annealed and the respective annealing condisions is presented in Table 4. Some of the tungsten coated and patterned chips, aluminum patterned chips, glass plates, and quartz windows that had been coated with plasma reaction

Table 4. *Substrate Annealing Conditions

Expt. No.	Substrate	Annealing Method	Time	Temp. (K)
861117 (78% He/ 22% CO)	plasma chamber glass window	pulsed CO_2 laser, 40 KV, unfocused	60 pulses	
861126A (100%)	W on pc SI chip; patterned W on sc Si chip	--radio frequency (rf) coil (in flowing air);	10 sec 60 sec	
		--rf coil in still air	70 sec	dull red
870326	W ribbon	Ar ion laser, 4.5 watts, unfocused	211 min (in situ)	
870416	ceramic feed-through	slow convective heating (cv.h.) in air while monitoring electrical resistance	141 min	(743) (max.)
870427	ceramic feed-through	same as above, except under H_2 flow	57 min	(763) (max.)
870721	W on pc and sc Si; patterned Al on sc Si chips	cv.h. under H_2 flow	18 hr + 1 hr + 2 hr	563 @ 563 @ 723
870901	W and Al on sc Si chips	cv.h. under H_2 flow	18 hr	563
880224	glass fiber filter (GFF)	cv.h. in air	1 hr + 3 hr	ca. 400 873
880229	GFF	cv.h. in air	24 hr + 1 hr	420 573
880304	GFF	cv.h. in air	8 hr	505
880307 (100% CH_4)	GFF	cv.h. in air	8 hr	505
880309 (48% H_2/ 52% CH_4)	GFF	cv.h. in air	8 hr	505

Table 4 (continued)

Expt. No.	Substrate	Annealing Method	Time	Temp. (K)
880311 (H_2/CO)	GFF	cv.h. in air	3 hr	515
880317 (H_2/CO_2)	GFF	cv.h. in air	24 hr	515
880527	W on pc and sc Si chips	--cv.h. under H_2 flow	18 hr	(533)
		--cv.h. in air	18 hr	(553)
	W on pc and sc Si chips	--cv.h. under H_2 flow	18 hr	(533)
		followed by cv.h. in air	+19 hr	(603)
880602	W on pc and sc Si chips	--cv.h. in air	18 hr	373
		--cv.h. in air	18 hr	(533)
		--cv.h. in air	18 hr	(593)
		--cv.h. in air	18 hr	(593)
		--cv.h. under H_2 flow	1 hr	(573)
		--cv.h. in air, followed by cv.h. under H_2	18 hr + 1 hr	(593) (573)
		--cv.h. under H_2, followed by cv.h. in air	1 hr +19 hr	(573) (603)
880623	W on pc Si chip glass plate	--rf coil in air	3 sec	red hot
		--drew lines with focused Ar ion laser beam (3.5 watts)	0.3 cm/sec	
880629	W on pc Si chip and glass plate	--rf coil, 0.013 Pascal	1 min	
		--cv.h. in air	85 min	(670)
		--drew lines with focused Ar ion laser beam (3.5 watts)	0.5 cm/sec	
		(2.0 watts)	0.5 cm/sec	
		(1.0 watts)	0.5 cm/sec	
880708	(-) dc potential aluminum plate	cv.h. in air	90 sec	(875)

Table 4 (continued)

Expt. No.	Substrate	Annealing Method	Time	Temp. (K)
880711	pieces of GFF	cv.h. in air	25 hr	383
			23 hr	(473)
			1 hr	(676)
			90 sec	(875)

*All experiments were conducted at a nominal pressure of 1,330 Pascals using a nominal gas mixture of 75% H_2 and 25% CH_4, except where noted.

products were annealed in air or hydrogen at temperatures ranging from 373-670 K for time intervals ranging from several seconds to several hours. These anneals were performed in the tube furnace described earlier. An annealing chamber was constructed from a 20 mm i.d. by 50 cm long borosilicate glass tube with O-ring seal joints on both ends (see Figure 10). The ends of this tube were connected to two matching O-ring seal joints that had ends tapered to 1/4 in. o.d. tubing. Quick couples were used to connect the chamber with the gas handling system for delivery of hydrogen at ca. 400 ml/min. Anneals in air were performed by disconnecting the chamber's gas inlet line and allowing ambient air to be drawn through the system by convective flow. A brass sample holder with a stainless steel insertion handle was used to place and hold the substrates in the center of the tube furnace, adjacent to the thermocouple.

Some glass fiber filters were also annealed in air at temperatures ranging from 390-873 K by placing them in borosilicate glass petri dishes and then into a laboratory drying oven or a muffle furnace. This was done to observe the onset of a development process that changed the color of the plasma reaction product coating from black to purple to pink/red.

Several patterned and unpatterned CVD tungsten on silicon chips, and one glass plate, were inserted into a radio frequency coil and heated inductively. Either a 30-year-old ham radio with ~ 100 watts of power at 13.56 Mhz, or an ICOM All Solid State HF SSB tranceiver feeding a Heath Kit tube-type linear amplifier at 14.000 Mhz and delivering ~ 250 watts of power, were used to power the 3 cm diameter 3

Figure 10. Substrate Annealing Chamber

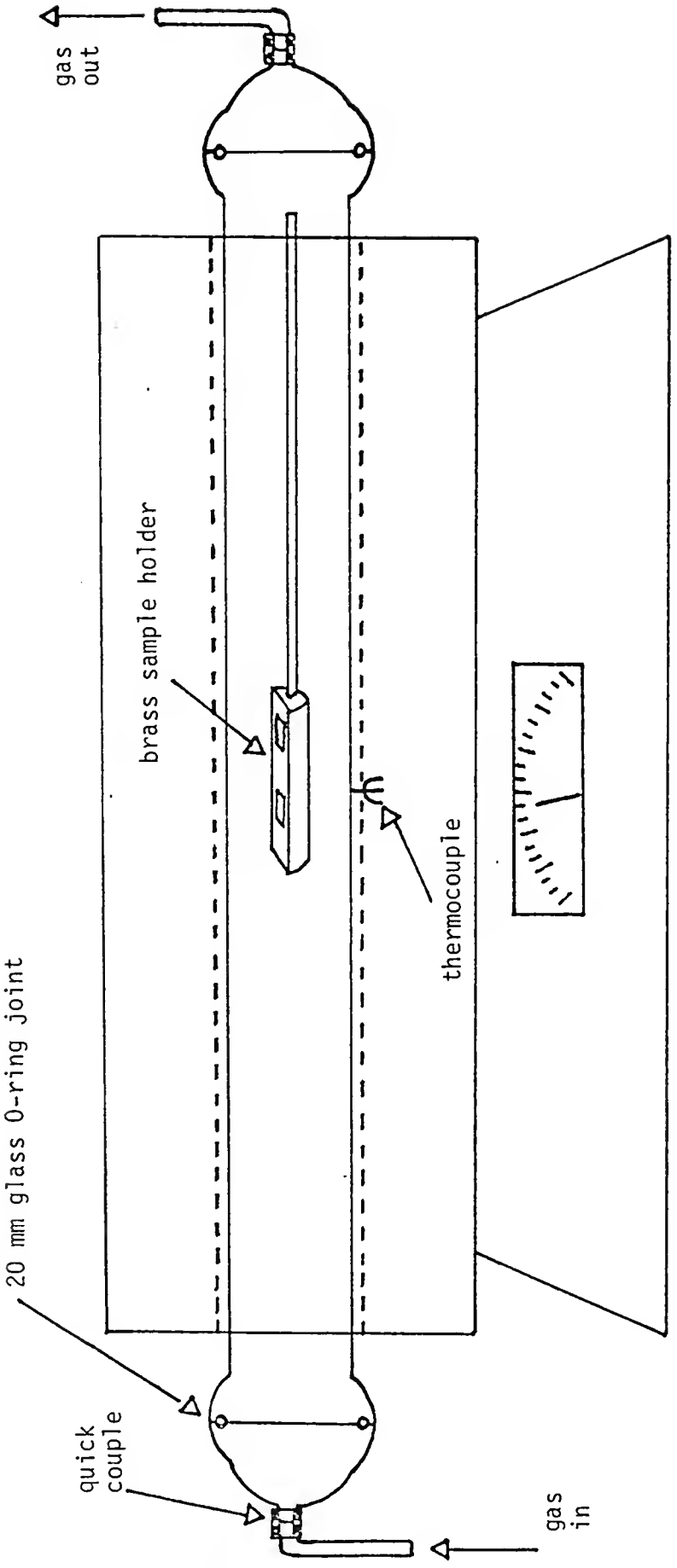
gas out
brass sample holder
thermocouple
20 mm glass O-ring joint
quick couple
gas in

turn coil. No temperature measurements were made in these tests, but several samples were heated to a red glow. Exposure time to the rf field was varied from 3-70 seconds. Some tests were performed in ambient air with or without a fan blowing air past the sample, and other samples were heated while under a pressure of 0.01 Pascals.

The unfocused pulsed CO_2 laser beam was used to anneal a coated chamber window and a coated quartz window. Exposures were varied from 1-100 pulses. The laser was operated at its maximum power level of 40 KV during all of these tests.

The Argon ion laser was used to write gold lines on coated substrates by focusing the beam through a 75 mm focal length quartz lens (Rolyn #11.0140) onto the coated surface. The laser was operated at power levels of 3.5, 2.0, and 1.0 watts. Glass plates and CVD tungsten on Si chips were taped to a carbon block and manually rastered in front of the laser beam at the focal point. Pull rates were varied from ~ 0.3 cm/sec to ~ 0.5 cm/sec. The focused beam was also fixed on one spot on a CVD tungsten on sc SI chip for 10 seconds.

Product Volatility Study

The search for volatile gold compounds in the plasma reaction products was divided into three categories, based on technique. The first category of tests involved attempts to sublime gold compounds at low pressure from the reaction products thermally and collect them in a cold trap. The second category of tests utilized quadrupole and ion cyclotron (ICR) mass spectrometers and several different methods of sample delivery in an attempt to isolate and identify gold compounds.

compounds. The third category consisted of one series of experiments using a time of flight mass spectrometer (TOFMS) to detect gold cluster compounds formed in a Nd/YAG pulsed laser stimulated plasma using a solid gold target and 1% methane in helium. Each experiment in the volatility study is described below.

Sublimation Experiments

The two sublimation experiments that were performed used the reaction products formed in a 75% He/25% CH_4 plasma and isolated in the product recovery system. The first experiment used the (195 K) U-tube cold trap from 861018. This trap had been positioned after a 300 K cold finger during the plasma reaction experiment. The second sublimation experiment utilized the first cold finger trap (195 K), and the glass wool plug contained in its outlet, from 861023. Both of these cold traps contained milligram quantities of the dark-colored plasma reaction products.

Both sublimation experiments were performed by attaching the plasma containing cold traps (which had been sealed and stored at 195 K) to a fresh U-tube cold trap kept at 195 K. This trap was connected to the mechanical vacuum pump, via a metering valve and a 195 K pump trap, and the system was evacuated slowly to < 1 Pascal. In the first test the products were warmed from 195-373 K over a period of four hours. A second collection trap was exchanged for the first one when the products reached 300 K. In the second test the plasma products were warmed from 300 to ~ 900 K over a period of 90 minutes. Only one collection trap was used in this test. All of the collection traps,

and both of the product recovery traps, were sealed in air and heated to ~ 900 K in a bunsen burner. Color changes in the trap contents, which indicated the presence of gold films, were observed visually.

Mass Spectrometer Experiments

Six experiments were performed using quadrupole or ICR mass spectrometers to detect compounds in the plasma reaction products. All of the instruments were located in the Department of Chemistry at the University of Florida (U.F.). A synopsis of these experiments is presented below in Table 5.

Table 5. Volatility Study Mass Spectrometer Experiments

Expt. No.	Plasma Expt. (Gas Mix)	Sample Type	MS Type	Sample Introduction Method
1	860704 (75% He/25% CH_4)	target residue	quadrupole	solids probe, heated to 670 K
2	870121 (93% H_2/8% C_2H_2)	chamber wall residue	GC/quad.MS	injected acetone suspension/solution
3	870819 (75% H_2/25% CH_4)	U-tube cold trap	quadrupole	connected to gas inlet, heated to 680 K
4	860722 (75% He/25% CH_4)	cold trap after GWP	FTICR	connected to gas inlet, heated to 380 K
5	870819 (75% H_2/25% CH_4)	coated glass plate	FTICR	placed adjacent to ICR cell; e-beam & laser desorption
6	870819 (75% H_2/25% CH_4)	residue from coated glass plate	FTICR	solids probe, heated to 450 K, CID reactions

The first experiment was done in the laboratory of Prof. R.A. Yost by Mr. M. Hail using a Finnigan/MAT 4515 quadrupole MS. Reaction products were recovered from the gold target used in test 860704 (75% He/25% CH_4) by scraping the tar-like residue with a teflon spatula. The sample was placed in a solids probe and heated to 673 K while observing the mass response from 0-494 atomic mass units (a.m.u.). The instrument's mass range was calibrated using perfluorotributylene.

The second experiment was done in the department's Analytical Service Laboratory by Dr. R.W. King using a Finnigan/MAT 4500 gas chromatograph/quadrupole mass spectrometer (GC/MS). A sample was recovered from the plasma chamber sidewall after test 870121 (93% H_2/8% C_2H_2) by rinsing the sidewall with spectral grade acetone. The extract/suspension was injected onto a 5 ft. x 1/4 in. glass chromatography column packed with an inert support coated with 3% SP2100 (an organo-silane polymer commonly used for hydrocarbon separations). Helium carrier gas flow rate through the column was 30 ml/min. The column temperature was increased from 318-573 K at 10 degrees per minute while observing the mass response from 0-300 a.m.u. This instrument was also calibrated using a standard hydrocarbon mixture (FC 43).

The third experiment was performed in the laboratory of Prof. M.T. Vala by the author using a Finnigan 3500 quadrupole MS. The U-tube cold trap used in test 870819 (75% H_2/25% CH_4) was connected to the instrument's solids probe inlet and heated to 680 K in a tube furnace while observing the mass response from 0-500 a.m.u. The instrument response was tested by placing a sample of triethylphosphine-gold

chloride (synthesized by Dr. E. Sczlick in the laboratory of G.J. Palenik at U.F.) in the solids probe and heating it to 570 K.

The fourth, fifth, and sixth experiments were performed in the laboratory of Prof. J.R. Eyler by Dr. M. Moini and the author. The fourth one used a sample from test 860722 (75% He/25% CH_4). The sample was collected in a 195 K cold trap positioned after a glass wool plug during the plasma experiment. This cold trap was connected to the gas inlet of an ICRMS (Nicolet FTMS-1000 equipped with a 3.0 Tesla superconducting magnet and described fully in the literature).[65] The sample trap was then evacuated to 0.1 Pascals while still immersed in dry ice. The valve to the MS was then opened and the mass response from 0-1000 a.m.u. was observed using Fourier transform techniques while the sample trap was slowly warmed to ~ 380 K. The instrument response was tested by placing a sample of triethylphosphine-gold chloride in a solids probe and warming it to ~ 450 K.

The fifth experiment used an inhouse fabricated ICRMS (equipped with a Nicolet FTICR MS data station and a Varian Fieldial 1.0 Tesla electromagnet) to examine plasma reaction products coated on a glass plate in run 870819 (75% H_2/25% CH_4). The sample was mounted on a solids probe and positioned in the vacuum chamber adjacent to the ICR cell. The mass response from 0-400 a.m.u. was monitored using Fourier transform methodology while the sample was exposed to a 500 nanoamp electron beam for one hour. The sample was then irradiated with an unfocused frequency doubled, 532 nm pulsed Nd:YAG laser (Quantel Model YG 580) at power levels of 50-500 mJ/pulse in an attempt to desorb compounds that would have then been ionized by co-desorbed potassium

ions. (The K+ ions came from the materials used to construct the ICR cell. This was considered a "soft" ionization technique.) The mass response was monitored for the next twenty minutes while the laser and e-beam were on, and then for another ten minutes with the laser on and the e-beam off.

The sixth experiment was performed in the Nicolet FTMS-1000 ICRMS using a sample generated in run 870819 (75% H_2/25% CH_4). The sample was placed in a capillary tube that was then inserted into the solids probe and warmed to ~ 450 K while the mass response from 0-1000 was observed. Collision-induced ion dissociation (CID) experiments were performed on compounds with mass numbers 44, 149, 195, 255, 334, and 348.

Time of Flight MS Plasma Experiment

This experiment was performed in the labortory of Prof. P.J. Brucat in the Department of Chemistry at U.F. by Mr. D.E. Lessen and the author. This laboratory was equipped with a cluster beam apparatus linked to a time of flight mass spectrometer (see Figure 11) that is described fully elsewhere.[66] The cluster beam was produced by irradiating a solid gold target with a focused pulsed Nd:YAG laser (Quantel Model YG-580) beam at a power level of 1-2 mJ/pulse at target impact (7 nsec pulses at 10 hz). Helium or helium/1% methane gas was introduced to the target at a pressure of ~ 1 atm. using a 1 msec pulsed valve. The resultant plasma exited the target holder through a 2 mm dia. hole and was hypersonically expanded into a large vacuum chamber maintained at a pressure of 0.01 Pascals. A skimmer in direct

Figure 11. Cluster Beam/TOFMS Apparatus

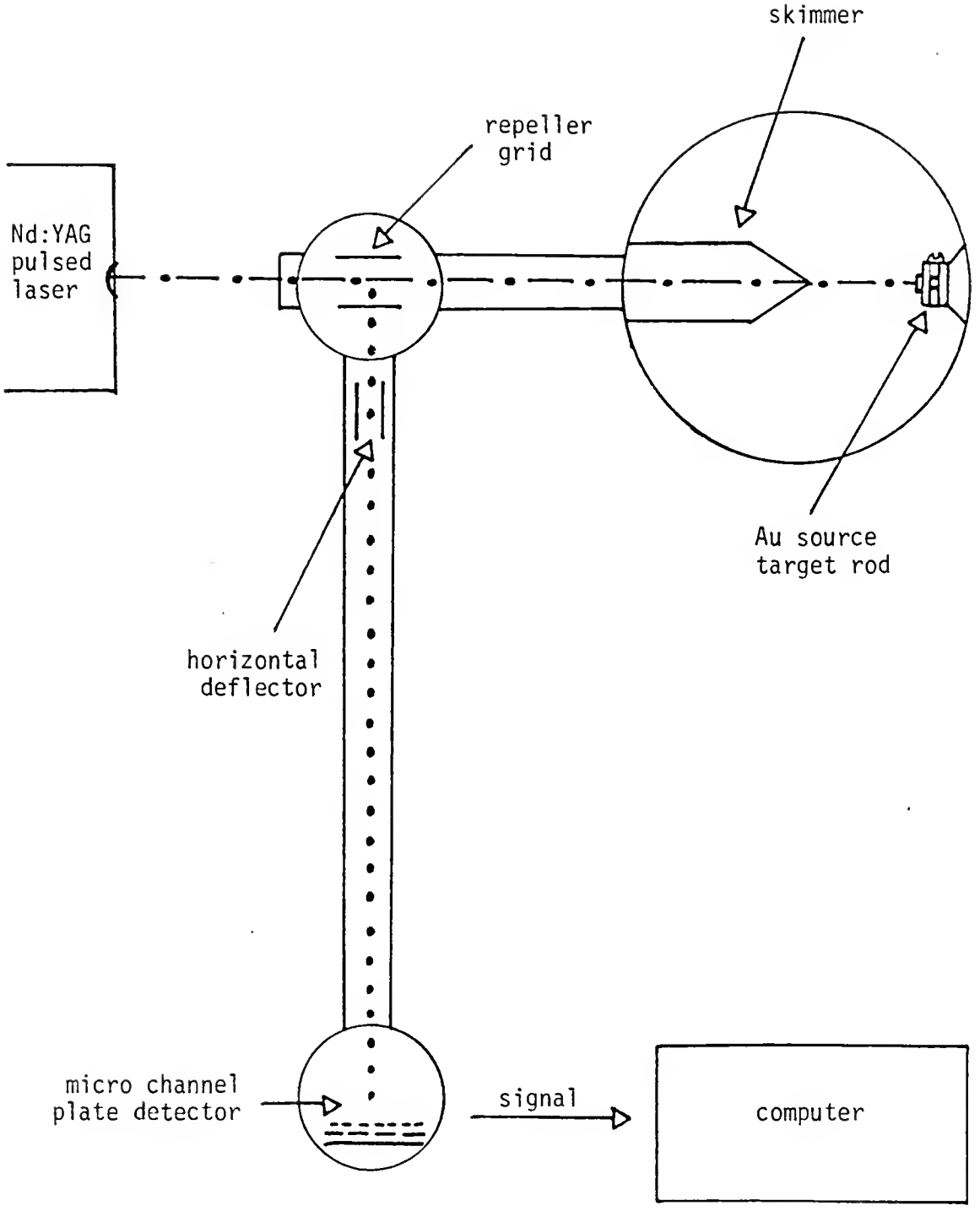
skimmer
repeller grid
Nd:YAG pulsed laser
Au source target rod
horizontal deflector
micro channel plate detector
signal
computer

line of sight with the plume exit allowed undeflected clusters to enter a repeller grid where they were redirected down a three meter TOF tube and into a multi-stage detector. A variable voltage horizontal deflector (HD) located at the beginning of the TOF tube optimized the transfer efficiency of various mass ranges of clusters.

During the course of the experiment the HD voltage was varied between 50-120 volts. This allowed the observation of signals from ionized gold clusters and cluster compounds from Au(1) to Au(7). At each voltage setting the signals from positive ion clusters produced in pure helium and in helium/1% methane plasmas were recorded.

Gold Thin Film Characterization

Six different techniques were utilized to characterize the plasma reaction products formed in the 3:1 hydrogen/methane-gold plasmas. Samples of the ultrafine particle product and coated substrates (both annealed and unannealed) were subjected to analyses. Most samples were in the form of thin films deposited on glass plates, ceramic feedthroughs, and CVD tungsten or aluminum on silicon chips. A major objective of these analyses was the determination of the relative abundance, and the physical state, of the gold present in the soot-like plasma reaction products. Film stoichiometry, structure, and electrical properties were also investigated. The analytical techniques utilized in this part of the study were

1) visible absorption spectroscopy,
2) optical microreflectometry (OMR),
3) x-ray photoelectron spectroscopy (XPS),

4) scanning electron microscopy (SEM) with

5) energy dispersive spectroscopy (EDS), and

6) electrical resistance (R)

The principle features of each technique are described briefly along with the relevant parameters employed to analyze the sample films. Detailed lists of the samples analyzed using each technique are presented in Chapter III along with the respective analytical results and a discussion of their meaning.

Visible Absorption Spectroscopy

A Hewlett-Packard Model 8450 diode array spectrometer was used by the author to measure the absorption spectra (300-800 nm) of acetone suspension/solutions of several samples recovered from the plasma chamber sidewalls. Samples from CH_4, He/CH_4, and He/CO plasma experiments were subjected to solvent dissolution tests using hexane, toluene, acetone, diethyl-ether, 1:1 solutions of the preceding solvents, water, hydrochloric acid, nitric acid, and aqua regia before determining that pure acetone yielded the best results (discussed in the next chapter). The absorption spectra of 10 ppm and 10,000 ppm Au standards in acetone/water were also measured. These standards were prepared by diluting 1 ml of the 1000 ppm and 10 ml of the 100,000 ppm AA standards, respectively, to 100 ml with spectral grade acetone. All of the sample and standard spectra were measured against an acetone reference cell. All measurements were made in standard matched 1 cm wide quartz cuvets.

The major objective of these analyses was the determination of the presence or absence of the metallic absorption band for gold in the 550-600 nm region of the spectrum. This indicated the presence or absence of gold particles large enough to exhibit metallic behavior.

Optical Microreflectometry

An optical microreflectometer located in the laboratory of Prof. P. Holloway in the Material Science Department at U.F. was used by the author to measure the reflectance spectra of several samples. The instrument consisted of a quartz halogen light source and focusing lens assembly, a 1200 1/mm grating monochromator, a binocular microscope with internal mirrors for directing reflected light to a GaAs photomultiplier tube, and a Keithley autoranging picoammeter (Model 485). Reflectance curves were determined by comparing the sample intensities to the intensities of a standard with known reflectivity in air, R(std). The reflectance intensity of a SiC standard, I(std), was measured at 10 nm intervals between 400 and 900 nm just prior to measuring the intensity of each sample's reflectance, I(samp), at the same wavelengths. The reflectance value for each sample point, R(samp), was then calculated using the following equation:

$$R[samp] = [I(samp) - DC] \times [R(std)]/[I(std) - DC]$$

where DC was the photomultiplier dark current. R(std) values for SiC are listed in Appendix C.

Sample films were examined visually to determine a representative area for reflectance measurements. The instrument analyzed an area 20 microns in diameter. The same spot on the SiC standard was measured

each time by aligning two small defects on the crystal surface with points on the microscope measurement grid. Reflectance curves were determined for annealed and unannealed films deposited on glass plate and on CVD tungsten on Si chips, as-deposited films on the two polymeric tapes, and the Harris Corp. standard sputtered Au film.

X-Ray Photoelectron Spectroscopy

X-ray photoelectron spectroscopy studies were carried out on several $CH_4/H_2/Au$ plasma reaction product coated and annealed W on Si substrates. The XPS analyses had three major objectives: 1) determination of the elemental surface composition of the film, 2) determination of the binding energy (BE) of the Au $4f_{5/2}$ and $4f_{7/2}$ peaks and the C 1s peak, and 3) determination of the gold and carbon concentrations in the bulk of the film. The first objective was achieved through the use of elemental survey scans from 0-1000 eV BE. The second objective was accomplished using narrow scans (~10 eV) of the respective Au and C peaks and observing the shift in BE and the peak shapes and widths at half height (whh). The determination of carbon and gold concentrations in the bulk of the films was accomplished using narrow scans with variable photoelectron takeoff angles and Ar^+ ion etching. Spectra were recorded in a fixed analyzer transmission mode, which allowed direct comparison of adjusted peak areas for semiquantitative analyses. A detailed list of all samples subjected to XPS analyses, along with the respective analytical conditions and results, is presented in Chapter III together with a detailed discussion of the results.

Two instruments were used to perform the analyses in these studies. One instrument, a Kratos XSAM 800, was located in the laboratory of Prof. V.Y. Young in the Department of Chemistry at U.F. and was operated by Mr. P.C. McCaslin and Mr. J.G. Davis, Jr. The instrument used a Mg anode (1254.6 eV Kα line) x-ray source operated at 15 kV accelerating potential. Samples were mounted to a grounded holder using stainless steel screws that contacted the surface of the sample films and the underlying W substrate near the edges. This arrangement prevented charging of the thin film while it was being exposed to the x-radiation and undergoing electron loss. Spectra were recorded at photoelectron takeoff angles of 10 and 70 degrees. This technique allowed observation and comparison of the signals produced predominantly by near surface species (~1.5 nm sampling depth at 10 degree takeoff angle) and those produced predominantly by bulk species (~7.5 nm, or three times the mean free path of 1.2 keV electrons in gold,[67,68] sampling depth at 70 degree takeoff angle). One sample was also etched with Ar^+ ions at 2.5 keV accelerating potential and 0.25 mA sample current for a total of 60 minutes. Spectra were recorded before the etch, after 15 minutes of etching and after 60 minutes of etching.

The second XPS instrument was a GCA/McPherson ESCA 36 located in the laboratory of Prof. A.T. D'Agostino in the Department of Chemistry at the University of South Florida and was operated by Mr. C. Biver. This instrument used an Al anode (1487.6 eV Kα line) x-ray source operated at 15 kV potential. An initial set of samples that was analyzed in this instrument was improperly grounded and thus did not yield valid BE data. However, since the charging effect reached an

equilibrium status within the first few seconds of exposure to the constant intensity x-ray beam,[69] the total areas of the Au and C peaks and the elemental survey scans provided useful information. One sample film and one Harris Corp. standard sputter deposited Au film were subjected to depth profiling using Ar^+ ion etching (13 μA ion current and 6.3 mA arc current). These two samples were grounded by pressing copper foil over them, with an open area for analysis, and attaching the foil securely to the grounded sample stand. All spectra were recorded at a photoelectron takeoff angle of 75 degrees. Peak areas were adjusted for elemental composition determinations using Scofield's photoionization cross sections[70] at 1254.6 and 1487.6 eV, respectively, for the two instruments. Since only gold and carbon were detectable in the films (the photoionization cross section for hydrogen is extremely small, 0.0002 relative to carbon, and was not detectable with these instruments), and the Scofield cross section value for the C 1s peak is taken as 1.00 relative (22,000 barns at 1254.6 eV, and 13,600 barns at 1487.6 eV), only the combined areas (XAu) of the Au 4f peaks were adjusted. This was done using the following equation for the Mg Kα source (1254.6 eV):

$$(XAu)/(7.68 + 9.79) = \text{adjusted Au area}$$

For the Al Kα source (1487.6 eV), the following equation was used:

$$(XAu)/(7.54 + 9.58) = \text{adjusted Au area}$$

Once the adjusted Au areas (adjAu) were calculated they were compared directly to the corresponding C 1s peak areas to yield relative percent atomic composition using the following equations:

$$(100)(adjAU)/(adjAu + C\ 1s) = \text{relative atomic \% Au}$$
$$(100)(C\ 1s)/(adjAu + C\ 1s) = \text{relative atomic \% C}$$

Relative percent mass concentrations were then calculated using the following equations, where ra%Au and ra%C are the relative atomic percent concentrations of gold and carbon, respectively:

$$(ra\%Au)(197)/[(ra\%Au)(197) + (ra\%C)(12.0)] = \text{relative mass \% Au}$$
$$(ra\%C)(12.0)/[(ra\%Au)(197) + (ra\%C)(12.0)] = \text{relative mass \% C}$$

In some discussions of the results in the following chapter references are made to the ratio of gold to carbon and vice versa. In all instances these discussions are referring to the atomic ratios of the two elements.

Scanning Electron Microscopy with Energy Dispersive Spectroscopy

The SEM/EDS analyses were carried out in order to determine 1) the average grain or particle size and shape of the species comprising the as deposited sample films and 2) the change in film structure associated with various annealing regimes. These analyses were performed in a JEOL SEM equipped with an EDS system located in the laboratory of Prof. M. Ammons in the College of Engineering Center for

Electron Microscopy at the University of South Florida. The instrument was operated by Prof. Ammons and Ms. A.S. Slater.

The optics in the EDS system precuded the observation of low Z elements, thus hydrogen and carbon were not observable. The EDS was used primarily to determine qualitatively the relative abundance of gold in the surface being scanned by the SEM. By varying the electron energy, and thus the mean free path in the sample film, a rough depth profile could be observed. This facilitated the interpretation of the signals produced by the underlying substrate. Plasma reaction products coated on glass chips, W on sc and pc SI chips and Scotch tape were examined along with the Harris Corp. standard sputtered Au film. Both annealed and as-deposited samples were examined. A detailed list of the samples analyzed is presented in the next chapter.

Electrical Resistance Measurements

Two methods of observing the electrical resistance properties of the sample films were employed. The first technique consisted of observing the resistance across a 3 mm wide ceramic junction in an electrical feedthrough that had been heavily coated with plasma reaction products. The feedthrough was inserted into the substrate annealing chamber described earlier along with a thermocouple junction. The resistance was monitored as the temperature was slowly increased from 300-750 K. In one experiment hydrogen gas was flowed through the system at 200 ml/min. In a second experiment the system was left open to the ambient atmosphere. The purpose of these two tests was to observe any minima in the resistance values versus the temperature as

the reaction product film connecting the electrodes was heated under hydrogen and under air.

The second resistance measurement method used a 4-point probe technique, described in detail by L.B. Valdes,[71] to determine the sheet resistance, Rs, in ohms/square, of sample films coated on nonconductors (glass, quartz, Scotch tapes). An Alessi CPA/1 Resistivity Test Fixture with a 4-point osmium head was available for use in the laboratory of Prof. P. Holloway. Since the sample films were unevenly coated, and thickness determinations of the delicate films was not obtainable with available instrumentation, the main objective of these measurements was the determination of relative sheet resistance values for various areas on the samples.

Measurements were made by adjusting the input current to an appropriate level, measured in amps, and reading the voltage drop between the two outer probes and the two inner probes. The sheet resistance was then calculated using the relationship:

$$Rs = (V/I)(4.2)$$

The correction factor, 4.2, is based on a probe spacing equal to ~10% of the average specimen diameter. Since the probe spacing was 1 mm and the average sample film dimensions were not discernible due to the microscopic discontinuities inherent in the films, the sheet resistance values can be viewed only in relation to each other and to the standard sputtered Au film sheet resistance.

CHAPTER III
RESULTS AND DISCUSSION

In this chapter the experimental results are presented along with interpretive discussions relating the observations to known theories appropriate to each subject. The three phases of the study are treated separately, as in the preceding chapter, with one exception. A probable mechanism of formation of the gas-phase gold bearing species in the pulsed laser stimulated plasma is not presented until the final section of this chapter, after all of the experimental evidence has been presented.

Production of Gas-Phase Gold Species

Screening Study Results

As mentioned earlier, the purpose of the screening study was to identify gases and/or gas mixtures, operating pressures, and laser power density parameters that would result in the production of copious amounts of gas-phase gold species. Several parameters had to be considered simultaneously. Thus, the first experiments addressed the operational limits of the plasma reaction system with respect to gas pressure and laser power density levels. The next group of experiments investigated the use of He, Ar, H_2, and mixtures of He/H_2 and Ar/H_2 in the production system. Negative results with these mixtures led to the

the next group of screening study experiments which investigated the use of carbonaceous gases [CO, CO_2, CH_4, C_2H_2, $(C_5H_5)_2$] mixed with helium or hydrogen in the production system. The most successful candidates from this group of experiments, along with several chlorofluorocarbon/He gas mixtures ($CHClF_2$, CCl_2F_2, and C_2F_6) were then subjected to a series of semi-quantitative filter catch runs in order to determine the optimum conditions for Au transport in the gas stream. Finally, the most successful conditions (75% H_2/25% CH_4 at 1,330 Pascals) were utilized in the substrate coating and annealing experiments described in the next section.

The onset of gas breakdown and subsequent energy loss in the gaseous plasma prior to target impact was the first parameter investigated. Since Araya et al. had reported a peak in the production rate of ultrafine metal (Ti, Fe, Ni, Al, and Mo) particles from pulsed, Nd:YAG laser stimulated plasmas at air pressures of ~100,000 Pascals and power densities of 10^4-10^7 watts/cm^2,[27] the first experiments in this study attempted to duplicate this result using the pulsed CO_2 laser and a gold target. However, on observing the first few pulses of the focused CO_2 laser beam in air at atmospheric pressure in front of the Au target, it was apparent that gas breakdown could be initiated under these conditions. This phenomenon results from multiphoton ionization of the gases by the leading photons in the pulse, followed by a cascade of ionization when the free carrier density reaches a critical value. The change in density of free carriers is proportional to the density of the atoms and/or molecules and the spectral irradiance, as well as the physical properties of the gas species, such

as the photoionization crosssections and the ionization potentials. (T.P. Hughes offers an excellent review of both theory and experiments dealing with this phenomenon.)[72] When the effects of Bremsstrahlung radiation are considered, most notably the continuum spectrum produced by electron-neutral atom collisions in the initial stages of gas breakdown, the cascade effect and subsequent gas plasma formation is not surprising. The high density of continuum radiation produces a correspondingly high density of free carriers, ions, atoms, and molecules in a multitude of energy states. This scenario leads to a rapid increase in absorption of the incoming laser photons by the gaseous species, resulting in low irradiance of the target.

Thus, it was necessary to define the pressure limits for gas breakdown occurrence in the plasma production system. In experiment 860530 H_2 was supplied to the chamber at 110,900 Pa and the laser energy density at the target surface was varied by moving the focusing lens back 3 cm. Gas breakdown was observed in the form of a gas plasma located about 2 cm in front of the target impact point. As the lens was moved away from the target, the gas plasma moved synchronously, always remaining approximately 18 cm from the back side of the 20 cm focal length lens.

In experiment 86062A (see Table 2) the target was removed and standard grade helium was supplied to the plasma chamber at pressures ranging from 18,800-161,500 Pascals while the laser beam was focused into the center of the chamber. At pressures greater than 88,000 Pascals all of the laser pulses resulted in gas breakdown plasma formation. At 72,000 Pa ~95% of the pulses resulted in gas breakdown;

at 58,800 Pa ~70% of the pulses resulted in breakdown and at 18,800 Pa no breakdown was observed (see Figure 12).

A similar experiment, 880602B, was performed with the system open to the atmosphere (101,500 Pa). The first few pulses did not initiate gas breakdown, as had occurred in the initial plasma chamber start-up test and in experiment 860530, when the gold target was in place. However, subsequent laser pulses into the targetless chamber caused gas breakdown to occur 20-50% of the time. These observations could be explained by considering the laser/solid interactions that took place on the surface of the Au target and on the surface of the glass chamber back wall.

As the incoming photons struck the solid gold target surface some were reflected and some were absorbed by conduction band electrons that were then raised to higher energy states. Heat was generated in the metal by collisions of these excited electrons with phonons. The mean relaxation time in the highly conducting Au solid is on the order of 10^{-12} to 10^{-13} seconds[73] and the duration of the laser pulse was > 250 nsec. Thus, there was ample time for heating and vaporization of some of the Au during the early stages of the incoming pulse. This metal vapor was then ejected into the atmosphere in the path of the laser beam. This increased the optical density of the gas and initiated the gas breakdown observed. When the ambient gas pressure was lowered enough (in subsequent experiments), the effect of the metal vapor was not great enough to initiate the ionization cascade leading to gas breakdown.

Figure 12. Percent of CO_2 Laser Pulses Resulting in Helium Gas Breakdown Versus Pressure

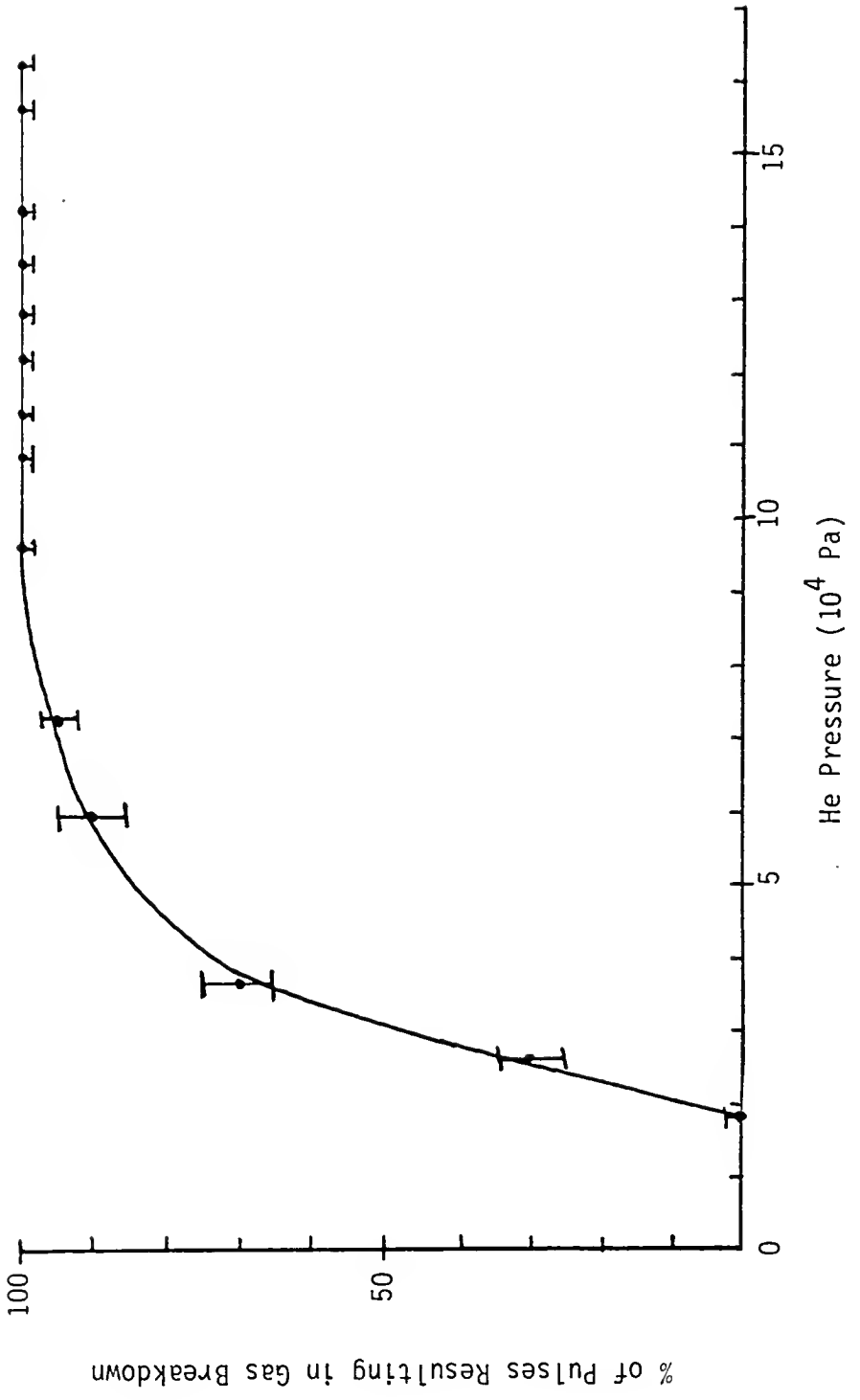
% of Pulses Resulting in Gas Breakdown
100
50
0
5
10
15
He Pressure (10^4 Pa)

When the target was removed and the system was left open to the atmosphere (no gas flow), the first few laser pulses impacted on the chamber back wall and no gas breakdown occurred. However, it was apparent from the visible interaction of the laser beam with the glass surface that material (probably hydrocarbon contaminants) was being vaporized and introduced into the chamber ambient. It was speculated that some of this material, in the form of small particles, randomly diffused to locations near enough to the beam focal point to be vaporized and increase the optical density of the local gas to a point great enough to initiate gas breakdown. Pulses that did not cause breakdown struck the back wall and introduced more particles into the chamber. The unpredictable appearance of the gas plasma during the part of the experiment following the first few pulses correlated well with this explanation.

As a result of these observations, all subsequent screening study experiments were performed at pressures < 18,000 Pa. Visual inspection of the product recovery systems, as described earlier, was used to indicate positive or negative results in this phase of the study. Referring to Table 2, a He/H_2 ~3:1 gas mixture was tried at pressures of 13,870, 6800, and 800 Pascals with negative results. Helium was then used alone at 800 and 1330 Pa, also with negative results. Argon at 1390 Pa also yielded negative results, as did a 3:1 mixture of Ar/H_2 at 1390 and 670 Pa, and a ~1:1 mixture at 750 Pa. Later in the study argon and helium were subjected individually to semiquantitative glass fiber filter catch experiments at ~1400 Pa (discussed below).

In all of these experiments, except the 100% Ar runs, the target was deeply cratered and there were pieces of Au in the bottom of the chamber. When 100% Ar was used the target impact point was a shallow crater and there was little Au debris in the chamber. The colinear shape of the plume in the Ar runs, compared to the more spherical plumes with the other gases, indicated that there was some partial gas breakdown occurring. This observation lead to the selection of He for use as the inert diluent gas in the remainder of the screening study.

The next experiment listed in Table 2 used a 3:1 mixture of helium and carbon monoxide at 4930, 2670, 1600, and 1200 Pa (expt. 860724). Gas breakdown occurred several centimeters in front of the target at pressures above ~2000 Pa. At 1600 Pa the entire chamber pulsed a bright white. The pressure was lowered to 1200 Pa and the system was allowed to run for ~13,000 laser pulses. By the end of the experiment a black, soot-like substance had thickly coated the glass plasma chamber and collected in the glass wool plug in the product recovery system. The next experiment listed (861106) started with 100% helium and then CO was added incrementally while maintaining the total pressure at 1600 Pa. Some soot formation was observed when the CO concentration reached 3.8%. As the concentration was increased to 5.2% and 10%, the production rate of the soot increased visibly. When the pressure was increased to 4000 Pa with the 10% mixture, no further production of soot was noted. Finally the CO concentration was increased to 12% and the pressure was increased to 9070 Pa (for a CO partial pressure of 1090 Pa. Again, no further soot production was noted.

The next experiment listed (861110) used a 4:1 mix of He/CO at 1530 Pa and ran for 14,400 pulses. A copious amount of soot was deposited on the plasma chamber walls and trapped on the glass wool plug (GWP) in the product recovery system. There were no visible deposits in the glass cold trap after the GWP. This trap was sealed and heated in a flame to ~900 K and then cooled with no resultant visible change in appearance (i.e., color change).

Extracts of the soot were prepared by placing pieces of the GWP in separate glass vials with hexane, toluene, acetone, water, and aqua regia and gently agitating them. There was no change in appearance of the systems containing hexane, toluene, or water, but the acetone extract took on a light purple color and the soot particles were visibly loosened from the glass fibers. The vial containing aqua regia showed complete dissolution of the soot. The extracts were then subjected to ultrasonic agitation for 30 minutes and allowed to stand for several days and were then analyzed by AA. Results indicated that the acetone extract contained Au in the bulk of the solution and associated with fine black particles that had settled to the bottom of the vial. There was no indication of Au in the other solvents that was not associated with the particles, except for aqua regia which had dissolved the particles.

The next series of experiments used mixtures of acetylene and helium containing 2.5, 8.3, and 19% C_2H_2 at 1400 Pa and ~10,000 laser pulses. The product recovery system used in these experiments had a test tube placed in the gas stream as it exited the chamber (see Figure 8). In two runs (19% and 2.5% C_2H_2) this tube was cooled to 195 K with

dry-ice and in the third run it was at room temperature. A very light amount of deep purple/black soot was deposited on this test tube and in the cold trap in the 2.5% C_2H_2 run; a very heavy coating of black soot resulted from the 8.3% run; and a moderate amount of black soot was collected in the 19% run.

The cold trap contents of the second run were subjected to the solvent extraction test described above with the same results. Figure 13 shows an example of the increase in the Au AA signal when the instruments sampling tube was placed in the bottom of the acetone extract vial. It was apparent that the Au particles were small enough to atomize in the instruments air/acetylene flame.

The remaining cold traps and all three coated test tubes were heated in a bunsen burner flame and yielded pink to red colored thin films indicating the presence of gold.[74] The thicker areas of the films on the test tubes and at the cold lines on the inlet sides of the cold traps were metallic yellow in color. The original black color film that coated the glassware changed to deep purple and then disappeared within a few seconds after heating to yield the red and yellow films which persisted. These tests were considered positive because of the relatively large amount of Au transported from the plasma zone to the cold trap, and CO was selected for further evaluation despite its moderate toxicity.

Experiment 861126 utilized the mixture of helium gas saturated with dicyclopentadiene described earlier. This test was run for 3660 laser pulses and produced a very heavy, sticky black soot-like residue that deposited on the chamber walls and in the cold trap. The cold

Figure 13. AA Spectrum of Cold Trap Acetone Extract Showing Enhanced Au Signal from Particles

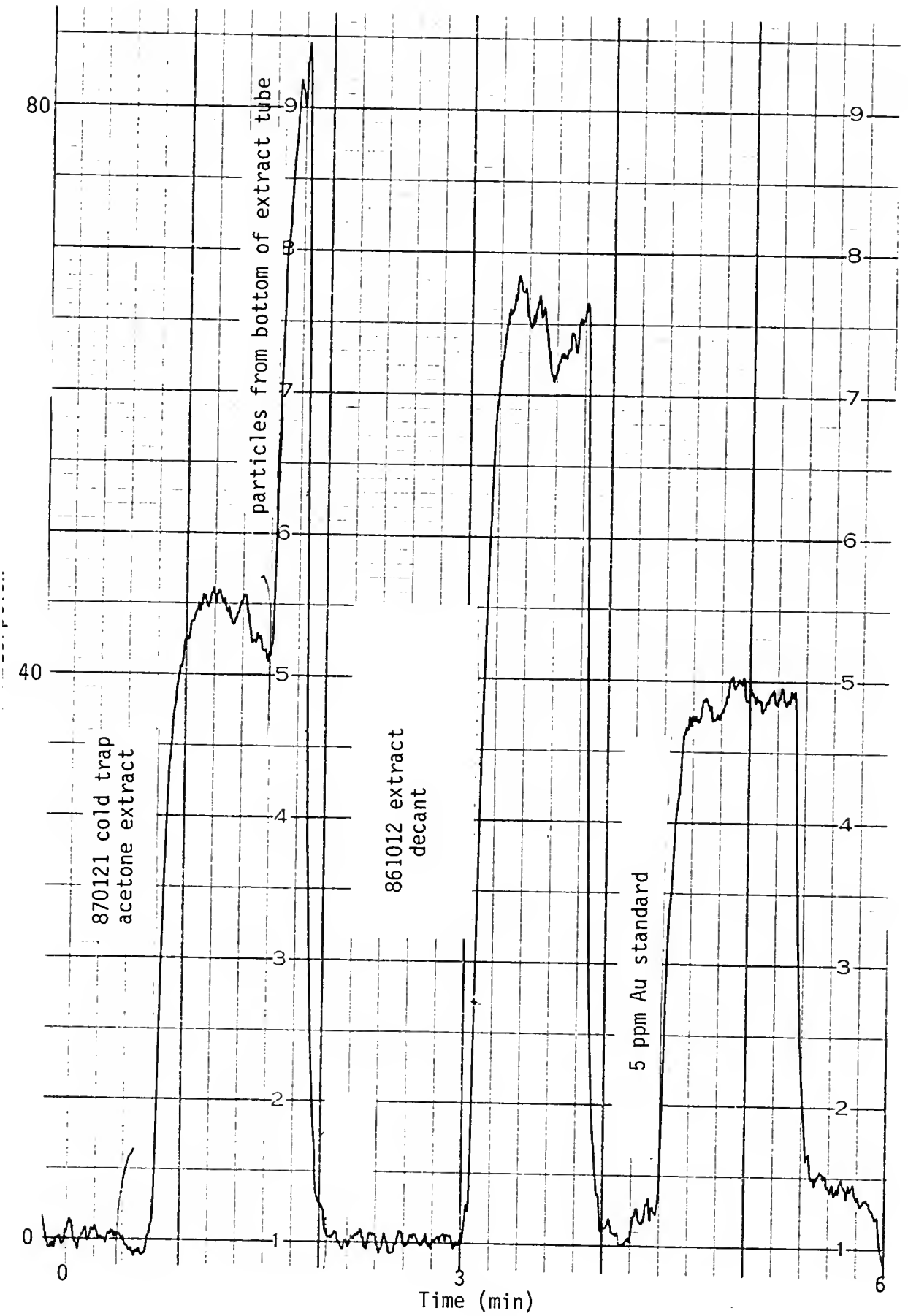
80
40
0
0
3
6
Time (min)
particles from bottom of extract tube
870121 cold trap
acetone extract
861012 extract
decant
5 ppm Au standard
9
8
7
6
5
4
3
2
1

trap was sealed and heated in a flame as described above. The dark deposit did not change significantly in appearance until the tube was unsealed and reheated in air. The dark deposits seemed to burn off and left behind a thin area of pink colored film associated with the heaviest deposits in the trap (these were located at the cold line on the inlet side). Thus, this test was considered negative.

Pure methane gas was used in experiment 861022A which was run for ~4000 laser pulses. Some light gray deposits were noted in the cold trap. Some grains of Au were also present in the bottom of the plasma chamber. The cold trap was heated in air as described above and yielded a very light pink film in the areas of heaviest deposition. This test was considered negative.

The next series of experiments listed in Table 2 utilized ~3:1 mixtures of CH_4/He at pressures between 1470 and 2000 Pa. The first two tests in this series, 860701 and 860702, used the heated quartz tube recovery system with a gas residence time of 3 msec and operated at temperatures of 893 and 573 K, respectively. In the first test, which lasted for 5400 laser pulses, a light purple residue was found in the middle of the heated tube and a dark purple to gold colored residue was found in the exit end of the tube. No colored deposits were collected in the cold trap after the heated tube. The second test was run for 7020 pulses and yielded similar results except all films were darker and some purple deposits were found in the cold trap. These tests were considered positive.

In the next experiment in this series, 860704, the focal point diameter at target impact was increased from the optimum to 1.2 mm,

effectively decreasing the power density from 3×10^9 to 9×10^8 watts/cm^2. The test was run for 2460 pulses at the lower power density with negative results. The focus was then optimized and within a few hundred pulses visible deposits had appeared in the first two cold traps (273 and 195 K). At the end of the run a moderate amount of product was present in the first trap and the remainder was in the second trap. No visible deposits were present in the third cold trap. This completed the experiments performed in the glass plasma reaction chamber. The aluminum chamber was used in the remainder of the study.

Two more experiments in the above series, 861012 and 861023, showed that the Au was associated with the soot-like product particles and could be isolated in the GWP. The cold traps after the GWP had clear deposits that turned yellow on warming to room temperature and then turned black when heated in the flame under He. The black deposits disappeared in a few seconds when the traps were reheated in air, leaving the glass clear.

At this point in the study a "blank" run was performed (861022C) using the same gas mixture at 800 Pa and a graphite target. No dark deposits were observed, but a clear condensate was found in the cold trap. This material behaved identically to the cold trap contents after the GWP in the last two runs. It was assumed that this material was a mixture of various unsaturated hydrocarbons that polymerized on heating in He and combusted on heating in air.

The next series of experiments utilized a mixture of ~18:6:1 He/CH_4/air at 1200 and 1600 Pa and ~7000-10,000 laser pulses. Results were similar to earlier He/CH_4 runs with one exception. The relative

abundance of the Au films in relation to the soot deposits appeared to be less. These tests (861016, 861017, and 861018) were considered positive.

The next two experiments, 870109 and 870324, used a ~4:1 mix of hydrogen and methane at ~1300 Pa. The first test gave the best results in the study up to that point. The dark purple deposits in the cold trap yielded the heaviest Au film observed up to that point and this gas mixture was selected for further investigation.

In experiment 870324 two focal point diameters larger than the optimum were investigated: 2.4 mm, corresponding to a power density of 2×10^8 watts/cm^2; and 1.1 mm, corresponding to a power level of 1×10^9 watts/cm^2. The plasma was very small with the lower power density and no deposits were observed in the cold trap after 4200 laser pulses. The plasma was somewhat larger with the 1.1 mm dia. focal point but only a light deposit was collected in the cold trap after ~3000 laser pulses. These tests were considered negative.

One experiment was performed using a 3:1 mixture of hydrogen and natural gas (870313) at 1420 Pa for a duration of 10,200 pulses. The results were positive, but the relative proportion of Au film left in the cold trap after heating the black deposits was less than the amounts observed in the H_2/CH_4 experiments.

This concluded the screening study experiments that used visual observations to evaluate results. The final series of screening study tests were performed using the glass fiber filters (GFF) and holder described in the last chapter. These tests provided a semi-quantitative measure of the amount of Au transported from the plasma

zone to the filter. The majority of these tests lasted over 20,000 laser pulses. The tests involving the chlorofluorocarbon gas $CHClF_2$ lasted 3660 and 5160 pulses and the tests involving graphite and copper targets lasted ~10,000 pulses (refer to Table 2 for pulse values). Table 6 lists the GFF runs with the gravimetric and AA results listed in weight per 1000 pulses. The GFF catches that consisted mainly of large particles (those discernible under visual microscopy) are asterisked. The bulk of the mass collected on the remaining filters was in the form of the superfine particles observed in earlier experiments.

The effectiveness of CH_4 and CO in transporting Au in the form of the superfine soot-like material was verified in these experiments. A strong dependency on the partial pressure of the carbonaceous gas in hydrogen was exhibited in these tests. Figure 14 shows a plot of this relationship for CH_4 and CO and indicates the optimum production rate occurred at ~350 Pa. Araya et al. also observed a strong dependency of the production of superfine Ti particles on the gas (air) pressure in their pulsed Nd:YAG stimulated plasma reaction system, although their peak production rate occurred at ~100,000 Pascals.[27]

The concentration of Au in the material produced in these tests ranged from 82-99%, with one outlying value of 37% (expt. 880224). The target was rotated only every 1.5-2.0 hours in this experiment, as opposed to every 30 minutes in the other experiments. The deep and variable cratering of the Au target produced varying nozzle configurations for the plume expansion during the test time and apparently affected the amount of carbonaceous material incorporated in

Table 6. Filter Catch Plasma Experiment Results

Expt. No.	Gas Mix	Target	Total Pres. (Pa)	Carbonaceous Gas Pres. (Pa)	Filter Catch (μg/1000 pulses) Total (grav.)		Gold (AA)	% Gold
880218	Ar	Au	1390	0	--		0.9	--
880222	He	Au	1370	0	27		0.7	2.6
880223	CH_4/H_2	Au	1350	324	264		217	82
880224	CH_4/H_2	Au	1390	360	782		291	37
880302	CH_4/H_2	Au	1380	261	347		343	99
880303	CH_4/H_2	Au	670	174	68	*	61	90
880304	CH_4/H_2	Au	2710	705	92	*	43	47
880307	CH_4	Au	1470	1470	226	*	26	12
880309	CH_4/H_2	Au	670	348	348		285	82
880311	CO/H_2	Au	1390	375	216		205	95
880317	CO_2/H_2	Au	1390	348	58		56	96
880239	$CHClF_2$/He	Au	1470	382	4830		--	--
880415	$CHClF_2$/He	Au	300	72	607		--	--
880421	CCl_2F_2/He	Au	1360	326	866	*	--	--
880425	$CCl_2F_2/He/H_2$	Au	1370	192	1307		--	--
880427	C_2F_6/He	Au	1240	335	225	*	--	--
880720	CH_4/H_2	Graphite	1350	351	<20	*	--	--
880723	CH_4/H_2	Copper	1350	351	163	*	--	--
880724	CH_4/H_2	Copper	1410	367	174	*	--	--

*Nearly all of the material was in the form of large particles.

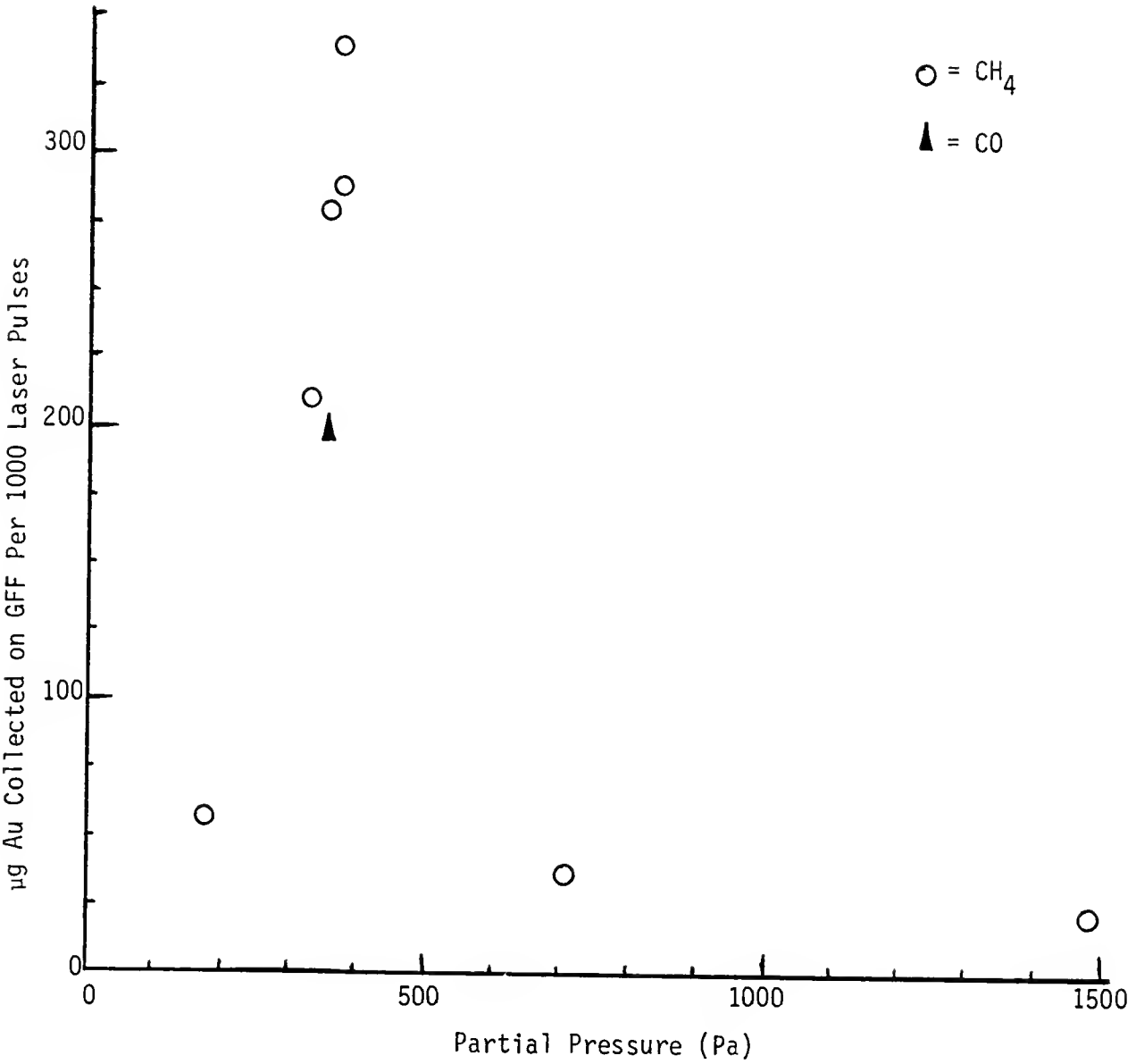

Figure 14. Weight of Au Collected by the GFF Versus CH_4 and CO Partial Pressures

the material. This apparent nozzle configuration dependency was also observed by Hagena and Obert when forming clusters from CO_2 in expanding supersonic jets.[75]

The three halogenated species examined also exhibited some pressure dependency on the production rate of particulate material collected on the GFF. This material ranged in color from light brown to black and was not wetted by aqua regia. In this respect it behaved very similarly to teflon. This was in sharp contrast to the immediate dissolution in aqua regia of the material produced by CH_4, CO, and CO_2. The Au target in all of the halogenated gas experiments was only slightly pitted with a shallow crater, indicating very little Au mass removal. This result was similar to that observed in other experiments where gas breakdown had occurred, but the gas plume before the target was not observed in these tests. There was also an indication that the presence of hydrogen enhanced the production rate of fine particulate material from the saturated chlorofluorocarbon, CCl_2F_2. These compounds were not investigated further due to their potential for contaminating the VLSI microcircuitry with Cl and F and their low incorporation of Au (as evidenced by the target impact).

The one test that used a graphite target and the 3:1 H_2/CH_4 gas mixture at 1350 Pa verified earlier observations of no soot production by plasmas under these conditions. The target was deeply pitted after 10,000 pulses and there was a large amount of particulate debris in the bottom of the chamber, but the GFF was essentially clean. This indicated that the Au was necessary for the formation of the

carbonaceous material that was transported to the GFF along with the superfine Au particles.

The two tests that used a copper target and the 3:1 H_2/CH_4 gas mix at ~1400 Pa yielded negative results in terms of superfine particle production. Inspection of the target after ~9000 pulses in the first test revealed very little Cu removal in the 1.5 mm dia. impact spot, despite operating at the optimum lens focal distance. In the second experiment with the Cu target (880724) the lens was moved 10 mm closer to and farther away from the target while the chamber pressure was at 200 Pa. The target was removed and inspected under the microscope after several hundred laser pulses at each focal distance adjustment. The greatest degree of cratering occurred at the optimum focal distance. The test was continued for ~10,000 pulses at 1410 Pa pressure and the optimum focal distance and again yielded negative results.

During these two experiments some gas breakdown was observed in the first few pulses. The metal surface at the impact point appeared to melt during these pulses and then became highly reflective to the laser beam as evidenced by reflected impacts on the plasma chamber wall. This phenomenon had not been observed previously in the study. This point is discussed further in the final section of this chapter.

From the results of the screening study the 3:1 H_2/CH_4 gas mixture at 1350 Pa was identified as the best conditions for production of the Au bearing species which appeared as superfine particles. The state of the Au in these particles was not known at this point, but the copious amounts produced in the plasma reaction system and the apparent ease of

formation of Au films on the glassware that had been coated with the product warranted further investigation of this material. Although CO appeared to produce similar products under the same conditions, its higher toxicity excluded it from further investigation.

Substrate Coating and Annealing Results

The substrates that were coated are listed in Table 3 in the experimental section. All coating experiments were performed at 1330 Pa and most utilized the 3:1 H_2/CH_4 gas mixture. One exception was the run where glass plates and W on Si chips were placed in the plasma chamber ~3 cm from the target impact and exposed to the plasma produced in 100% He at 1330 Pa. After 15,000 laser pulses these plates had a shiny metallic Au coating similar to those produced in Au evaporation systems. There was no carryover of Au into the recovery system and the substrates displayed stratified films consistent with line of sight deposition.

The 5 cm long piece of W ribbon placed in the recovery system glass tubing and irradiated with the Ar ion laser while being exposed to the reaction products produced in a H_2/natural-gas/Au plasma showed a stratified color change from yellow-brown to purple to black starting ~1 mm away from the laser impact point. The pattern was symmetrical on both sides and indicative of the expected thermal gradient.

The 1 cm long piece of W ribbon that was irradiated with the same laser through a quartz window while being exposed to the reaction products from a H_2/CH_4/Au plasma was completely free of deposits at the end of the run. Recall that this ribbon glowed red under vacuum and

was a very dull red under the experimental conditions. Thus, it appeared that the surface temperature of the W was too high to allow the plasma reaction products, or their resultant thermal decomposition products, to stick.

The Scotch brand transparent tape, adhesive side, that was exposed to the H_2/CH_4 reaction products in the substrate coating chamber had a shiny metallic gold appearance even though the glass and W substrates adjacent to it appeared black when coated. This behavior was consistent throughout the study whenever the tape was used to hold other substrates in place or exposed by itself. This was a very interesting phenomenon and the coated tape was selected for further characterization of the Au film. When the other side of the tape was coated the film was purple-black in color, similar to the appearance of the film when coated on glass.

The Scotch brand black electrical tape displayed the reverse behavior: The plasma reaction products could not be seen on the sticky side, but the deposits appeared as a dull metallic yellow film on the back side of the tape. Samples of this surface were also subjected to further tests.

All of the product coatings were easily wiped off of the substrates, except for the metallic films on the two tapes, and thus were not capable of withstanding a profilometry test for thickness determination. The tape samples were not flat enough to undergo profilometry. The remaining substrates that were coated were subjected to annealing and/or further testing.

Substrate annealing conditions were described in the last chapter and listed in Table 4. The Au bearing material behaved consistently in all experiments. Substrates heated in air to 470 K changed in color from black to deep purple. This color persisted even when left at 470 K for 12 hours. When the temperature was increased to 500 K the color changed to pink within a few minutes. At temperatures > ~650 K the color change took place in a few seconds. Similar results were observed in substrates heated in H_2, except the final color had a brown tint. Samples that were first annealed in air and then H_2, and vice versa, did not exhibit a change in color after the first anneal.

Early in the study the unfocused pulsed CO_2 laser beam was used to anneal a coated glass chamber window. The first few pulses produced a visible vapor cloud originating at the coated surface. At the same time the black coating turned purple. After ~20 pulses the coating had turned pink, and after ~40 pulses the coating had turned a bright gold. Under an optical microscope relatively large flakes of Au (hundreds of microns) were clearly visible. These flakes formed an overlapping discontinuous film. The surface was exposed to another 20 pulses of the laser with no change in appearance. The coating was very tenacious and was difficult to scratch off the glass surface.

The W on Si substrate that was annealed in the rf coil by bringing it to red heat appeared to lose most of the product coating in the form of a vapor cloud. This may have been caused by the rapid heating and vaporization of the carbonaceous species that caused the small Au particles to be physically blown off the substrate surface with the expanding gas plume.

The same type of substrate was subjected to pulsed rf heating under a vacuum (0.013 Pa) and looked similar to convectively heated samples. A coated glass substrate annealed under the same conditions did not exhibit a color change. These observations indicated that the annealing effect on the W coated chip was due to the heating of the W layer and not the Au plasma product thin film.

The coated W on Si substrates that were heated with the focused argon ion laser beam in air showed a very light, thin line of discoloration (dark brown) at all laser power levels and substrate pull rates. The one sample that was exposed to the beam continuously for 10 seconds in one spot was subjected to SEM analysis and showed only a slight change in appearance between the annealed and unannealed areas. This difference appeared as an increase in size of pores between grains, as would be expected if material had volatilized rapidly. It was also apparent from the micrographs that the W substrate had conducted the incoming heat away from the impact point, thus limiting the local heating effect of the laser beam. These micrographs are presented in the section on thin film characterization.

The coated glass substrates that were exposed to the focused Ar ion laser beam displayed radically different behavior. At the higher power levels the beam path appeared as a strip of bright metallic gold islands. At the lowest power level the line was a semi-continuous double ridge of metallic Au with a trough in the middle where the center of the beam had passed. These observations were indicative of direct and rapid heating of the product film by the beam on the non-conductive glass surface. This meant that the thermal conductivity of

the product film must have been of the same order of magnitude as W in order to not exhibit formation of metal islands on the W surface even after the extremely long exposure times relative to the glass substrates.

Product Volatility Study Results

This phase of the overall study was divided into three sections, as described in the last chapter. The results of the first two sections, described below, indicated that there were no detectable volatile Au compounds present in the reaction products that were capable of being isolated by differential condensation or sublimation. The results of the third section indicated that gold-carbide compounds could be formed in a pulsed Nd:YAG laser stimulated plasma in 1% CH_4 in He at ~100,000 Pa.

Sublimation Experiments

The two sublimation experiments described in the last chapter were both negative. The Au was associated with the purple-black soot-like superfine particles in all tests and could not be isolated by thermal desorption even at reduced pressure. In addition, all attempts to isolate or separate volatile Au compounds from the product gas stream by differential condensation using staged cold traps were also negative. These results lead to the next section of mass spectrometer tests that attempted to identify Au compounds in the plasma reaction products.

Mass Spectrometer Experiments

Samples subjected to MS analyses and the pertinent conditions are listed in Table 5 in Chapter II. In the first experiment a sample of the black tar-like residue found on the Au target after a plasma run that utilized a 3:1 He/CH_4 gas mixture at 1330 Pa was placed in a solids probe and slowly heated to 670 K while observing the mass response from 0-494 a.m.u. A total ion count spectra from this test is presented in Figure 15. The most striking feature is the prominent peak at mass 155 and the preponderance of compounds between mass 100 and 200. There were also significant amounts of compounds over mass 200, but there were no prominent peaks. These results were considered encouraging at the time and prompted further MS investigations.

In the second MS analysis a sample from the chamber sidewall that was recovered after a plasma run that utilized a 93% H_2/8% C_2H_2 gas mixture at 1330 Pa was dissolved/suspended in acetone and injected into the GC/MS system described earlier. No mass peaks larger than the background signal were observed over 59 a.m.u. The most prominent peak appeared at mass 43. Table 7 lists the mass response and relative counts of the peaks between 0-60 a.m.u. Note that the measured mass values listed are off by 1 a.m.u. as evidenced by the N_2 and O_2 peaks appearing at listed values of 27 and 31 a.m.u., respectively.

All of the remaining tests in the MS study used plasma reaction products formed in 75% He/25% CH_4/Au plasma experiments. These compounds are referred to as "P.R.P." throughout the remainder of the text and figure headings. Any different conditions are noted explicitly.

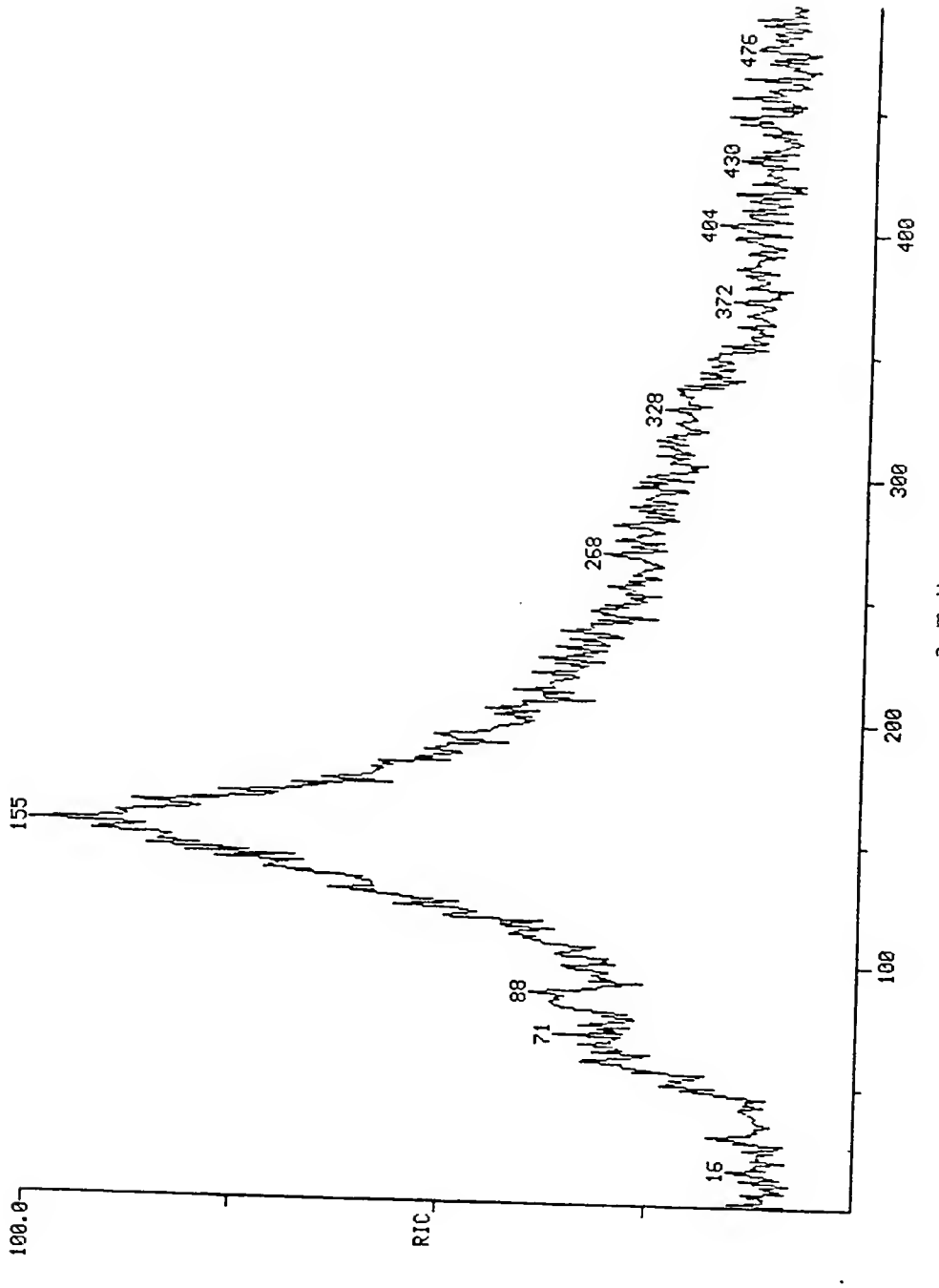

Figure 15. Total Ion Count Mass Spectra of Target Residue

Table 7. GC/MS Results from an Acetone Extract of H_2/C_2H_2/Au Plasma Reaction Products

Measured Mass	No. Points	Absolute Intensity	% Int. Base	
60	10	230.	0.02	
59	25	3610.	0.32	
58	35	101848.	8.89	
57	25	3293.	0.29	
55	21	1318.	0.12	
53	25	1708.	0.15	
52	14	524.	0.05	
45	25	2935.	0.26	
44	43	31945.	2.79	
43	10	218.	0.02	
43	10	260.	0.02	
43	10	294.	0.03	
43	100	1145792.	100.00	↑
43	14	397.	0.03	
43	10	222.	0.02	
43	8	243.	0.02	
42	51	97096.	8.47	
41	51	31701.	2.77	
40	71	15236.	1.33	
39	35	64466.	5.63	
38	29	40396.	3.53	
38	25	1340.	0.12	
37	29	37884.	3.31	
36	43	13643.	1.19	
35	14	313.	0.03	
32	21	573.	0.05	
32	29	12302.	1.07	
31	29	16568.	1.45	
30	21	1662.	0.15	
30	25	3212.	0.28	
29	35	53504.	4.67	*
29	35	71524.	6.24	*
28	25	38747.	3.38	*
28	43	121284.	10.59	*
27	71	241396.	21.07	
26	51	168440.	14.70	
25	35	41736.	3.64	
24	29	8783.	0.77	
20	35	6703.	0.59	
19.5	29	4904.	0.43	
19	29	8404.	0.73	
18	29	51041.	4.45	

In the third experiment a cold trap coated with the P.R.P. was connected to the solids probe inlet and heated to 680 K while observing the mass response from 0-500 a.m.u. The results of this test were similar to the first MS test with the most prominent peaks occurring at 44 and 150 a.m.u. (results not shown). No significant peaks appeared over 150 mass units, while a preponderance of the peaks appeared below 100 a.m.u.

The fourth experiment utilized the Nicolet ICRMS to look at a sample of the cold trap contents collected after a glass wool plug during a P.R.P. production experiment. The most prominent peak was at mass 44 and the remainder of the peaks were below 100 a.m.u. (results not shown). A sample of triethylphosphinegold chloride (TEPGC) was placed in the solids probe following this analysis and the resultant spectra of the volatile Au compound (Figure 16) confirmed the instrument's response. The parent ion peak (minus one H) appeared at 349 a.m.u. and the parent ion minus Cl appears at 315 a.m.u.

In the fifth MS experiment a glass plate coated with P.R.P. was placed in the inhouse fabricated ICRMS adjacent to the ICR cell and observed as it rose to 180^{o}C over one hour. Figure 17 shows the large amount of low mass peaks that appeared at two minutes. After 10 minutes mass 44 was the most prominent peak (Figure 18) and mass 150 was starting to grow in. By 25 minutes mass 150 had become very prominent, mass 296 was prevalent, and mass 44 was still the highest peak (Figure 19). After 55 minutes the mass 44 signal had decreased substantially and mass 149 was the highest peak while mass 296 had also increased (Figure 20).

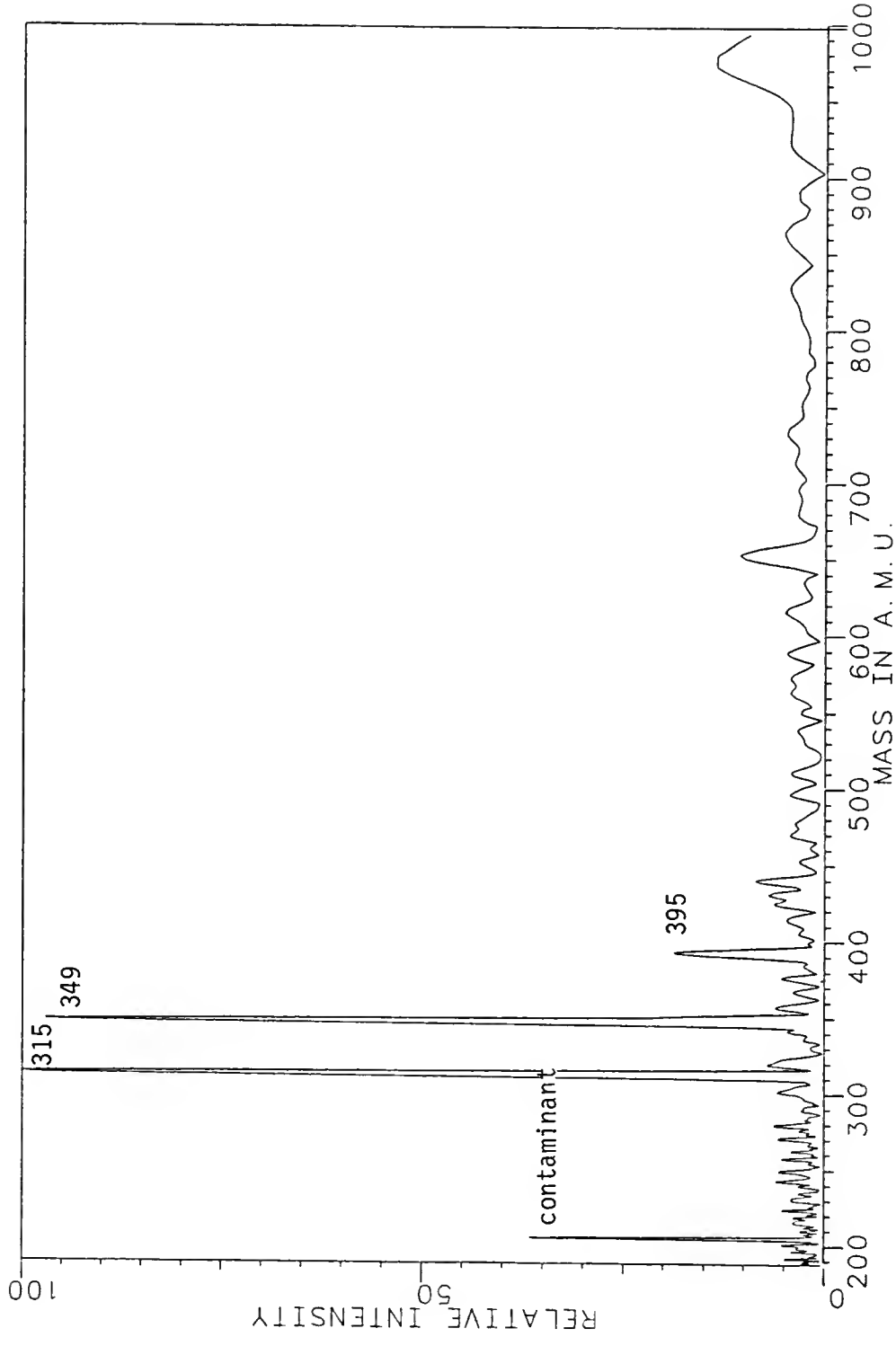

Figure 16. ICRMS of Triethylphosphine Gold Chloride

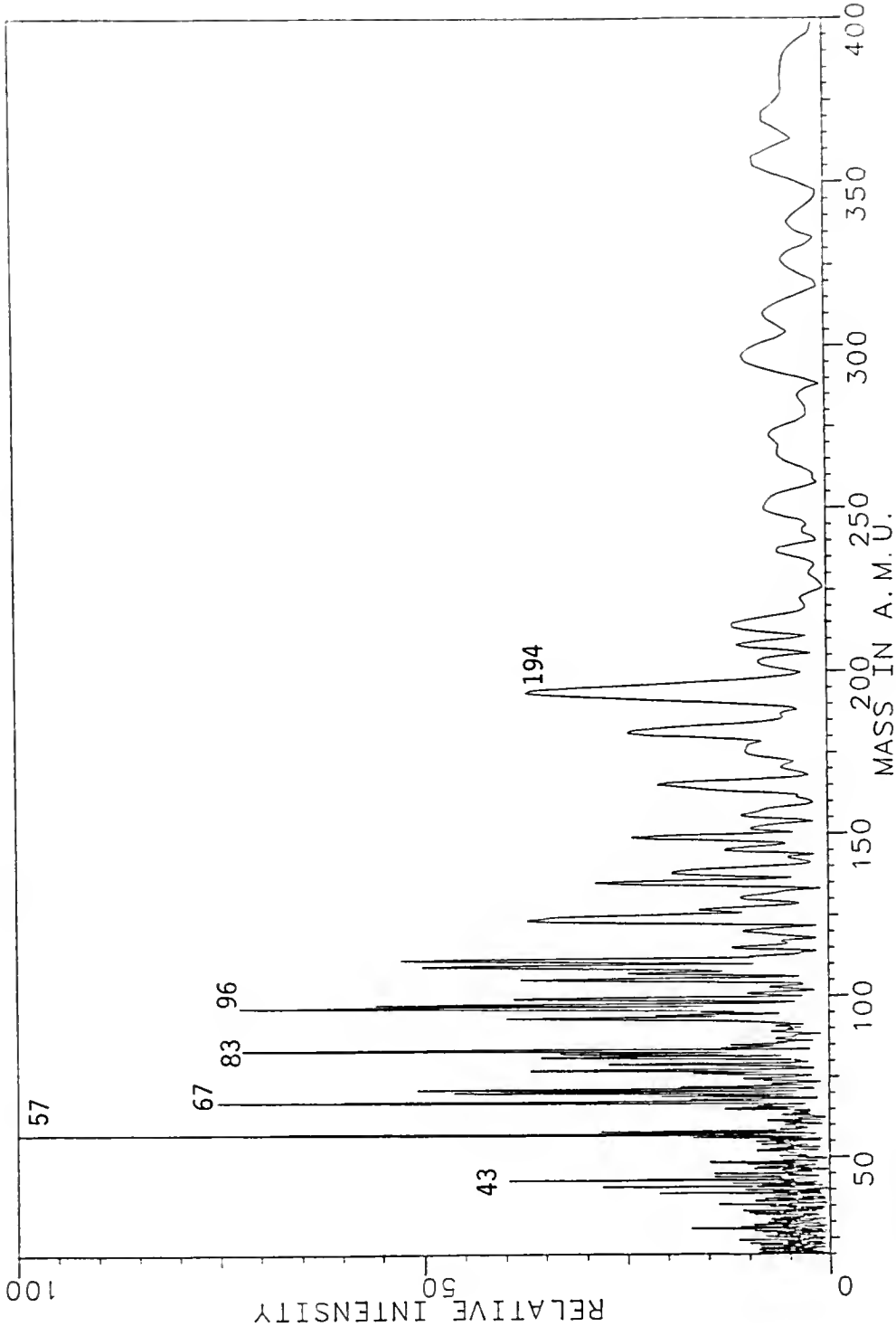

Figure 17. ICRMS (0-400 a.m.u.) of P.R.P., 2 Minutes

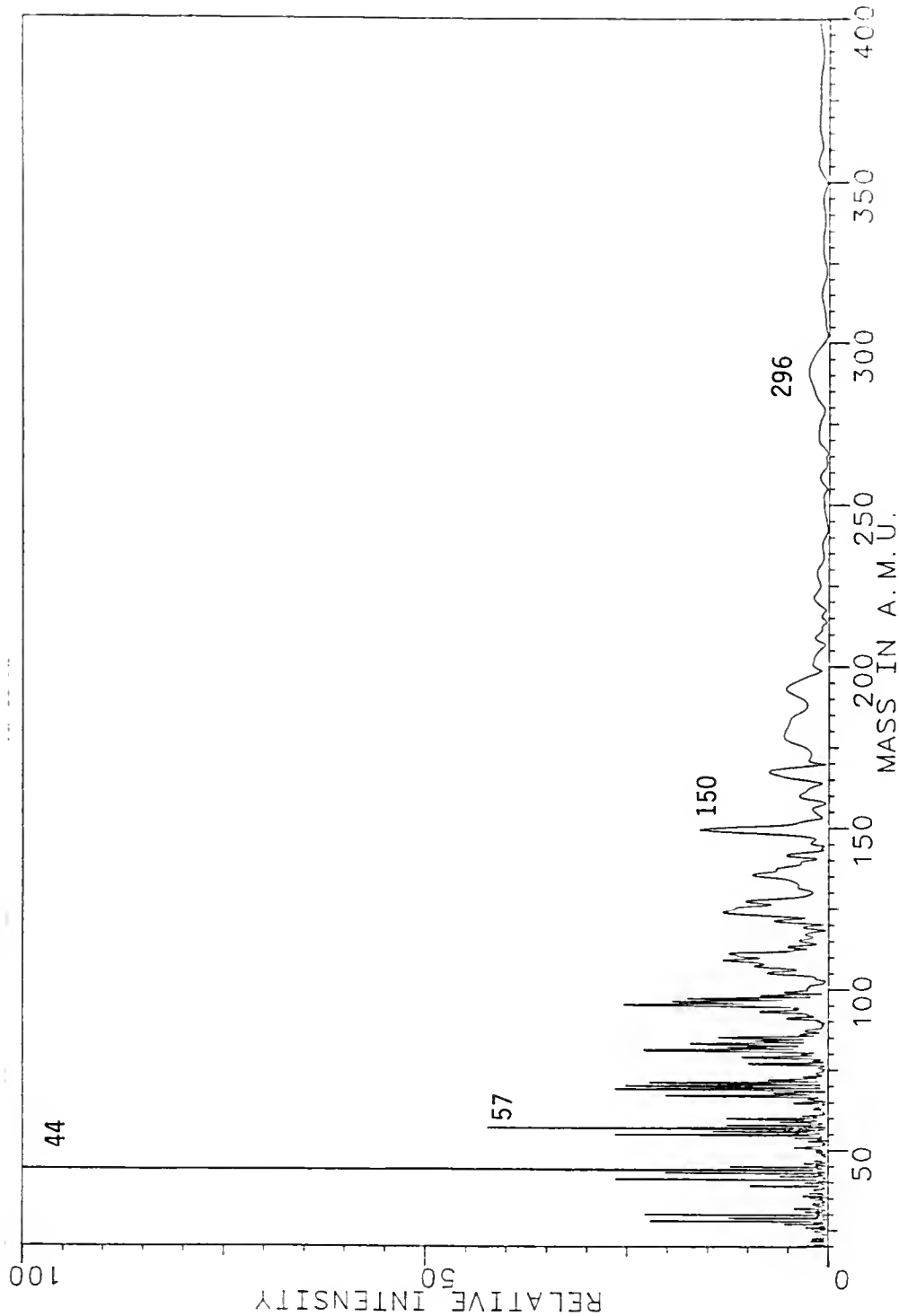

Figure 18. ICRMS (0-400 a.m.u.) of P.R.P., 10 Minutes

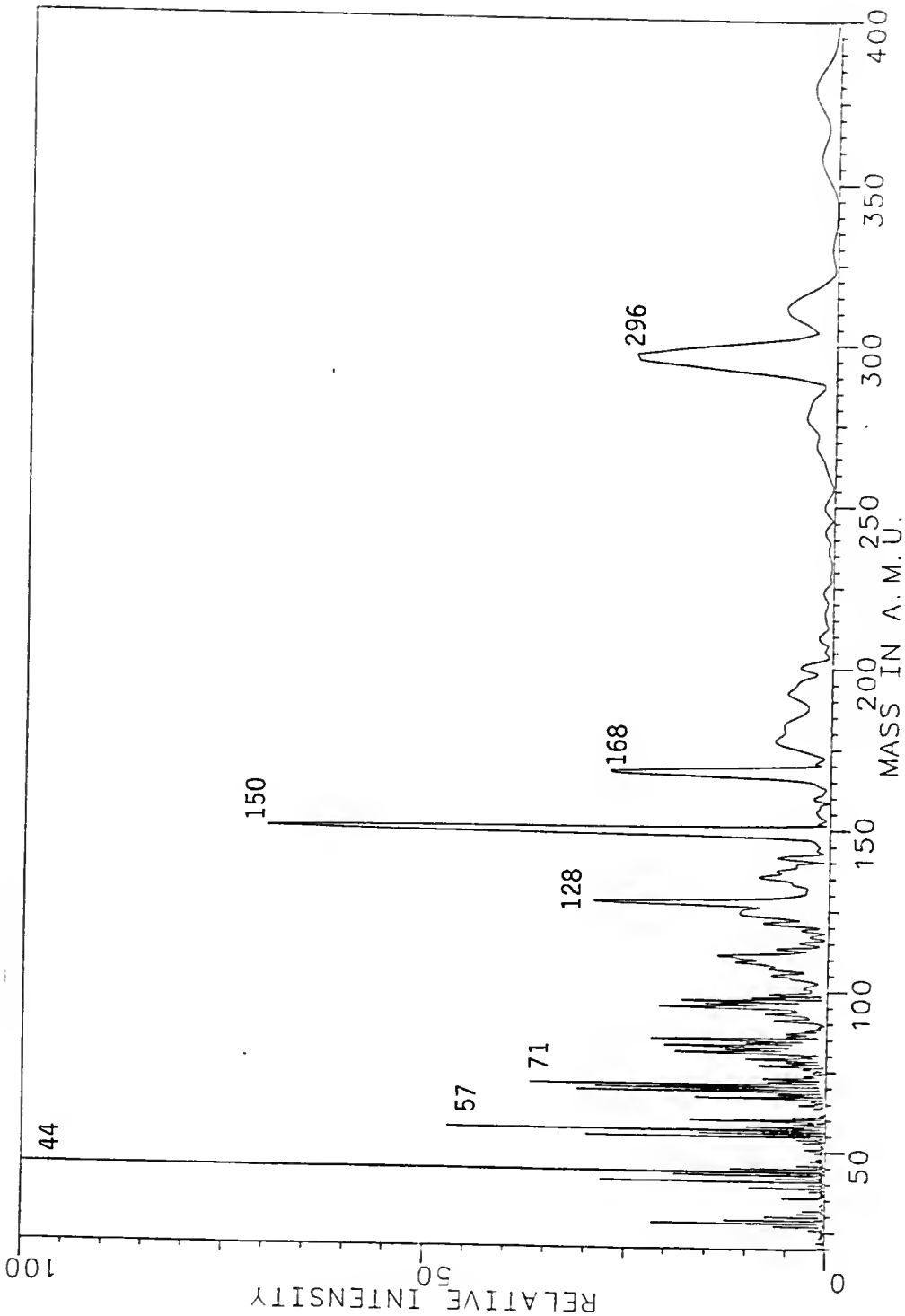

Figure 19. ICRMS (0-400 a.m.u.) of P.R.P., 25 Minutes

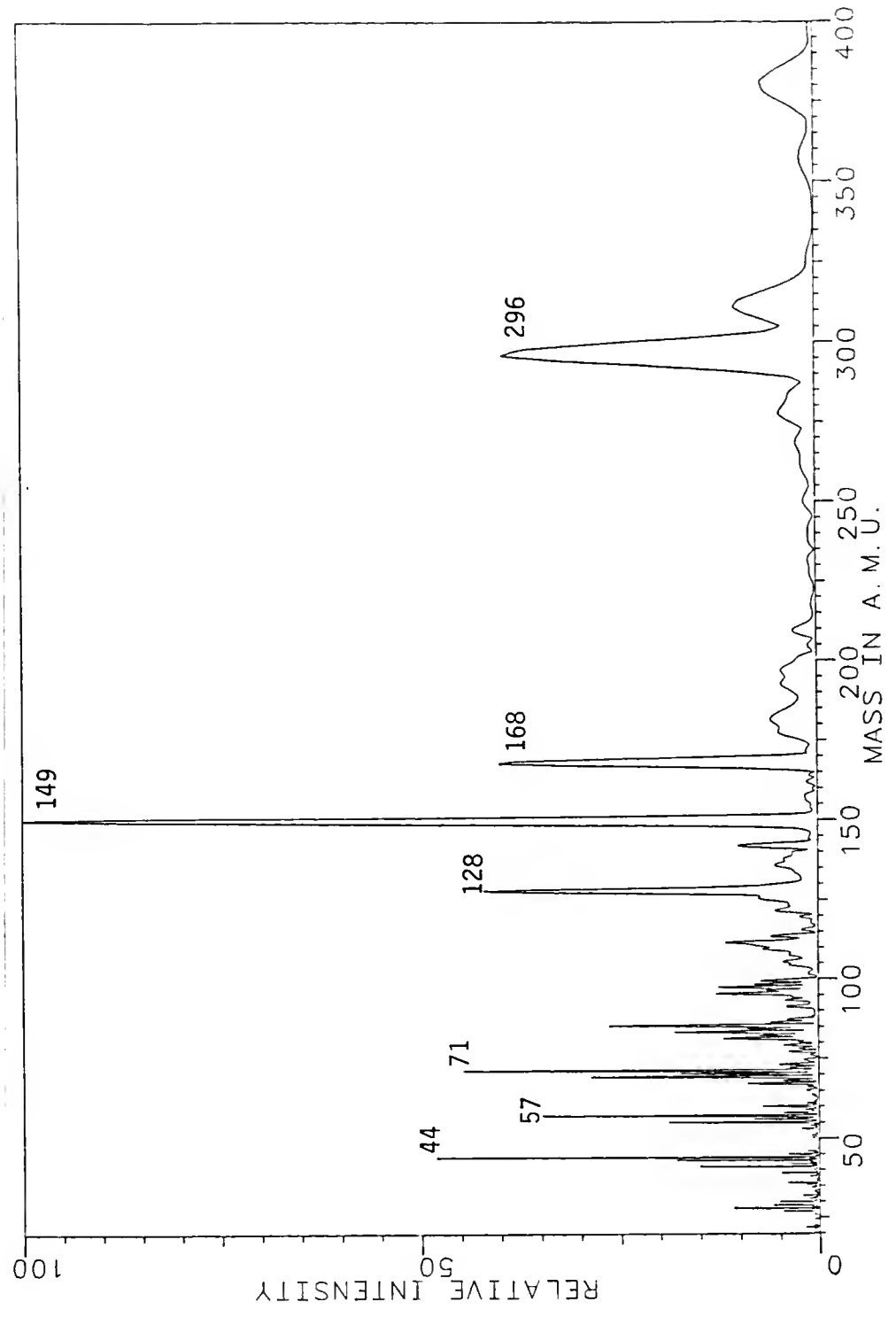

Figure 20. ICRMS (0-400 a.m.u.) of P.R.P., 55 Minutes

At this point the pulsed Nd:YAG laser was used to irradiate the sample and the mass 44 signal increased dramatically (Figure 21). Even after 20 minutes of continuous pulsing with the laser, the mass 44 signal still dominated the spectrum (Figure 22). Next, the electron beam was turned off and the spectrum was recorded while the laser was still pulsing. Figure 23 shows the resultant mass spectra with no peaks over ~20 a.m.u. significantly stronger than the background.

This experiment was repeated in the Nicolet ICRMS and spectra were recorded at temperatures of ~50^{o}C (Figures 24 and 25), 125^{o}C (Figure 26), and 175^{o}C (Figures 27 and 28). The low mass hydrocarbon pattern that had been observed in all previous mass spectra of the P.R.P. was again present along with several prominent high mass peaks at 195, 255, 334, and 349 a.m.u. These peaks had not been observed before and there was a sharp cutoff at mass 349 as shown in the 0-1000 a.m.u. spectra in Figure 28. This spectra also shows the mass 44 and 149 peaks that were noted in previous work.

Since there was some question of possible contamination from other sources (the instrument was used extensively to analyze a variety of samples), CID reactions were run on the high mass peaks 195, 255, 334, and 349. Figures 29 and 30 show the results of CID on mass 334 at -0- collision time and after 50 msec of collision time, respectively. The major product appeared at mass 255. The CID on mass 349 under the same conditions is shown in Figures 31 and 32. Some increase in mass 255 signal, and the appearance of a moderate signal at 178 a.m.u., were the only changes noted. The CID reactions on the remaining compounds

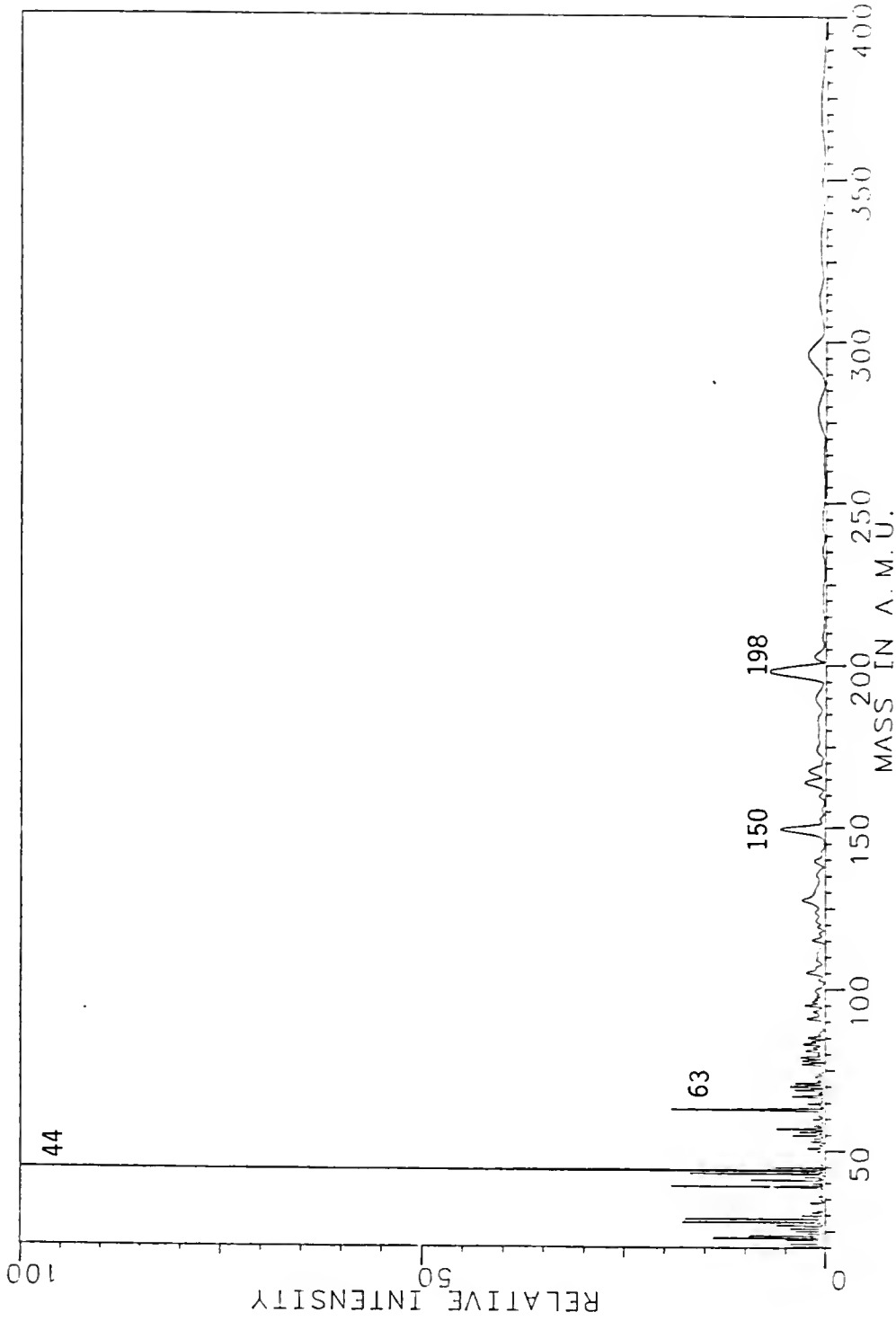

Figure 21. ICRMS (0-400 a.m.u.) of P.R.P., 60 Minutes, Laser On

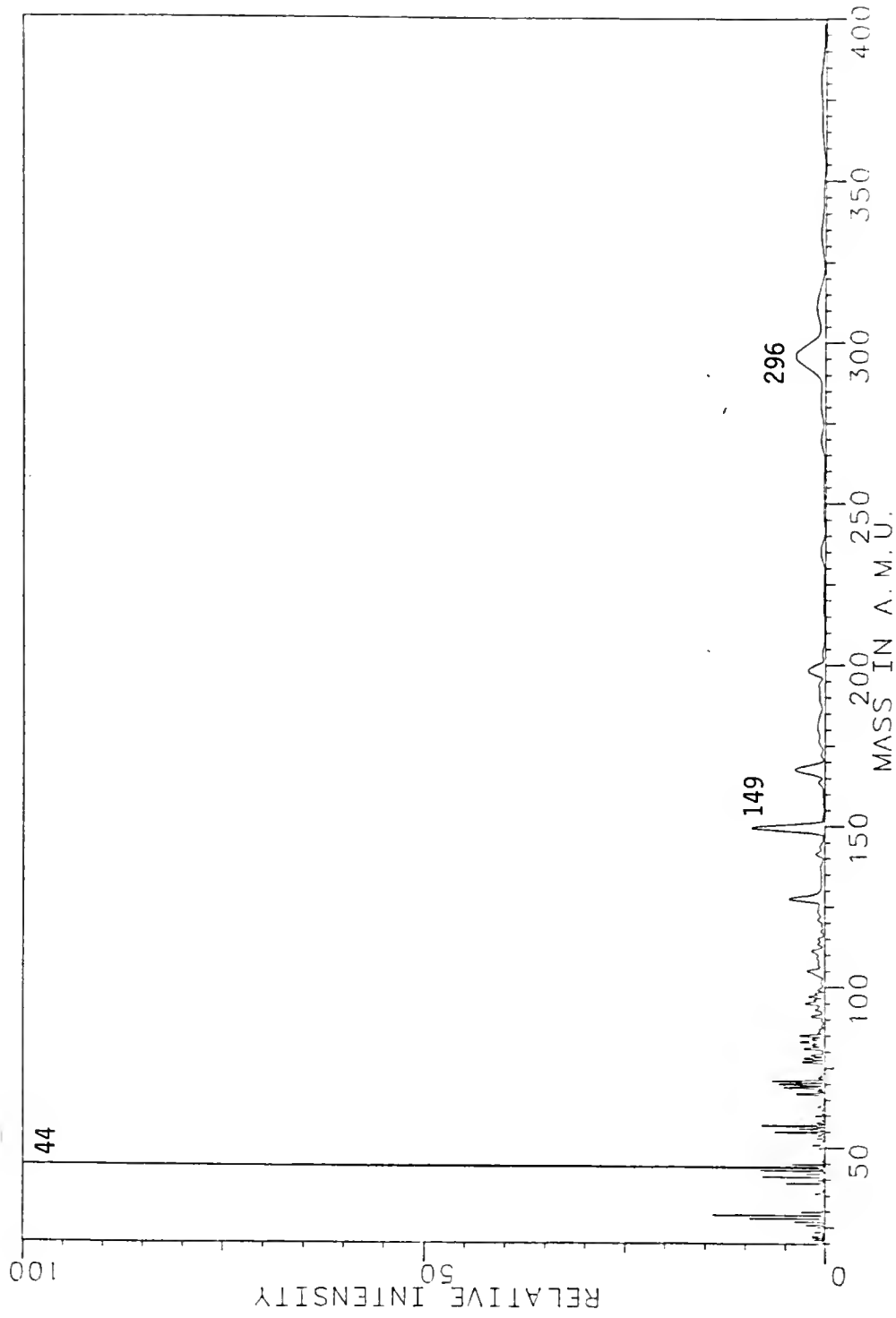

Figure 22. ICRMS (0-400 a.m.u.) of P.R.P., 80 Minutes, Laser On

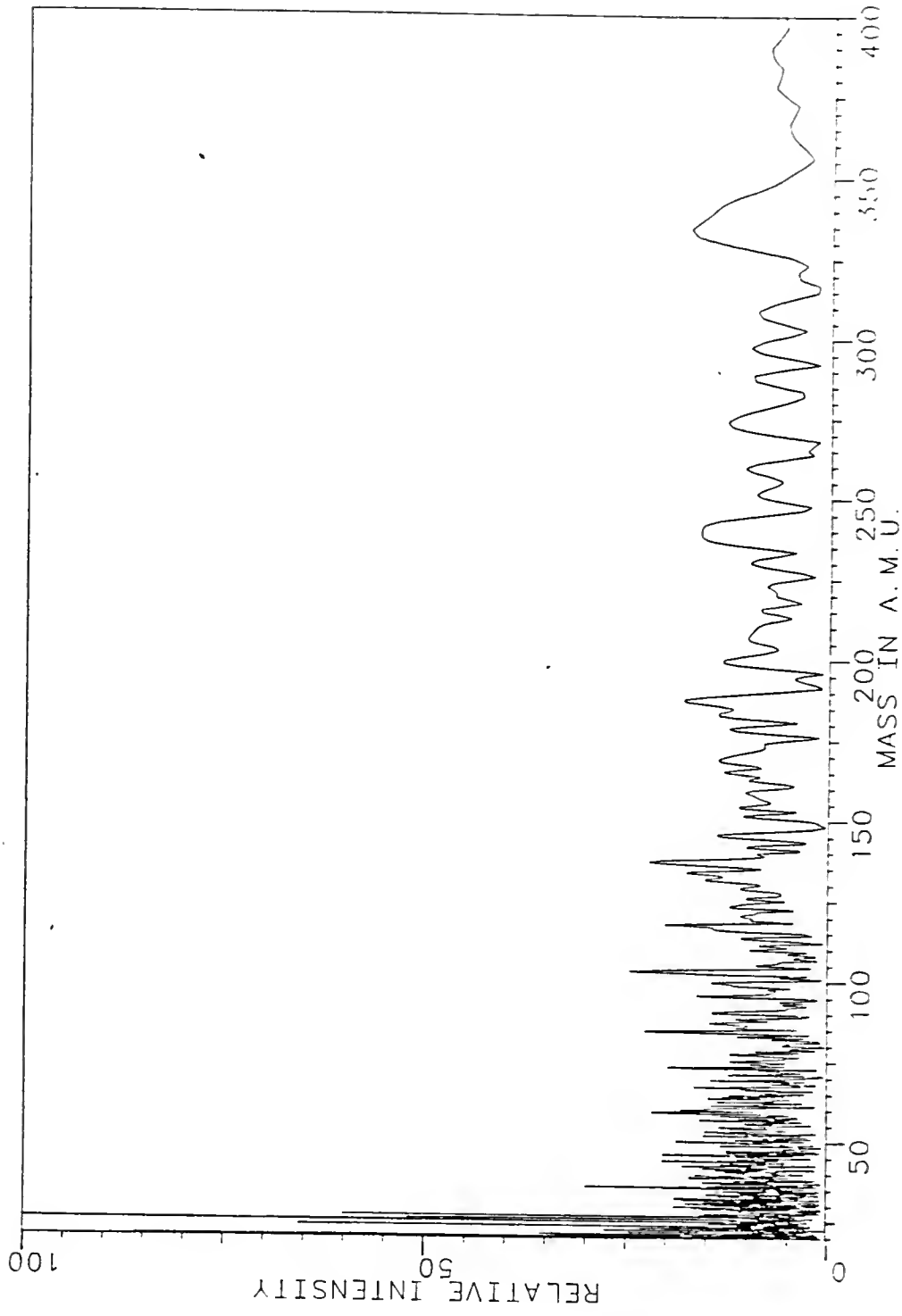

Figure 23. ICRMS (0-400 a.m.u.) of P.R.P., Laser On, e-Beam Off

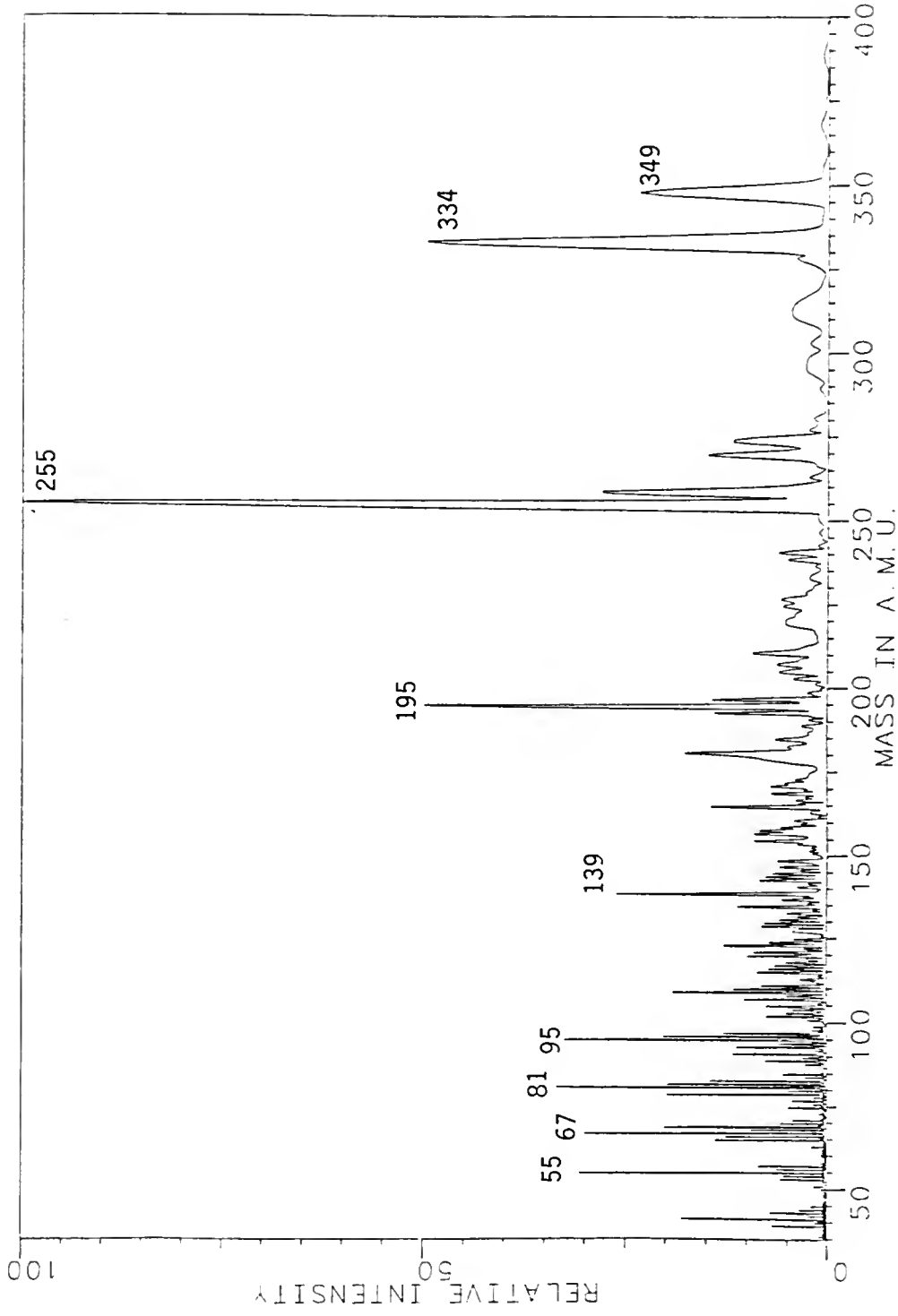

Figure 24. ICRMS (0-400 a.m.u.) of P.R.P. at ~50°C

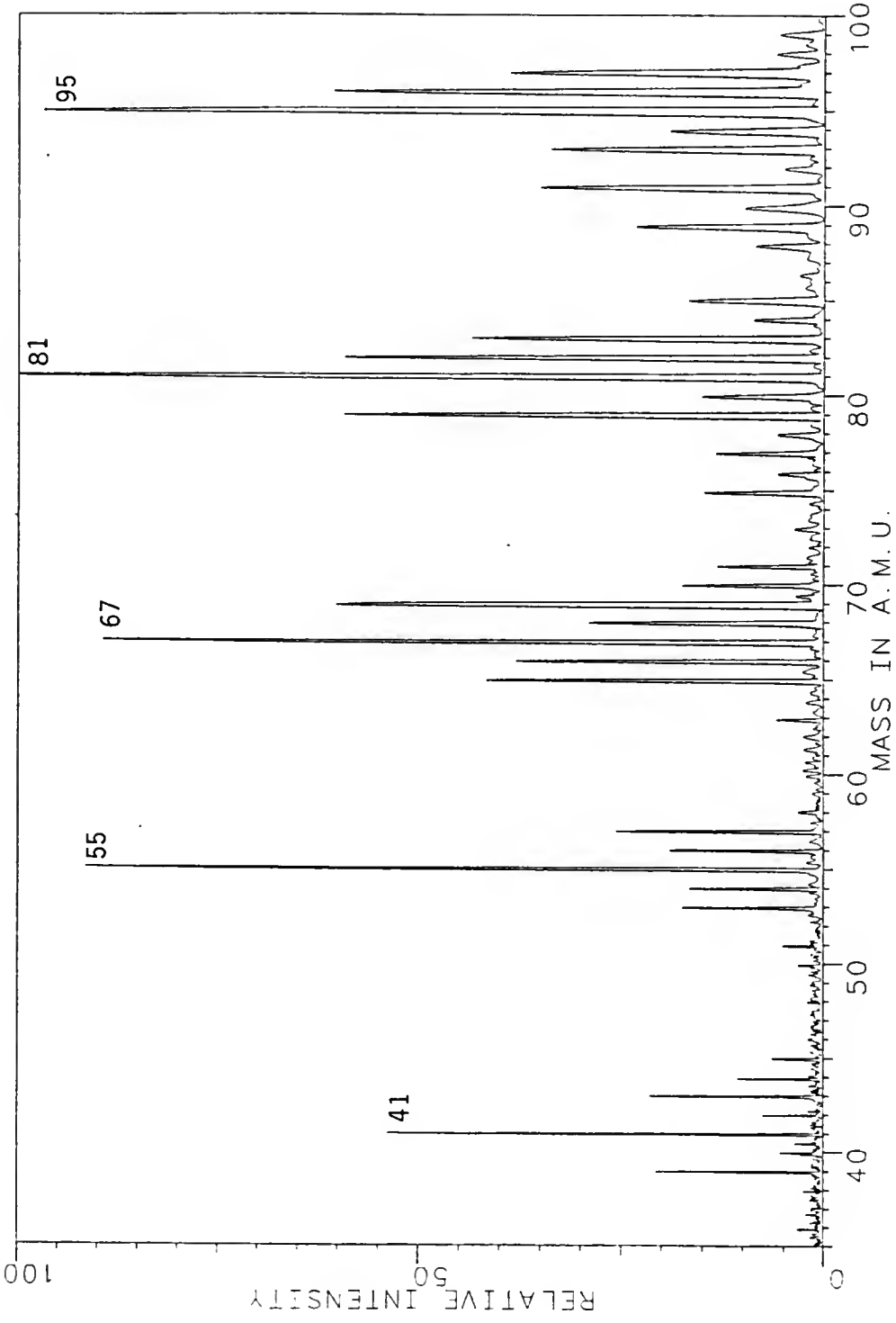

Figure 25. ICRMS (0-100 a.m.u.) of P.R.P. at ~50°C

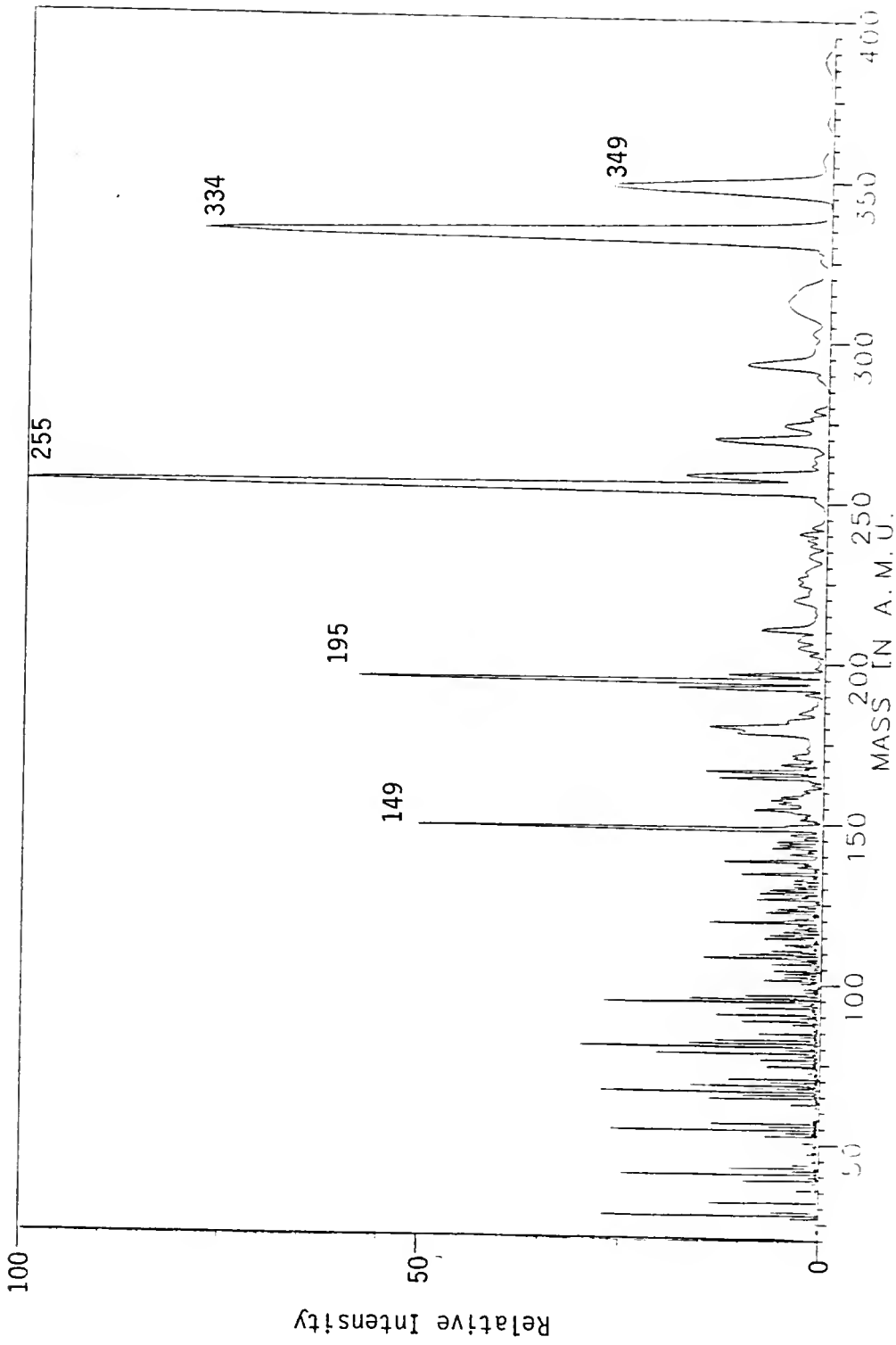

Figure 26. ICRMS (0-400 a.m.u.) of P.R.P. at 125°C

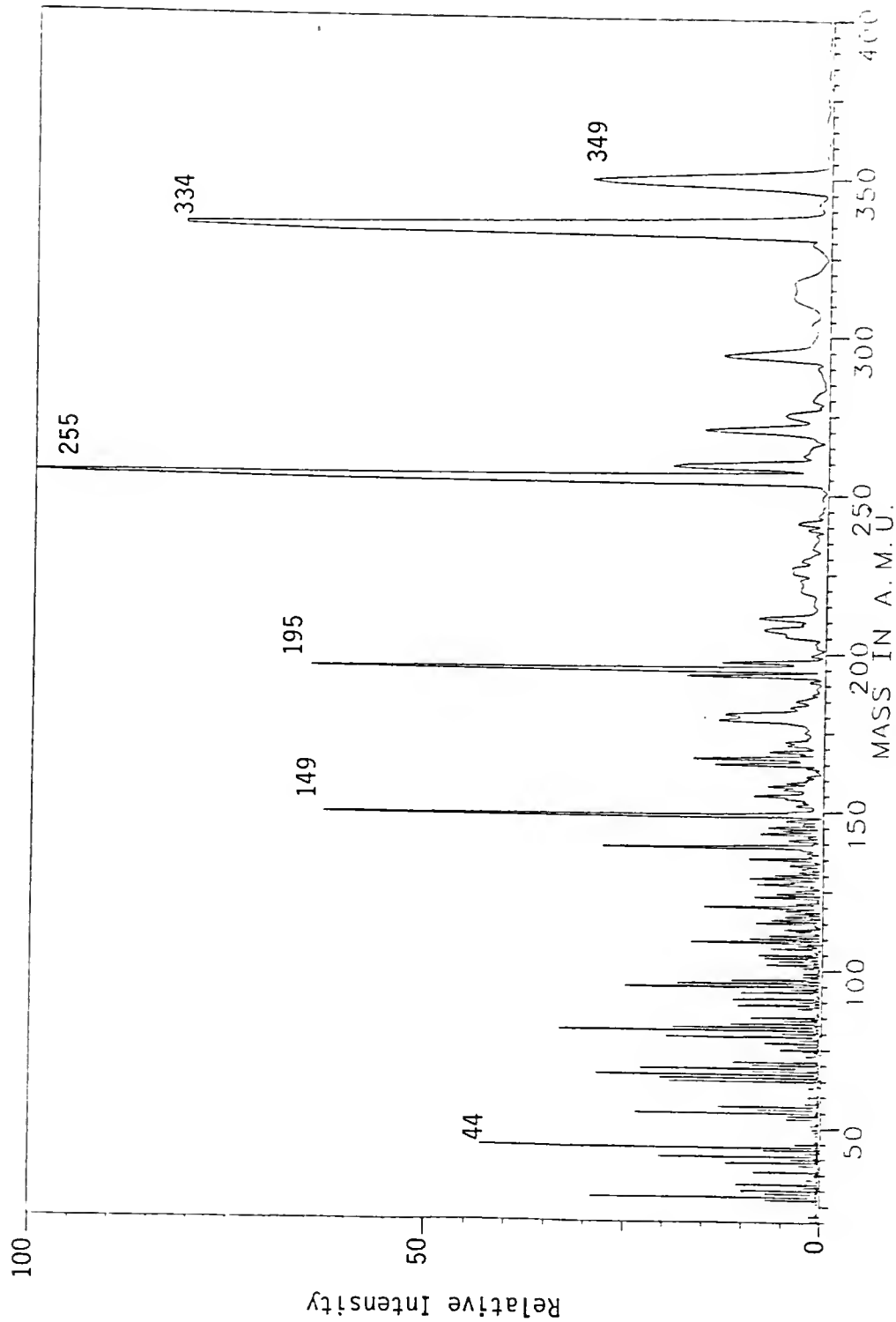

Figure 27. ICRMS (0-400 a.m.u.) of P.R.P. at 175°C

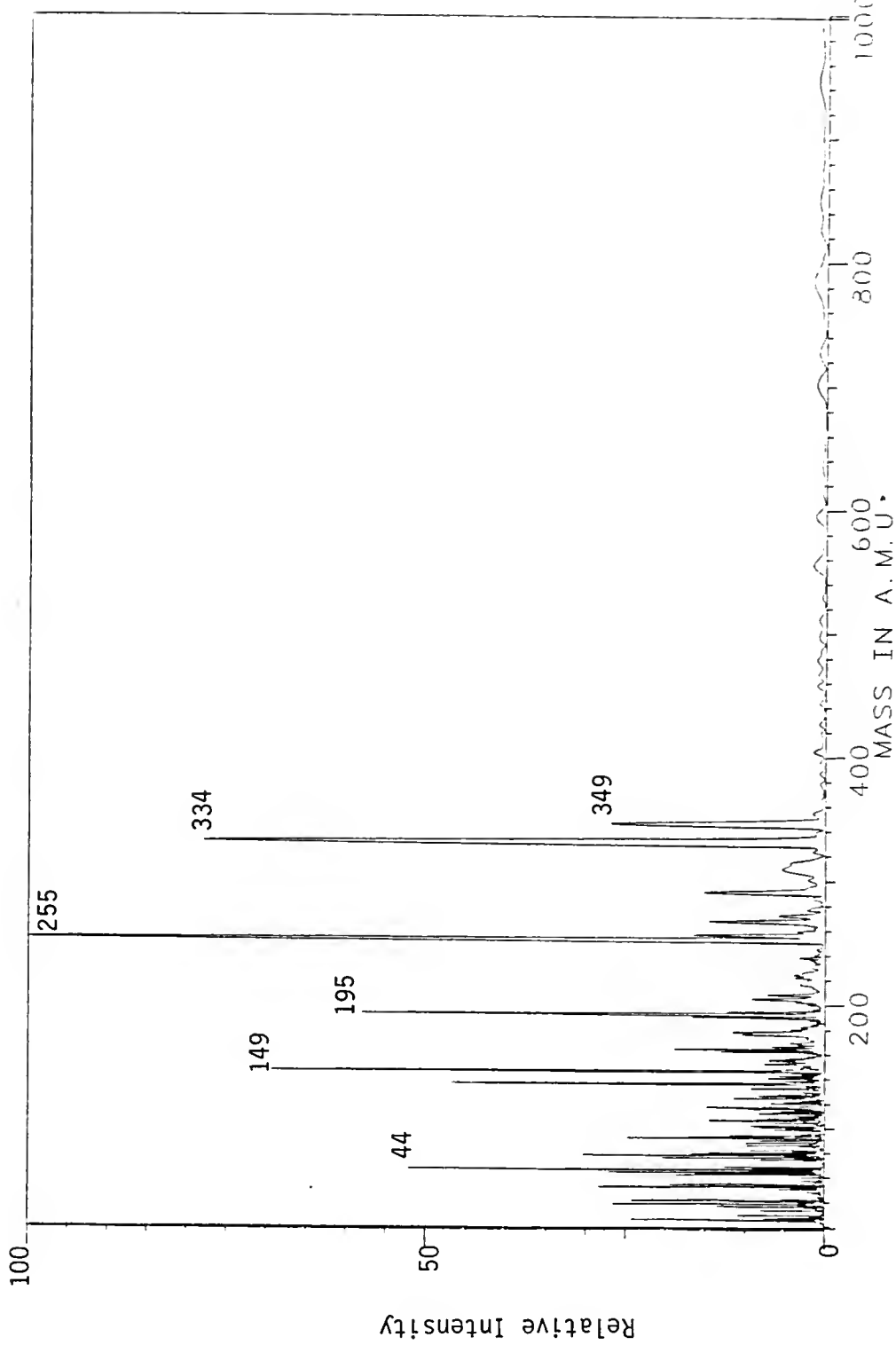

Figure 28. ICRMS (0-1000 a.m.u.) of P.R.P. at 175°C

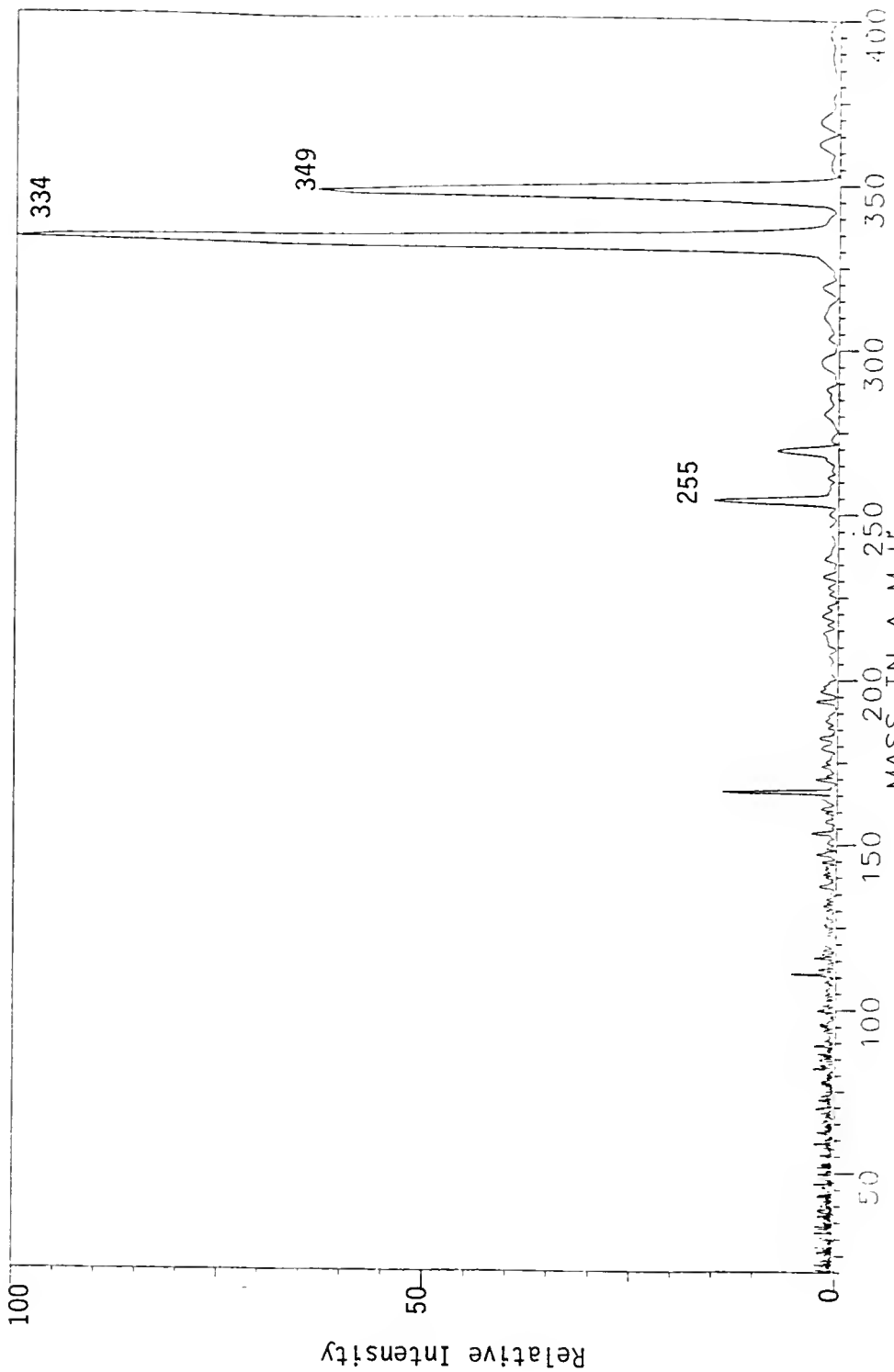

Figure 29. ICRMS of CID of Mass 334, No Collission Time

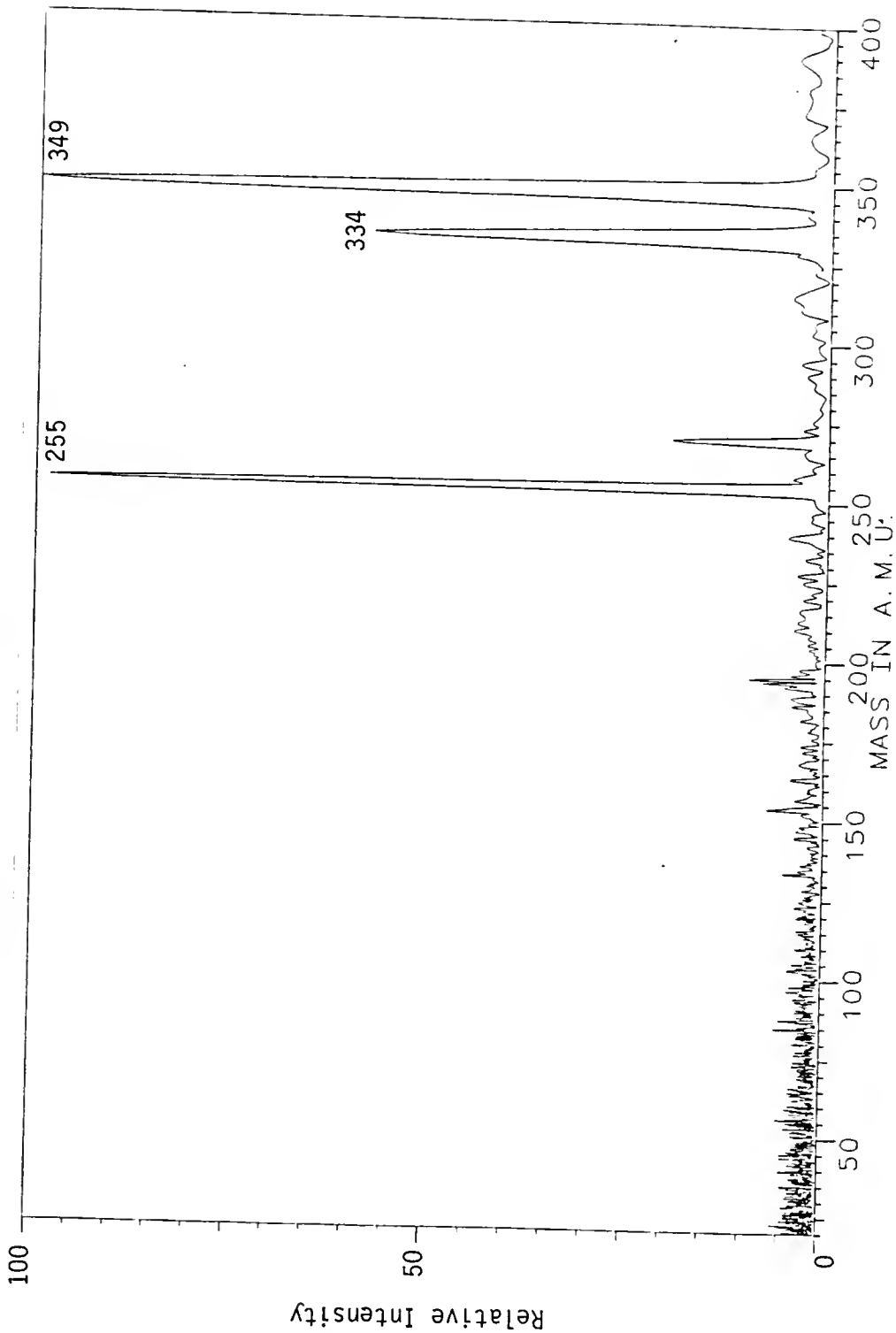

Figure 30. ICRMS of CID of Mass 334, 50 msec Collision Time

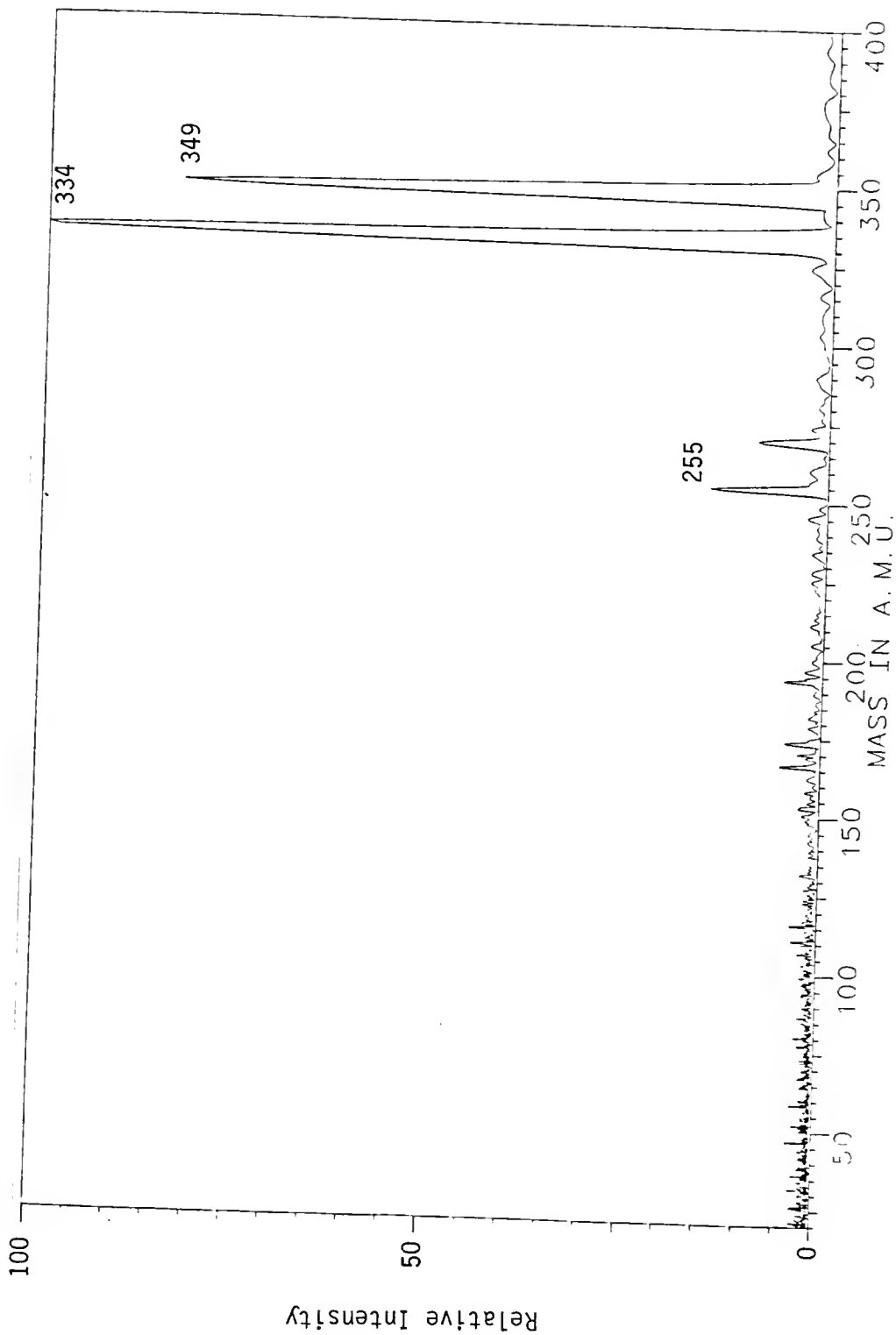

Figure 31. ICRMS of CID of Mass 349, No Collision Time

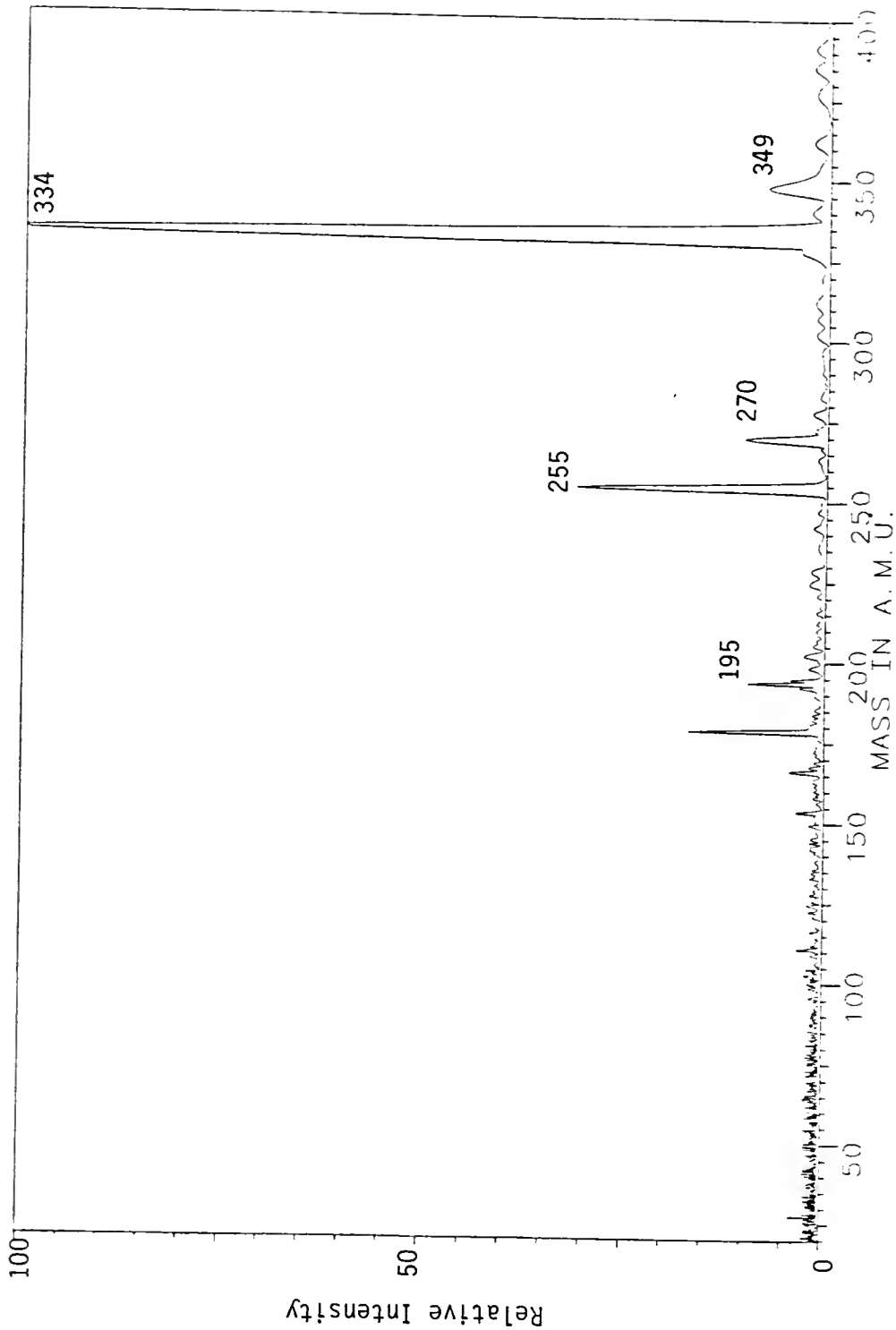

Figure 32. ICRMS of CID of Mass 349, 50 msec Collision Time

mentioned were all negative with respect to the appearance of Au^+ ion. Mass 44 was identified as CO_2 by a charge transfer reaction with water.

Thus, the presence of volatile Au compounds could not be established by the MS study results. The identification of CO_2 and the ubiquitous presence of a compound with a charge to mass ratio of 149 or 150 was firmly established, as was the presence of many low mass compounds (<100 a.m.u.) that exhibited a hydrocarbon type pattern. These results seem reasonable considering the H_2/CH_4 plasma reactants. The abundance of CO_2, especially under highly energetic conditions, would seem to indicate its ease of formation within the system. These points are discussed further in the last section of this chapter.

Time of Flight MS Experiment

In this experiment Au to Au_7 positive ion clusters were produced in the pulsed Nd:YAG stimulated plasma described earlier and observed with the TOFMS. The purpose of this experiment was to determine if Au/carbonaceous ion clusters could be produced (and detected) by adding CH_4 to the He gas normally used in the cluster beam apparatus. The results confirmed that this was possible.

Recall that the horizontal deflector (HD) voltage directly affected the ion signals as previously discussed. Thus, when a spectra scanning several hundred a.m.u. was recorded the greatest sensitivity was for the central mass region. This limitation did not apply to the narrow range scans (< 100 a.m.u.). All of the comparative spectra of species formed in He and He/CH_4 plasmas were recorded at the same HD voltages.

It should also be noted that there are several possible mechanisms responsible for the observed changes in the positive ion spectra when the CH_4 gas was added to the plasma. The three major mechanisms are

1) neutralization

$$Au(n)^+ + R^- = Au(n) + R$$

2) combination/dissociation

$$Au(n)^+ + Au = Au(n+1)^+$$

3) ion product reactions

$$Au(n)^+ + R + He = Au(n)R^+ + He^*$$

$$Au(n) + R^+ + He = Au(n)R^+ + He^*$$

$$Au(n)R + He^* = Au(n)R^+ + He + e^-$$

$$Au(n-1)R^+ + Au + He = Au(n)R^+ + He^*$$

where the * denotes a translationally hot species. No attempt was made to identify any of these, or any other mechanisms, as the one(s) responsible for the changes in ion signals observed.

Figure 33 shows the Au to Au_5 ion signals, along with respective first and second oxide peaks, which were formed in the He plasma. (The oxide peaks were ubiquitous in this apparatus and most likely were formed from residual moisture in the target and holder.) When ~1% CH_4 was added to the He gas stream, a dramatic change in the ion spectra occurred (Figure 34). The Au and Au_2 signals decreased by nearly two orders of magnitude, the Au_3 signal decreased by a factor of three, the Au_4 signal decreased by a factor of seven and the Au_5 signal increased

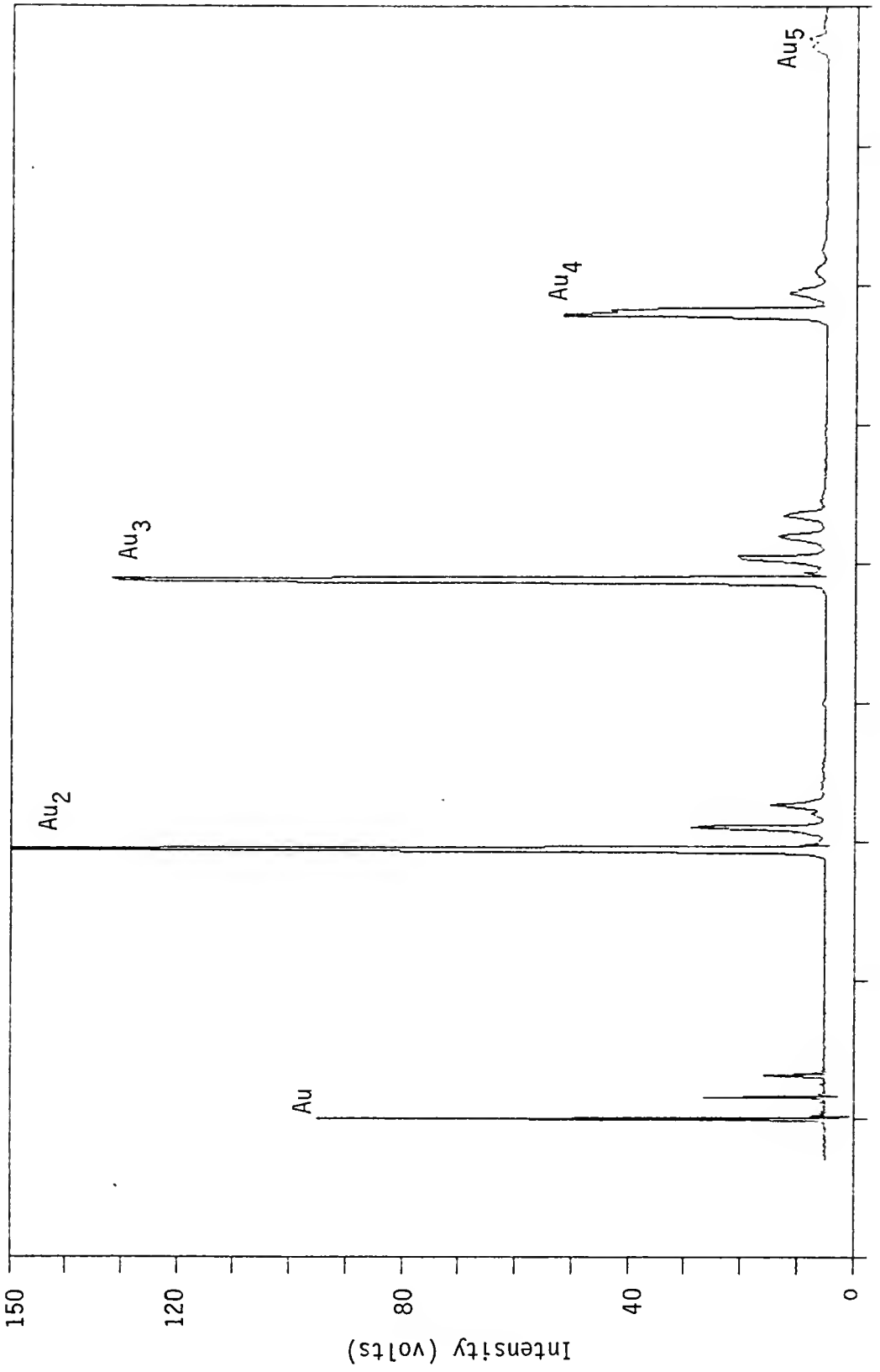

Figure 33. TOFMS of Au to Au_5 Clusters Formed in Helium Plasma

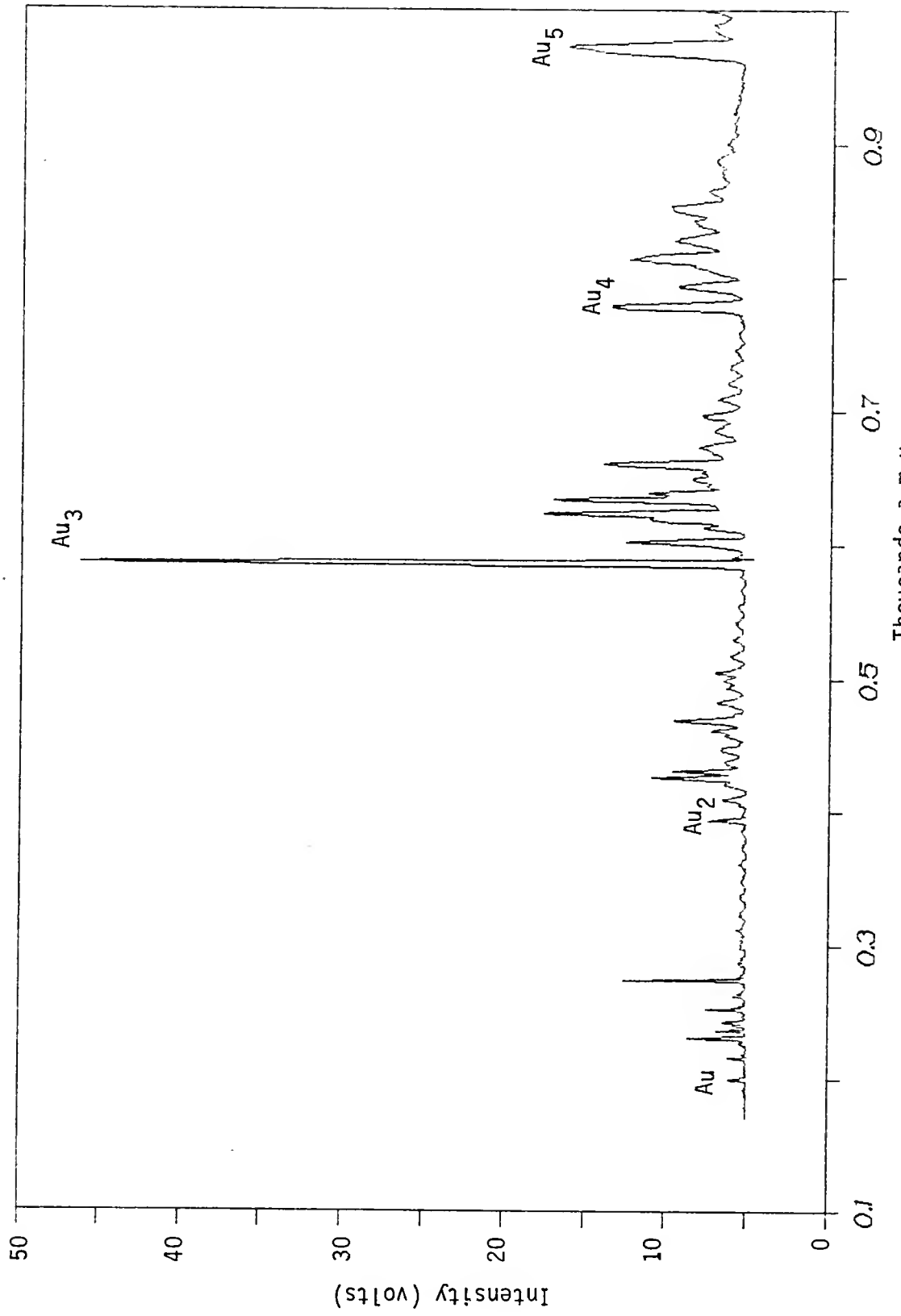

Figure 34. TOFMS of Au to Au_5 Clusters Formed in 1% CH_4/He Plasma

by one order of magnitude. There was also a plethora of new peaks which appeared at staggered intervals after each Au cluster peak.

Similar scans of the Au_3 to Au_7 region (Figures 35 and 36) showed the same effect of additional peaks appearing when CH_4 was added to the plasma. These spectra also show the large increase in the Au_5 signal (and its oxides) as well as moderate increases in the Au_6 and Au_7 signals. Once again the Au_3 signal appeared to be relatively insensitive to the addition of CH_4 to the plasma.

The experiment was repeated with the HD set to optimize the Au signal. Figures 37 and 38 show the spectra from species produced in the helium and helium/methane plasmas, respectively. These spectra indicate the high sensitivity of the Au, AuO, and AuO_2 signals to the plasma conditions. The most prominent new peaks occurred at 38, 44, 54, and 76 mass units above 197 (the Au mass). These peaks were evidently due to the addition of carbon and hydrogen to the Au and AuO species. For example, the largest peak at +76 mass units could have been due to either AuC_6H_4 or $AuOC_5$, among other possibilities.

The Au_2 region was observed in the next experiment and the spectra are presented in Figures 39 and 40. The pattern of additional peaks was even more pronounced in this test. They appeared at 12, 13, 25, 37, 49, 61, 73, 85, 97, 109, and 121 mass units above the Au_2 signal at 394 a.m.u. This was strongly suggestive of the ordered addition of C, CH, C_2H, C_3H, C_4H, C_5H, C_6H, C_7H, C_8H, C_9CH, and $C_{10}H$ to the Au_2 dimer. The signals at +37 and +61 dominated the new peaks.

Very similar results were observed in the Au_3 spectrum when CH_4 was added to the plasma. The before and after spectra, presented in

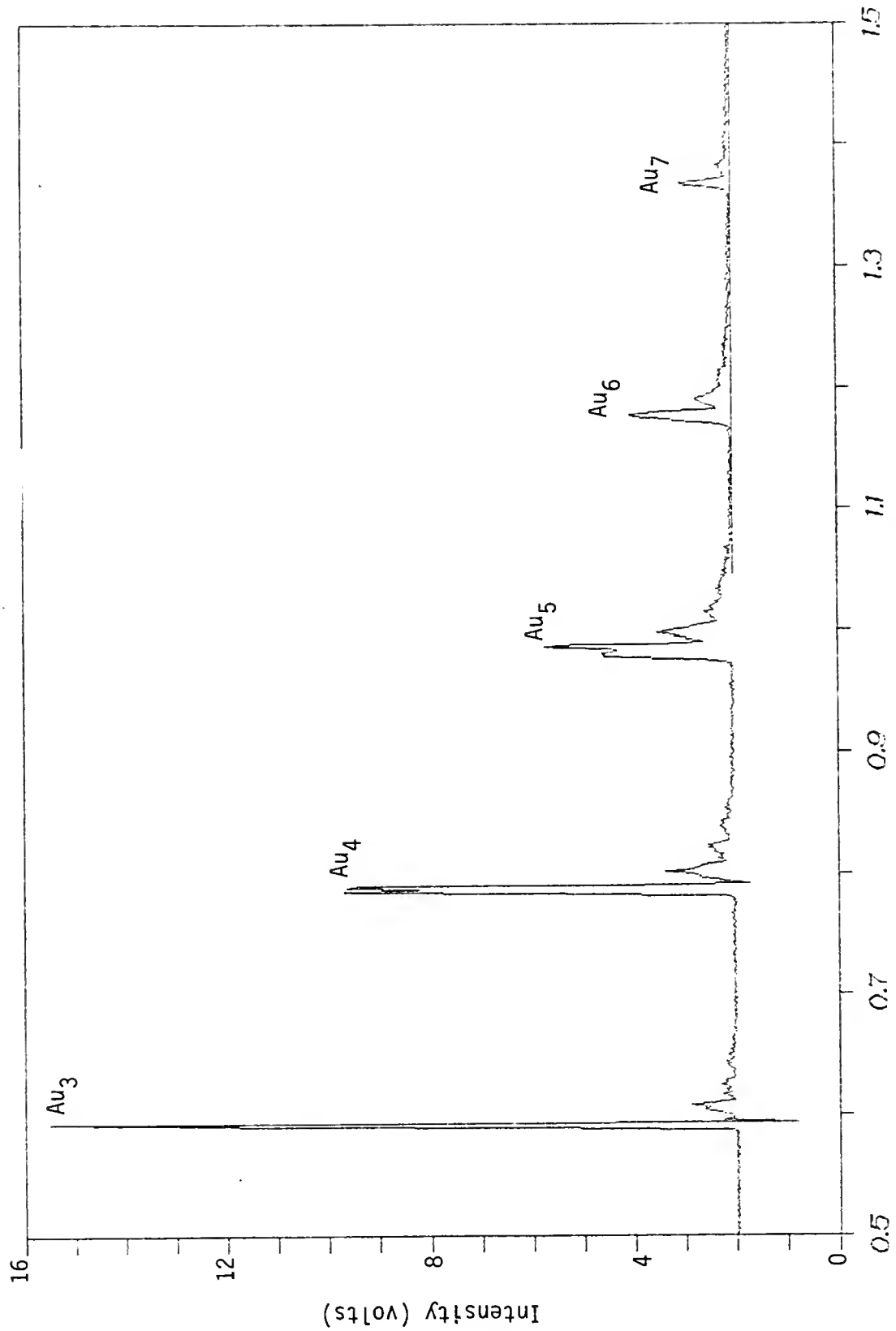

Figure 35. TOFMS of Au_3 to Au_6 Formed in Helium Plasma

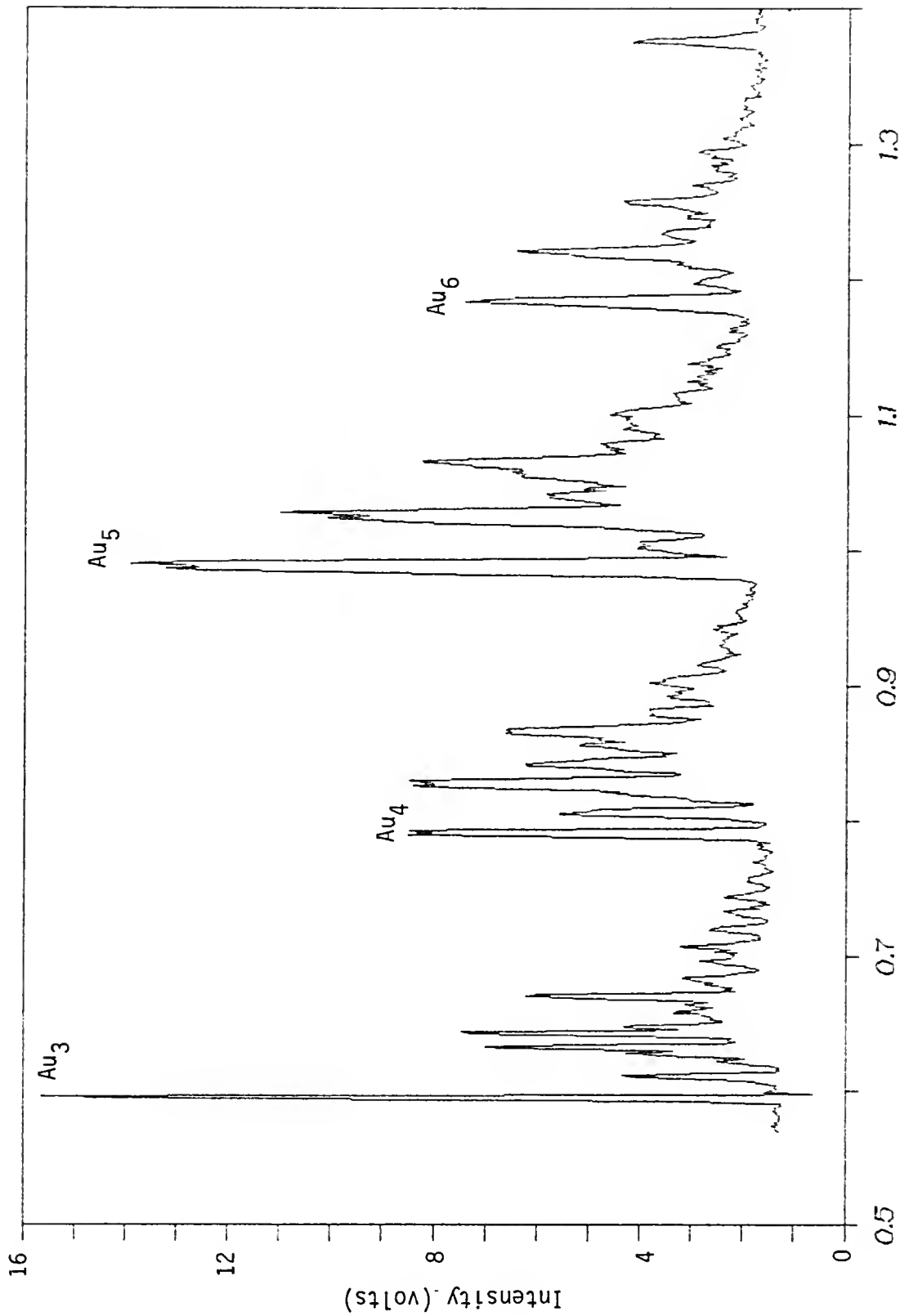

Figure 36. TOFMS of Au_3 to Au_6 Formed in 1% CH_4/He Plasma

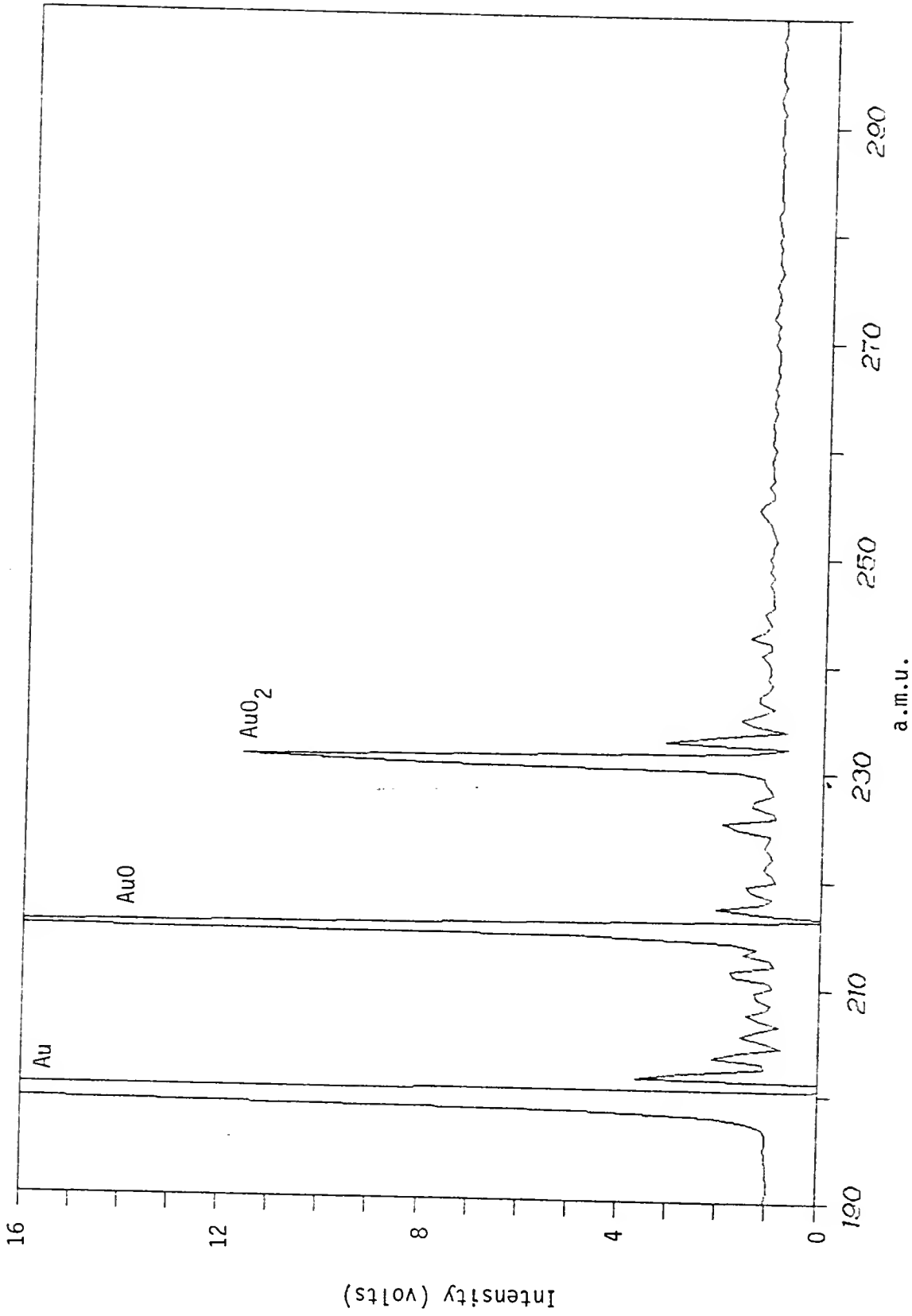

Figure 37. TOFMS, Expanded Au Region (from Helium Plasma)

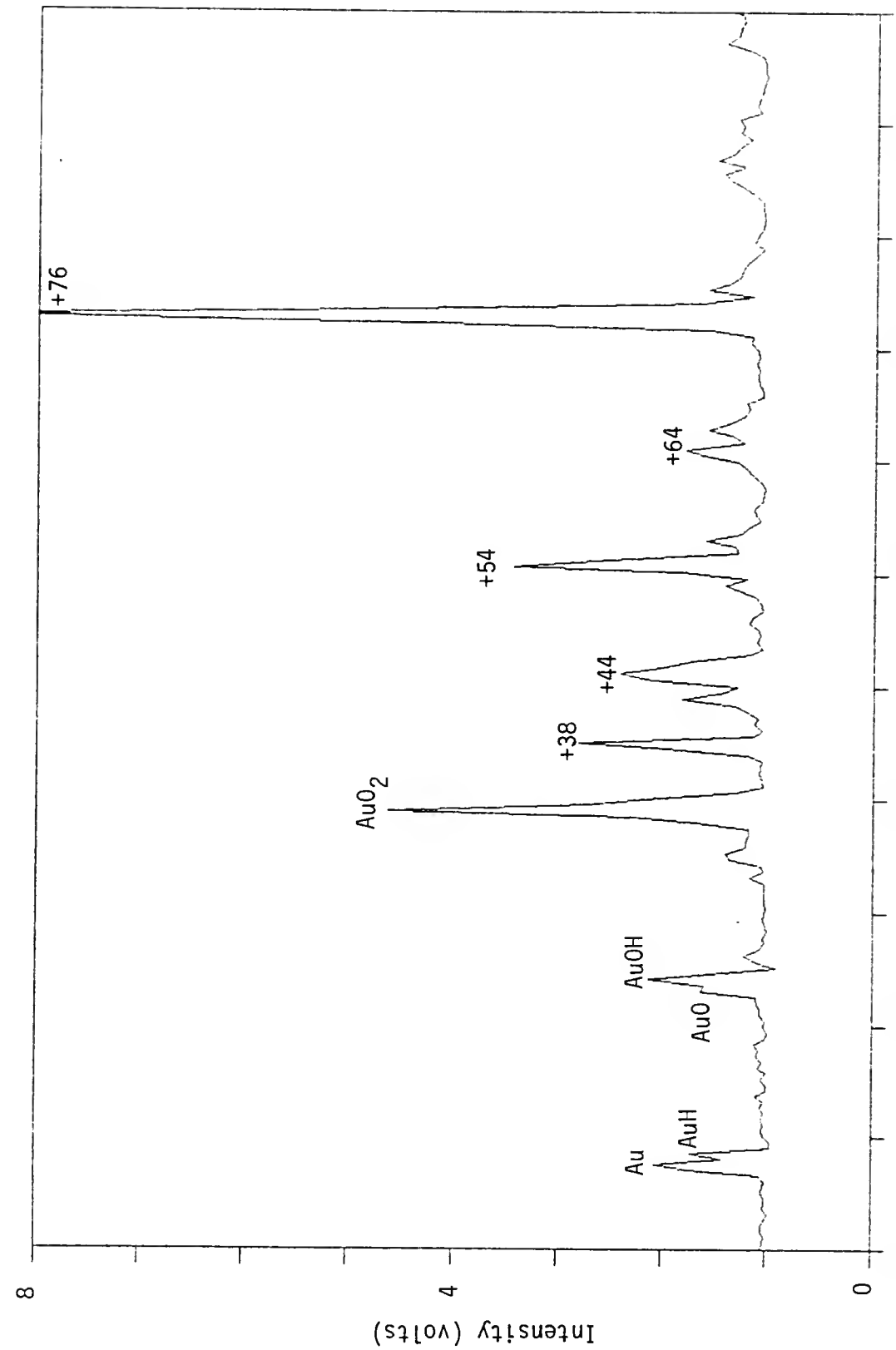

Figure 38. TOFMS, Expanded Au Region (from 1% CH_4/He Plasma)

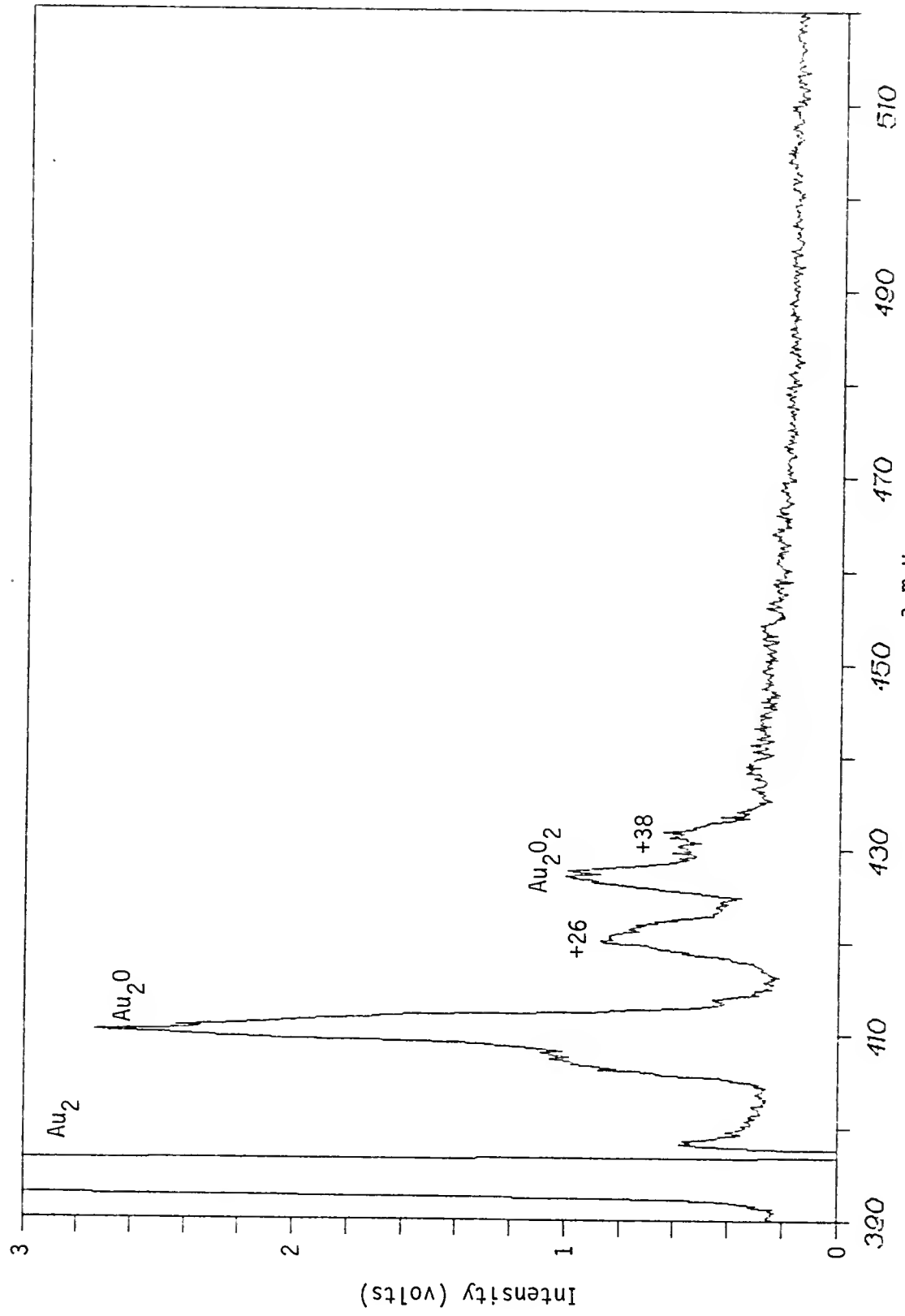

Figure 39. TOFMS, Expanded Au_2 Region (from He Plasma)

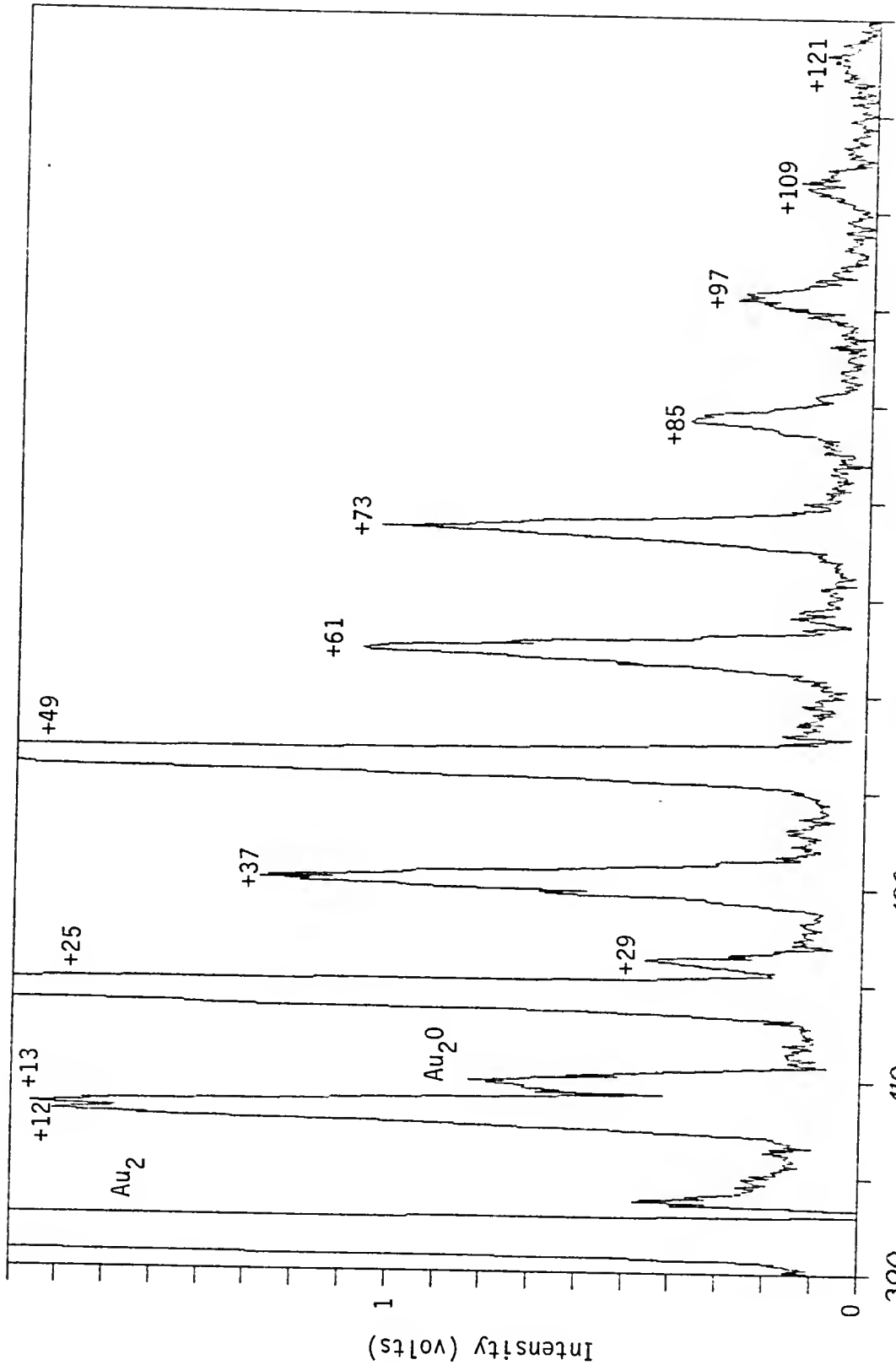

Figure 40. TOFMS, Expanded Au_2 Region (from 1% CH_4/He Plasma)

Figures 41 and 42, show the major additional peaks occurring at 37, 49, 61, 73, 85, 97, and 109 mass units above the Au_3 signal at 591 a.m.u. This was highly suggestive of the ordered addition of C_3H, C_4H, C_5H, C_6H, C_7H, C_8H, and C_9H. The +37 peak was the dominant new peak in this spectra. The low reactivity of Au_3 was again demonstrated by the comparatively low signals of the additional peaks arising from the addition of CH_4 to the plasma.

This series of experiments showed that the addition of CH_4 to the He/Au plasma formed by the pulsed Nd:YAG laser had a significant impact on the mass of the positive ion clusters detected by the TOFMS. The evidence suggested that the ordered addition of carbon atoms, along with one hydrogen atom, to the Au clusters was the probable cause of the additional ion peaks observed. The +38 and +76 mass peaks dominated the Au spectral additions, the +37 and +61 peaks dominated the Au_2 spectrum additions, and the +37 mass peak was the strongest additional signal in the Au_3 positive ion spectrum. Also, the Au_3^+ ion appeared to be significantly less sensitive to the addition of CH_4 to the He/Au plasma.

Despite the fact that the cluster beam experiments showed that Au was very reactive with CH_4 in an energetic plasma, the overall results of the volatility study indicated that significant quantities of volatile gold compounds could not be isolated from the plasma reaction products. However, the P.R.P. were very effective in transporting Au downstream from the plasma reaction chamber and could be collected on substrates to yield gold films of varying quality, depending on deposition and annealing conditions. Thus, the P.R.P. films were

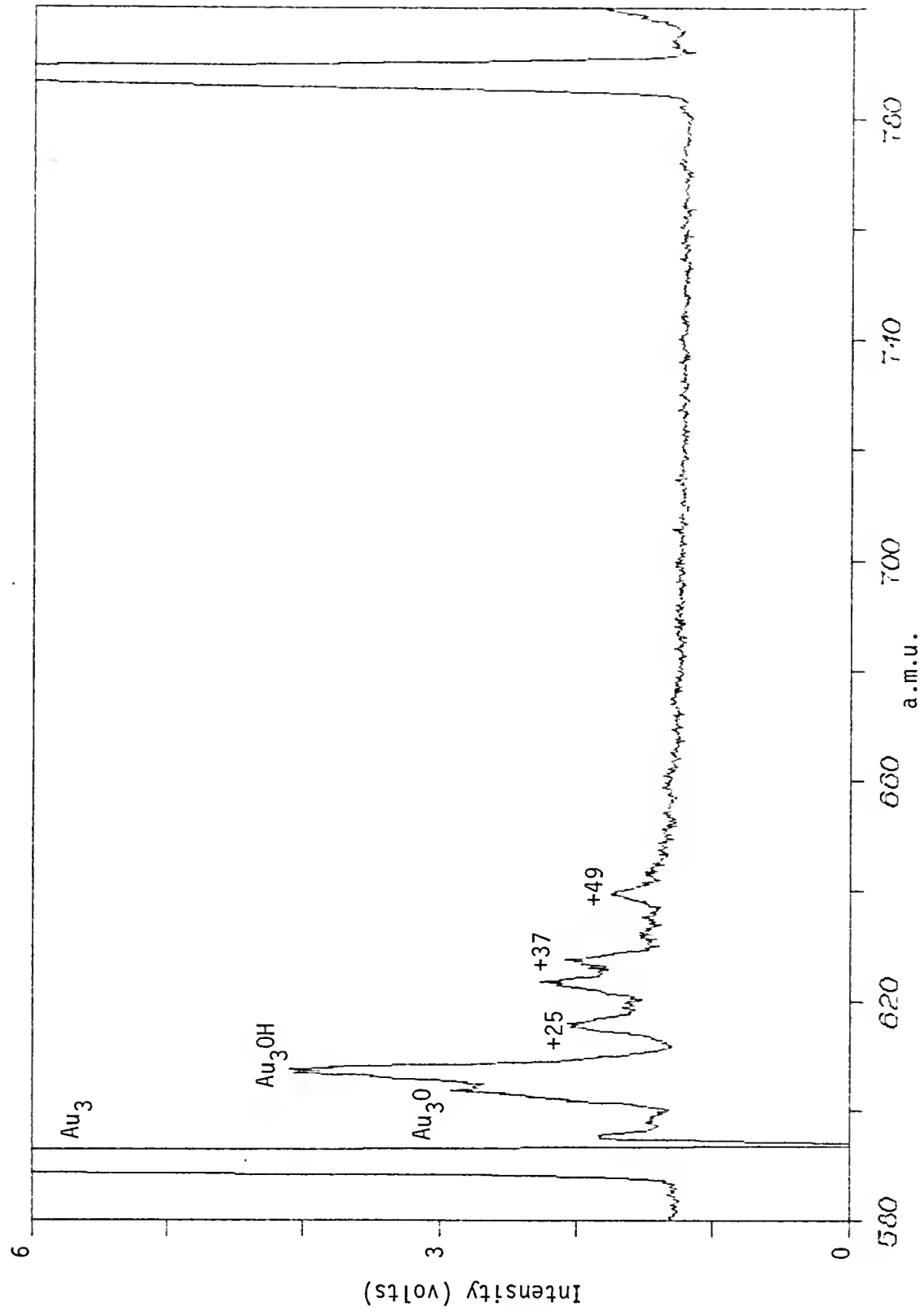

Figure 41. TOFMS, Expanded Au_3 Region (from He Plasma)

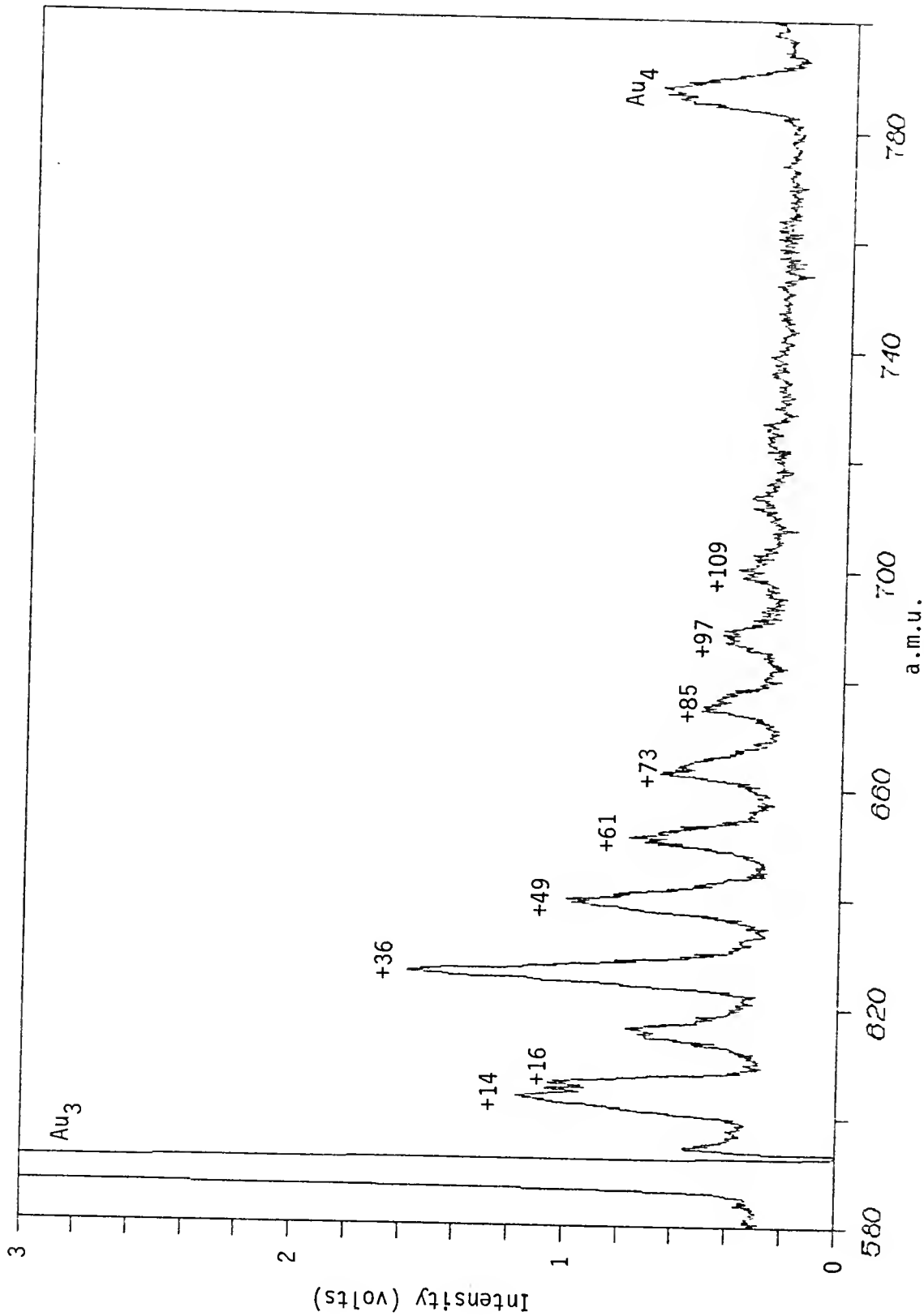

Figure 42. TOFMS, Expanded Au_3 Region (from 1% CH_4/He Plasma)

subjected to further analyses to determine some of their properties. These analyses were also intended to determine the state of the Au in the P.R.P.

Gold Thin Film Characterization Results

Visible Absorption Spectroscopy

Figure 43 shows the results of visible absorption spectra (325-800 nm) of acetone extract/suspensions of P.R.P. formed in pure CH_4, He/CO, and He/CH_4/air plasmas. The spectra of 10,000 μg Au/ml (water) and 10 μg Au/ml (acetone) are also included in this figure. The most significant feature of these spectra is the presence of the Au metallic absorption band centered at ~560 nm in the He/CO and He/CH_4/air P.R.P. extract/suspensions, denoting the presence of suspended Au particles. The conspicuous absence of this band in the CH_4 P.R.P. extract/suspension agreed with earlier observations in the screening study.

Optical Microreflectometry

Reflectance spectra, 400-900 nm, were recorded for the Harris Standard sputtered Au film (Figure 44), P.R.P. coated W/Si (Figure 45), P.R.P. coated glass (Figure 47), and P.R.P. coated Scotch brand black electrical tape and transparent tape (Figure 46). The major comparative features in these spectra are the sharp increase in reflection of Au between 500 and 550 nm and the relatively high reflectivity of Au from 600-900 nm (see Figure 44).

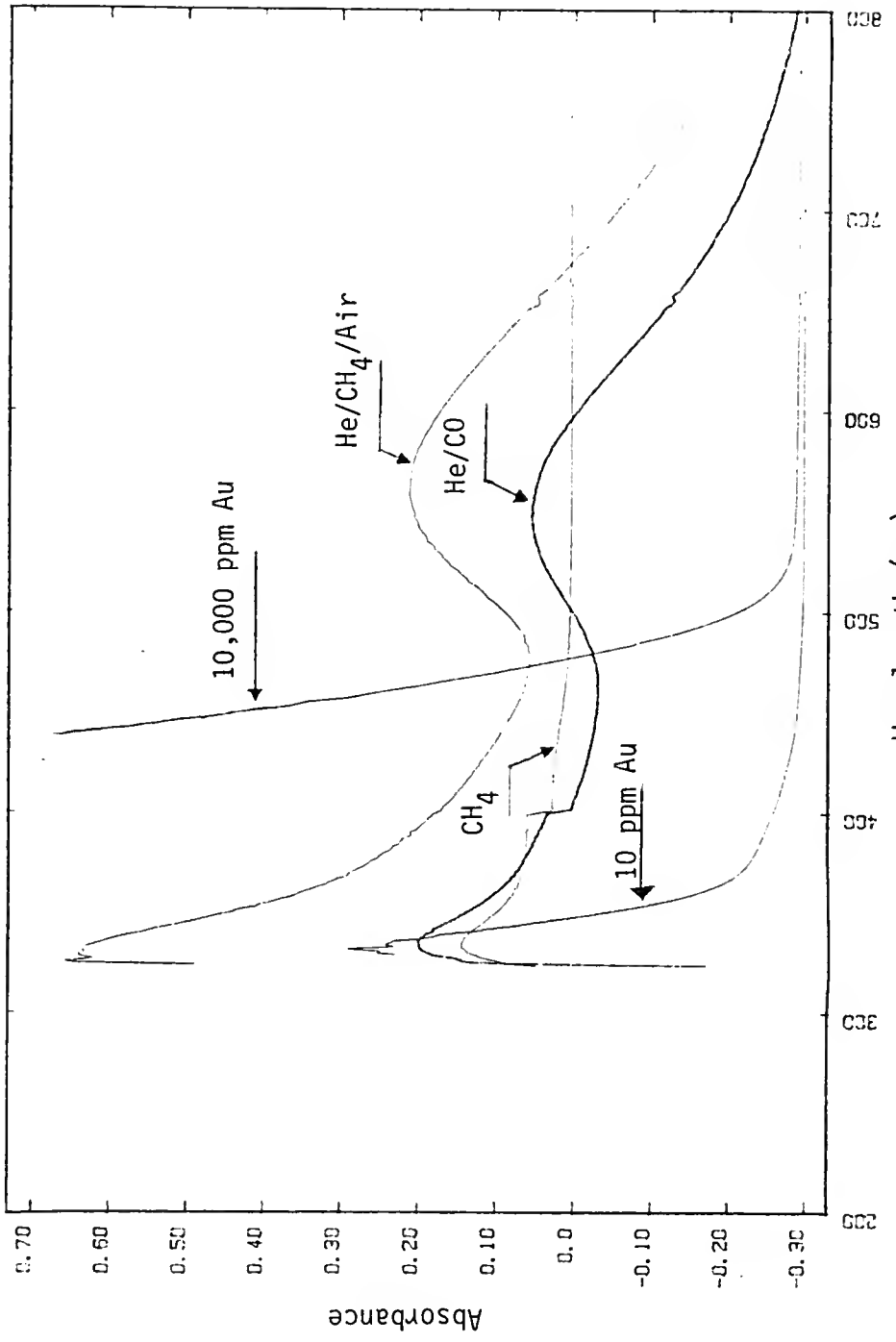

Figure 43. Visible Absorbance Spectra of Acetone Extracts of Reaction Products from CH_4/Au, He/CO/Au, and He/CH_4/Air/Au Plasmas

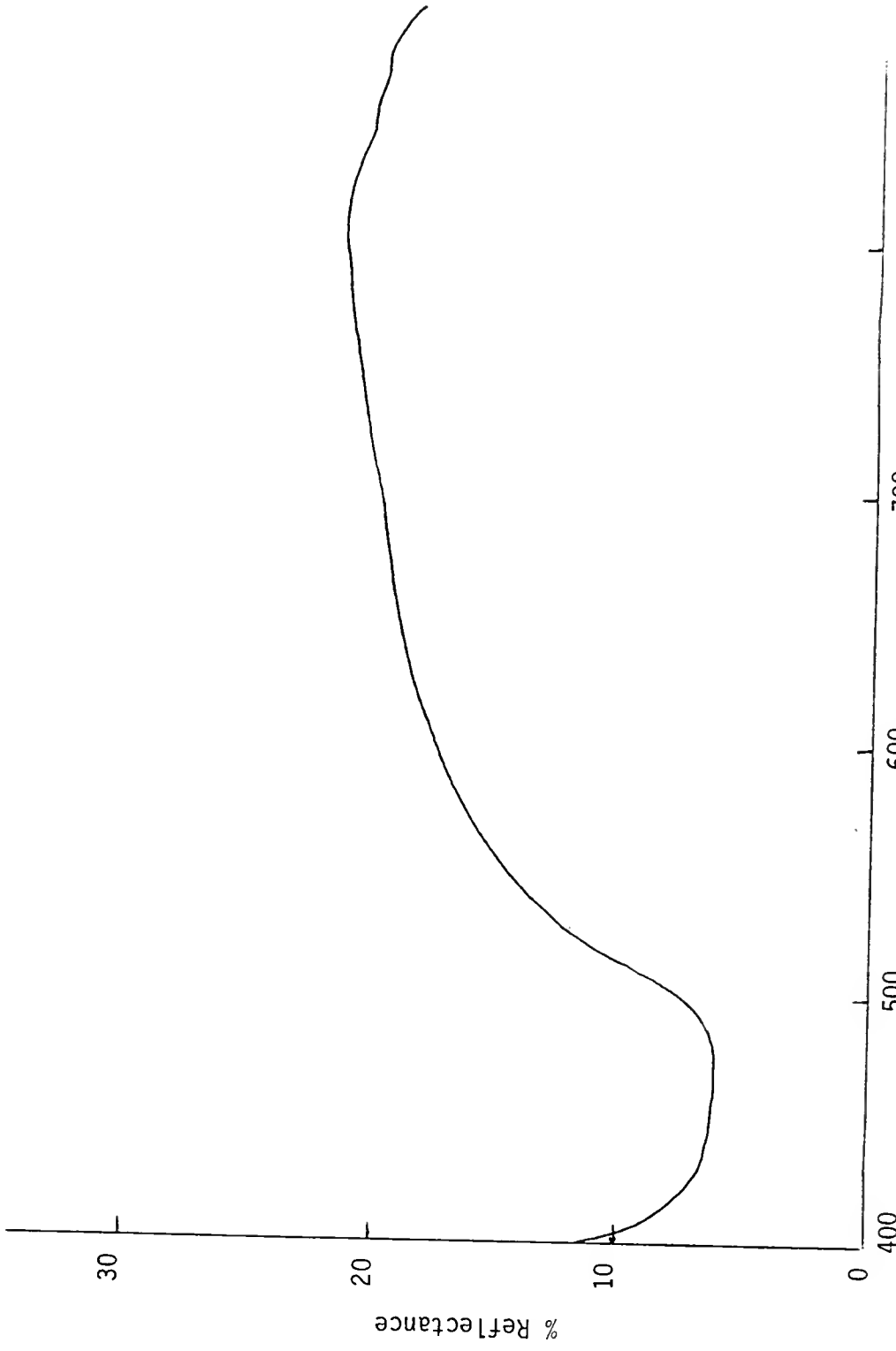

Figure 44. Visible Reflectance Spectra of Harris Stnd. Sputtered Au Film

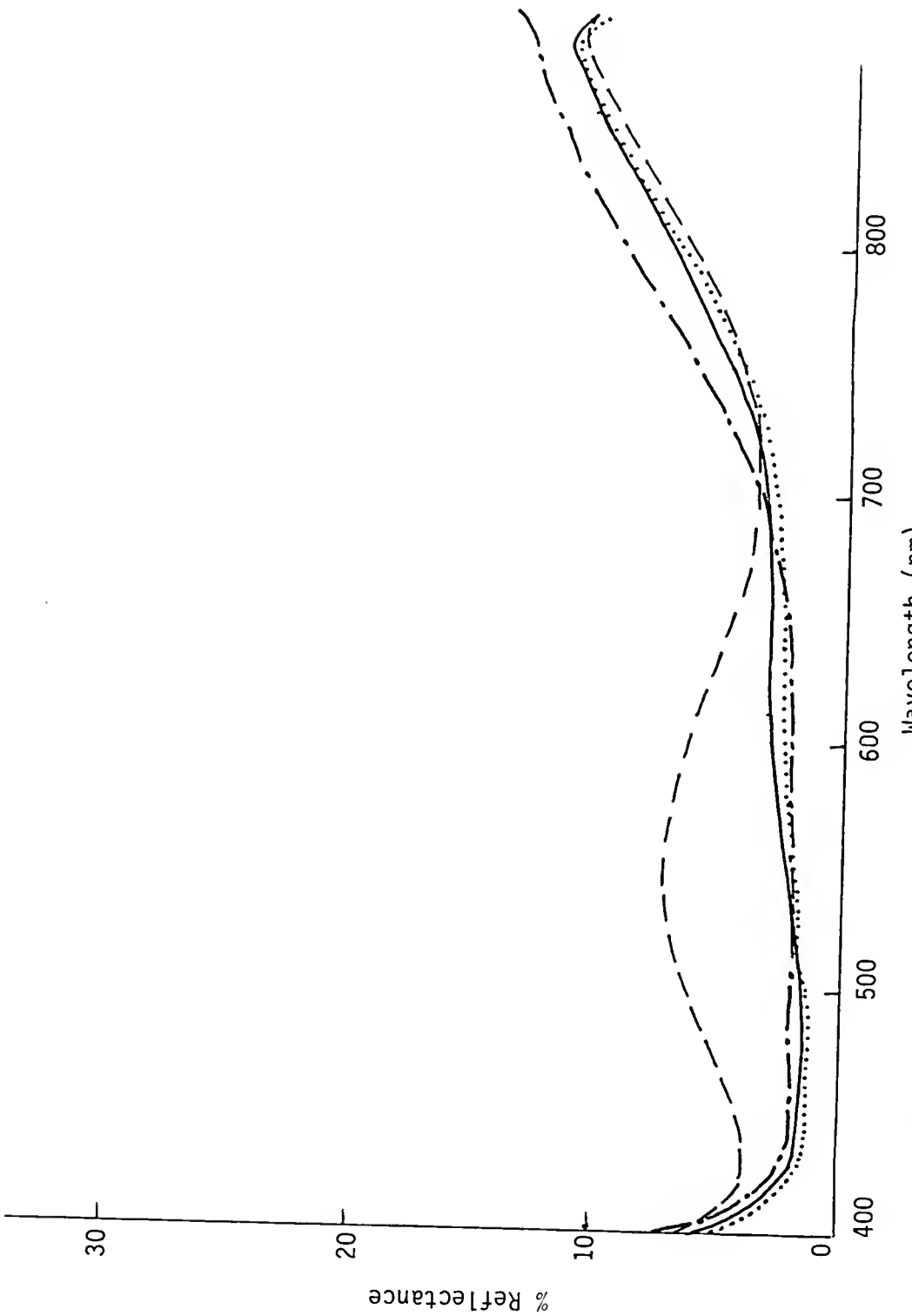

Figure 45. Visible Reflectance Spectra of P.R.P. on W/Si
—·— As Deposited
···· Annealed in Air, 320°C, 18 hrs
—— Annealed in H_2, 400°C, 1 hr
- - - Etched Spot on Air Anneal Sample

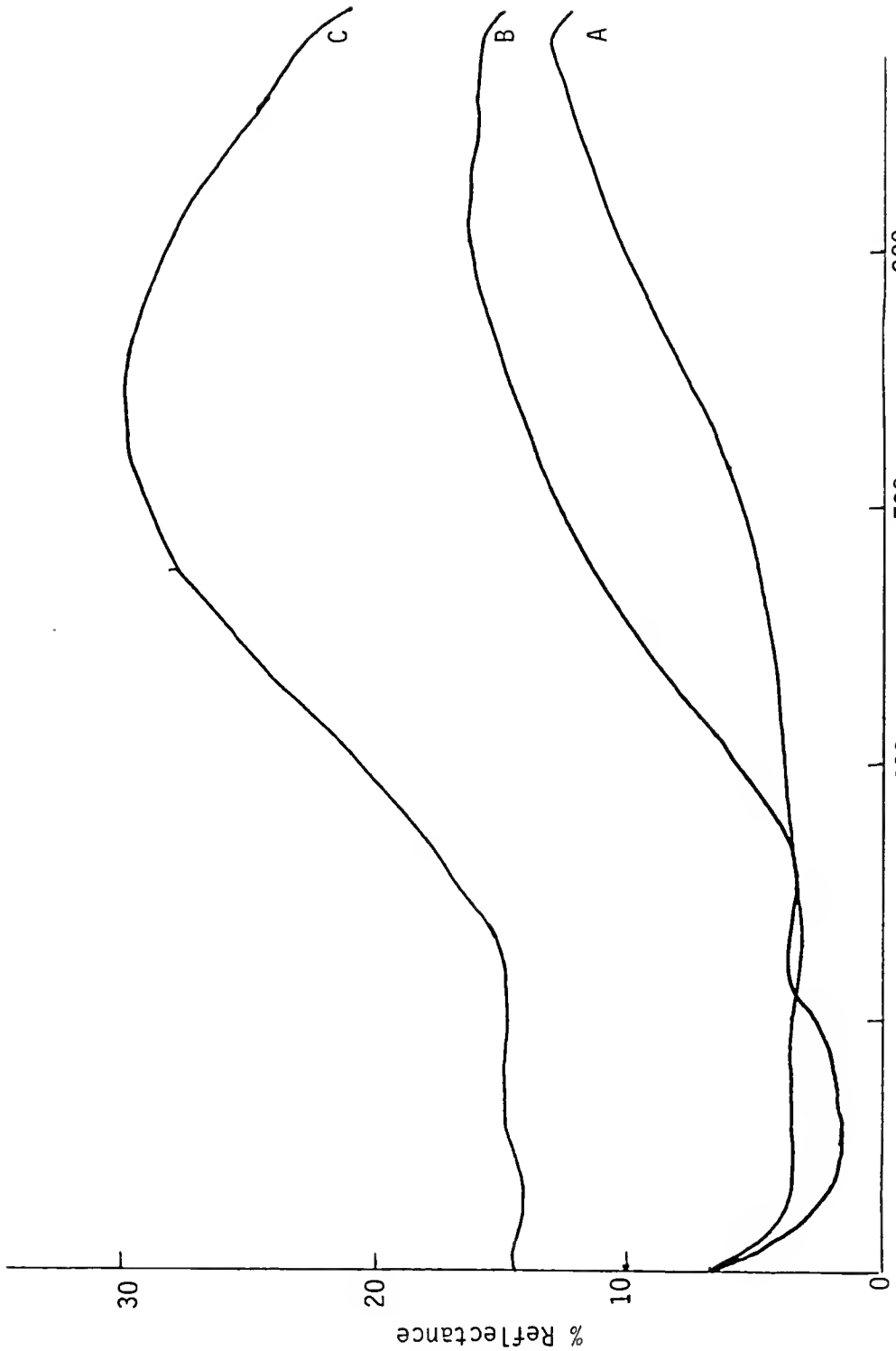

Figure 46. Visible Reflectance Spectra of P.R.P. on Glass
A) 25°C Deposition,
B) After 400°C, 1.5 hr H_2 Anneal, and
C) 100°C Deposition

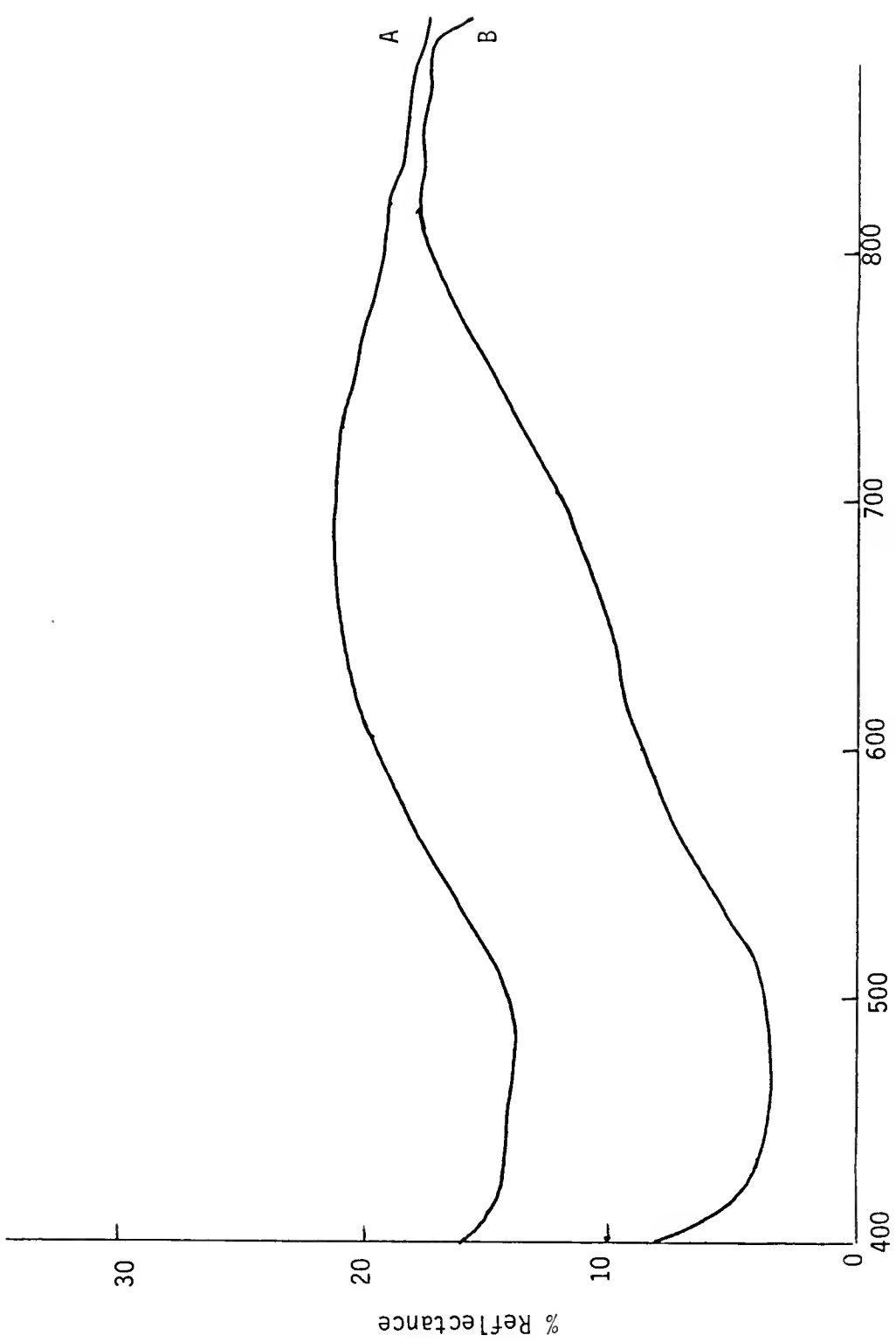

Figure 47. Visible Reflection Spectra of P.R.P. on
A) Adhesive Side, Scotch Brand Transparent Tape
B) Back Side, Scotch Brand Black Electrical Tape

In Figure 45 the reflectance spectra for the P.R.P. on W/Si are compared for four different samples. As-deposited, air-annealed, and hydrogen-annealed samples all had similar spectra with no sharp increase in reflectivity, and overall low reflectivity below 800 nm. This was indicative of highly carbon contaminated films. The sample that was subjected to argon ion etching displayed the W reflection spectrum, indicating removal of the annealed P.R.P. film by the etching process.

The coated glass substrates displayed the most variable spectra. The as-deposited sample spectrum was similar to the coated W/Si spectra, while the air-annealed sample on glass displayed the sharp transition at ~500 nm but was not highly reflective until 600 nm. The glass plate that was coated with P.R.P. at 100^{o}C was the most similar to the Au standard in its reflectance properties, with the sharp transition occurring at ~550 nm and high reflectivity lasting to ~800 nm.

The two tape samples also displayed sharp transitions at ~500 nm, indicating that the P.R.P. film was highly reflective as deposited on these substrates. The coated adhesive side of the transparent tape was particularly reflective, as its spectrum shows (Figure 47).

These spectra provided a measure of the P.R.P. reflectance properties on the different substrates. They also indicated the low reflectivity of the dark colored films on W/Si substrates, and the highly reflective, metallic looking film on the transparent tape (25^{o}C deposition) and the 100^{o}C deposited film on glass.

X-Ray Photoelectron Spectroscopy

The XPS studies determined the P.R.P. film compositions and the binding energy of the Au in the films. Three types of P.R.P. samples coated on W/Si were analyzed along with the Harris standard Au film: as deposited, annealed in air at 250°C or 320°C for 18 hours, and annealed in H_2 at 320°C for 18 hours and 300°C for one hour. The Harris standard, and one each of the air and H_2 annealed samples, were subjected to Ar ion etching, as described earlier. The photoelectron takeoff angle (Theta) was relatively low (30°) in the first two etch runs listed. The third etched sample was also subjected to initial analyses at Theta equal to 10° and 70°. The other samples were subjected to surface analyses at a high Theta of 75°. The XPS anaytical conditions and results are listed in Table 8.

The heavy atomic concentration of C on the surface (84.6%) of the standard Au film was indicative of the handling that the sample experienced before analysis. The C concentration fell to ~1/2 of its starting concentration after 15 minutes of etching. After one hour of etching the C mass concentration was stable at ~1.5%. The atomic concentration of the Au in the bulk (i.e., after one hour of etching) was 80%, or 98.5% mass concentration.

The P.R.P. film sample from experiment #880602 that had been annealed in air and subjected to profile analysis showed a maximum gold mass concentration of 91% after 30 minutes of etching. After 50 minutes of etching the Au concentration dropped to 88 mass percent and

Table 8. XPS Analytical Conditions and Results

Instrument	Sample	Angle	Etch Time (min)	Au $4f_{7/2}$ B.E. (eV)	Au $4f_{7/2}$ Width (eV)	Au Atomic %	Au Mass %	C 1s B.E. (eV)	C 1s Width (eV)	C Atomic %	C Mass %	C Relative %
GCA	Harris Stnd.	30°	0	*	1.45	15	75	*	1.92	85	25	100
		30	15	*	--	--	--	*	1.80	--	--	53
		30	30	*	--	--	--	*	1.78	--	--	37
		30	45	*	1.60	76	98	*	1.92	24	1.8	35
		30	60	*	1.61	80	98.5	*	1.88	20	1.5	29
GCA	880602 Air, 320°C, 18 hr	30	0	84	1.49	23	83	284	2.01	77	17	100
		30	30	84	1.60	39	91	284	2.03	61	8.7	80
		30	50	84	1.52	32	88	284	1.74	68	12	89
Kratos	870901 H_2, 300°C, 18 hr	10	0	--	--	2.4	29	--	--	97	81	100
		70	0	--	--	45	93	--	--	55	7.0	57
		70	15	--	--	51	95	--	--	49	5.3	51
		70	60	--	--	61	96	--	--	39	3.7	40
Kratos	Harris Stnd.	75	0	83.9#	1.10	56	95	283.7	1.73	44	4.6	--
Kratos	880602 H_2, 300°C, 1 hr	75	0	84.1	1.15	37	91	283.6	1.78	63	9.3	--
Kratos	880527 Air, 250°C, 18 hr	75	0	84.1	1.12	52	95	283.8	1.76	48	5.3	--
Kratos	880527 as deposited	75	0	84.1	1.19	51	94	283.5	1.78	49	5.6	--

*Sample not grounded properly. #Used as calibration standard to adjust instrument scale.

it was obvious from visual inspection after the run that the film was nearly etched away.

The second sample P.R.P. film that was subjected to depth profile analysis was an air annealed film from experiment #870901. This film had a near surface C atomic concentration of 97%, determined by a Theta = 10^{o} initial scan. A Theta = 70^{o} initial scan showed a C atomic concentration of 55%, indicating the near surface nature of the carbon. The Au concentration was 45 atomic percent (93% mass) under the same conditions. After 15 minutes of etching the Au concentration was 51 atomic percent (95% mass). After one hour of etching the bulk Au atomic concentration in this film was determined to be 61%, or 96% mass concentration. Figure 48 shows the XPS survey scan spectra of the film before and after etching. The appearance of strong W bands indicated that the underlying substrate had been exposed by the process, probably be removal of the hydrocarbon layer that coated the entire film. The P.R.P. formed a discontinuous film and areas of the substrate were visible after the sample was removed. Figures 49 and 50 show the XPS spectra associated with the high and low Theta analyses for the C 1s peak and the Au $4f_{5/2}$ and $4f_{7/2}$ peaks, respectively, and indicates the near surface nature of the carbon.

The remaining samples that were subjected to high Theta (75%) surface analyses in order to observe binding energy (B.E.) shifts had Au atomic concentrations of 56% (Harris std.), 37% (880602 H_2 anneal), 52% (880527 air anneal), and 51% (880527 as deposited). These concentrations were consistent with the other analyses and showed that the Au/C ratios were more dependent on the sample source than on the

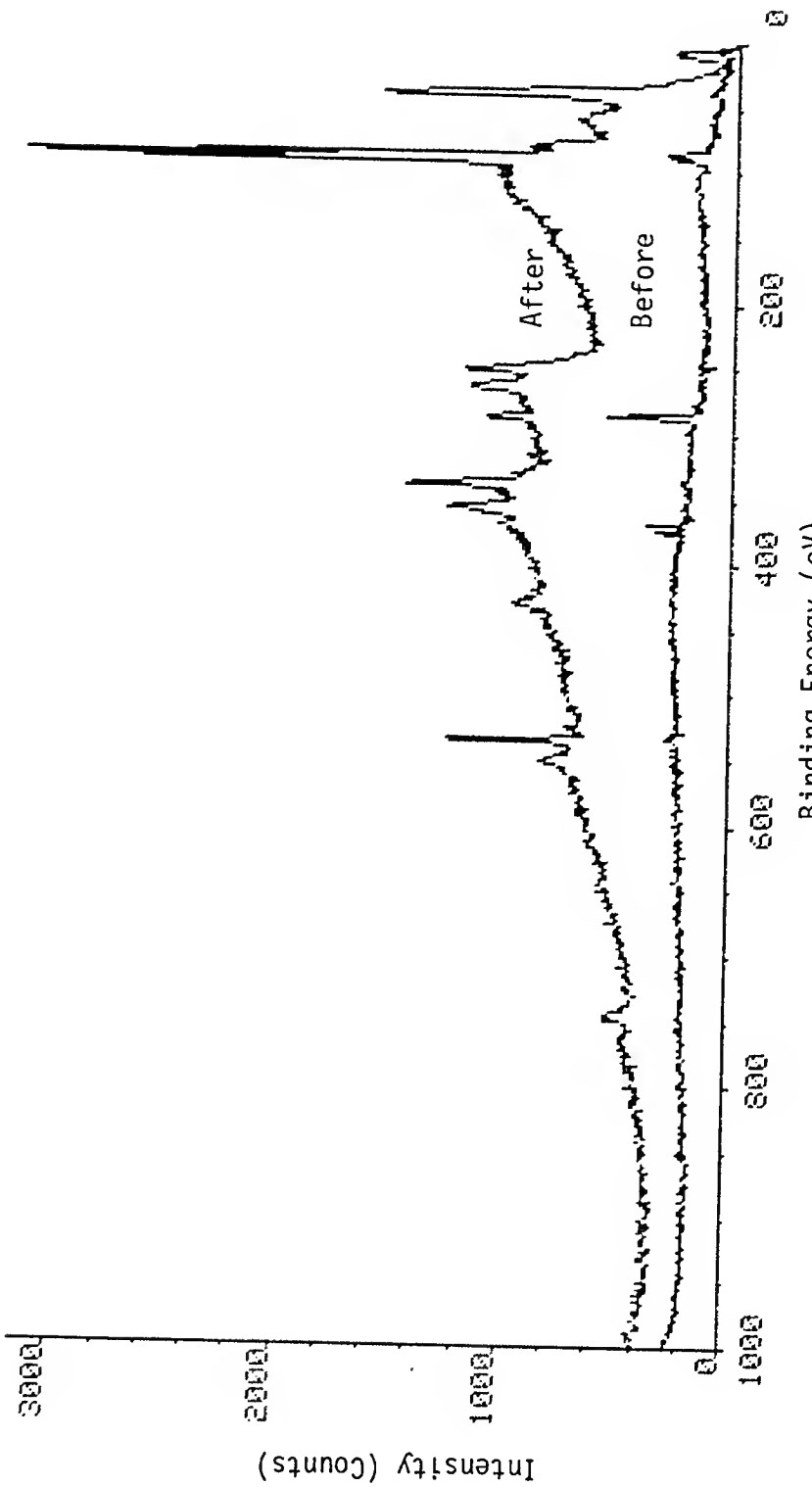

Figure 48. XPS Survey Scan of P.R.P. on W/Si (300°C H_2 Anneal) Before and After Etching

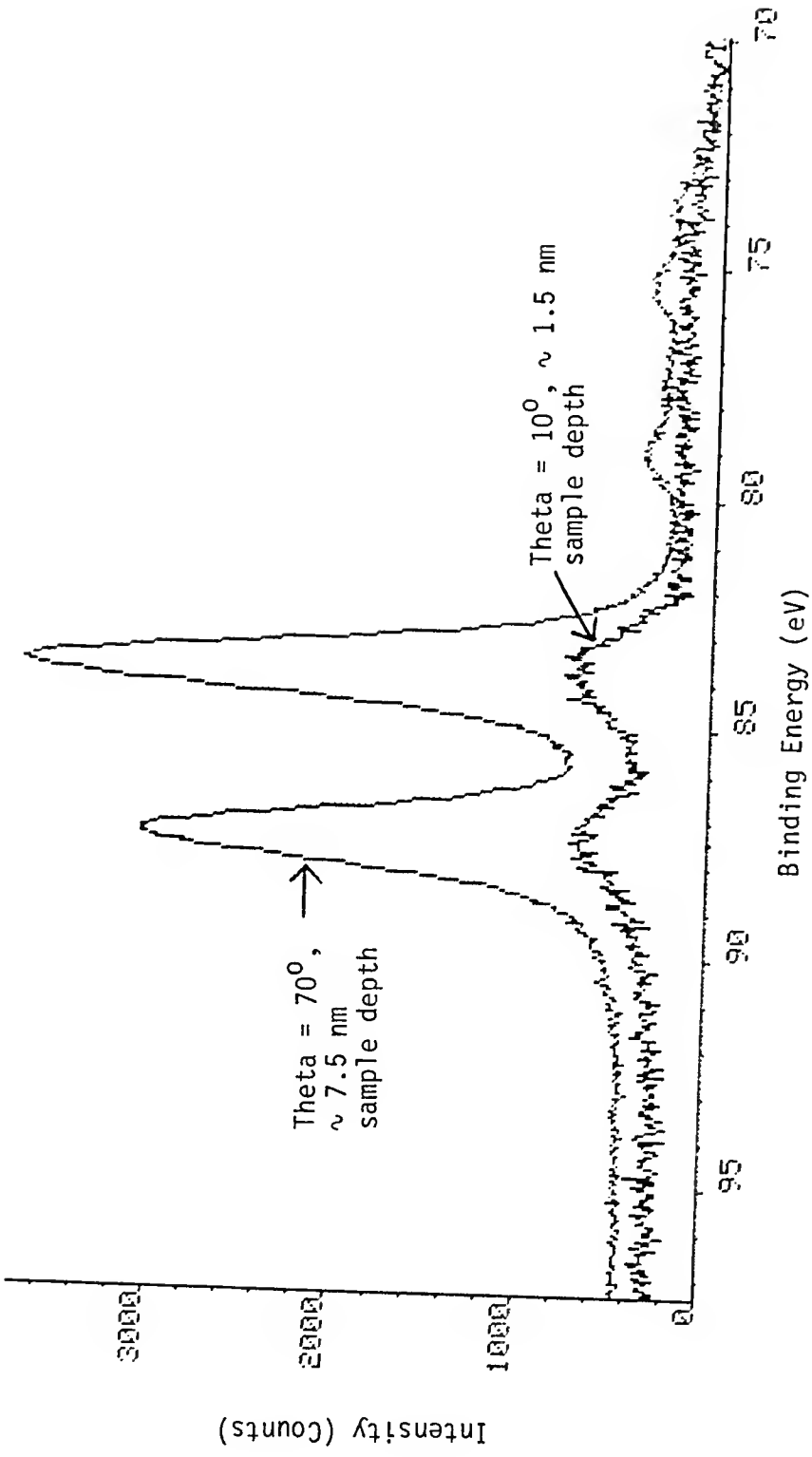

Figure 49. XPS Scan of Au $4f_{5/2,7/2}$ Peaks at High and Low Photoelectron Takeoff Angles

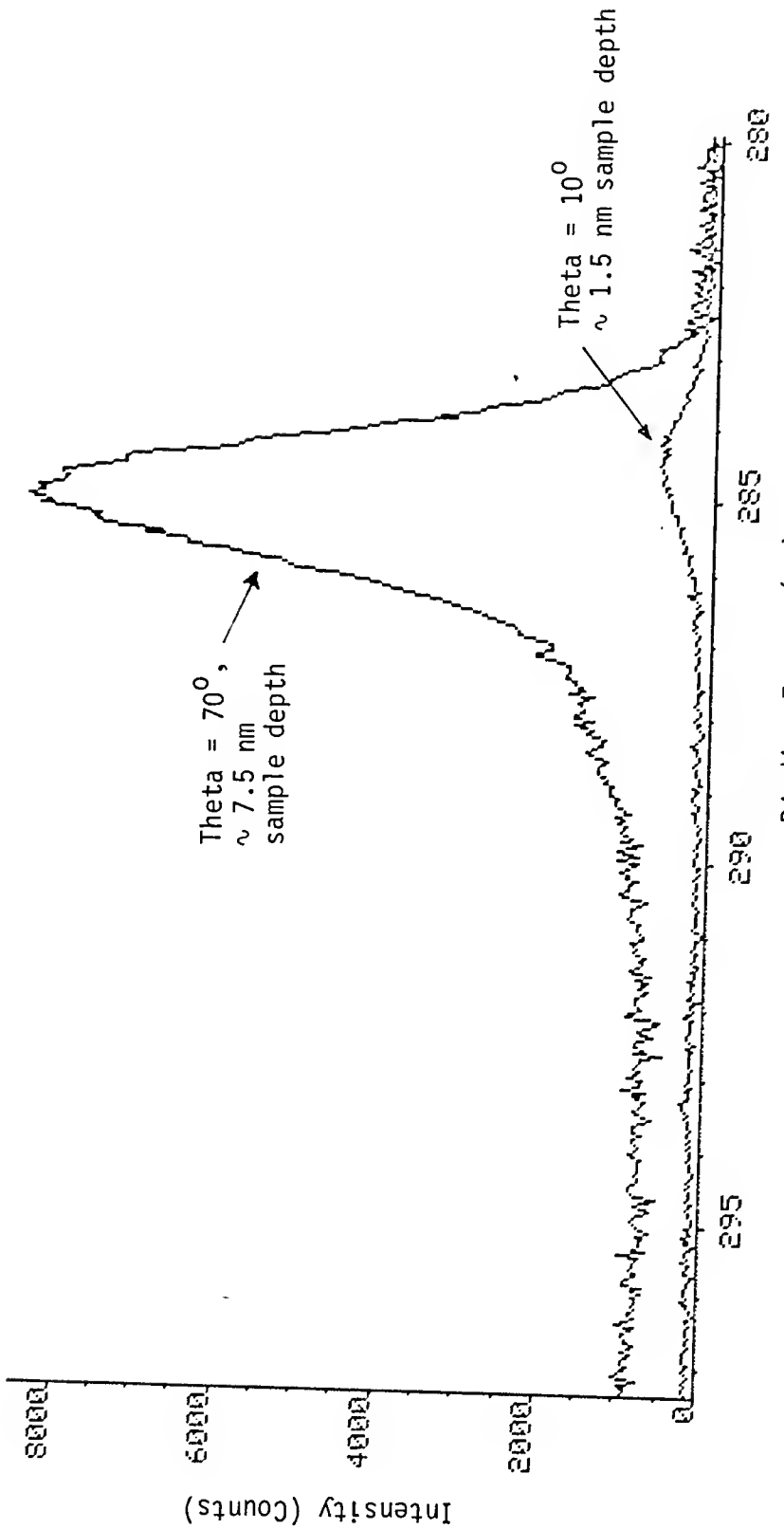

Figure 50. XPS Scan of C_{15} Peak at High and Low Photoelectron Takeoff Angles

annealing conditions. Both the H_2 and air annealed samples from 880602 had the same bulk Au mass concentration of 91%. Even the unannealed sample from 880527 had the same bulk Au mass concentration as its air annealed counterpart (~94%). These results were also consistent with the results of the gravimetric/AA study which indicated a range of 82-99% Au mass concentration in the as deposited films, with an average value of 91%.

The B.E.s and widths of the Au 4f peaks in all of the samples were not significantly different from the B.E.s and widths of the standard Au film. This was a critical factor in determining the probable formation mechanism of the P.R.P. superfine particles. The Au existed in the metallic state in the as deposited, air annealed and H_2 annealed sample films. The 0.2 eV difference in B.E. was not considered significant in the Kratos instrument and in fact similar shifts were observed in spectra of the Au standard taken several hours apart. Shifts due to Au-C bonding were expected to be 0.4 eV or greater.[76-78]

Scanning Electron Spectroscopy with Energy Dispersive Spectroscopy

The SEM/EDS analyses were performed on the standard Au film and P.R.P. coated sc W/Si, glass and polymeric tape substrates in order to determine grain size and film morphology. The Harris standard sputter deposited Au film was photographed as received and after undergoing one hour of Ar ion etching in the XPS study (Figures 51 and 52). The pebble-like film had a surface grain size of ~1000 nm and was fairly uniform in appearance. This is a typical structure for a sputter deposited Au film and is indicative of three dimensional hillock growth

Figure 51. SEM Photograph of Harris Stnd. Sputtered Au Film

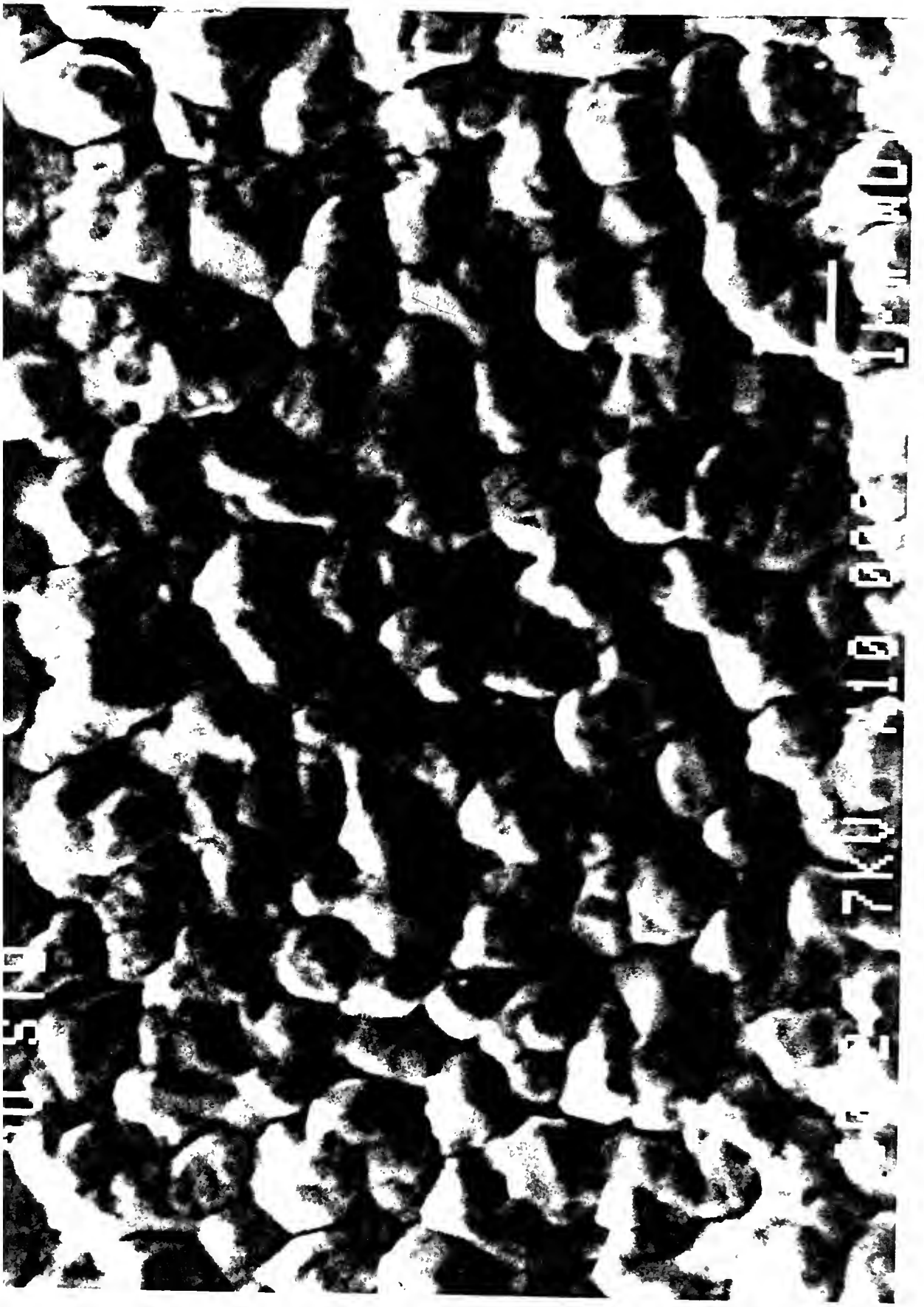

Figure 52. SEM Photograph of Harris Stnd. Sputtered Au Film After 1 Hour of Argon Ion Etching

Au film #9
SEI 8.15kV X10,000 1μm WD14

on islands. This was verified by the SEM of the same film after etching, which revealed the underlying Au island structure. The early stages of the hillock formation are visible on the larger island structures (Figure 52). These photographs also serve to illustrate some of the limitations of the sputter deposition process mentioned in Chapter I.

The EDS spectrum of the as etched film is presented in Figure 53. The large Au signal is the most prevalent peak, but the significant Si signal from the underlying substrate illustrates the sampling depth of several hundred Angstroms typical of EDS systems at 15 KV.

Figure 54 shows the EDS spectrum at 15 KV of the P.R.P. as formed and placed in a pile on the SEM mount. The strong Au signal is apparent. (Note that the intensity scales of the EDS spectra are given at the bottom right of each figure.) The SEM view of this sample was not revealing due to the mounting technique.

However, the as deposited P.R.P. film on sc W/Si clearly showed a uniform grain of ~4000 Angstroms (Figure 55). The 15 KV EDS spectrum of this surface (Figure 56) indicated that the Au/C film was very thin. A lower energy spectrum was not recorded for this sample.

The SEM photograph of the air annealed P.R.P. film on sc W/Si (Figure 57) shows a similar uniform grain size, but the structure is altered significantly. The Au particules appear to have joined to form a chain-mail type of structure with the carbonaceous material located in the interstitial areas. The 5 and 15 KV EDS spectra of this surface are presented in Figures 58 and 59. The strong Au signal in the former spectrum versus the higher energy spectrum again illustrates the

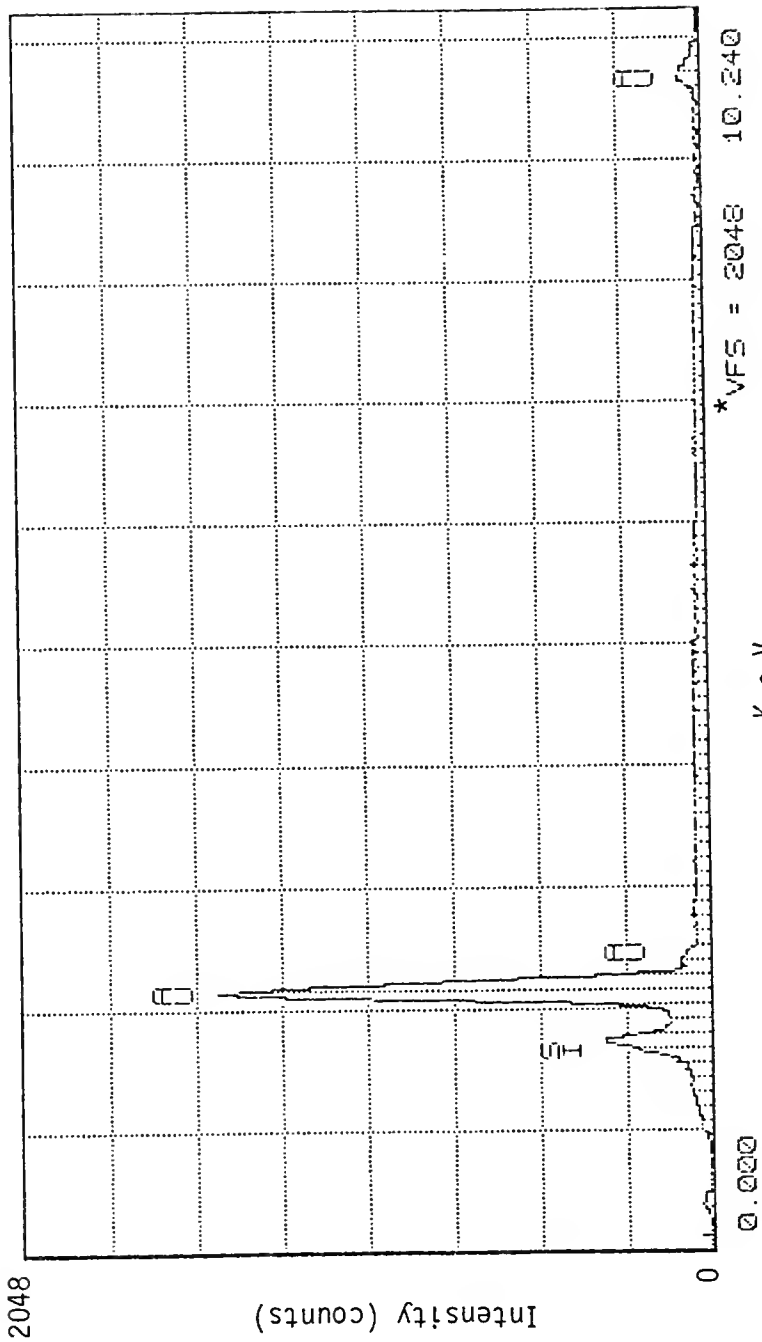

Figure 53. EDS of Harris Stnd. Sputtered Au Film on Si; 15 KV

*Vertical Full-Scale, Counts

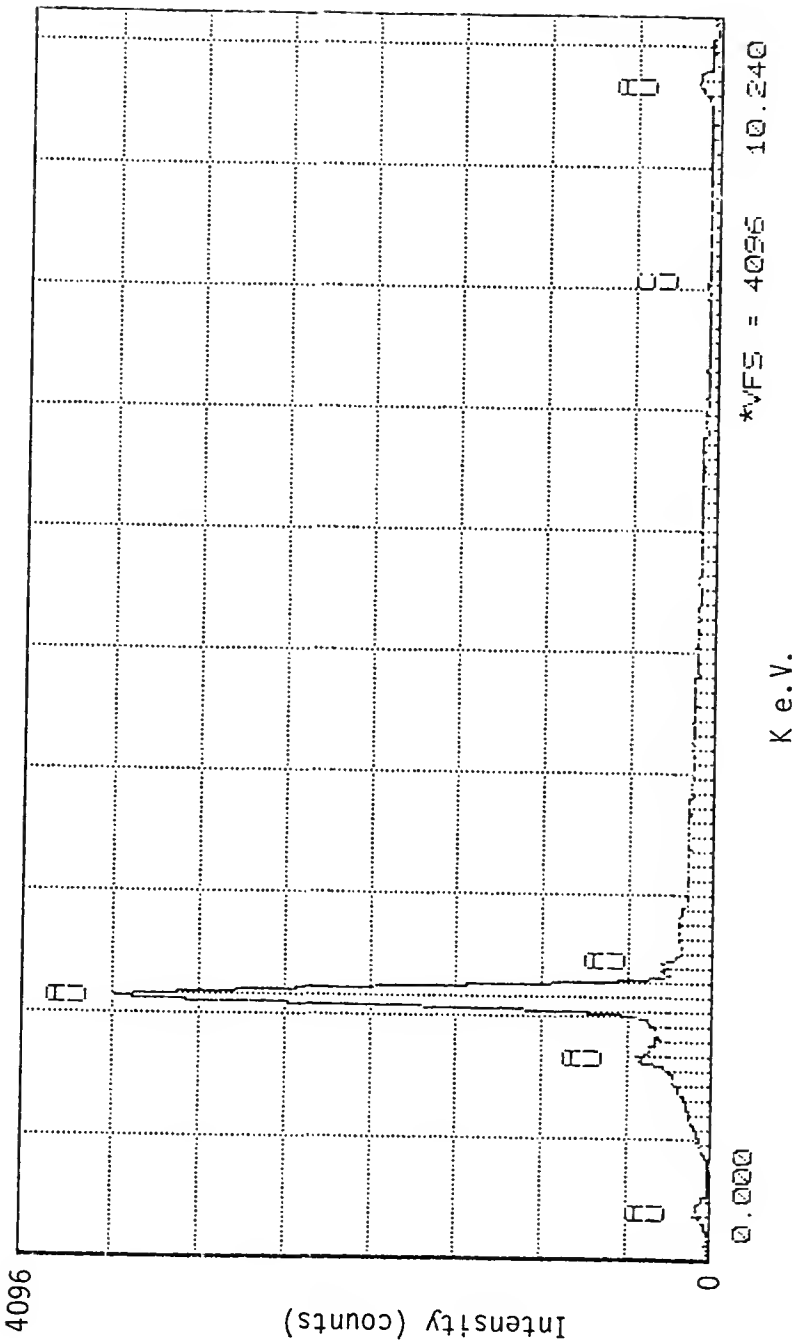

Figure 54. EDS of H_2/CH_4/Au Plasma Reaction Product (P.R.P.); 15 KV

*Vertical Full-Scale, Counts

Figure 55. SEM Photograph of P.R.P. on W/Si

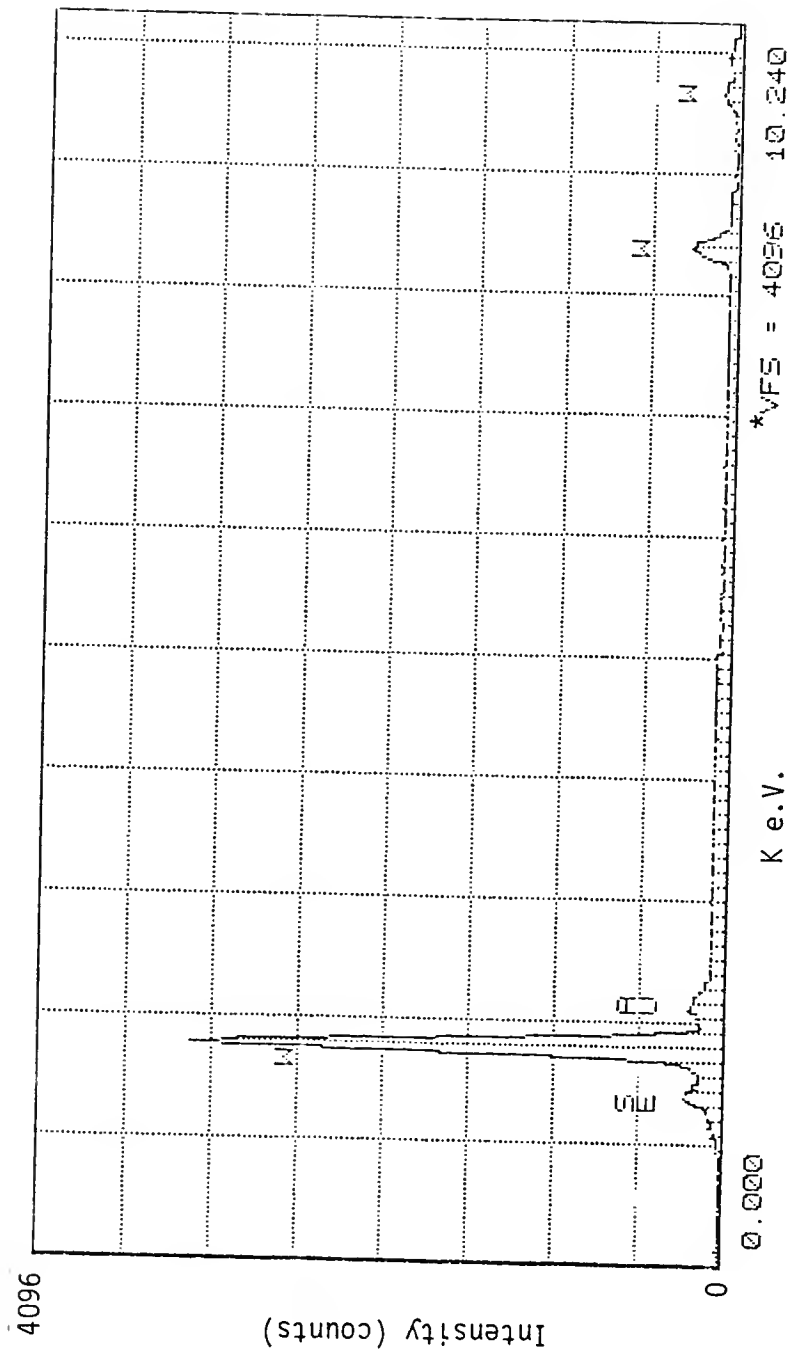

Figure 56. EDS of P.R.P. on W/Si; 15 KV

*Vertical Full-Scale, Counts

Figure 57. SEM Photograph of P.R.P. on W/Si After 250^{o}C, 18 Hour Anneal in Air

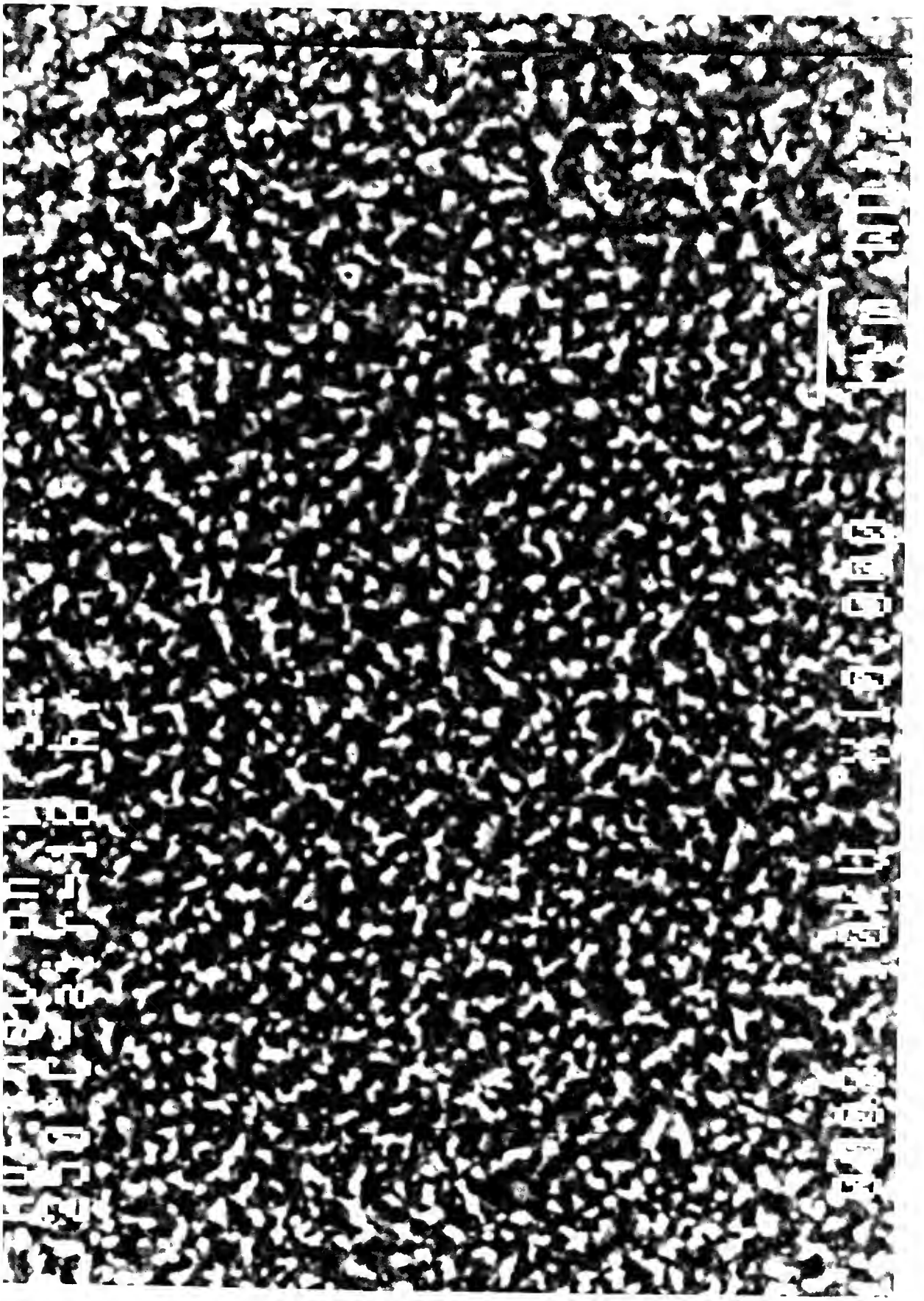

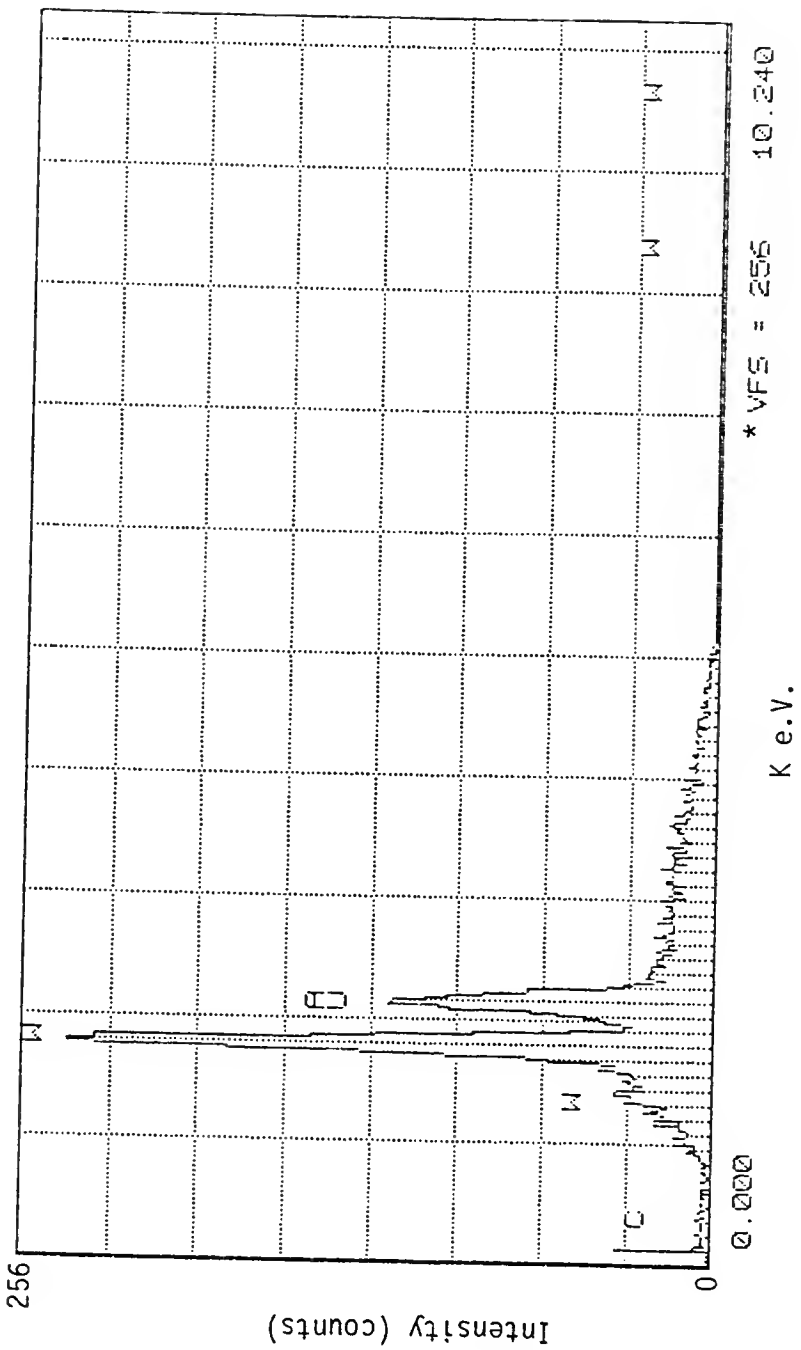

Figure 58. EDS of P.R.P. on W/Si After 250°C, 18 Hour Anneal in Air; 5 KV

*Vertical Full-Scale, Counts

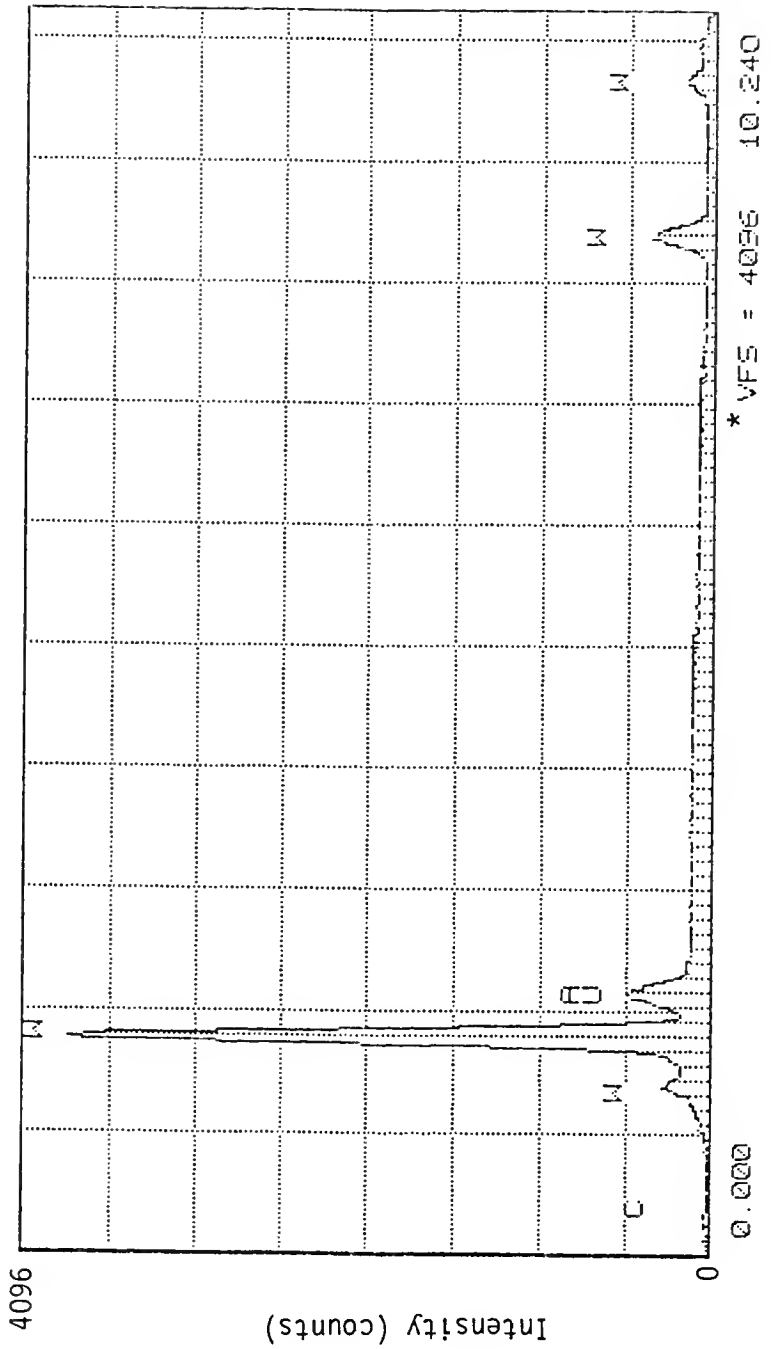

Figure 59. EDS of P.R.P. on W/Si After 250°C, 18 Hour Anneal in Air; 15 KV

*Vertical Full-Scale, Counts

thinness of the film and verifies that the photographed surface is composed of the Au/C system.

The SEM/EDS analysis of a hydrogen annealed P.R.P. film yielded results similar to the air annealed sample. The SEM photograph shows the same chain-mail structure but has less contrast between the Au and C areas (Figure 60). This may be due to the presence of a surface hydrocarbon film, as was indicated by the XPS results. Only the high energy EDS spectrum was recorded for this sample (Figure 61), and it verifies the presence of a thin Au surface film.

The SEM photograph of a P.R.P. film on sc W/Si that was deposited at 100^{o}C is presented in Figure 62. The three dimensional crystal structure of the Au film is very apparent, indicating advanced stages of growth. This can be explained by considering the high substrate temperature in the deposition process that formed the film. The increased motion of Au atoms and clusters on this surface allowed the small Au particles to agglomerate in the lowest energy structure accessible, i.e., the face centered cubic crystal structure. The overlapping crystals formed a very thin film, similar to the other P.R.P. samples, as indicated by the low and high energy EDS spectra pictured in Figures 63 and 64, respectively.

The P.R.P. coated on glass and annealed in air showed no discernible grain structure under SEM analysis. The 5000X image is shown in Figure 65, but images up to 50,000X were observed during the course of the analysis with the same results. The low and high energy spectra (Figures 66 and 67) were similar to the other samples with

Figure 60. SEM Photograph of P.R.P. on W/Si After 320°C, 18 Hour Anneal in Hydrogen

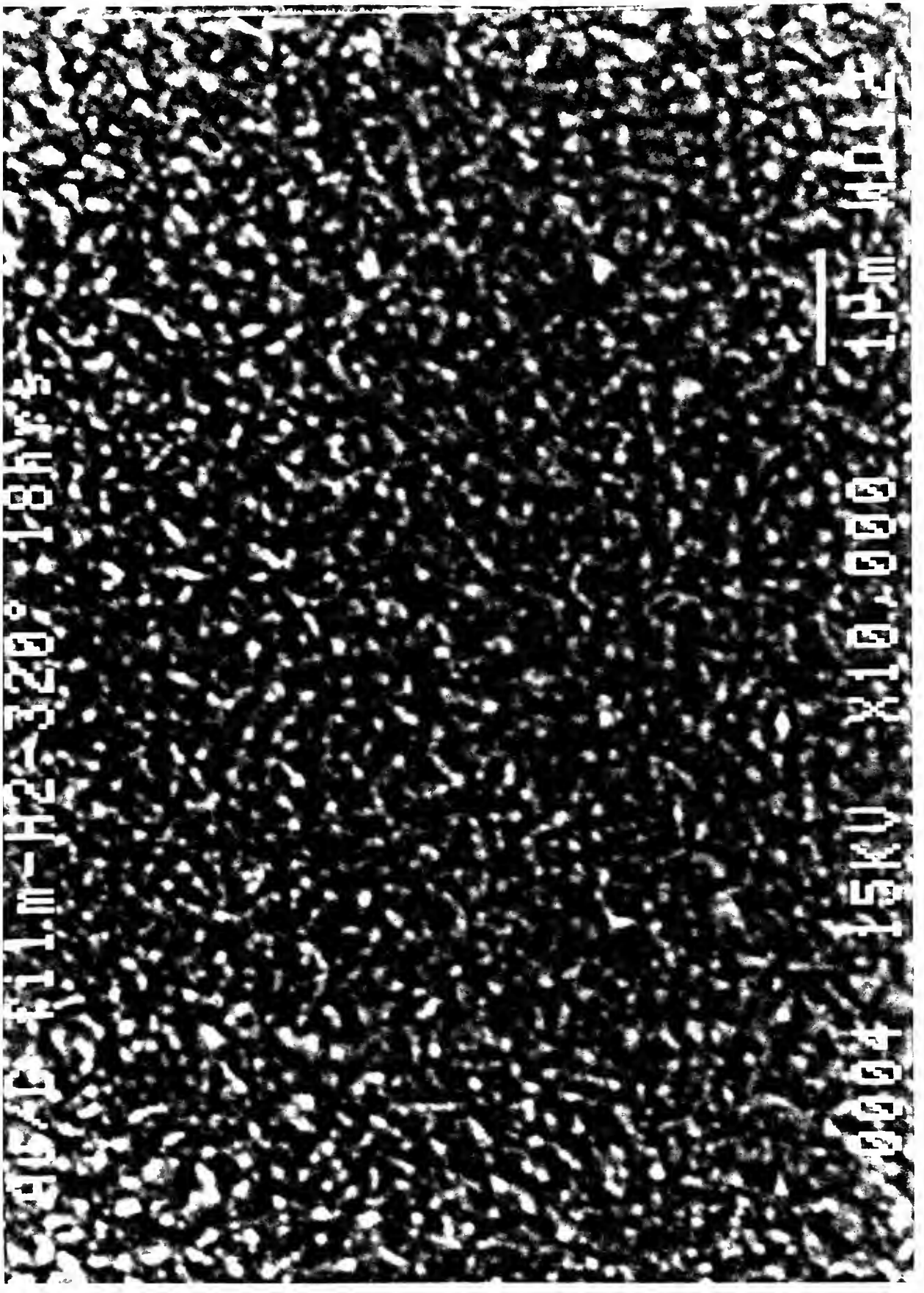
Ar+ 1.0 mA H2 320° 18hr
15kV X10,000 1μm

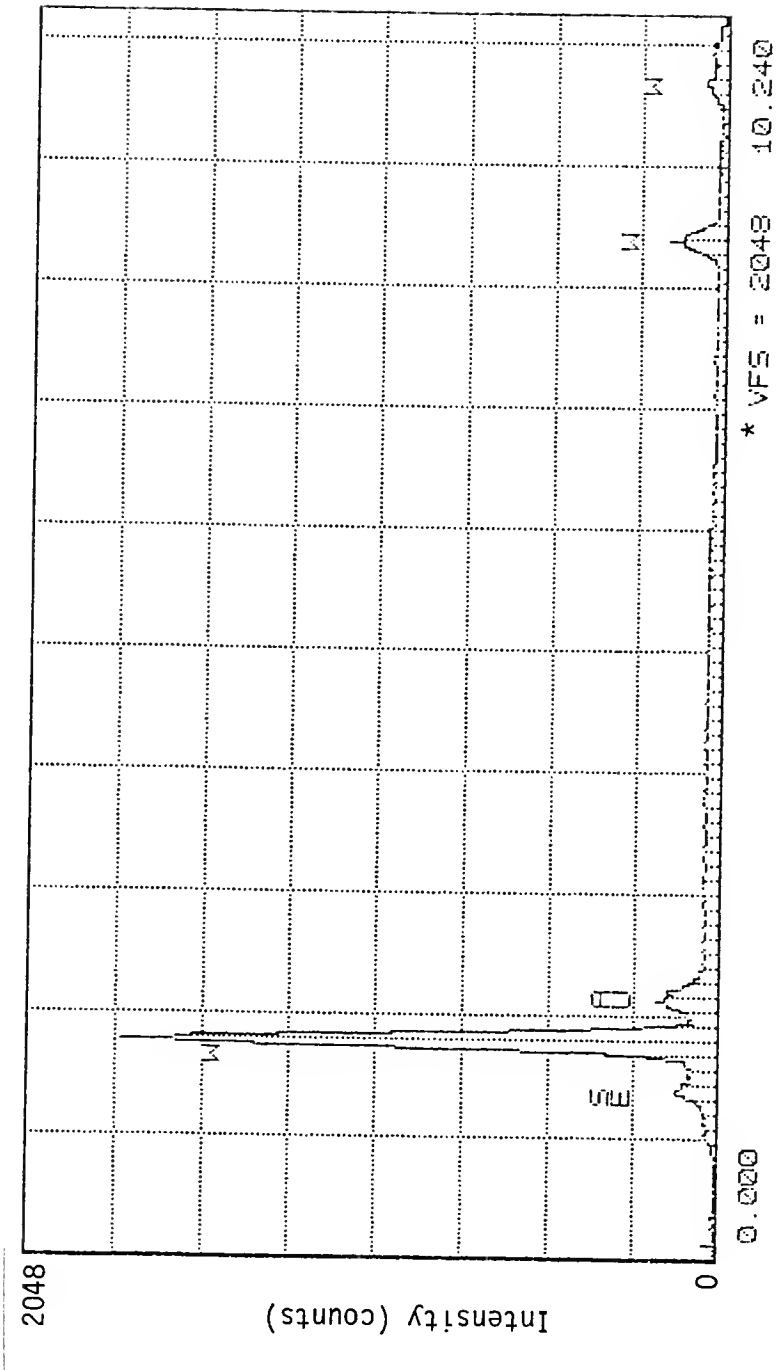

Figure 61. EDS of P.R.P. on W/Si After 320°C, 18 Hour Anneal in Hydrogen; 15 KV

*Vertical Full-Scale, Counts

Figure 62. SEM Photograph of P.R.P. on W/Si, 100°C Deposition

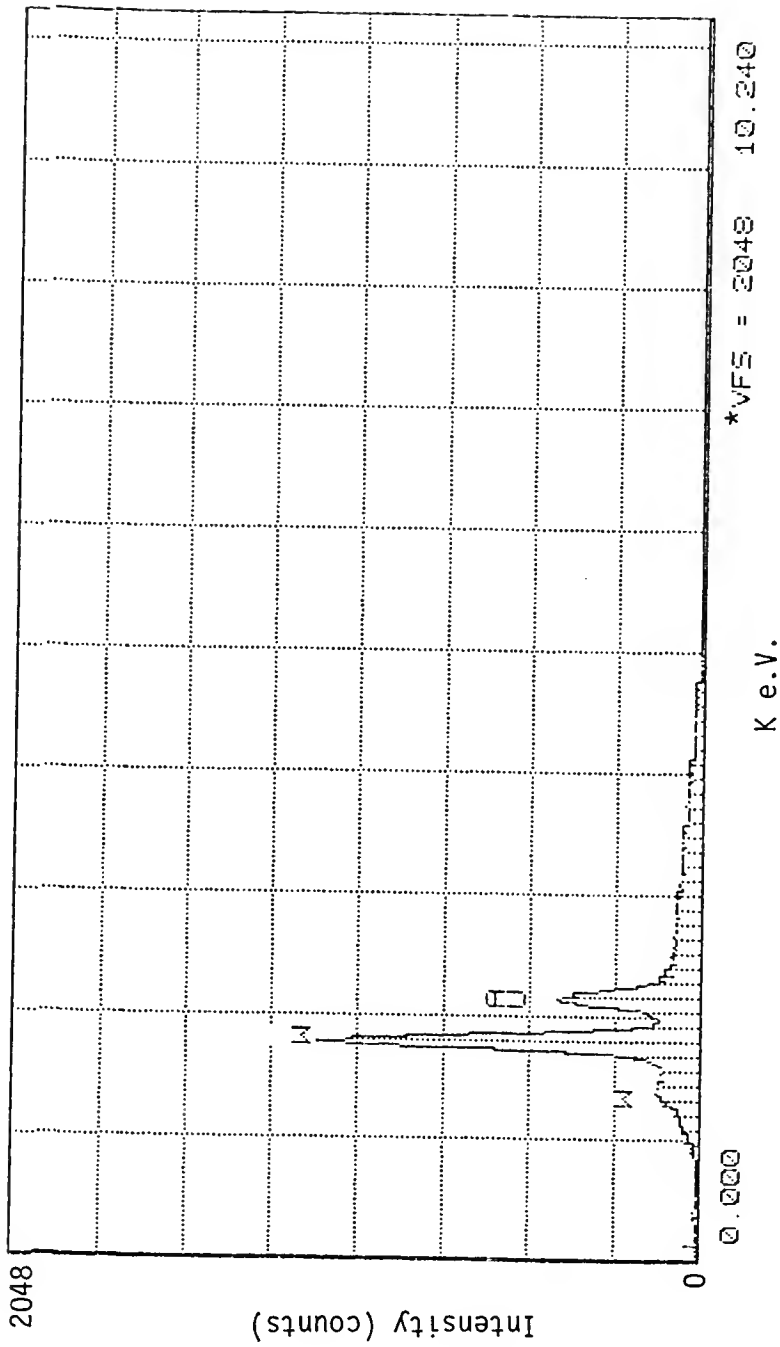

Figure 63. EDS of P.R.P. on W/Si, 100°C Deposition; 5 KV

*Vertical Full-Scale, Counts

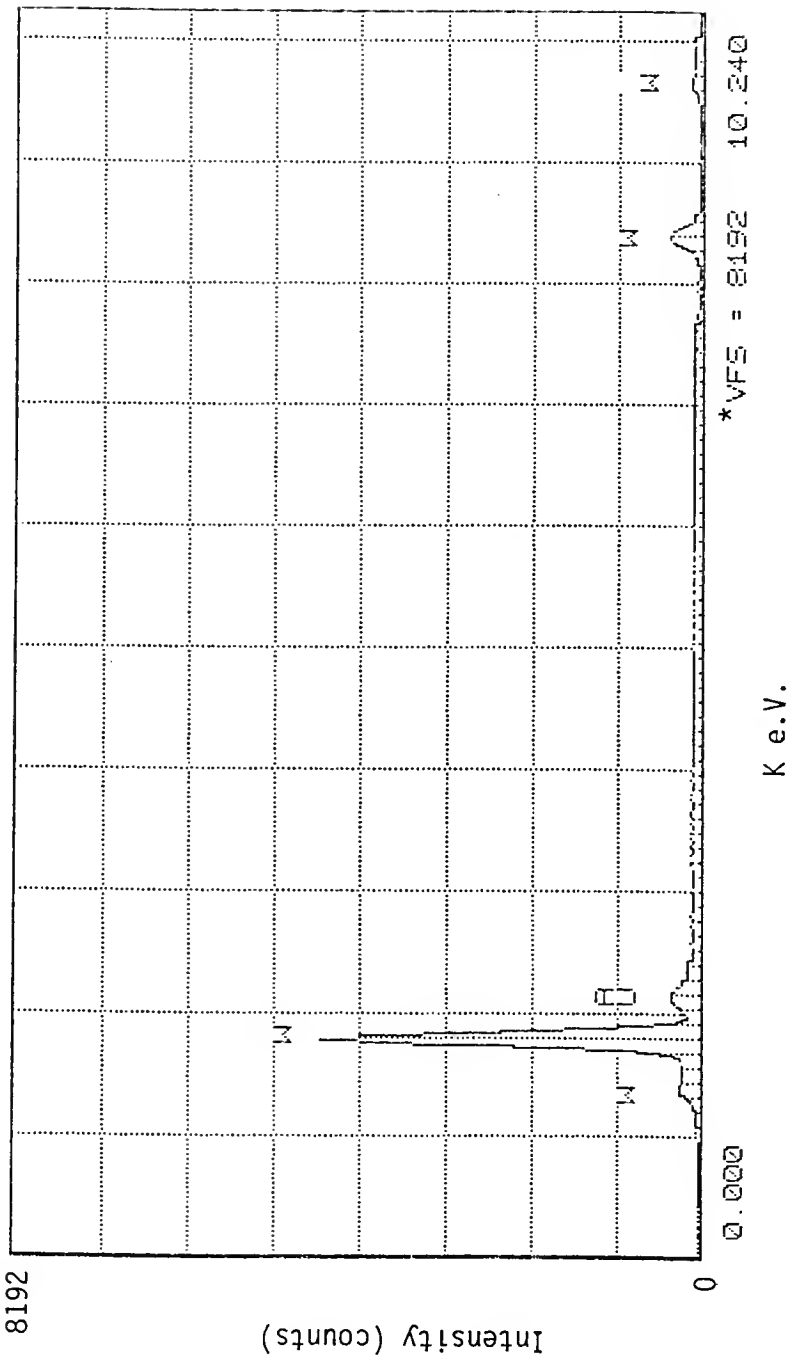

Figure 64. EDS of P.R.P. on W/Si, 100°C Deposition; 15 KV

*Vertical Full-Scale, Counts

Figure 65. SEM Photograph of P.R.P. on Glass After 400°C, 1.5 Hour Anneal in Air

Au soot on glass
400°C-air-1.5 hr
0005 4KV X5,000 1μm

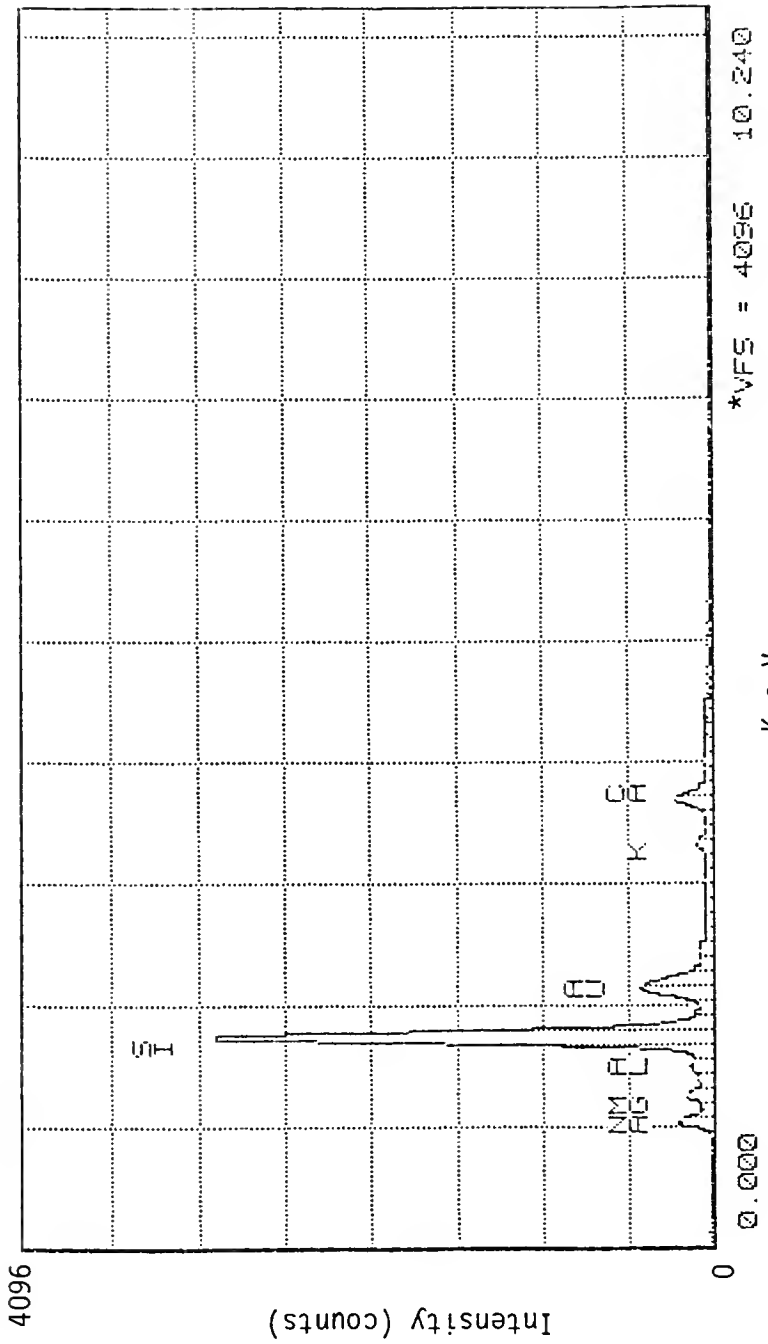

Figure 66. EDS of P.R.P. on Glass After 400°C, 1.5 Hour Anneal in Air; 15 KV

*Vertical Full-Scale, Counts

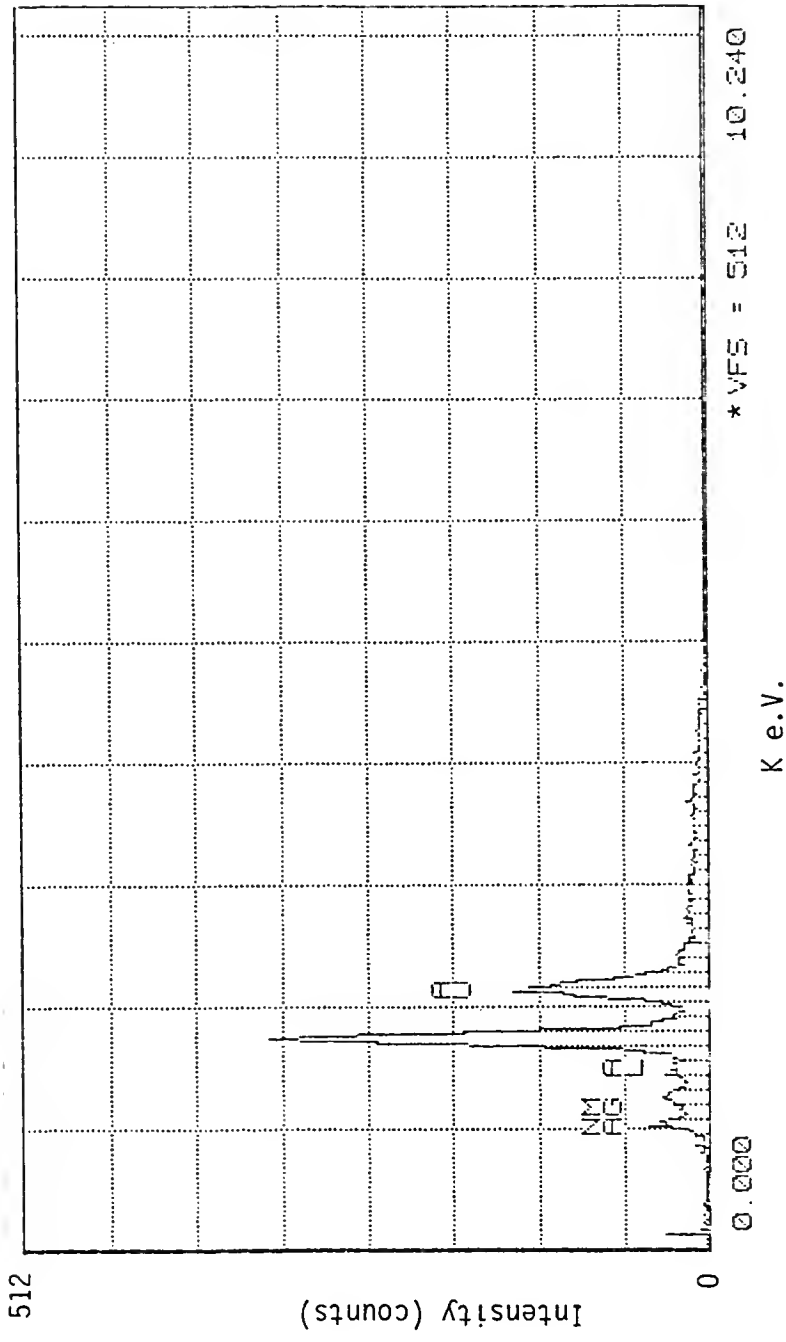

Figure 67. EDS of P.R.P. on Glass After 400°C, 1.5 Hour Anneal in Air; 5 KV

*Vertical Full-Scale, Counts

respect to the strong substrate signal (from Si in this case) indicating the thinness of the Au film.

The SEM photograph of a P.R.P. sample deposited on glass at 100°C showed an even more uniform, grainless structure (Figure 68). Again, the film was viewed under much higher magnification than pictured without obtaining additional structural information. The low and high energy EDS spectra for this surface (Figures 69 and 70) indicated that this was also a very thin film.

The P.R.P. deposited on the adhesive side of Scotch brand transparent tape and subjected to SEM analysis is pictured in Figure 71. A uniform dispersion of ~1000 Angstrom size grains is visible on the even finer grained background. The EDS spectrum (Figure 72) verified the presence of Au on this surface.

The last three SEM photographs included in this section (Figures 73, 74, and 75) show the laser annealed P.R.P. coated sc W/Si surface described earlier. Figure 73 clearly shows the dissipation front of the heat wave generated by the laser beam. The target spot is near the center of the photograph. Figures 74 and 75 show the effect of the heat described earlier. The increased openness of the grain structure is clearly evident in these shots taken at a 30° angle.

Electrical Resistance Measurements

The electrical feedthroughs that were subjected to air and hydrogen anneals while observing the resistance across a P.R.P. coated surface experienced problems with the electrode contacts. The electrodes were coated with a low melting alloy that was apparently

Figure 68. SEM Photograph of P.R.P. on Glass, $100^{o}C$ Deposition

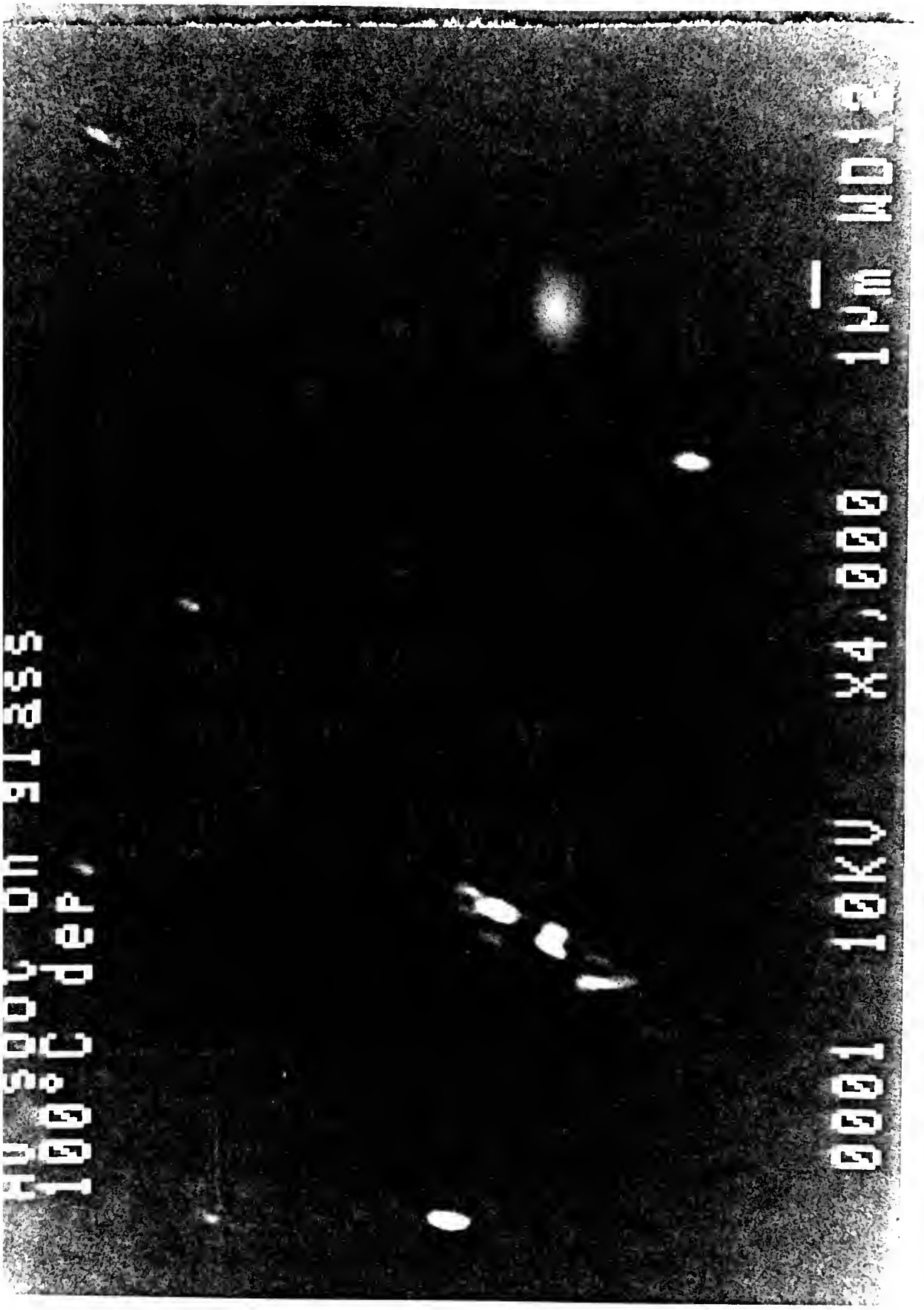
Au sputtered on glass
160°C dep.
0001 10KV X4,000 1μm WD15

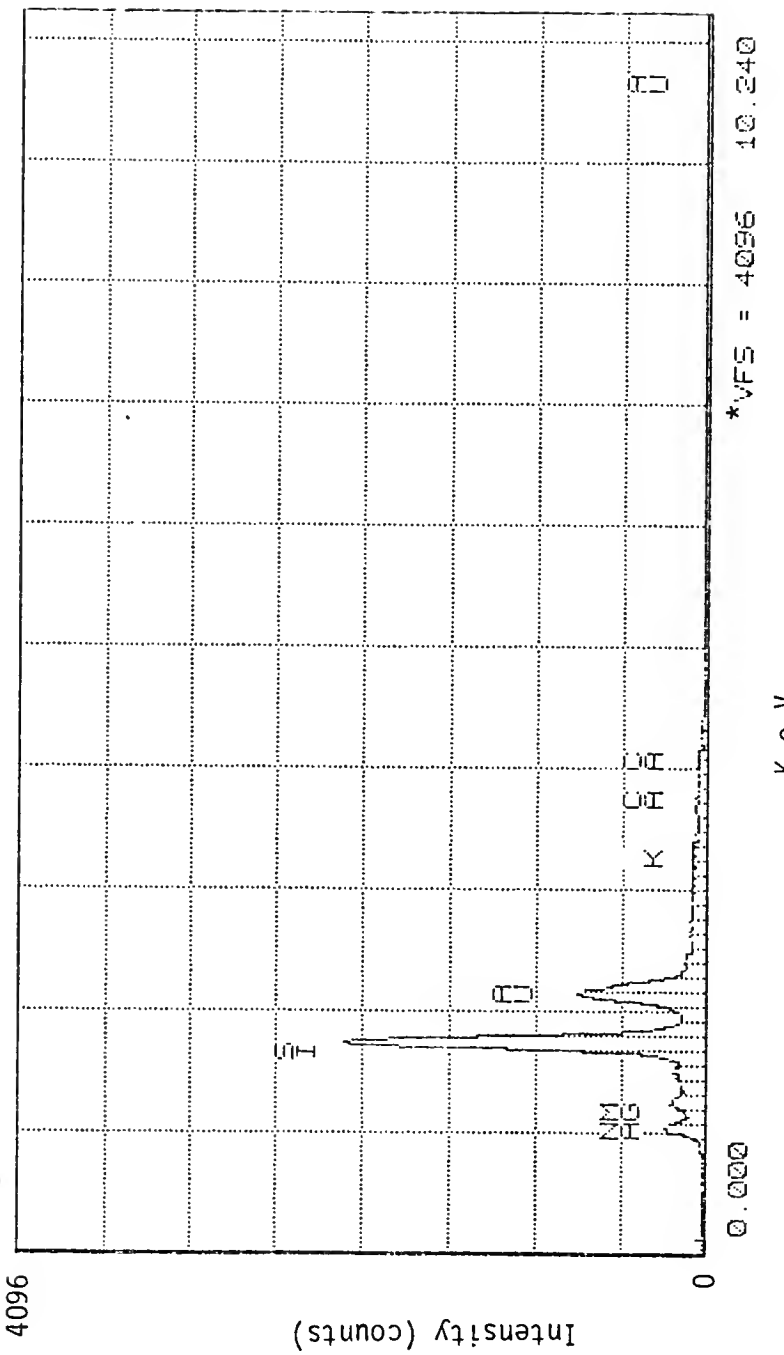

Figure 69. EDS of P.R.P. on Glass, 100°C Deposition; 5 KV

*Vertical Full-Scale, Counts

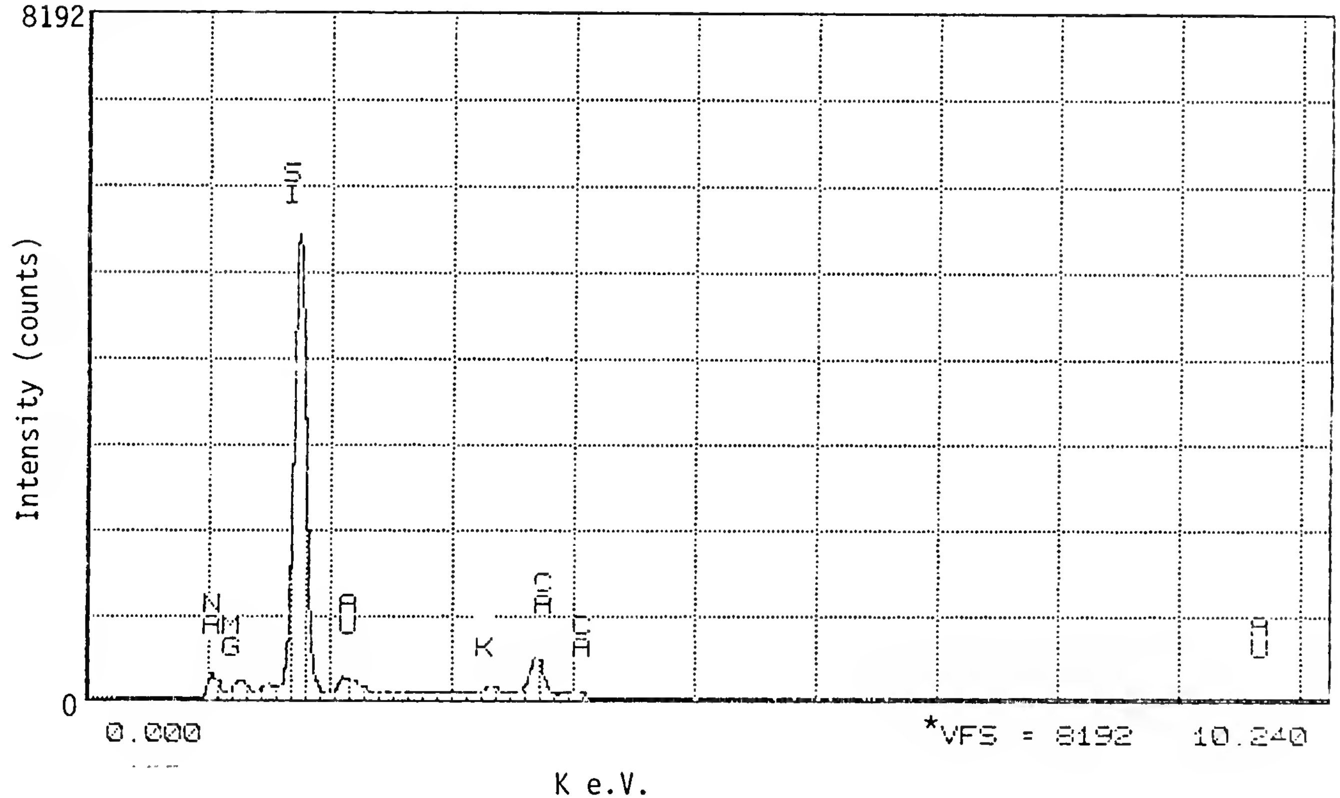

Figure 70. EDS of P.R.P. on Glass, 100^{o}C Deposition; 15 KV

*Vertical Full-Scale, Counts

Figure 71. SEM Photograph of P.R.P. on Adhesive Side of Scotch Brand Transparent Tape

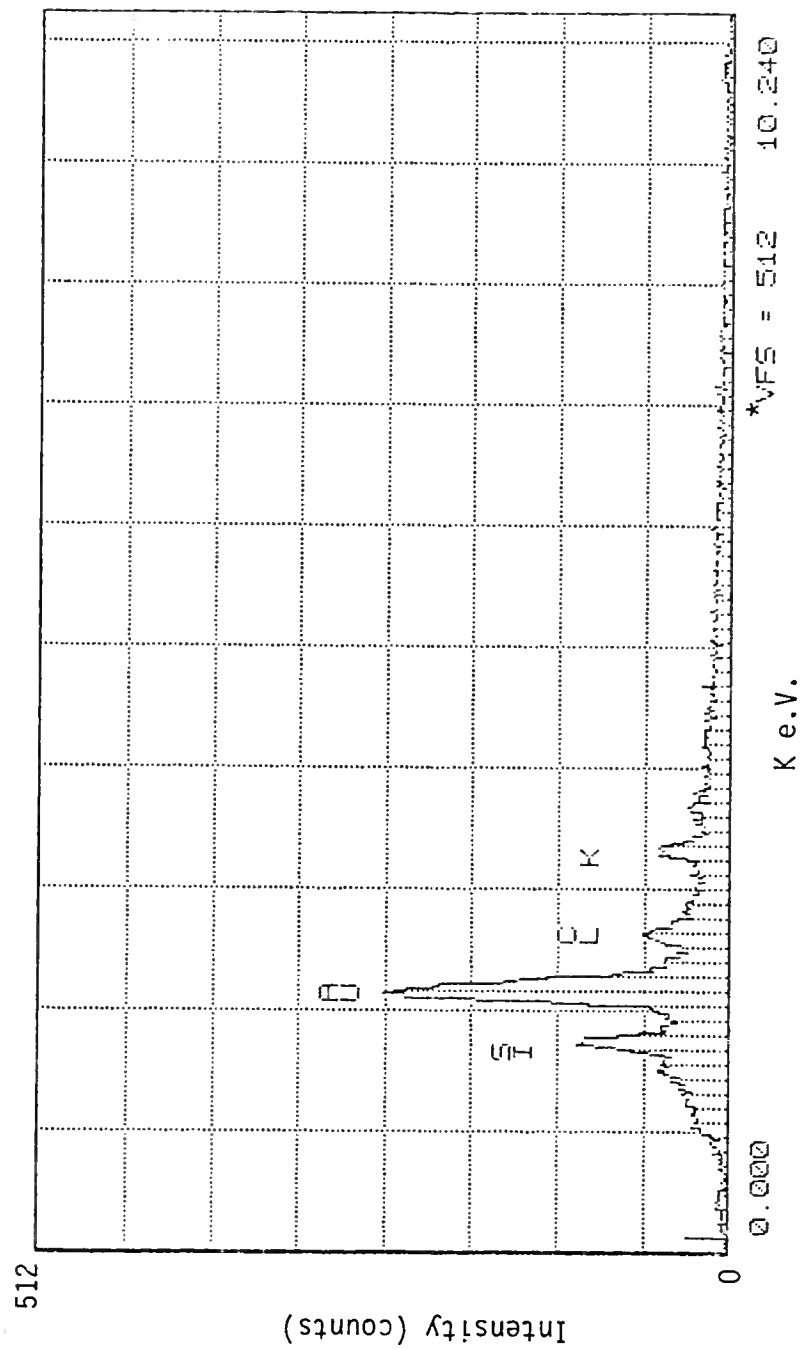

Figure 72. EDS of P.R.P. on Adhesive Side of Scotch Brand Transparent Tape; 14 KV

*Vertical Full-Scale, Counts

Figure 73. SEM Photograph of Laser Annealed Area of P.R.P. on W/Si


0009 15KV

Figure 74. SEM Photograph of Unannealed P.R.P. on W/Si

AU SOOT
P1/3 10/20 X20,000 1μm

Figure 75. SEM Photograph of Laser Annealed Spot of P.R.P. on W/Si

0.4K SOOT LASER SPOT

meant to facilitate soldering. This film melted and broke the contact in the first test (air annealed sample). The feedthrough used in the second test (H_2 anneal) was etched in con. HCl and baked at 600°C for 18 hours before being coated with the P.R.P. The results of this test are presented in Figure 76.

Figure 76 illustrates the electrical properties of a forming Au film. The early conductance (low resistance) of the film indicated that the closely packed particles had enough contact to complete the circuit. As the temperature was increased the particles coalesced into separated islands and lost contact with one another. As the temperature rose to over 300°C the Au islands began merging and eventually completed the circuit again. This island formation and coalescence has been observed by other investigators and is typical of Au film growth.[79,80]

Four point probe resistance measurements showed a sheet resistance value (Rs) of 0.09 Ohms per square mm for the Harris standard Au film. The two coated glass plates that were analyzed by SEM/EDS showed infinite resistance at all input settings, indicating the discontinuity of the films. The same results were observed with the coated black electrical tape, the coated transparent tape, and an air annealed coated GFF sample.

The glass plate coated with Au from He plasma (by line of sight deposition) had a Rs value of 2.3 Ohms/mm^2 and a quartz window thickly coated with P.R.P. had a Rs value of 5600 Ohms/mm^2. These two samples indicated the effectiveness of the He plasma for producing conductive

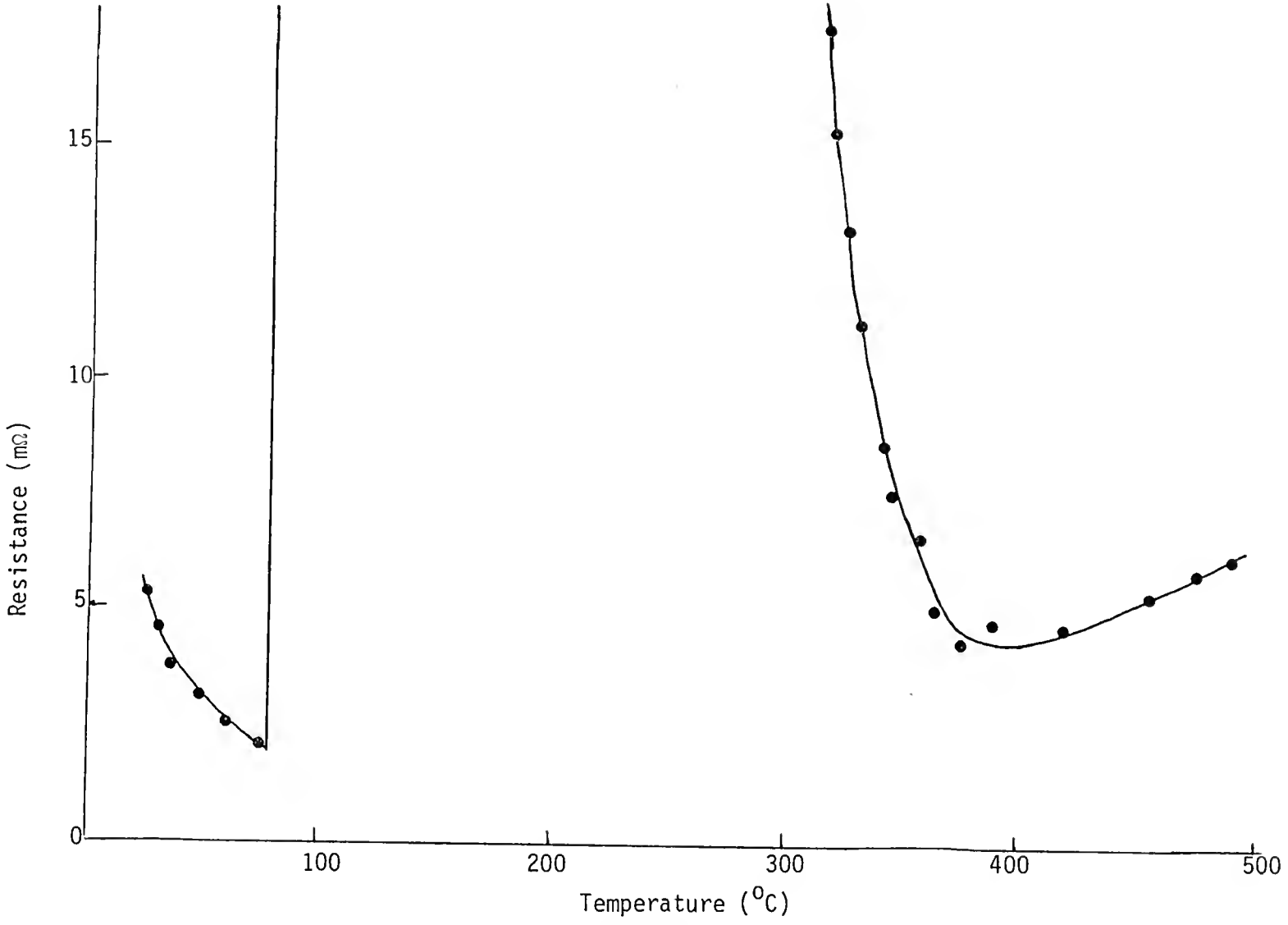

Figure 76. Electrical Resistance vs. Temperature for a P.R.P. Coated Feedthrough

Au films in close proximity to the plasma zone, and the conductivity possible with a thick layer of the P.R.P., presumably due to the close proximity of the Au particles to each other and the limited conductivity of the carbonaceous material.

CHAPTER IV
SUMMARY AND CONCLUSIONS

Discussion of Plasma Reaction Product Formation

The extensive experimental evidence gathered in the production and characterization of the P.R.P. can be appropriately summarized in a discussion of its formation. Only a general description of the gold/carbon ultrafine particle formation can be deduced from this evidence. A definitive formation mechanism could not be deduced without substantial additional analytical information, such as transmission electron microscopy of isolated particles, in situ diagnostic spectroscopy of the plasma, and in situ mass spectrometry of plasma generated ions. While these efforts were beyond the scope of this study, the general mechanism presented below is strongly supported by the experimental evidence. There are necessarily some missing details in the proposed mechanism. Each step is presented sequentially below along with a brief discussion.

1) The first photons in the 250 nanosecond pulse to reach the gold surface were partially reflected and partially absorbed by conduction band electrons via an internal photoelectric effect. Electron-phonon collisions, which occur on a time scale of 10^{-12} to 10^{-13} sec in good conductors, changed the energy input into heat and caused rapid vaporization of some of the metal.[73] Because of the speed

of this process, the vapor front was initially the same density as the solid phase and was highly ionized due to its high temperature.[72]

2) As the dense, ionized vapor front expanded into the reactive gas mixture, the shock wave generated by the explosive heating process traveled in the opposite direction, through the molten surface material and into the solid bulk. This shock wave caused large chunks of molten material to be blown off the target. The smallest of these particles appeared as spheroids greater than 10 microns in diameter. Larger particles had irregular globular surfaces. Since these particles ended up in the bottom of the reaction chamber, it is assumed that their role in the formation of the ultrafine gold/carbon particles collected downstream from the reaction zone was minimal. However, their presence complicated the mass-balance determination of the amount of material that was actually vaporized during each laser pulse. Instead, a reverse calculation based on the amount of material collected in four filter catch experiments showed that an average of 8.7×10^{14} atoms of Au per pulse were vaporized and subsequently reacted to form the captured product. (The range of averages for the four experiments was $6.6\text{-}10.5 \times 10^{14}$ atoms/pulse.)

3) The advance of the ionized plume was preceded by hot electrons which excited the ambient gas before the gold arrived. This resulted from the production of high energy electrons during step 1) that had a most probable thermal velocity, $V_p = (2kT/m)^{1/2}$, and expanded from the surface in all directions, but with a distribution that favored coaxial dispersion of the highest energy electrons.[81] These electrons caused a rapid increase in the optical density of the ambient gas (via inverse

bremsstrahlung) which led to further excitation of the species present in a manner analogous to the gas breakdown phenomena described earlier. This effect also limited the amount of incoming laser energy that reached the surface of the target. Since electron temperatures are typically an order of magnitude higher than ion temperatures in this regime,[80-82] and the electron mass is five orders of magnitude smaller than the Au ion mass, the velocity of the hot electron front was three orders of magnitude faster than the ion plume front.

Tan et al.[82] determined an empirical relationship between the fastest ion velocities in cm/sec, Vi, and the peak laser fluxes from Nd glass lasers and CO_2 lasers in W/cm_2, Ip. They found that Vi was independent of atomic number and the laser wavelength and was proportional to the peak irradiation, Ip:

$$Vi = 5.7 \times 10^6 \, Ip^{1/6}$$

Using this relation and the peak irradiation value of 3×10^9 W/cm^2 yields a Vi of 2.2×10^8 cm/sec. The experimental evidence presented by Tan et al. showed that over 80% of the ions have velocities in excess of 1/2 Vi. This calculated value is in reasonably close agreement with the experimentally determined value of 3×10^7 cm/sec for aluminum ion velocities in similar plasmas with Ip = 2×10^8 W/cm^2 reported by Dyer et al. (Note that Tan et al.'s empirical relationship predicts a Vi of 14×10^7 cm/sec for this case.) Thus, an upper limit for the total distance traveled by the ionized plasma front during the 250 ns laser pulse is given by

$$(2.5 \times 10^{-7} \text{ sec}) \times (2.2 \times 10^{8} \text{ cm/sec}) = 55 \text{ cm}$$

Of course the plasma front never extended out to this distance due to collisional energy losses within the expanding plume itself, and between the plume front and the ambient gas. The point to be made here is that the expanding Au plasma was continuously irradiated with the incoming laser photons during its reactive expansion, and thus ample energy was available not only from the hot plasma but also from the incident laser radiation to stimulate high energy reactions in the core of the plume. Tonon and Rabeau[83] measured a mean ion temperature of 30 eV in a hydrocarbon plasma produced by a 100 ns CO_2 laser pulse incident on a solid polyethylene target with a peak intensity of 6×10^9 W/cm^2. Assuming an analogous situation occurred in the plasmas generated in this study, the Au ions were hot enough to be in the plus 2 state (2nd ionization potential of Au = 20.5 eV).

The high temperature (light emitting portion) plasma generated in this study extended approximately 5 cm from the target surface and was roughly spherical initially. The plasma shape became more prolate as target cratering progressed and took on the classic shape of a candle flame after several minutes of pulsing on the same spot (Figure 77). The coaxial core of the plasma was white, indicating high temperature broadband emission, and extended from the target surface to about 2/3 of the distance to the edge of the light emitting zone. This hot core was only a few millimeters in diameter and it was apparent from photographs that the plasma was radially symmetric and the brightest emission was from a hemispherical plume 2-3 mm in diameter that originated at the garget impact point.

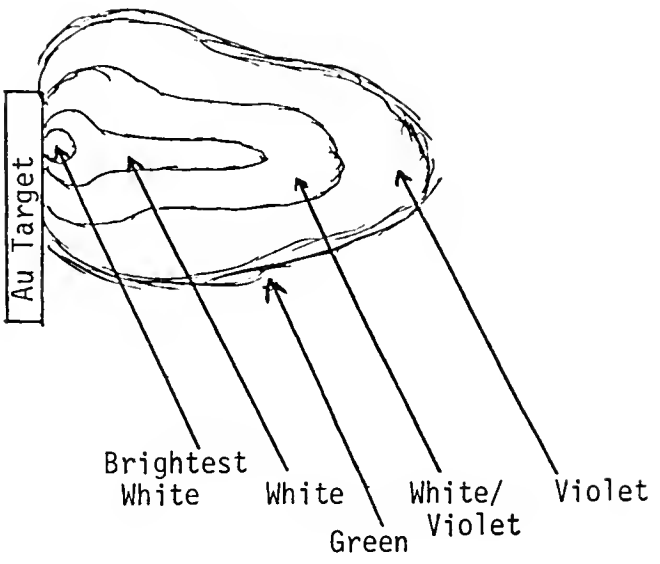

(Actual Size Pictured)

Figure 77. Typical Plasma Produced by the Pulsed CO_2 Laser Incident on a Solid Gold Target in 1350 Pa of 3:1 H_2/CH_4

4) Thus, the ionized gold plume expanded into an excited state methane/hydrogen atmosphere and approximately 10^{15} ions/atoms of Au ultimately reacted with the carbonaceous species present and were collected downstream from the reaction zone. This step contains the greatest amount of uncertainty. It was not apparent from the experimental evidence if the Au and C were intermixed at all levels in the particles, or if the C was associated primarily with the exterior of the particles. It was shown conclusively by XPS studies that the Au exists in the metallic state in particles, or equivalent connected network structures, no smaller than 50 Angstroms in diameter. This lower size limit can be assigned since pure Au particles smaller than this, or Au/C in a bonded state, produce significant shifts in the Au 4f binding energies.[84-86] No such shifts were observed in the spectra.

High angle XPS studies of unannealed and air annealed particle films formed during the same plasma experiment showed only a small decrease in the C/Au ratio, from 0.96 to 0.92. Profile XPS studies of an air annealed and a hydrogen annealed sample (from different plasma experiments) showed C/Au ratios in the film bulk of 1.56 and 0.64, respectively. (This compares to a C/Au ratio of 0.25 in the Harris standard Au film bulk.) However, the conductivity tests, the reflectance spectra, the MS studies, and the observation of visible clouds rising from the surface of films during laser anneals, all indicated that carbon compounds were associated with the exterior surfaces of the particles.

Thus, there is evidence that the carbon is present on the exterior of the particles, and that is may also be present in the interior of

the particles. It is not clear whether the C is incorporated in the interior of the particles or is trapped in grain boundaries between particles in the annealed films. Therefore, it is not possible to define a mechanism that would accound for the incorporation of C in the Au particles. It is possible, however, to speculate on the particle nucleation and growth mechanism by considering the above discussion and the experimental results.

The total volume of the luminescent plasmas represented by Figure 77 was approximately 40 cm^3. At a CH_4 partial pressure of 1350 Pa, there were 3.2×10^{18} molecules of CH_4 present in the plasma sweep volume under static conditions. This was more than three orders of magnitude greater than the number of Au atoms that reacted to form the P.R.P. during each pulse. When the plume expanded at $\sim 10^8$ cm/sec this gas was compressed and partially swept away. The high order of P.R.P. formation dependency on the CH_4 pressure under static conditions indicated that the density of carbonaceous species at the plume front (where most of the collisions between Au and C species took place) was a critical parameter. The formation of P.R.P. using CO and CO_2 in place of CH_4 indicated that carbon, rather than some unique hydrocarbon, was the dominant (along with gold) species involved in the P.R.P. formation. A more exhaustive study of the pressure dependency on these three gases would yield further insight into the mechanism of C inclusion.

5) It seems probable that the Au underwent homogeneous nucleation in the expanding, cooling, plasma front and formed Au particles larger than 50 A which then contacted the carbonaceous species and became

coated with the C material. At this point more Au may have been incorporated in the growing pargicle, or the C coating may have prevented further Au addition. A detailed TEM study of individual particle cross sections would show which scenario is correct.

Of the four CH_4/H_2 P.R.P. filter experiments, two had C/Au ratios of 3.5, one had a ratio of 0.16, and one had a ratio of 28. The CO and CO_2 filter experiments had ratios of 0.85 and 0.69, respectively. This larger range of ratios supports the exterior growth mechanism for C addition. Figure 78 shows a plot of the relation of particle size to the ratio of C/Au required to form a monolayer coating of C on the exterior of a solid Au particle. (This plot was constructed using a hard-sphere model with the diameters of Au = 2.9 A and C = 1.4 A.) For particles in the size range of 100 to 1000 A, ratios of C/Au in the range of 1.0 to 0.1 would be required. This is consistent with the XPS data and the experimentally determined C/Au ratios for most of the tests. The higher ratios, 3.5 and 28, were probably due to additional C buildup on the exterior of the particle. This point was evident in the highest ratio sample which lost the bulk of its C weight during an air anneal. (A precise measurement of the loss was not possible due to nonreproducible binder losses from the glass fiber filters during the annealing process.)

So, while a limited amount of C may be incorporated along with Au on top of a pure Au core in the growing particle, it seems likely that the majority of the C is added to the exterior of the Au core. Agglomeration of these C coated particles in the gas phase may account for their entrainment in the gas phase, or the growth mechanism of the

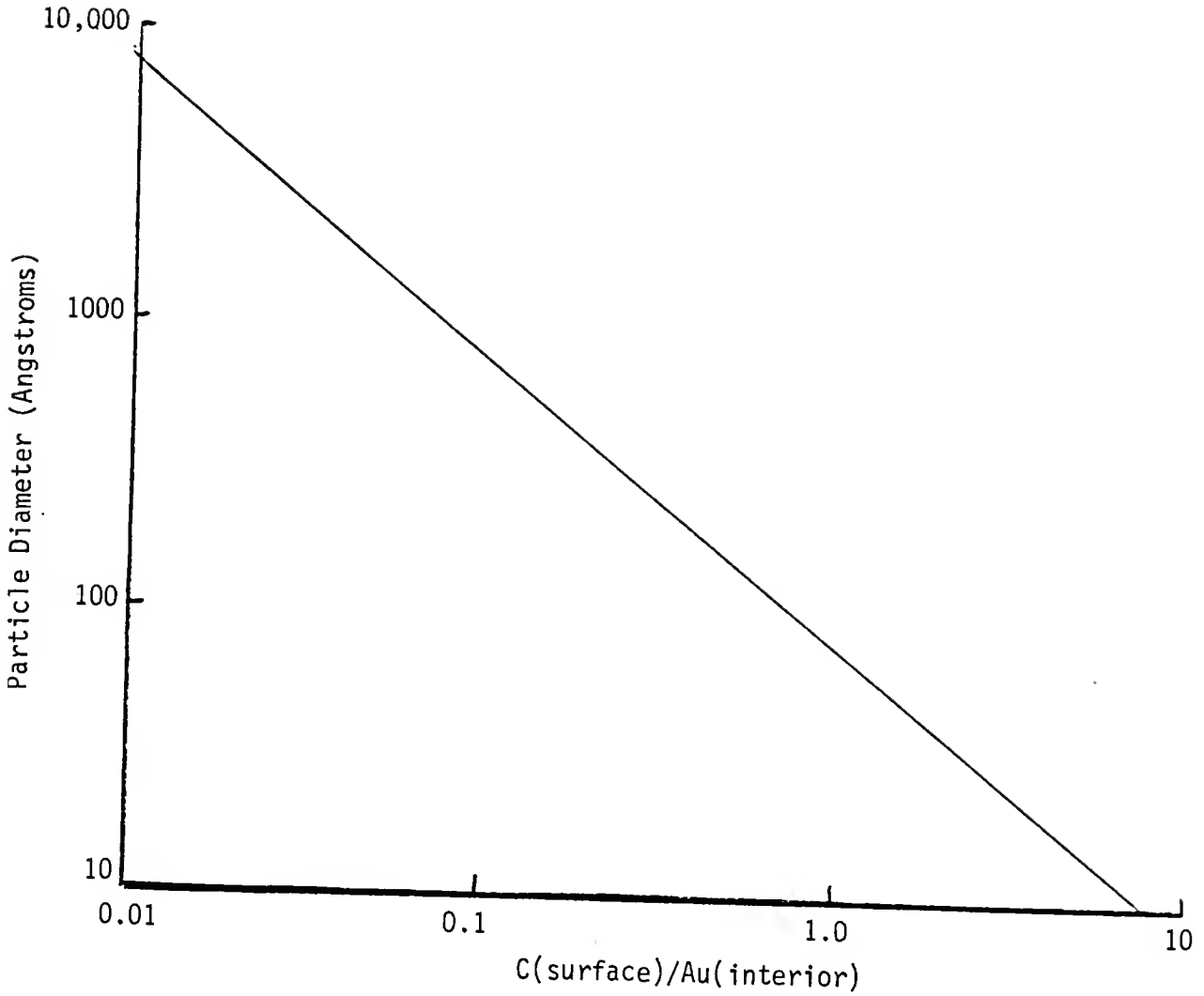

Figure 78. Particle Diameter Versus Ratio of Carbon Atoms, Required to Form a Monolayer on the Surface, to Gold Atoms in the Particle

individual particles in the presence of the carbon compounds may be responsible for producing a particle of sufficient size and density to be entrained in the gas stream. Both of these scenarios depict a heterogeneous formation mechanism for the P.R.P. The lack of Au transported to the filter in plasma experiments that utilized inert gases and hydrogen under similar gas flow regimes, and the lack of soot collected on the filter in a CH_4/H_2/graphite plasma experiment, both support the assumption of a heterogeneous mechanism.

Conclusions

The results of this study showed that superfine particles, or particle agglomerates, of gold/carbon in the 100-400 nm size range could be produced in a pulsed CO_2 laser stimulated carbonaceous gas plasma and transported in a gas stream at several hundred Pascals pressure. The study also showed that the production of these plasma reaction products was highly dependent on the carbonaceous gas pressure, even when diluted in helium or hydrogen, and on the incident laser power density. This suggested a heterogeneous nucleation mechanism. The best conditions determined for production of the superfine gold/carbon particles were a partial pressure of 350 Pascals of methane in hydrogen and a laser power density of 3×10^9 watts/cm^2. (Higher power densities were not investigated.) The XPS analyses showed that the Au was present in the metallic state in the reaction product. The nucleation and growth of thin Au films from the products resembled other Au film growth scenarios from evaporation and sputter

sources, with the exception of the inclusion of substantial amounts of carbon (~50 atom %).

Although the plasma products gave no indications of being suitable for use in microelectronic interconnect formation, the optical properties of the thin Au cluster films were not thoroughly investigated. Preliminary infrared reflection and transmission measurements (not reported in the text due to the cursory nature of the analyses) indicated very high broadband absorption. These properties may be of interest to the electronic industry for use in bolometers or other devices requiring infrared absorbers of low thermal mass. Gold blacks have historically been used for this purpose,[87-90] but there is an operational upper temperature limit of 100-150°C. Above these temperatures the gold black films, which are composed of agglomerates of 0.1 to 4 nm diameter Au particles loosely packed in a high porosity matrix collapse and lose their high absorption characteristics. These films also are subject to contamination from the crucible and/or heating element materials that are used in the formation process (evaporation of Au in the presence of 14 to 2800 Pa of N_2, H_2, or air). The P.R.P. reported on in this text has the advantages of being free from metallic oxide impurities and being resistant to collapse (as indicated by a sharp color change in the film) at temperatures in excess of 200°C, presumably due to the thin carbonaceous coating on the Au particles.

In addition to the infrared characteristics of the P.R.P. films, the visible properties could also be of great interest to the electronic industry. There were three distinct colors that could be

produced in the P.R.P. films, depending on annealing conditions (and thus on the amount and location of carbon inclusion): black, purple, and red/yellow. Since it was shown that an Ar ion laser could cause local annealing, this material could be utilized as a multi-level, micro optical encoding medium.

These properties warrant a further investigation of the P.R.P. formation mechanism and further characterization of its optical properties.

APPENDIX A
GLASS FIBER FILTER BLANKS

Three borosilicate glass fiber filters of the type used in the study (Micro Filtrations Systems GB100R47 mm) were chosen randomly from the box and subjected to blank gravimetric analyses using the Mettler analytical balance. The filters were placed in glass petri dishes and dried overnight in a 375 K oven. They were then removed from the oven and allowed to come to room temperature in a desiccator before being weighed. Each filter was weighed separately in the bottom half of the glass petri dish and then transferred to the filter holder and installed in the plasma reaction system. The petri dish was then weighed and returned to the desiccator. The initial filter weights were determined by difference using this method.

The filters were subjected to blank runs by evacuating the plasma reaction system and then pulling a mixture of 75% H_2/25% CH_4 gas through the system at a nominal (atmospheric) flow rate of 200 ml/min and a nominal pressure of 1,330 Pascals (10 torr) for 30 minutes. The system was then filled to atmospheric pressure with the gas mixture and the filter holder was removed. The filter was then removed from the holder and placed into a pre-weighed petri dish that was already on the balance. Final filter weights were determined by difference using this technique.

All weights were recorded to the nearest 0.01 mg. Great care was taken to assure that no particles or flakes were produced during the handling of the delicate filters, as was the practice during production runs. The initial and final filter weights and the differences (D) are listed in Table 9. The standard deivation (S) of the blank filter weights was calculated using the following equation:

$$S = \{[E(D)^2]/3\}^{1/2}$$

The value of S for the three filters was determined to be 0.434 mg.

Table 9. Glass Fiber Filter Blank Weights

Filter	Initial Weight (mg)	Final Weight (mg)	Difference (mg)
1	187.80	187.13	-0.67
2	167.79	168.00	+0.21
3	192.73	193.00	+0.21

In order to determine the contribution of the normal standard deviation of the balance to the standard deviation of the filter blank weights, five copper penny weights were each weighed three times (see Table 10). The sample standard deviation (s) for each penny weight was calculated using the following equation:

$$s = \{[E(m - x)^2]/2\}^{1\backslash 2}$$

where m is the average of the three weights and x is the individual weight value. The mean value for s for all five weights was determined to be 0.220 mg.

Table 10. Repetitive Weighings on the Mettler Analytical Balance

Penny #	Weight (mg)			Average	Standard Deviation
	(1)	(2)	(3)		
1	3088.02	3087.80	3087.55	3087.79	0.235
2	2515.84	2516.00	2516.07	2515.97	0.118
3	2537.43	2536.78	2537.00	2537.07	0.331
4	2554.08	2554.00	2554.40	2554.16	0.212
5	2487.14	2487.32	2486.91	2487.12	0.206

APPENDIX B
ATOMIC ABSORPTION SPECTROMETER CALIBRATION

The Perkin Elmer Model 303 AA spectrometer was fitted with a Fisher Scientific Au hollow cathode tube and tuned to the 242.8 nm line. The lamp was operated at 9.0 mamp. A stock solution of concentrated Au standard was prepared by dissolving 1.0068 grams of 0.999% pure Au wire in 20 ml of aqua regia. This solution was then diluted to 100.0 ml in a volumetric flask and sealed. Serial dilution in either deionized water or spectral grade acetone was used to prepare 1-100 ppm (grams per million ml) working standards at the beginning of each day that analyses were performed.

The instrument's burner flame (acetylene/air) was adjusted to give the greatest linear response range for each type of solvent. In practice, this consisted of leaning the gas mixture substantially when running samples and standards dissolved (or suspended) in acetone compared to those dissolved in water. The instrument response was recorded as percent absorption, to the nearest 0.5%, on a stripchart recorder (see Figure 77). Straight line calibration plots of absorbance (A) versus concentration were prepared from the transmission data using the Lambert-Beer relationship, where T = (100 - % absorption)/100:

$$-\log T = A$$

Figure 79 shows a typical calibration plot for the instrument. No significant differences in instrument performance were noted, once the flame conditions were optimized, when using acetone solvent versus water solvent.

Figure 79. Typical AA Calibration Plot of Absorbance vs. Au Concentration

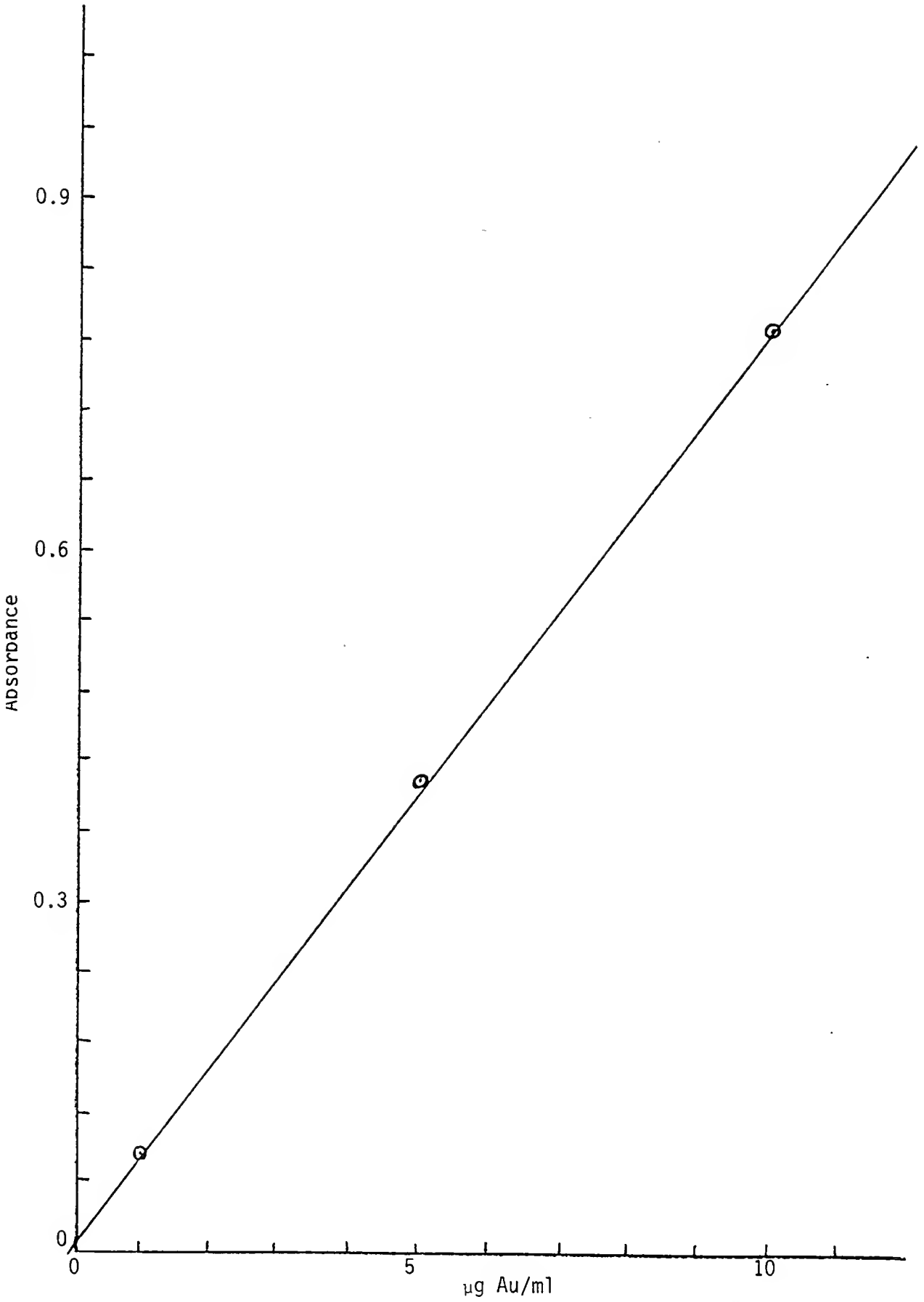
0.9
0.6
0.3
0
Absorbance
0
5
10
µg Au/ml

APPENDIX C
STANDARD REFLECTANCE VALUES FOR SILICON CARBIDE

R(stnd) for single crystal SiC used to calculate reflectance curves for microreflectometry analyses are listed below.

Table 11. R(stnd) Values for SiC

Wavelength (nm)	R(stnd) (%)	Wavelength (nm)	R(stnd) (%)
400	22.2	660	20.0
410	22.1	670	20.0
420	21.9	680	19.9
430	21.8	690	19.9
440	21.6	700	19.9
450	21.5	710	19.9
460	21.3	720	19.8
470	21.2	730	19.8
480	21.1	740	19.8
490	21.0	750	19.8
500	20.9	760	19.7
510	20.8	770	19.7
520	20.7	780	19.7
530	20.6	790	19.7
540	20.6	800	19.7
550	20.5	810	19.7
560	20.5	820	19.7
570	20.4	830	19.7
580	20.3	840	19.7
590	20.3	850	19.7
600	20.2	860	19.6
610	20.2	870	19.6
620	20.1	880	19.6
630	20.1	890	19.6
640	20.0	900	19.6
650	20.0		

REFERENCES

1. Simon S. Cohen, VLSI Electronics Microstructure Science, Vol. 15: VLSI Metallization, N.G. Einspruch, S.S. Cohen, and G.S. Gildenblat, eds. (Academic Press, Inc., Orlando, FL, 1987), Chap. 1.

2. B.M. Welch, D.A. Nelson, Y.D. Shen, and R. Venkataraman, VLSI Electronics Microstructure Science, Vol. 15: VLSI Metallization, N.G. Einspruch, S.S. Cohen, and G.S. Gildenblat, eds. (Academic Press, Inc., Orlando, FL, 1987), Chap. 9.

3. I. Blech, H. Sello, and L.V. Gregor, Handbook of Thin Film Technology, L.I. Maissel and R. Glang, eds. (McGraw-Hill Book Company, Inc., New York, 1970), Chap. 23.

4. H.B. Huntington and A.R. Grone, J. Phys. Chem. Solids 25, 335 (1971).

5. F.M. d'Heurle and P.S. Ho, in Thin Films--Interdiffusion and Reactions, J.M. Poate, K.N. Tu, and J.W. Mayer, eds. (J. Wiley and Sons, New York, 1978), 243-303.

6. R.C. West, CRC Handbook of Chemistry and Physics, 67th Edition, R.C. West, M.J. Astle, and W.H. Beyer, eds. (CRC Press, Inc., Boca Raton, FL, 1986).

7. B.E. Douglas, D.H. McDaniel, and J.J. Alexander, Concepts and Models of Inorganic Chemistry, 2nd Edition (J. Wiley and Sons, New York, 1983), Chap. 1.

8. James A. Schwartz, VLSI Electronics Microstructure Science, Vol. 15: VLSI Metallization, N.G. Einspruch, S.S. Cohen, and G.S. Gildenblat, eds. (Academic Press, Inc., Orlando, FL, 1987), Chap. 8.

9. J.C. Blair, C.R. Fuller, P.B. Ghate, and C.T. Haywood, J. Appl. Phys. 43(2), 307 (1972).

10. S.O. Colgate, G.J. Palenik, D.W. Schoenfeld, Florida High Technology and Industry Council Project Report, No. 85092726 (1986).

11. S. Wolf and R.N. Tauber, Silicon Processing for the VLSI Era, Vol. 1: Process Technology (Lattice Press, Sunset Beach, CA, 1987).

12. E.K. Broadbent, U.S. Patent 4,517,225 (1985).

13. J.L. Beauchamp and P.M. George, U.S. Patent 4,324,854 (1982).

14. S.C. Baber and V.R. Porter, U.S. Patent 4,465,716 (1984).

15. M.F. Rubner and P. Cukor, U.S. Patent 4,486,463 (1984).

16. P.B. Ghate, Thin Solid Films, 93, 359 (1982).

17. D.S. Cambell, Handbook of Thin Film Technology, L.I. Maissel and R. Glang, eds. (McGraw-Hill Book Company, Inc., New York, 1970), Chap. 5.

18. Y.P. Butylin, Ukr. Khim. Zh., 53(10), 1021 (1987).

19. C. Patton, Electronics Design 46 (1986).

20. F. Jansen, Plasma Deposited Thin Films, J. Mort and F. Jansen, eds. (CRC Press, Inc., Boca Raton, FL, 1986), Chap. 1.

21. R.A. Dugdale, Nature, 249, 440 (1974).

22. M.L. Green and R.A. Levy, J. Metals, June, 63 (1985).

23. F.O. Sequeda, J. Metals, May, 43 (1985).

24. T. Tagaki, J. Vac. Sci. Technol. A 2, 382 (1984).

25. W. Knauer and R.L. Poeschel, J. Vac. Sci. Technol. B 6 (1), 456 (1988).

26. D.B. Fraser, U.S. Patent 4,072,768 (1978).

27. Matsushito Electric Industrial Co., Ltd., Jpn. Patent 57/65324 (1982).

28. T. Araya, A. Matsunawa, S. Katayama, S. Kioki, Y. Ibaraki, and Y. Endo, U.S. Patent 4,619,691 (1986).

29. F.G. Mann, A.F. Wells, and D. Purdie, J. Chem. Soc., Pt. 2, 1828 (1937).

30. V.E. House and S.O. Colgate, 39th Annual Meeting of the Florida Section of the American Chemical Society, Tampa, FL (1988).

31. R.J. Puddephat and I. Treurnicht, J. Organometallic Chem. 319, 129 (1987).

32. A. Shiotani and H. Schmidbaur, J. Amer. Chem. Soc. 92, 7003 (1970).

33. C.E. Larson, T.H. Baum, and R.L. Jackson, J. Electrochem. Soc. 134(1), 266 (1987).

34. H. Schmidbaur, Gmelin Handbuch der Anorganische Chemie: Gold-Organic Compounds (Springer-Verlag, Berlin, 1980).

35. Cyanopure Corporation, Product Bulletin 159 (1986).

36. R.Y. Jan and S.D. Allen, SPIE 459, 71 (1984).

37. T.H. Baum and C.R. Jones, Appl. Phys. Lett. 47(5), 538 (1985).

38. T.H. Baum and C.R. Jones, J. Vac. Sci. Tech. B 4(5), 1187 (1986).

39. T.H. Baum, E.E. Marinero, and C.R. Jones, Appl. Phys. Lett. 49(18), 1213 (1986).

40. T.T. Kodas, T.H. Baum, and P.B. Comita, J. Appl. Phys. 2(1), 281 (1987).

41. T.H. Baum, J. Electrochem. Soc. 134(10), 2616 (1987).

42. G.M. Shedd, H. Lezec, A.D. Dubner, and J. Melngailis, Appl. Phys. Lett. 49(23), 1584 (1986).

43. K. Gamo, N. Takakura, N. Samoto, R. Shimuzu, and S. Namba, Jap. J. Appl. Phys. 23(5), 293 (1984).

44. H.W.P. Koops, R. Weid, D.P. Kern, and T.H. Baum, J. Vac. Sci. Tech. B 6(1), 477 (1988).

45. E.D. Wolley, U.S. Patent 3,440,113 (1969).

46. W.L. Grady and M.M. Bursey, Int. J. Mass. Spectrom. Ion Phys. 55, 111 (1983).

47. W.L. Grady and M.M. Bursey, Int. J. Mass. Spectrom. Ion Phys. 55, 247 (1983).

48. A.K. Chowdhury and C.L. Wilkins, J. Am. Chem. Soc. 109(18), 5336 (1987).

49. D.A. Weil and C.L. Wilkins, J. Am. Chem. Soc. 107, 7316 (1985).

50. E. Kay, A. Dilks, and U. Hetzler, J. Macromol. Sci.-Chem. A 12(9), 1393 (1978).

51. E. Kay and A. Dilks, Thin Solid Films 78, 309 (1981).

52. H. Biederman and L. Holland, Nucl. Instrum. Methods 212, 497 (1983).

53. R.A. Roy, R. Meissier, and S.V. Krishnaswamy, Thin Solid Films 109, 27 (1983).

54. E. Kay and M. Hecq, J. Appl. Phys. 55(2), 370 (1983).

55. H. Biederman, Vacuum 34(3-4), 405 (1984).

56. L. Martinu, Thin Solid Films 140, 307 (1986).

57. L. Martinu, Solar Energy Mater. 15, 21 (1987).

58. S.A.Y. Al-Ismail and C.A. Hogarth, J. Phys. E: Sci. Instrum. 20, 344 (1987).

59. D. McIntosh and G.A. Ozin, Inorg. Chem. 16(1), 51 (1977).

60. P.H. Kasai and P.M. Jones, J. Am. Chem. Soc. 107(22), 6385 (1985).

61. P.H. Kasai, J. Am. Chem. Soc. 105(22), 6704 (1983).

62. P.H. Kasai, J. Am. Chem. Soc. 106(11), 3069 (1984).

63. G.M. Schragg, Doctoral Dissertation, University of Florida (1987).

64. H. Khalifa, G. Suehla, and L. Erdey, Talanta 12, 703 (1965).

65. J.R. Eyler, TRAC 5(2), 44 (1986).

66. D. Lesson and P.J. Brucat, J.C.P., submitted December 1988.

67. M. Klasson, J. Hedman, A. Berndtsson, R. Nilsson, and C. Nordling, Physica Scripta 5, 93 (1972).

68. B.L. Henke, Phys. Rev. A 6(1), 94 (1972).

69. Kratos, Inc., XSAM800 Operators Handbook (1984).

70. J.H. Scofield, J. Electron. Spectros. 8, 129 (1976).

71. L.B. Valdes, Proc. IRE 42, 420 (1954).

72. T.P. Hughest, Plasmas and Laser Light (J. Wiley and Sons, New York, 1975), Chaps. 5 and 6.

73. J.F. Ready, J. Appl. Phys. 35(2), 462 (1965).

74. N.F. Mott and H. Jones, The Theory of the Properties of Metals and Alloys (Dover Publications, Inc., New York, 1958), Chap. III.

75. O.F. Hagena and W. Obert, J. Chem. Phys. 56(5), 1793 (1971).

76. A. Fritsch and P. Legare, Surface Sci. 162, 742 (1985).

77. C.J. Sofield, C.J. Woods, C. Wild, J.C. Riviere, and L.S. Welch, Mat. Res. Soc. Symp. Proc. 28, 197 (1984).

78. M. Fuggle and R. Martensen, J. Elect. Spect. 24, 275 (1980).

79. I.H. Khan, Handbook of Thin Film Technology, L.I. Maissel and R. Glang, eds. (McGraw-Hill Book Company, Inc., New York, 1970), Chap. 10.

80. P.E. Dyer, D.J. James, G.J. Pert, S.A. Ramsden, and M.A. Skipper, Laser Interaction and Related Phenomena--Interaction of High Power CO_2 Lasers With Solid Targets, Volume 3A, H.J. Schwarz and H. Hora, eds. (Plenum Press, New York, 1973).

81. N.A. Ebrahim and C. Joshi, Phys. Fluids 24(1), 138 (1981).

82. T.H. Tan, G.H. McCall, and A.H. Williams, Phys. Fluids 27(1), 296 (1984).

83. G. Tonon and M. Rabeau, Phys. Lett. 40A, 215 (1972).

84. C.G. Granquist and O. Hunderi, Phys. Rev. B 16(8), 3513 (1976).

85. S.B. Dicenzo and G.K. Wertheim, Comments Solid State Phys. 11(5), 203 (1985).

86. L. Oberli, R. Monot, H.J. Mathieu, D. Landolt, and J. Buttet, Surface Sci. 106, 301 (1981).

87. L. Harris, R.T. McGinnies, and B.M. Siegel, J. Opt. Soc. Am. 38(7), 582 (1948).

88. L. Harris, and J.K. Beasley, J. Opt. Soc. Am. 42, 134 (1951).

89. V.N. Sintsov, Zhurnal Prikladnoi Spektroskoppi 4(6), 503 (1966).

90. D.R. McKenzie, J. Opt. Soc. Am. 66(3), 249 (1975).

BIOGRAPHICAL SKETCH

Charles George Simon was born in West Palm Beach, Florida, on August 18, 1954. He received the Bachelor of Science degree in chemistry, under the guidance of Prof. D. Neal Boehnke, from Jacksonville University in Jacksonville, Florida, in 1976. He then entered the Graduate School at the University of South Carolina (U.S.C.) where he worked under the direction of Prof. Terry Bidleman in the Analytical Chemistry Division. He received the Master of Science degree from U.S.C. in 1979. From 1979-1985 he worked in the specialty chemicals and forest products industries as an environmental/analytical chemist and industrial hygienist. In 1985 he entered the University of Florida graduate school and worked under the direction of Prof. Sam Colgate in the Physical Chemistry Division. Subsequent to his pending completion of the requirements for the Doctor of Philosophy degree, he has accepted a position with the Extraterrestrial Materials Group, McDonnell Center for the Space Sciences, Washington University, St. Louis, Missouri.

I certify that I have read this study and that in my opinion it conforms to acceptable standards of scholarly presentation and is fully adequate, in scope and quality, as a dissertation for the degree of Doctor of Philosophy.

Samuel O. Colgate, Chairman
Associate Professor of Chemistry

I certify that I have read this study and that in my opinion it conforms to acceptable standards of scholarly presentation and is fully adequate, in scope and quality, as a dissertation for the degree of Doctor of Philosophy.

Martin Vala
Professor of Chemistry

I certify that I have read this study and that in my opinion it conforms to acceptable standards of scholarly presentation and is fully adequate, in scope and quality, as a dissertation for the degree of Doctor of Philosophy.

Willis B. Person
Professor of Chemistry

I certify that I have read this study and that in my opinion it conforms to acceptable standards of scholarly presentation and is fully adequate, in scope and quality, as a dissertation for the degree of Doctor of Philosophy.

John R. Eyler
Professor of Chemistry

I certify that I have read this study and that in my opinion it conforms to acceptable standards of scholarly presentation and is fully adequate, in scope and quality, as a dissertation for the degree of Doctor of Philosophy.

Donald J. Huber
Associate Professor of Biochemistry and Molecular Biology

This dissertation was submitted to the Graduate Faculty of the Department of Chemistry in the College of Liberal Arts and Sciences and to the Graduate School and was accepted as partial fulfillment of the requirements for the degree of Doctor of Philosophy.

December, 1988

Dean, Graduate School